Competitive interplay between xenophagy and viral evasion mechanisms of autophagy during human cytomegalovirus infection

Dissertation submitted for the achievement of the

academic degree

"Doctor rerum naturalium"

(Dr. rer. nat.)

At the department of Biology of

the Johannes Gutenberg-University

in Mainz

submitted by

Nadine Krämer

Born on June 02, 1994 in Erbach (Odenwald)

Mainz 2023

Dean Department of Biology: Prof. Dr. Eckhard Thines

1.Referee:

2.Referee:

Day of the oral examination: 16.02.2024……

I, Nadine Krämer, declare that I have authored this dissertation independently, that I have not used other than the declared sources / resources, and that I have explicitly marked all material which has been quoted either literally or by content from the used sources.

Mainz, …… ……

(Signature)

Some of the data on which this work is based have already been published:

Nadine Krämer, Martin Schütz, Uxía Gestal Mato, Lina Herhaus, Manfred Marschall, Christine Zimmermann (2022): Recombinant Human Cytomegalovirus Expressing an Analog-Sensitive Kinase pUL97 as Novel Tool for Functional Analyses. Viruses 2022, 14(10)

Summary

Infection with the human cytomegalovirus (HCMV) is controlled on multiple levels by intrinsic defense mechanisms of the cell. Selective autophagy functions as such a mechanism by degrading viral components. In this process, which is also called xenophagy, autophagy receptors play a central role. These receptors recognize the viral cargo and direct it to the developing autophagosomes. After fusion of the autophagosome with the lysosome, the cargo is degraded and recycled. The interplay between HCMV and autophagy is only poorly understood and both antiviral and proviral roles of autophagy have been described. To gain a better knowledge of these processes, the roles of the two autophagy receptors SQSTM1/p62 and optineurin and some potential autophagy receptors of the tripartite motif (TRIM) family proteins during HCMV infection were analyzed.

Co-immunoprecipitation (Co-IP) experiments combined with mass spectrometry (MS) analyses revealed that SQSTM1/p62 precipitates with several viral proteins in HCMV-infected cells. Almost all viral capsid proteins were found to interact, confirming the results of our previous study. Strikingly, the experiments also revealed that SQSTM1/p62 interacts with several proteins of the nuclear pore complex (NPC). This is in line with the knowledge that SQSTM1/p62 shuttles between the nucleus and cytoplasm via the NPC. These combined findings suggest that SQSTM1/p62 transports capsid structures from both the cytoplasm and the nucleus to autophagosomes for degradation. To further investigate the impact of the receptor on HCMV infection, SQSTM1 knockout cells were generated. Infection of these cells revealed that the absence of the receptor had no impact on viral DNA replication. Surprisingly, however, enhanced release of viral progeny was found after HCMV infection of SQSTM1 knockout cells, compared to controls. This suggests that SQSTM1/p62 expression induces an antiviral effect downstream of the initiation of viral genome replication. This fits into the hypothesis that viral infection is controlled by autophagy via the interaction of SQSTM1/p62 with viral capsid components in the process of particle morphogenesis and the subsequent degradation of these proteins.

The absence of SQSTM1/p62 in HCMV-infected cells also led to an increase in the levels of interferon stimulated gene products (ISGs). ISGs are known to restrict viral replication on multiple levels. Thus SQSTM1/p62 impedes viral progeny production via degradation of capsid proteins while seemingly supporting viral infection by restricting type I interferon (IFN-I) signaling. This contradiction may be explained by the known function of autophagy to control excessive interferon responses. SQSTM1/p62 may thus play a balancing role during HCMV infection between degrading viral components and preventing cell damage by an extreme interferon response. The results suggest that SQSTM1/p62 is a key regulator of autophagic processes during HCMV infection, controlling both viral and cellular mechanisms.

In a next part of the study, the impact of SQSTM1/p62 phosphorylation on HCMV infection was addressed. The functions of autophagy receptors, such as to link the cargo with the autophagic machinery is partly regulated by phosphorylation. Phosphoproteomic analyses revealed that SQSTM1/p62 was exclusively hyperphosphorylated at S272 upon HCMV infection. The phosphorylation status of all other known sites on SQSTM1/p62 was not affected by HCMV infection. To address the role of this S272 phosphorylation on HCMV infection, HCMV mutants were generated, which expressed different versions of SQSTM1/p62. The receptor was expressed from these recombinant viruses in either (i) its wild-type configuration (S272), or (ii) serine was replaced by aspartic acid or glutamic acid, thereby either mimicking the phosphorylation (S272D and S272E), or (iii) by replacing serine by alanine, representing a non-phosphorylated status (S272A). Infection of SQSTM1 knockout cells with these mutants, followed by Co-IP and MS analyses, did not reveal any differences between the mutant viruses, showing that the phosphorylation at S272 had no effect on binding to cellular and viral proteins. However, S272 phosphorylation impaired proteasomal degradation of SQSTM1/p62, leading to an enrichment of this receptor and increased ISG protein levels in HCMV-infected cells, accompanied by reduced viral progeny release. Thus, although SQSTM1/p62 restricts ISG protein levels, as seen in the first part of the study, phosphorylation at S272 increased IFN-I responses. This indicated that S272 phosphorylation appears to be a key switch that regulates the interference of SQSTM1/p62 and autophagy in IFN-I responses.

To determine whether the HCMV kinase pUL97 was involved in the phosphorylation of SQSTM1/p62 at S272, a mutant version of this kinase (pUL97-as1) was used. The mutated gene (*UL97-as1*) expresses an analog-sensitive version of pUL97 which can be specifically and reversibly inhibited by treatment with the ATP analog 3MB-PP1. A recombinant HCMV mutant was generated by replacing the *wt-UL97* gene with *UL97-as1*. Infection of cells with this virus in the presence of 3MB-PP1 resulted in decreased phosphorylation of SQSTM1/p62 at S272, suggesting that pUL97 was involved in the phosphorylation of the receptor. This was confirmed by co-transfection experiments using plasmids expressing either *UL97-as1* or *GFP-SQSTM1* and the addition of 3MB-PP1 with subsequently phosphoproteomic analysis. Subsequent in-vitro kinase assay, however, could not provide evidence for direct phosphorylation of SQSTM1/p62 by pUL97, indicating an indirect effect of the viral kinase on phosphorylation of the receptor. The results were surprising, as the experiments in the previous section had shown that S272 phosphorylation impeded HCMV progeny production. It remains unclear why pUL97 should mediate an antiviral effect, but this may be explained by the multiple functions of the viral kinase to support viral infection, which may fortuitously also lead to S272 phosphorylation by a cellular kinase. Further experiments are necessary to investigate the impact of pUL97 on SQSTM1/p62 function and on autophagy.

Besides SQSTM1/p62, the autophagy receptor optineurin and its role during HCMV infection was addressed. Surprisingly, Co-IP and MS analyses could identify only one HCMV

protein, namely pUL84, as an interactor with optineurin. Interestingly, pUL84 also interacted with SQSTM1/p62. As the viral protein is a key component of the DNA-replication complex, this suggested that there might be an interference of optineurin with viral genome replication. However, infection of optineurin knockout cells showed no impairment in HCMV genome replication and progeny release. Further analyses of this, e.g., with respect to different cell types were beyond this work and shall be addressed in further studies.

In a further section, the role of selected TRIMs during HCMV infection was investigated. TRIM25, TRIM26, and TRIM32 had been identified before as components of HCMV virions. TRIM21 and TRIM28 are known regulators of autophagy. Interestingly, some of these TRIMs again interacted with viral capsid proteins. Consequently, individual knockout cells were established. The knockout of any of these TRIMs did not have an impact on the induction of autophagy in HCMV-infected cells. However, knockout of particularly *TRIM25* and *TRIM32* resulted in increased release of viral progeny following infection of the respective knockout cells with HCMV. Thus, some TRIMs indeed seem to function in the cellular defense against HCMV infection.

In a final section, the role of the immunity related GTPase Q protein (IRGQ) during HCMV infection was analyzed in collaboration with Lina Herhaus, Institute of Biochemistry II, Goethe University Frankfurt/Main, Germany. This group had identified IRGQ as a new candidate in the regulation of autophagy upon *Salmonella* infection. Knockdown of IRGQ by siRNA transfection did not impair HCMV genome replication. Interestingly, the downregulation of this gene resulted in a marked increase in viral progeny release. The knockdown of gamma-aminobutyric acid receptor-associated protein-like 2 (GABARAP-L2), which is an interactor of IRGQ, also resulted in elevated HCMV progeny production. Moreover, the results demonstrated that the antiviral impact of IRGQ was dependent on the presence of GABARAP-L2. Together these data identify IRGQ as a novel regulator of HCMV infection. The antiviral mechanisms that are mediated by IRGQ await further analysis.

Zusammenfassung

Die Infektion mit dem humanen Cytomegalovirus (HCMV) wird auf verschiedenen Ebenen durch zelleigene Abwehrmechanismen kontrolliert. Die selektive Autophagie stellt einen derartigen Mechanismus dar. Bei dieser Form der Autophagie, die auch als Xenophagie bezeichnet wird, spielen Autophagierezeptoren eine zentrale Rolle. Diese Rezeptoren erkennen die viralen Moleküle (*Cargo)* und leiten sie zu den Autophagosomen. Nach der Verschmelzung des Autophagosoms mit dem Lysosom wird das *Cargo* abgebaut und recycelt. Bislang war jedoch das Zusammenspiel zwischen HCMV und Autophagie nur unzureichend verstanden, es wurde sowohl eine antivirale als auch eine provirale Rolle der Autophagie beschrieben. Um ein besseres Verständnis über diese Vorgänge zu erlangen, wurde die Rolle der beiden Autophagierezeptoren SQSTM1/p62 und Optineurin, sowie einiger potenzieller Autophagierezeptoren aus der Tripartite-motif (TRIM) Proteinfamilie während einer HCMV-Infektion analysiert.

Zur Analyse der Interaktion von SQSTM1/p62 mit viralen Proteinen wurde die Methodik der Ko-Immunopräzipitation (Ko-IP) in Kombination mit massenspektrometrischen (MS) Analysen eingesetzt. Es zeigte sich, dass SQSTM1/p62 mit fast allen viralen Kapsidproteine interagierte. Dies bestätigte die Ergebnisse unserer früheren Studie. Auffallend war, dass auch mehrere Proteine des Kernporenkomplexes (NPC) als Interaktionspartner von SQSTM1/p62 identifiziert wurden. Da SQSTM1/p62 als nukleozytoplasmatisches Shuttleprotein bekannt ist, sind diese Ergebnisse plausibel und legen nahe, dass SQSTM1/p62 über die Interaktion mit dem NPC Kapsidstrukturen aus dem Zellkern, ähnlich wie aus dem Zytoplasma zum Abbau zu den Autophagosomen transportiert. Um den Einfluss des Rezeptors auf die HCMV-Infektion weiter zu untersuchen, wurden SQSTM1/p62-Knockout-Zellen erzeugt. Diese Zellen wurden infiziert und anschließend die virale DNA-Replikation und die Synthese von Tochterviren untersucht. Das Fehlen von SQSTM1/p62 hatte keinen Einfluss auf die virale Genomreplikation, wohl aber auf die Freisetzung von viralen Nachkommen, die erhöht war. Dies deutete darauf hin, dass die antivirale Wirkung von SQSTM1/p62 auf Vorgänge abzielt, die zur späten Phase der viralen Infektion, nach Beginn der viralen Genomreplikation ablaufen. Dies stimmte auch mit der Vorstellung überein, dass die virale Infektion durch die Interaktion von SQSTM1/p62 mit viralen Kapsidkomponenten im Prozess der Partikelmorphogenese kontrolliert wird.

Weitere Analysen zeigten, dass das Fehlen von SQSTM1/p62 bei einer HCMV-Infektion die Interferon-Antwort durch einen Anstieg an Interferon-stimulierten Genprodukten (ISGs) verstärkt. ISGs sind dafür bekannt, dass sie die virale Replikation auf mehreren Ebenen einschränken. Aus diesen Ergebnissen ließ sich ableiten, dass SQSTM1/p62 durch Kontrolle der ISG-Expression die Virusinfektion begünstigt, während es gleichzeitig den Abbau von viralen Kapsidproteinen vermittelt. Dieser Widerspruch lässt sich durch die bekannte

Funktion der Autophagie in der Kontrolle einer übermäßigen Interferonantwort erklären. SQSTM1/p62 könnte so während einer HCMV-Infektion eine ausgleichende Rolle zwischen dem Abbau viraler Komponenten und der Verhinderung von Zellschäden durch eine überschießende Interferonantwort spielen. Die Ergebnisse deuten zusammengefasst darauf hin, dass SQSTM1/p62 ein wichtiger Regulator der Autophagie während einer HCMV-Infektion ist, der sowohl virale als auch zelluläre Mechanismen kontrolliert.

In einem weiteren Teil der Arbeit wurden die Auswirkungen der Phosphorylierung von SQSTM1/p62 auf die HCMV-Infektion untersucht. Einzelne Funktionen der Autophagierezeptoren, wie z.B. ihre Affinität zum *Cargo* und den autophagosomalen Membranen werden durch Phosphorylierung reguliert. Die MS Analysen zeigten, dass SQSTM1/p62 bei einer HCMV-Infektion ausschließlich an Position S272 verstärkt phosphoryliert wird. Der Phosphorylierungsstatus aller anderen, bekannten Phosphorylierungsstellen von SQSTM1/p62 wurde durch die HCMV-Infektion nicht beeinflusst. Um die Rolle der Phosphorylierung an S272 bei einer HCMV-Infektion näher zu untersuchen, wurden HCMV-Mutanten hergestellt, die verschiedene Versionen von SQSTM1/p62 exprimierten. So wurde ein Virus hergestellt, das den Rezeptor in seiner Wildtyp-Konfiguration (S272) exprimierte. Weitere Viren wurden kloniert, die eine Version von SQSTM1/p62 exprimierten, in der Serin durch Asparaginsäure oder Glutaminsäure ersetzt wurde (S272D und S272E). Eine derartige Modifikation ahmt die Phosphorylierung an Position S272 nach. Schließlich wurde ein Virus hergestellt, in dem Serin durch Alanin an Position S272 ersetzt wurde (S272A). Alanin kann nicht phosphoryliert werden. Die Bindung der verschiedenen Versionen des Rezeptors an das *Cargo* wurde in Ko-IP- und MS-Analysen nach Infektion von SQSTM1-Knockout-Zellen mit den rekombinanten Viren untersucht. Hierbei zeigten sich keine Unterschiede in der Bindungsfähigkeit von SQSTM1/p62 an zelluläre und virale Proteine. Die Phosphorylierung an S272 reduzierte jedoch den proteasomalen Abbau von SQSTM1/p62, was zu einer Anreicherung des Rezeptors und zu erhöhten ISG-Proteinspiegeln in HCMV-infizierten Zellen führte. Dies war von einer verringerten Freisetzung von Tochterviren begleitet. Obwohl SQSTM1/p62 also die ISG-Proteinkonzentration einschränkt, wie im ersten Teil der Arbeit festgestellt wurde, scheint die Phosphorylierung an S272 die IFN-I-Induktion zu verstärken. Die S272-Phosphorylierung scheint also ein entscheidender Faktor zu sein, der die Interferenz von SQSTM1/p62 und Autophagie bei IFN-I-Reaktionen reguliert.

Um festzustellen, ob die HCMV-Kinase pUL97 an der Phosphorylierung von SQSTM1/p62 an S272 beteiligt ist, wurde eine analog-sensitive Version dieser Kinase (pUL97-as1) verwendet. Das mutierte Gen (*UL97-as1*) exprimiert eine Version von pUL97, die durch Behandlung mit dem ATP-Analogon 3MB-PP1 spezifisch und reversibel gehemmt werden kann. Durch Ersetzen des *wt-UL97*-Gens durch *UL97-as1* wurde ein rekombinantes HCMV erzeugt. Die Infektion von Zellen mit dieser Mutante in Gegenwart von 3MB-PP1 führte zur verminderten Phosphorylierung von SQSTM1/p62 an S272. Dies deutet darauf hin, dass pUL97 an der Phosphorylierung des Rezeptors beteiligt ist. Das Ergebnis konnte durch Ko-

Transfektionsexperimente bestätigt werden. Eine *In-vitro*-Kinase-Analyse konnte jedoch keine direkte Phosphorylierung von SQSTM1/p62 durch pUL97 nachweisen, was auf eine indirekte Wirkung der viralen Kinase auf die Phosphorylierung des Rezeptors hinweist. Diese Ergebnisse waren überraschend, da die Experimente im vorangegangenen Abschnitt gezeigt hatten, dass die S272-Phosphorylierung die Produktion von HCMV-Tochterviren behindert. Es bleibt unklar, warum pUL97 eine antivirale Wirkung vermitteln sollte. Dies könnte jedoch durch die vielfältigen Funktionen der viralen Kinase zur Unterstützung der viralen Infektion erklärt werden, die zufälligerweise auch zur S272-Phosphorylierung durch eine zelluläre Kinase führen könnten. Weitere Experimente sind notwendig, um die Auswirkungen von pUL97 auf die Funktion von SQSTM1/p62 und auf die Autophagie zu untersuchen.

Neben SQSTM1/p62 wurde auch der Autophagierezeptor Optineurin und seine Rolle während einer HCMV-Infektion untersucht. Überraschenderweise konnte durch Ko-IP- und MS-Analysen nur ein HCMV-Protein, nämlich pUL84, als Bindepartner von Optineurin identifiziert werden. Interessanterweise interagierte pUL84 auch mit SQSTM1/p62. Da pUL84 eine Schlüsselkomponente des DNA-Replikationskomplexes ist, deutet dies auf eine mögliche Interferenz von Optineurin mit der viralen Genomreplikation hin. Die Infektion von Optineurin-Knockout-Zellen zeigte jedoch keine Beeinträchtigung der HCMV-Genomreplikation und der Freisetzung von Nachkommen. Weitere Analysen hierzu, z.B. in Bezug auf verschiedene Zelltypen, gehen über den Rahmen dieser Arbeit hinaus und sollen in weiteren Studien untersucht werden.

In einem weiteren Abschnitt wurde die Rolle von ausgewählten TRIMs während der HCMV-Infektion untersucht. TRIM25, TRIM26 und TRIM32 konnten wir in Vorarbeiten als Bestandteile von HCMV-Virionen identifizieren. TRIM21 und TRIM28 sind bekannte Regulatoren der Autophagie. Interessanterweise konnte in Ko-IP/MS-Analysen wiederum eine Interaktion einiger dieser TRIMs mit Kapsidproteinen nachgewiesen werden. Zur weiteren Analyse wurden individuelle Knockout-Zellen hergestellt. Der Knockout der TRIMs hatte keinen Einfluss auf die Induktion der Autophagie in HCMV-infizierten Zellen. Allerdings führte der Knockout insbesondere von *TRIM25* und *TRIM32* zu einer erhöhten Freisetzung von Tochterviren. Einige TRIMs scheinen also tatsächlich eine Funktion bei der zellulären Abwehr bei HCMV-Infektionen wahrzunehmen.

In einem letzten Abschnitt der Arbeit wurde die Rolle der immunity related GTPase Q (IRGQ) im Rahmen der HCMV-Infektion zusammen mit der Arbeitsgruppe von Lina Herhaus vom Institut für Biochemie II der Goethe-Universität Frankfurt am Main untersucht. Herhaus und Kollegen hatten IRGQ als einen neuen Regulator der Autophagie bei der *Salmonella*-Infektion identifiziert. Der Knock-down von IRGQ hatte keinen Einfluss auf die virale Genomreplikation. Interessanterweise führte jedoch der Knock-down dieses Proteins zu einer deutlich erhöhten Freisetzung viraler Nachkommen. Ein gleicher Effekt wurde auch nach dem Knock-down des Gamma-aminobutyric acid receptor-associated protein-like 2 (GABARAP-L2) beobachtet. Dieses Protein ist ein bekannter

Bindungspartner von IRGQ. Die Ergebnisse haben außerdem gezeigt, dass die antivirale Wirkung von IRGQ von GABARAP-L2 abhängig ist. Zusammengefasst konnten diese Experimente IRGQ als einen neuen Regulator der HCMV-Infektion identifizieren. Der Mechanismus der antiviralen Wirkung von IRGQ muss in nachfolgenden Arbeiten adressiert werden.

.

Table of contents

Table of figures

Table of tables

List of abbreviations

3MB-PP1	3-methylbenzyl pyrazolopyrimidine
AEC	3-Amino-9-Ethyl-Carbazole
ARF6	ADP-ribosylation factor 6
ARL6IP1	ADP-ribosylation factor-like protein 6-interacting protein 1
BAC	Bacterial Artificial Chromosome
Bafi	Bafilomycin A1
bFGF	basic Fibroblast Growth Factor
BSA	Albumin fraction V (from bovine serum)
CDK	Cyclin-Dependent Kinase
CDK1	Cyclin-Dependent Kinase 1
cGAS	cyclic GMP-AMP synthase
Co-IP	Co-immunoprecipitation
CRISPR/Cas9	Clustered Regularly Interspaced Short Palindromic Repeats/Cas9
CVB3	Coxsackievirus B3
d.p.i.	days post infection
ddH_2O	double-distilled water
dH_2O	distilled water
DMEM	Dulbecco's Modified Eagle Medium
DMF	N,N-Dimethylformamide
DMSO	Dimethyl sulfoxide
dNTPs	Deoxynucleotide Triphosphates
DOG	2-deoxy-galactose
DPBS	Dulbecco's Phosphate Buffered Saline
DTT	1.4-Dithiothreitol
EBV	Epstein–Barr virus
EDTA	Ethylene Diamine Tetra acetic Acid
EtOH	Ethanol
FACS	Fluorescence-Activated Cell Sorting
FCS	Fetal Calf Serum
FDR	False Discovery Rate
fwd	forward
GABARAP	Gamma-aminobutyric acid receptor-associated protein
GABARAP-L2	Gamma-aminobutyric acid receptor-associated protein-like 2
galK	galactokinase
GAPDH	Glyceraldehyde 3-Phosphate Dehydrogenase

gB	glycoprotein B
GFP	Green Fluorescent Protein
GGH	Gamma-Glutamyl Hydrolase
GO	Gene Ontology
gRNA	guide RNA
h.p.i.	hours post infection
h.p.t.	hours post transfection
HCMV	Human Cytomegalovirus
HEPES	4-(2-hydroxyethyl)-1-piperazineethanesulfonic acid
HFF	Human Foreskin Fibroblasts
HIV	Human Immunodeficiency Virus
HSV	Herpes Simplex Virus
ICP34.5	Infected Cell Protein 34.5
IE1	Immediate-early protein
IFN-I	Interferon type I
IFN-β	Interferon β
IP	Immunoprecipitation
IRGQ	Immunity Related GTPase Q protein
ISG	Interferon Stimulated Gene
ISG15	Interferon Stimulated Gene 15
IVKA	In-Vitro Kinase Assay
ko	knockout
KSHV	Kaposi's sarcoma-associated herpesvirus
LC3	Microtubule-associated protein 1 light chain 3
LC3B	Microtubule Associated Protein 1 Light Chain 3 Beta
LIR	LC3-interacting region
m.o.i.	Multiplicity of infection
MCP	Major capsid protein
MCMV	Murine Cytomegalovirus
MEM	Minimum Essential Medium
MIEP	Major Immediate Early Promotor
MS	Mass Spectrometry
Mx1	Interferon induced GTP-binding protein MX1
NF-κB	Nuclear Factor 'kappa-light-chain-enhancer' of activated B-cells
NPC	Nuclear Pore Complex
PAGE	Polyacrylamide Gel Electrophoresis
PCR	Polymerase Chain Reaction

PEP	Posterior Error Probability
PEST	proline (P), glutamic acid (E), serine (S) and threonine (T)
POM121	Nuclear envelope pore membrane protein POM 121
pp150	phosphoprotein 150
pp28	phosphoprotein 28
pp65	phosphoprotein 65
p-Rb	Phosphorylated Retinoblastoma protein
PSM	Peptide Spectrum Match
p-SQSTM1/p62 S272	Phosphorylated SQSTM1/p62 at S272
PVDF	Polyvinylidene Fluoride
qPCR	Real Time quantitative Polymerase Chain Reaction
Rb	Retinoblastoma protein
rev	Reverse
RT	Room temperature
S272	Serine 272
S272A	Serine 272 Alanine
S272D	Serine 272 Aspartate
S272E	Serine 272 Glutamate
S272wt	Serine 272 wildtype
SCP	Small Capsid Protein
SD	Standard Deviation
SDS	Sodium Dodecyl Sulphate
SDS-PAGE	Sodium Dodecyl Sulphate Polyacrylamide Gel Electrophoresis
siCDK1	CDK1 siRNA
siControl	Control siRNA
siGABARAP-L2	GABARAP-L2 siRNA
siIRGQ	IRGQ siRNA
SQSTM1	Sequestosome-1
STING	Stimulator of IFN Genes
STRING	Search Tool for the Retrieval of Interacting Genes
T269	Threonine 269
TAF15	TATA-binding protein-associated factor 2N
TBE	Tris/Borate/EDTA
TBK1	TANK-Binding kinase 1
TBS-T	Tris buffered saline, containing 0.2% Tween 20
TFA	Trifluoroacetic acid
TRAM1	Translocating chain-associated membrane protein 1

TRIM	Tripartite motif
Tris	Tris-hydroxymethyl-amino methane
UBD	Ubiquitin-Binding Domain
UL	Unique Long
UniProtKB	Universal Protein Knowledge Base
US	Unique Short
VZV	Varicella zoster virus
WB	Western blot
wt	Wildtype

1 Introduction

Many human viruses share a long time of co-evolution with their host, leading to mutual adaptation. On the one hand, viruses are successfully recognized, antagonized and removed from the organism by various innate and adaptive host mechanisms. However, on the other hand, viruses have developed multiple strategies to interfere with such defense mechanisms. The human cytomegalovirus (HCMV) is one example of a pathogen which evades control by its host on various levels. One such level is the intrinsic process of autophagy. This work addresses on the interaction of HCMV with the molecular regulation of autophagy with a particular focus on autophagy receptors.

1.1 HCMV

The HCMV, also termed Human Herpesvirus 5 (HHV-5), is a member of the herpes virus family (Schottstedt et al., 2010). In addition to HCMV, there are eight other human herpesviruses, listed below in their systematic nomenclature and under their synonyms: HHV-1 Herpes simplex virus-1 (HSV-1), HHV-2 Herpes simplex virus-2 (HSV-2), HHV-3 Varicella zoster virus (VZV) and HHV-4 Epstein–Barr virus (EBV), HHV-6A and 6B Roseolovirus, and HHV-8 Kaposi's sarcoma-associated herpesvirus (KSHV) (Lan and Luo, 2017). Among human herpesviruses, HCMV has the largest genome, consisting of a double-stranded DNA enclosed in an icosahedral capsid (Figure 1) (Murphy and Shenk, 2008; Schottstedt et al., 2010). The capsid is covered by a protein layer termed the tegument, which serves both structural and functional roles, such as stabilizing the capsid (Dai et al., 2013; Kalejta, 2008a, b; Phillips et al., 2012; Smith et al., 2014). The viral particle is surrounded by a lipid envelope, containing different glycoproteins which interact with host cells and finally mediate penetration (Schauflinger et al., 2013).

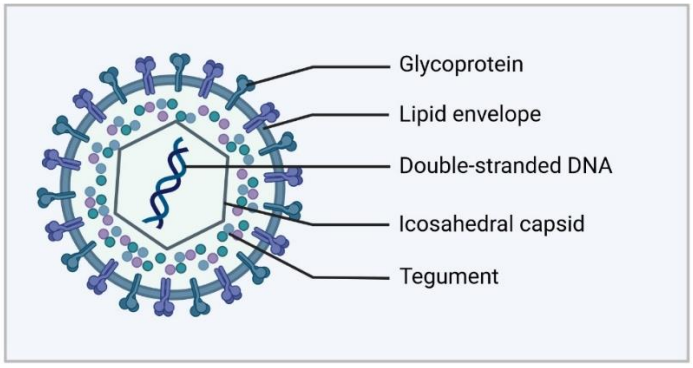

Figure 1. Schematic structure of the HCMV virion. The particle contains double-stranded DNA enclosed in an icosahedral capsid, which is surrounded by a protein layer of tegument proteins. A lipid envelope, containing glycoproteins cover the particle. The picture was created with BioRender.com

A special characteristic of the herpesvirus family is the establishment of life-long latency (Lan and Luo, 2017). In the case of HCMV, the prevalence of latent infection ranges from 40 and 70% in industrialized countries, whereas nearly 100% of the population is seropositive in developing countries (Lamberson and Dock, 1992). People carrying HCMV may pass the virus both horizontally and vertically (Gugliesi et al., 2020). Horizontal transmission occurs through body fluids such as breast milk, urine, saliva, genital secretions, tears, blood transfusion or organ transplantations (Gugliesi et al., 2020; Handsfield et al., 1985; van den Berg et al., 1990). The virus can be vertically transmitted via the placenta in pregnancy or during birth (Diosi et al., 1967; Stagno et al., 1984).

The primary infection is usually asymptomatic or is associated with mild symptoms like fever or enlarged lymph nodes (Horwitz et al., 1986; Rafailidis et al., 2008). While the reactivation in immunocompetent individuals, in most cases, again remains asymptomatic, HCMV may cause severe and even life-threatening complications in immunocompromised individuals such as transplant recipients or AIDS patients. Known disease conditions are pneumonia, colitis, hepatitis, or esophagitis in these patients (de Jong et al., 1998; Drew, 1992; Griffiths and Reeves, 2021; Griffiths et al., 2000; Steininger, 2007).

Congenital HCMV infection, in addition, is the most common viral infection in utero, associated with serious disease conditions in the fetus and in neonates (Canfield et al., 2023; Razonable et al., 2020). At birth, most infected newborns are healthy, however 10-15% may display clinical signs like rash, microcephaly, jaundice, hepatosplenomegaly or retinitis (Fowler and Boppana, 2018; Kenneson and Cannon, 2007). Some of the affected neonates also suffer from long-term health issues such as hearing loss, motor and mental retardation, or vision impairment (Fowler and Boppana, 2018; Goderis et al., 2014; Nance et al., 2006). In severe cases, congenital HCMV infection may result in pregnancy loss (Boppana et al., 1992; Kenneson and Cannon, 2007). Currently, no approved therapy or vaccine for prevention of congenital HCMV infection is available (Liu, 2014; Lomonte, 2017; Schottstedt et al., 2010).

1.2 Autophagy

Autophagy is a cellular degradation and recycling process to maintain a homeostatic state in the cell (Chun and Kim, 2018; Parzych and Klionsky, 2014). Basically, autophagy occurs constitutively at a low level, but can be further stimulated under stress conditions such as nutrient deficiency. Upon autophagy initiation, cytoplasmic components are sequestrated into a cup-shaped double-membrane called the phagophore, the precursor of the future autophagosome (Kuma and Mizushima, 2010; Parzych and Klionsky, 2014; Rabinowitz and White, 2010) (Figure 2). The phagophore elongates by recruiting members of the microtubule-associated protein 1 light chain 3 (LC3) family to the membrane. In addition, proteins of the gamma-aminobutyric acid receptor-associated protein (GABARAP) family are required for the maturation of the autophagosome, thereby enclosing its cargo (Schaaf et al., 2016; Weidberg et al., 2010). For degradation, the autophagosome fuses with the hydrolytic lysosome. At this stage, the building blocks of the cargo, such as amino acids, nucleic acids, and lipids are recycled (Kuma and Mizushima, 2010; Parzych and Klionsky, 2014; Rabinowitz and White, 2010).

Unlike this "bulk autophagy", which is considered to randomly sequester cargo, autophagy can be highly selective (Vargas et al., 2023). In this process, autophagy receptors selectively bind either directly to the cargo or to biochemical tags conjugated to cargo, for the most part ubiquitin (Chu et al., 2013; Gubas and Dikic, 2022; Rogov et al., 2014; Sun et al., 2018). The recognition occurs via a dedicated receptor region, which is often the ubiquitin-binding domain (UBD) (Khaminets et al., 2016; Kirkin and Rogov, 2019). Subsequently, autophagy receptors recruit the cargo to the phagophore, where they mainly interact with LC3 proteins, located in the autophagosomal membrane via their LC3-interacting region (LIR) (Birgisdottir et al., 2013). Finally, the cargo is degraded in the autolysosome. Depending on the cargo, several types of selective autophagy are defined such as mitophagy, i.e. the degradation of mitochondria. Aggrephagy involves sequestration of protein aggregates by autophagy (Ding and Yin, 2012; Lamark and Johansen, 2012). In recent years, selective autophagy has gained considerable attention in relation to the degradation of pathogens (Jordan and Randall, 2012). Xenophagy is a form of selective autophagy that targets intracellular microorganisms for degradation. When referring specifically to viruses, this process is also called virophagy. Here, similarly to other cargo, viral components are detected for degradation (Dong and Levine, 2013; Paul and Münz, 2016; Richetta and Faure, 2013; Schlegel et al., 1996). Therefore, autophagy has been recognized as an intrinsic defense mechanism of the cell against viruses and other pathogens (Jordan and Randall, 2012). Furthermore, autophagy also foster pathogen recognition and inflammatory cytokine responses, controlling cell survival and regulating inflammation (Choi et al., 2018). Moreover, autophagy plays a promotive role in adaptive immunity by providing antigens for major histocompatibility complex (MHC) class I and II molecules (Choi et al., 2018; Paludan et al., 2005; Paul and Münz, 2016; Verweij et al., 2015).

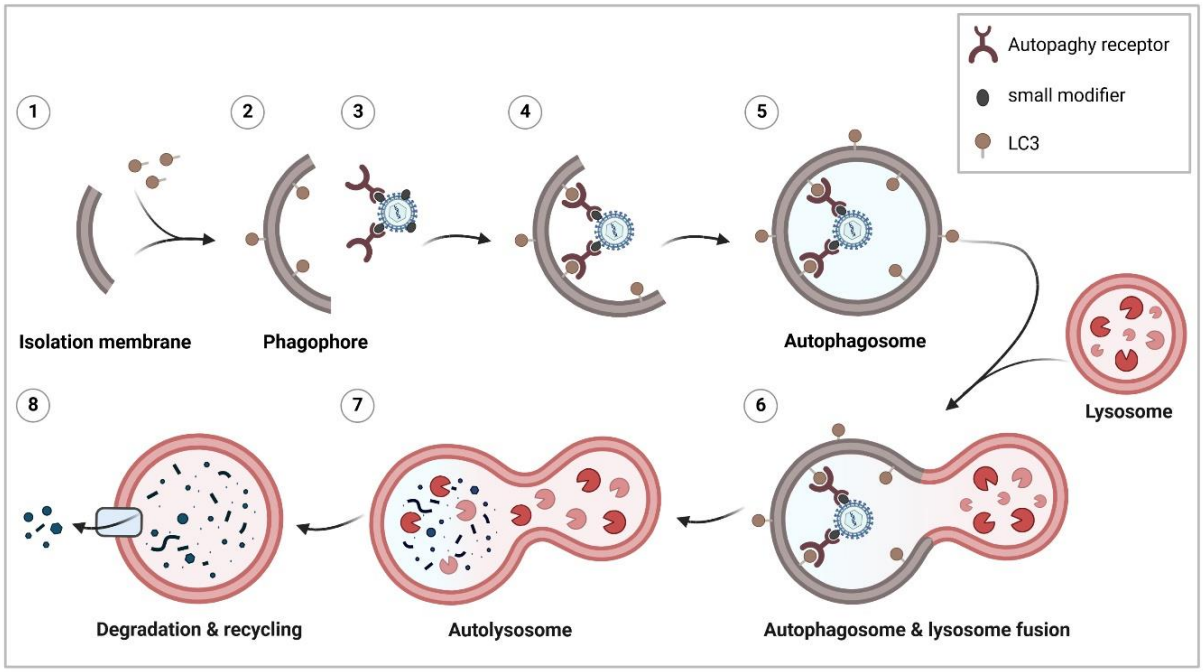

Figure 2. Schematic overview of virophagy, a selective form of autophagy, targeting viral cargo for degradation. (1) Viral infection triggers selective autophagy, leading to the nucleation of the phagophore. (2) LC3 molecules are anchored on both sides of the membrane to expand the phagophore. (3) Autophagy receptors recognize the viral cargo, which can be tagged with small modifiers, and transport it towards developing autophagosomes. (4) Autophagy receptors bind via their LIR domain to LC3 and linking the viral cargo with the autophagic machinery. (5) The expanding membrane closes around its cargo to form an autophagosome. (6) The autophagosomal membrane fuses with the lysosome. (7) The lysosomal content is released into the formed autolysosome to degrade the sequestered cargo. (8) Degraded viral material is released and can serve to trigger innate and adaptive immune responses. The schematic autophagy process was created with BioRender.com.

However, several herpesviruses have established mechanisms to antagonize autophagy, interfering with the autophagic process by interacting directly with autophagy receptors and other components of the autophagy machinery (Choi et al., 2018; Dong and Levine, 2013; Jordan and Randall, 2012). For example, HSV-1 encoded neurovirulence factor infected cell protein 34.5 (ICP34.5) targets Beclin-1, a positive regulator of autophagy, to inhibit autophagosome formation (Orvedahl et al., 2007). A different strategy is exhibited by KSHV, which has a viral homolog of B-cell lymphoma 2 (Bcl-2), ORF16, to mimic the cellular counterpart and attenuate autophagy by interference with Beclin-1 (Pattingre et al., 2005). Some viruses even use autophagy for their benefit to support viral replication, like VZV and EBV utilize autophagic membranes for their secondary envelopment and viral egress (Buckingham et al., 2014; Münz, 2017; Nowag et al., 2014). Therefore, both antiviral and proviral effects of autophagy can be identified in human viral infections (Jackson, 2015; Levine et al., 2011).

In the case of HCMV and its interplay with autophagy, conflictive data have been published. It is commonly seen that autophagy is induced almost immediately after infection (Chaumorcel et al., 2012), Zimmermann, Krämer et al., 2021). Chaumorcel and colleagues described that the virus developed mechanisms to evade autophagosomal degradation. They identified that the HCMV protein TRS1 interacts with Beclin-1 to inhibit autophagy (Chaumorcel et al., 2012). However, other studies did not describe a limiting effect of HCMV on autophagy but showed an increase of autophagy after infection (Belzile et al., 2016), Zimmermann, Krämer et al., 2021). In general, induction of autophagy was found to hamper viral replication, reflecting its antiviral impact (Belzile et al., 2016; Clark et al., 2018). Also, controversial data regarding its pro- or antiviral function in HCMV infection have been described. Some groups detected a restricting effect of autophagy on HCMV infection (Belzile et al., 2016; Clark et al., 2018), Zimmermann, Krämer et al., 2021). Others found a proviral role of autophagy, describing that the silencing of several autophagy proteins leads to increased viral production (König et al., 2021; Mouna et al., 2016; Taisne et al., 2019).

1.3 Autophagy receptors

Autophagy receptors are known to be associated in different types of selective autophagy and form a linkage between the cargo and the phagophore. All autophagy receptors are able to selectively bind their cargo and to promote the recruitment of the cargo to the phagophore, mainly by interacting with the anchored LC3 proteins (Galluzzi et al., 2017; Stolz et al., 2014). Several mammalian autophagy receptors exist and some of them have been shown to play a role in virophagy, such as sequestosome-1 (SQSTM1/p62), optineurin, calcium binding and coiled-coil domain-containing protein 2/nuclear dot 10 protein 52 (CALCOCO2/NDP52) and Tax1-binding protein 1 (TAX1BP1) (Ames et al., 2021; Kirkin and Rogov, 2019; Mohamud et al., 2019; Thinwa et al., 2022). In addition, some members of the tripartite motif (TRIM) family have been identified as autophagy receptors, of which the tripartite motif containing protein 5 (TRIM5α) also interacts with viral proteins (Mandell et al., 2014b). In this work, the focus was on known autophagy receptors SQSTM1/p62 and optineurin, and potential autophagy receptors of the TRIM family, which are briefly reviewed below.

1.3.1 SQSTM1/p62

The best-described autophagy receptor is SQSTM1/p62, expressed by its gene *SQSTM1*. It was the first characterized selective receptor in mammalian cells (Bjørkøy et al., 2005; Pankiv et al., 2007). SQSTM1/p62 contains both LIR and UBD domains, the latter one functions as a "ubiquitin sensor" and allows the delivery of the ubiquitinated cargo for autophagolysosomal degradation (Johansen and Lamark, 2011; Kim et al., 2008). However, the receptor is also able to bind native cargo (Lamark et al., 2017; Sagnier et al., 2015). In addition, the receptor is composed of further domains, including the Phox-BEM1 domain (PB1), through which SQSTM1/p62 can oligomerize, stabilizing its interaction with LC3B, a member of the LC3 family, and ubiquitin and allowing it to better fulfill its role as a linker between cargo and the autophagic machinery (Berkamp et al., 2021; Lin, 2013; Liu et al., 2016; Wurzer et al., 2015). SQSTM1/p62 plays a role in various viral infections. In coxsackievirus B3 (CVB3) infection, for example, SQSTM1/p62 targets a ubiquitinated capsid component for degradation (Mohamud et al., 2019; Shi et al., 2014). In human immunodeficiency virus (HIV) infection SQSTM1/p62 interacts ubiquitin-independently with the viral factor Tat, leading to its selective degradation (Sagnier et al., 2015). We have found, that SQSTM1/p62 co-immunoprecipitated with various HCMV proteins, although it is not established, whether this interaction leads to autophagosomal degradation (Zimmermann, Krämer et al., 2021). Besides its function as a cargo receptor for autophagy, SQSTM1/p62 is involved in several important pro- and anti-inflammatory pathways, including the activation of the transcription factor nuclear factor 'kappa-light-chain-enhancer' of activated B-cells (NF-κB) in distinct contexts (Hennig et al., 2021; Moscat et al., 2016; Ning and Wang, 2019). SQSTM1/p62 can also transport ubiquitylated substrates to

the proteasome, such as the cellular protein tau, which is involved in Alzheimer's disease (Babu et al., 2005; Seibenhener et al., 2004). Another feature of SQSTM1/p62 is the ability to shuttle between the nucleus and cytoplasm using its nuclear localization signals (NLS) and a nuclear export signal (NES) (Lobb et al., 2021; Pankiv et al., 2010). Thus, SQSTM1/p62 is a multifunctional protein and a key player in different forms of autophagy, such as virophagy.

1.3.2 Optineurin

Optineurin is also involved in pathogen degradation and is encoded by the *OPTN* gene (Rezaie et al., 2002; Ying and Yue, 2012, 2016). Due to its respective LIR and UBD domains, optineurin can recognize and recruit ubiquitinated cargo to the nascent autophagosome (Ying and Yue, 2012). Similar to SQSTM1/p62, optineurin can regulate autophagic clearance in a ubiquitin-independent manner, by recognizing protein aggregates (Korac et al., 2013). In virophagy, for example, it can limit HSV-1 infection in the brain and cornea by selectively targeting to two HSV-1 proteins, which are the tegument protein VP16 and the glycoprotein gB (Ames et al., 2021). Interestingly, optineurin has been less frequently identified as an autophagy receptor in viral infections than SQSTM1/p62. In addition to its role as an autophagy receptor, optineurin was found to regulate autophagy induction and autophagosome formation (Bansal et al., 2018; Ying and Yue, 2016). Furthermore, it functions and participates in cellular processes such as vesicle trafficking, maintenance of the Golgi apparatus, the NF-ϰB pathway and cell division control (Kachaner et al., 2012; Ying and Yue, 2012, 2016). Optineurin thus plays several roles and is important as an autophagy receptor for the degradation of pathogens.

1.3.3 TRIM proteins as (potential) autophagy receptors and regulators of autophagy

The members of the TRIM protein family are known for their antiviral activities by either directly limiting viral replication or modulating immune sensing and signaling (Eldin et al., 2009; Gack et al., 2009; Giraldo et al., 2020; Koepke et al., 2021; Schneider et al., 2014; van Gent et al., 2018). TRIM proteins are defined by a RING domain, B-box domains, and an associated coiled-coil domain(s) (Borden, 1998; Reddy et al., 1992; Reymond et al., 2001). All TRIM proteins possess ubiquitin E3 ligase activity and are therefore able to determine the fate of the target protein by attaching ubiquitin or ubiquitin like proteins (Chu and Yang, 2011; Ikeda and Inoue, 2012; Wu et al., 2020b). For most TRIM proteins, this modification is required for their ability to restrict viral infections (Ozato et al., 2008).

A recent study showed that several members of the TRIM family, for example TRIM5α, 6, 21, 23, 26, 28, 32 and 50, are also linked to autophagy (Mandell et al., 2014a). Moreover, it has been demonstrated that TRIMs may represent a new class of autophagy receptors (Kimura et al., 2017a; Mandell et al., 2014a; Mandell et al., 2014b; Overå et al., 2019). TRIM5α has been described as an autophagy receptor that recognizes the capsid protein of HIV-1

(p24). The interaction results in early virus uncoating, followed by restricting HIV-1 infection. Accordingly, the binding of the p24 and TRIM5α induces the autophagic flux and the capsid protein gets degraded in the autolysosome (Mandell et al., 2014b). In addition, other TRIMs have been identified as autophagy receptors. For example, TRIM21 targets a component of the type I interferon (IFN-I) response system, while TRIM16 acts as an autophagy receptor in secretory autophagy (Kimura et al., 2015; Kimura et al., 2017b). It is likely that other TRIM proteins are able to function as autophagy receptors. Besides acting as an autophagy receptor directly, TRIMs can regulate the activity of other autophagy receptors and thereby indirectly function in cargo recognition. This is for instance the case for TRIM32. This member of the TRIM family mono-ubiquitinates SQSTM1/p62 to promote its cargo binding properties (Overå et al., 2019). Upon virus infection, TRIM23 recruits and activates TANK-binding kinase 1 (TBK1), which leads to TBK1-mediated phosphorylation of SQSTM1/p62, thereby regulating viral cargo recognition and degradation (Sparrer et al., 2017).

TRIMs are also associated in regulating the autophagic process. They can directly impact autophagy at different steps in the process, including upstream signaling pathways, autophagosome formation and transcriptional regulation of autophagy genes (Mandell et al., 2014a). Here, both positive and negative regulation of the autophagy machinery has been described (Di Rienzo et al., 2020; Koepke et al., 2021). TRIM50 for example induces autophagy through non-degradative ubiquitination of Beclin-1, whereas TRIM37 inhibits bulk autophagy induction (Fusco et al., 2018; Wang et al., 2018).

However, only few TRIM proteins that are involved in virus-induced autophagy are described so far (Sparrer et al., 2017). In addition, the precise mechanism of their action in this context is described for only very few members, like TRIM23 or TRIM5α (Mandell et al., 2014b; Sparrer et al., 2017). Given their multifaceted role in autophagy, TRIMs may also turn out to have important functions in virus control.

1.4 Phosphorylation of autophagy receptors

Post-translational modification events regulate autophagy receptors in regard to their function in selective autophagy, in fostering the binding towards its cargo or their proteasomal degradation. Several post-translational modifications play an important role in these processes such as phosphorylation, ubiquitination and acetylation (Gubas and Dikic, 2022).

Phosphorylation is one major regulator of autophagy receptors determining the selectivity towards their cargo and their interaction with the autophagic machinery (Farré et al., 2013; Gubas and Dikic, 2022; Rogov et al., 2017). In mammalian cells, SQSTM1/p62 is phosphorylated at Ser403 by various kinases, which promotes the binding towards ubiquitinated cargo and, subsequently, its degradation (Matsumoto et al., 2011; Pilli et al., 2012). Furthermore, during proteotoxic stress, phosphorylation of SQSTM1/p62 at Ser407 enables its formation from a dimer to a monomer, thereby facilitating its binding towards ubiquitin (Lim et al., 2015). However, there is also the reverse case, in which phosphorylation leads to the prevention of the binding to members of LC3 family and thus preventing initiation of mitophagy, as can be seen in the example of the autophagy receptor FUN14 domain containing 1 (FUNDC1) at Tyr18 (Kuang et al., 2016).

In the restriction of pathogens, in general, receptor phosphorylation has been shown to promote their degradation. For example, optineurin is phosphorylated by TBK1 at Ser177. This facilitates its interaction with LC3, thereby limiting *Salmonella* growth (Wild et al., 2011). Thus, several viruses have developed strategies to block, activate or modify autophagy receptors to evade autophagosomal degradation or to use them for their own benefit (Viret et al., 2021; Ylä-Anttila, 2021). Phosphorylation thereby is one regulatory mechanism that might be manipulated during infection. HSV-1 for example uses the viral ICP34.5 protein to prevent the phosphorylation of SQSTM1/p62 and optineurin by TBK1, thereby impairing the affinity of the receptors towards their viral cargo (Richter et al., 2016; Verpooten et al., 2009). Besides phosphorylation other post-translational modifications, proteasomal degradation and proteolytic cleavage are used by viruses to manipulate autophagy receptors and the autophagic process. Thus, autophagy receptors can be instrumentalized by viruses on various levels to control autophagy (Viret et al., 2021; Ylä-Anttila, 2021).

2 Materials and Methods

2.1 Materials

2.1.1 Chemicals and reagents

Name	Order number	Supplier
0.5 M Ethylenediaminetetra-acetic acid (EDTA)	46034CI	Thermo Fisher Scientific (Fisher Scientific)
1 M 4-(2-hydroxyethyl)-1-piperazineethanesulfonic acid (HEPES)	15630080	Thermo Fisher Scientific
1.4-Dithiothreitol (DTT)	6908.2	Carl Roth GmbH + Co. KG
10% NP-40 Alternative	492018	Merck KGaA (Calbiochem®)
2-deoxy-galactose (DOG)	D4407-5G-A	Merck KGaA (Sigma-Aldrich)
3-Amino-9-ethylcarbazole (AEC)-tablets	A6926	Merck KGaA (Sigma-Aldrich)
6× DNA gel loading dye	R0611	Thermo Fisher Scientific
Agar-agar	2266.1	Carl Roth GmbH + Co. KG
Agarose	35-1020	Peqlab Biotechnology GmbH
Albumin fraction V (from bovine serum) (BSA)	1.12018	Merck KGaA
Bacto agar	214010	Becton, Dickinson and Company
basic fibroblast growth factor (bFGF)	13256-029	Thermo Fisher Scientific (Invitrogen)
Boric acid	6943.1	Carl Roth GmbH + Co. KG
Bromophenol blue sodium salt	1.11746.0005	Merck KGaA
Complete protease inhibitor cocktail tablets in easypacks, complete mini	04693159001	Roche Holding AG
CutSmart buffer	B7204	New England Biolabs
D-Biotin	3822.1	Carl Roth GmbH + Co. KG

Name	Order number	Supplier
Deoxynucleotide Triphosphates (dNTPs)	733-1855	VWR International GmbH
D-Glucose	X997.2	Carl Roth GmbH + Co. KG
Dimethyl sulfoxide (DMSO) ≥ 99,8%	4720.2	Carl Roth GmbH + Co. KG
di-Sodium hydrogen phosphate dihydrate $Na_2HPO_4 \times 2\ H_2O$	4984.1	Carl Roth GmbH + Co. KG
di-sodium tartrate dihydrate $Na_2C_4H_4O_6$	A2662	AppliChem GmbH
Dulbecco's Phosphate Buffered Saline (DPBS)	D8537	Merck KGaA (Sigma-Aldrich)
Ethanol (EtOH) 99.6%	P076	Carl Roth GmbH + Co. KG
Fetal calf serum (FCS)	F7524 Batch number: BCBW6329	Merck KGaA (Sigma-Aldrich)
Galactose	4987.1	Carl Roth GmbH + Co. KG
GeneRuler Ladder mix	11873963	Thermo Fisher Scientific
Glycerin (86%)	7533.3	Carl Roth GmbH + Co. KG
HD-Green plus safe DNA dye	ISII-HDGreen Plus	Intas Science Imaging
Hydrogen peroxide H_2O_2 (30%)	9683.1	Carl Roth GmbH + Co. KG
Isopropanol	07001123B	Aug. Hedinger GmbH & Co. KG
L-Glutamine	G7513	Merck KGaA (Sigma-Aldrich)
Lipofectamine 2000 Transfection Reagent	11668019	Life Technologies
L-Leucine	L-8000	Merck KGaA (Sigma-Aldrich)
MacConkey-Agar	X922.1	Carl Roth GmbH + Co. KG
Magnesium sulfate $MgSO_4 \times 7\ H_2O$	T888.2	Carl Roth GmbH + Co. KG

Name	Order number	Supplier
Manganese(II) chloride tetrahydrate $MnCl_2 \times 4\ H_2O$	105927	Merck KGaA (Supelco)
Methanol	20874307	VWR International GmbH
Milk powder	T145.2	Carl Roth GmbH + Co. KG
Minimum Essential Medium (MEM) without Glutamine	21090-022	Thermo Fisher Scientific (Gibco)
N,N-Dimethylformamide (DMF)	D4254	Merck KGaA (Sigma-Aldrich)
Na-Tatrat powder	T110.1	Carl Roth GmbH + Co. KG
OptiMEM	31985070	Thermo Fisher Scientific
PageRuler™ Prestained Protein Ladder	11812124	Thermo Fisher Scientific
PhosSTOP phosphatase inhibitor cocktail tablets	4906837001	Roche Holding AG
Polybrene	sc134220	Santa Cruz Biotechnology
Potassium dihydrogen phosphate KH_2PO_4	JB4921-04	Avantor Performance Materials
RNAiMAX	13778150	Thermo Fisher Scientific
SDS Running Buffer Novex®, Bolt™ MES (SDS Running Buffer)	B0002	Thermo Fisher Scientific
Sodium chloride NaCl	3957	Carl Roth GmbH + Co. KG
Sodium dodecyl sulphate (SDS)	4360.1	Carl Roth GmbH + Co. KG
Sodium phosphate monobasic monohydrate $NaH_2PO_4 \times H_2O$	T878.1	Carl Roth GmbH + Co. KG
Transfer Buffer Novex®, Bolt™ (Transfer Buffer)	BT00061	Thermo Fisher Scientific
Trifluoroacetic acid (TFA)	74564	Merck KGaA (Sigma-Aldrich)
Tris-hydroxymethyl-amino methane (Tris)	5429.2	Carl Roth GmbH + Co. KG
Triton-X-100	3051.3	Carl Roth GmbH + Co. KG
Trypan Blue Solution (0.4%)	T8154	Merck KGaA
Trypsin	27250-018	Thermo Fisher Scientific

Name	Order number	Supplier
Trypsin-EDTA	1540054	Thermo Fisher Scientific
Tryptone Soya broth	CM0129	OXOID
Tween® 20	8221840500	Merck KGaA
Urea > 99.7%	7638.2	Carl Roth GmbH + Co. KG
Yeast extract Servabacter powder	24540.02	SERVA Electrophoresis GmbH
β-Mercaptoethanol	4227.1	Carl Roth GmbH + Co. KG

2.1.2 Solutions and buffers

Reagent/Solution	Composition
0.1% Trypan blue solution	0.1% trypan blue solution (v/v) in 1× DPBS, stored at room temperature.
1× TBE buffer	54 g Tris, 27.5 g boric acid and 20 mL of 0.5 M EDTA were dissolved in 1 L dH_2O. This solution is diluted 1:10 in dH_2O and stored at room temperature.
1× Trypsin/ EDTA	0.5 g/L trypsin; 0,2 g/L EDTA in 1× DPBS (10×). This buffer is diluted 1:10 in dH_2O and stored at room temperature.
15% di-sodium tartrate-glycerol	80.9 g di-sodium tartrate dehydrate, diluted in 150 mL 86% glycerol and 275 mL 0.04 M sodiumphosphate buffer pH= 7.4, autoclaved and stored at room temperature.
2× SDS sample buffer	125 mM Tris; 2% (v/v) β-Mercaptoethanol; 10% (v/v) glycerol; 2% (w/v) SDS; 1 mM EDTA, pH 8,0 and 0.005% (v/v) bromphenolblue were mixed in 50 mL ddH_2O; stored at -20°C.
35% di-sodium tartrate	207.5 g di-sodium tartrate dihydrate, diluted in 325 mL 0.04 M sodiumphosphate buffer; pH= 7.4, at 65°C, autoclaved and stored at room temperature.
Acetate buffer	13.6 g/L sodium-acetate × 3 H_2O and 2.88 mL/L glacial acetic acid were mixed in dH_2O. pH= 4.9
AEC-staining solution	AEC-stock solution 1:20, diluted in acetate buffer and 1:1000 in H_2O_2 (30%)
AEC-stock solution	60 mg of AEC was dissolved in 15 mL DMF, 4 mg/mL. 1 mL aliquots were stored at -20°C.
bFGF	Stock concentration 0,1 mg/mL (w/v) in 10 mM; pH 7.6 Tris-HCl + 0,1% BSA. bFGF solution was filtered through a Spin-X centrifuge tube (0.22 µm) by centrifugation at 14000 rpm for 1 minute. 5 µL aliquots were prepared and stored at -20°C.
Blocking buffer	5% (w/v) BSA or milk powder in TBS-T

Reagent/Solution	**Composition**
FACS-buffer	1× DPBS with 1% FCS + 2 mM EDTA
IVKA buffer	20 mM Tris/Cl (pH 7.5), 0.5 mM $MnCl_2$ and 0.5 mM DTT in dH_2O.
Lysis buffer	0.5 M NaCl, 0.05 M Tris-HCl (pH = 8.5), 0.5% NP-40 alternative, 1 mM DTT, 1 complete protease inhibitor cocktail tablet/10 mL and 1 PhosSTOP phosphatase inhibitor cocktail tablet/10 mL in ddH_2O.
Lysis buffer + urea	Lysis buffer supplemented with 8 M Urea > 99.7%
TBS-T	0.2% (v/v) Tween-20 in TBS, stored at room temperature.
Wash buffer	0.5 M NaCl, 0.05 Tris-HCl (pH = 8.5), 1 tablet/10 mL complete protease inhibitor cocktail tablet and 1 tablet/10 mL PhosSTOP phosphatase inhibitor cocktail tablet in ddH_2O.

2.1.3 Media

2.1.3.1 Bacterial growth media

Designation	Composition
1× M9 medium	6 g Na_2HPO_4, 3 g KH_2PO_4, 1g NH_4Cl and 0.5 g NaCl were dissolved in 1 L dH_2O, sterile filtrated and stored at 4°C.
5× M63 minimal medium	10 g $(NH_4)_2SO_4$, 68 g KH_2PO_4 and 2 mg $FeSO_4$× 7 H_2O were dissolved in 1 L dH_2O and adjusted to pH 7 with 2 M KOH. Subsequently, the solution was sterile filtrated and stored at 4°C.
LB agar	6 g agar were dissolved in 400 mL LB medium and autoclaved, optionally and antibiotic was added to the agar cooled to 65°C.
Lysogeny broth (LB) medium	10 g tryptone, 5 g yeast extract, and 5 g NaCl were dissolved in 1 L dH_2O and adjusted to pH = 7.2 using NaOH followed by autoclaving; optionally, antibiotic was added to the agar cooled to 65°C.
M63 minimal agar plate	8 g Bacto agar were dissolved in 400 mL dH_2O (20 g/L) and autoclaved. Subsequently, 100 mL 5× M63 minimal medium, 0.5 mL 1 M $MgSO_4$×7 H_2O, 2 mg/mL d-Biotin, 10 mg/mL L-Leucine and 15 µg/mL chloramphenicol were added to the agar cooled to 65°C.
	For galK positive selection + 0.2% d-galactose
	For galK negative selection + 0.2% DOG + 0.2% glycerol
MacConkey plates/ galK indicator plates	25 g MacConkey agar were dissolved in 400 mL dH_2O (50 g/L) and autoclaved. 0.2% d-galactose and 15 µg/mL chloramphenicol were added to the agar cooled to 65°C.

2.1.3.2 Cell culture media

Medium for cells	Composition
HEK293T (Cell culture)	Dulbecco's Modified Eagle Medium (DMEM), supplemented with different volumes of FCS (5, 10 or 20%), 2 mM L-Glutamine, and 50 mg/l gentamycin.
HEK293T (Lentiviral harvest medium)	DMEM, supplemented with 20% FCS, 50 mg/L gentamycin, and 10 mM HEPES.
HFF (Cell culture)	Minimal Essential Medium Eagle (MEM), supplemented with 10% FCS, 2 mM L-Glutamine, 0.5 ng/mL bFGF and 50 mg/L gentamycin.

2.1.4 Commercial kits

Designation	Application	Order number	Supplier
High Pure Viral Nucleic Acid Kit	Isolation of viral DNA from cells and cell culture media	11858874001	Roche Holding AG
MaxiPrep High Purity Plasmid Kit	Plasmid-Preparation	11452-026	BioCat GmbH
NucleoBond® PC 500 Kit	BAC-Maxi-Preparation	740574.25	Macherey-Nagel GmbH & Co. KG
Pierce BCA Protein Assay Kit	Measurement of protein concentrations	23225	Thermo Fisher Scientific (Life Technologies GmbH)
QIAGEN GMBH Plasmid Mini Kit	Plasmid-Preparation	12123	QIAGEN GmbH
QIAquick Gel Extraction Kit DNA	Elution of DNA fragments from agarose gels	28704	QIAGEN GmbH
QIAquick PCR Purification Kit	Cleanup of DNA	28104	QIAGEN GmbH
SuperFect Transfection Reagent (3 mg/mL)	Virus reconstitution from BACmid-constructs in human cells	301305	QIAGEN GmbH

2.1.5 Antibiotics

Designation	Final concentration	Order number	Company
Ampicillin	100 µg/mL	K029.2	Carl Roth GmbH + Co. KG
Chloramphenicol	15 µg/mL	3886.1	Carl Roth GmbH + Co. KG
G148 Geneticin	500 µg/mL	10131-027	Thermo Fisher Scientific (Gibco)
Gentamycin	50 µg/mL	15750-037	Thermo Fisher Scientific (Gibco)

2.1.6 Inhibitors

Designation	Final concentration	Order number	Company
3MB-PP1	40 µM	529582-5MG	Merck KGaA (Calbiochem®)
Bafilomycin A1	200 µM	sc-201550A	Santa Cruz Biotechnology
MG132	10 µM	M7449	Merck KGaA (Sigma-Aldrich)

2.1.7 Enzymes

2.1.7.1 Restriction enzymes

Designation	Order number	Company
*Bam*HI-HF	R3136	New England Biolabs
*Dpn*I	R0176	New England Biolabs
*Eco*RI-HF	R3101	New England Biolabs
FastDigest *Bsm*BI (*Esp*3I)	FD0454	Thermo Fisher Scientific
*Hind*III-HF	R3104	New England Biolabs

2.1.7.2 Polymerases and Ligase

Designation	Order number	Company
Expand™ High Fidelity PCR-System	11732641001	Roche Holding AG
Hot Star Taq DNA Polymerase (5000 Units)	203205	QIAGEN GmbH
mi-Taq Only Polymerase	mi-E8015	Metabion GmbH
T4 DNA Ligase	M0202	New England Biolabs

2.1.8 Antibodies

2.1.8.1 Primary Antibodies

WB: Western Blot; IP: Immunoprecipitation

Antibody	Designation	Animal of origin	Dilution	Supplier
ARF6	mAb-ARF6 (3A-1)	mouse	WB: 1:1000	Santa Cruz Biotechnology sc-7971 donated by Lina Herhaus, Institute of Biochemistry II, Goethe University Frankfurt/Main, Germany
ARL6IP1	pAb-ARL6IP1	rabbit	WB: 1:1000	Merck KGaA (Sigma-Aldrich) HPA045307 donated by Lina Herhaus, Institute of Biochemistry II, Goethe University Frankfurt/Main, Germany
CDK1	mAb-CDK1 (AC5A6)	mouse	WB: 1:500	Thermo Fisher Scientific (Invitrogen) MA5-15629
GABARAP-L2	pAb-GABARAP-L2	rabbit	WB: 1:1000	Medical & Biological Laboratories Co., LTD. PM038 donated by Lina Herhaus, Institute of Biochemistry II, Goethe University Frankfurt/Main, Germany
GAPDH	mAb-GAPDH	mouse	WB: 1:500	Merck KGaA (Sigma-Aldrich) G87955
GFP	mAb-GFP (GF28R)	rabbit	WB: 1:1000	Thermo Fisher Scientific (Invitrogen) MA5-15256

Antibody	Designation	Animal of origin	Dilution	Supplier
GGH	pAb-GGH	rabbit	WB: 1:1000	Proteintech 13264-1-AP
IE1	mAB-IE1 (p63-27) hybridoma culture supernatant	mouse	WB: Un-diluted	donated by William Britt, UAB, Birmingham, U.S.A.
IRGQ	p-Ab-IRGQ	rabbit	WB 1:1000	Merck KGaA (Sigma-Aldrich) HPA043254 donated by Lina Herhaus, Institute of Biochemistry II, Goethe University Frankfurt/Main, Germany
ISG15	mAb-ISG15 (F-9)	mouse	WB: 1:500	Santa Cruz Biotechnology sc-166755
LC3B	mAb-LC3B (D11) XP	rabbit	WB 1:1000	Cell Signaling Technology 3868S
MCP	mAb-MCP (28-4) hybridoma culture supernatant	mouse	WB: Un-diluted	donated by William Britt, UAB, Birmingham, AL, U.S.A.
Mx1	pAb-Mx1	rabbit	WB: 1:1000	Thermo Fisher Scientific (Invitrogen) PA5-22101
Optineurin	pAb-Optineurin	rabbit	WB: 1:1000	Abcam ab23666
POM121	pAb-POM121	rabbit	WB: 1:1000	Thermo Fisher Scientific (Invitrogen) PA5-36498
pp150	mAB-pp150 (XPA36.14) hybridoma culture supernatant	mouse	WB: 1:2	donated by William Britt, UAB, Birmingham, AL, U.S.A.

Antibody	Designation	Animal of origin	Dilution	Supplier
pp28	mAb-pp28 (41-18) hybridoma culture supernatant	mouse	WB: 1:2	donated by William Britt, UAB, Birmingham, AL, U.S.A.
pp65	mAb-pp65 (65-33) hybridoma culture supernatant	mouse	WB: 1:500 IP: 1:50	donated by William Britt, UAB, Birmingham, AL, U.S.A.
p-RB 807/811	mAb-Phospho-Rb (Ser807/811) (D20B12) XP	rabbit	WB 1:1000	Cell Signaling Technology 8516
Rb	mAb-Rb (4H1)	mouse	WB 1:1000	Cell Signaling Technology 9309
SQSTM1/p62	mAb-SQSTM1/p62 [2C11]	mouse	WB: 1:1000	Abcam ab56416
SQSTM1/p62	mAb-SQSTM1/p62 (D5E2)	rabbit	IP: 1:100	Cell Signaling Technology 8025
pSQSTM1/p62 S272	pAb-SQSTM1/p62 (phospho Ser272)	rabbit	WB: 1:500	Biozol GTX133943-100
TAF15	mAb-TAF15	rabbit	WB: 1:1000	Abcam ab134916
Thiophosphate ester	mAb-Thiophosphate ester [51-8]	rabbit	WB: 1:5000	Abcam ab92570
TRAM1	pAb-TRAM1/TRAM	rabbit	WB: 1:1000	Abcam ab96106
TRIM21	mAb-TRIM21 (D1O1D)	rabbit	WB: 1:1000	Cell Signaling Technology 92043
TRIM25	mAb-TRIM25/EFP [EPR7315]	rabbit	WB: 1:2000 IP: 1:50	Abcam ab167154
TRIM26	pAb-TRIM26	rabbit	WB: 1:1000 IP: 1:200	Proteintech 27013-1-AP

Antibody	Designation	Animal of origin	Dilution	Supplier
TRIM28	mAb-TRIM28	mouse	WB: 1:500	Thermo Fisher Scientific (NOVEX by Life Technologies) 730029
TRIM32	mAb-TRIM32 (8H8)	mouse	WB: 1:1000	Santa Cruz Biotechnology sc-135588
UL44	mAb-UL44/p52 (28-21) hybridoma culture supernatant	mouse	WB: 1:2	donated by William Britt, UAB, Birmingham, AL, U.S.A.
UL48a/ small capsid protein (SCP)	mAb-UL48a hybridoma culture supernatant	mouse	WB: 1:2	donated by William Britt, UAB, Birmingham, AL, U.S.A.
UL97	UL97	mouse	IP: 1:200	donated by Manfred Marschall, Clinical and Molecular Virology, University Medical Centre Erlangen, Germany

2.1.8.2 Secondary Antibodies

Antibody	Designation	Animal of origin	Dilution	Supplier
Anti-mouse	HRP-coupled rabbit anti-mouse IgG (H+L)	rabbit	IE1 staining: 1:500	Agilent (Dako) P026002-2
Anti-mouse	IRDye® 800CW Donkey anti-mouse	donkey	WB: 1:15,000	LI-COR Biosciences 926-32212
Anti-rabbit	Donkey anti-rabbit, Alexa Fluor 680	donkey	WB: 1:10,000	Thermo Fisher Scientific A10043

2.1.9 Oligonucleotides

Unless otherwise stated, the oligonucleotides were obtained from Metabion GmbH. The respective forward (fwd) and reverse (rev) primers are listed.

2.1.9.1 Primers for galactokinase (galK) amplification

Sequence in bold represents respective *galK* homologies.

Primer	**Sequence (5'to 3')**	**Application**
UL1-Galk-fwd	AAATTGTTATTGCCAGTCGCACT AATACCGGTTGTAATCATCCTAA TTGG**CCTGTTGACAATTAATCAT CGGCA**	Amplification of the *galK* sequence with respective homologies to *UL1* and *UL6* using the plasmid pGalK
UL6-Galk-rev	CGTTCTTCATCGTCCACGTGGCT TCGCCAGCGTCGCCAAGCCGATT GAGG**TCAGCACTGTCCTGCTCCTT**	
UL97-GalK-fwd	CACCGCGGTCTGCTCACGGCCA CGGGCTGCTGTCTGCTGCACAACG TCAC**CCTGTTGACAATTAATCAT CGGCA**	Amplification of the *galK* sequence with homologies to *UL97* using the plasmid pGalK.
UL97-GalK-rev	ATGCACGCCAGCTTCCACTGGTC GTGATGAAACATGTCTGTGTGGA AACG**TCAGCACTGTCCTGCTCCTT**	

2.1.9.2 Primers for colony PCR

Primer	Sequence (5‘to 3‘)	Application
UL97-as1-fwd	CCAACGACCAGATCATCAC	Respective primer pair used in colony PCR to detect either the insertion of *galK* in pBAD-ΔUL97 or *UL97-as1* in pBAD-UL97-as1.
UL97-as1-rev	GCCAGAATGAGCAGACAG	
GalK-rev	ATCGGGTCCAGTTCATGC	
UL1-fwd	CCGCATTACACCAAACTTCC	Respective primer pair used in colony PCR to detect the insertion of *galK* in pBAD-ΔUL1-6.
UL1-rev	TCTGGAGACGGAGTAAGAAC	
GalK-rev	ATCGGGTCCAGTTCATGC	
SQSTM1-fwd	TCCAGTGACGAGGAATTGAC	Primer pair used in colony PCR to detect the presence of *SQSTM1* sequence in pBAD-SQSTM1-S272wt, -S272A, -S272D, and -S272E, but not the correct insertion in the Δ*UL1-6* gene region.
SQSTM1-rev	CCGCTCCGATGTCATAGTTC	
UL1-SQSTM1-fwd	TGCCAGTCGCACTAATAC	Primer pair used in colony PCR to detect the correct insertion of the respective *SQSTM1*-S272 version into pBAD-SQSTM1-S272wt, -S272A, -S272D, and -S272E, amplifying the DNA-sequence between the remaining sequence of *UL1* and the first nucleotides of *SQSTM1*.
UL1-SQSTM1-rev	CTTGCCCAGAAGGTAGG	
SQSTM1-UL7-fwd	CTCTGGGCATTGAAGTTG	Primer pair used in colony PCR to detect the correct insertion of the respective *SQSTM1*-S272 version into pBAD-SQSTM1-S272wt, -S272A, -S272D, and -S272E, amplifying the DNA-sequence between the last nucleotides of *SQSTM1* and the remaining sequence of *UL7*.
SQSTM1-UL7-rev	GTGCGCTGATGTTTGAAG	

2.1.9.3 Primers for qPCR

Primer pair and sensor to detect the viral gene *UL54* of HCMV by qPCR.

Primer	**Sequence (5‘to 3‘)**	**Supplier**
CMV-fwd	TCATCTACGGGGACACGGAC	Eurofins MWG Operon
CMV-rev	TGCGCACCAGATCCACG	Eurofins MWG Operon
RT-PCR-sensor fused to tetramethylrhodamine (TMR) fluorescent reporter dye)	CCACTTTGCCGATGTAACGT TTCTTGCAT-TMR	TIB Molbiol Synthesis laboratory GmbH

2.1.9.4 Primers for sequencing

Primer	**Sequence (5‘to 3‘)**	**Application**
pLKO-U6-Seq-fwd	TTTGCTGTACTT TCTATAGTG	Control of respective gRNA insertion into pLKO5.U6.sgRNA(BsmBI,stuffer).EFS.SpCas9.P2A.tageGFP
Seq SQSTM1-fwd	TCCAGTGACGA GGAATTGAC	Sequence analysis of each inserted *SQSTM1*-S272 version in the corresponding BACmid (pBAD-SQSTM1-S272wt, -S272A, -S272D or -S272E). The primer binds in the gene of *SQSTM1* to determine the presence and nucleotides coding for the respective modified amino acid at position 272. The analysis does not provide information about the correct insertion into the BACmid. For this purpose, sequence analysis was performed using Seq UL1-SQSTM1_fwd and Seq SQSTM1-UL7_fwd.
Seq SQSTM1-UL7-fwd	CTCTGGGCATT GAAGTTG	Control of the correct insertion position of each SQSTM1-S272 version in the corresponding BACmid (pBAD-SQSTM1-S272wt, -S272A, -S272D, or -S272E). The analysis shows the sequence between *SQSTM1* and the remaining nucleotides of *UL7*.
Seq UL1-SQSTM1-fwd	TGCCAGTCGCA CTAATAC	Control of the correct insertion position of each SQSTM1-S272 version in the corresponding BACmid (pBAD-SQSTM1-S272wt, -S272A, -S272D, or -S272E). The analysis shows the sequence between the remaining nucleotides of *UL1* and *SQSTM1*.
Seq-plKObv-fwd	GGTGTCGTGAG GAATTAG	Control of *GFP-SQSTM1* insertion into in plKO based vector.

2.1.9.5 Oligonucleotides for clustered regularly interspaced short palindromic repeats/Cas9 (CRISPR/Cas9) system

gRNAs targeting the gene of interest coding region	**gRNA name**	**gRNA sequences (5‘to 3‘)**
OPTN exon 1 at nucleotide 113	gRNA OPTN_Fwd	CACCGCCTGGACACGTTTACCCCGG
	gRNA OPTN_Rev	AAACCCGGGGTAAACGTGTCCAGGC
SQSTM1 exon 2 at nucleotide 67	gRNA SQSTM1_Fwd	CACCGAATGGCCATGTCCTACGTGA
	gRNA SQSTM1_Rev	AAACTCACGTAGGACATGGCCATTC
TRIM21 exon 1 at nucleotide 194	gRNA TRIM21_Fwd	CACCGCATGTTGGCTAGCTGTCGAT
	gRNA TRIM21_Rev	AAACATCGACAGCTAGCCAACATGC
TRIM25 exon 1 at nucleotide 442	gRNA TRIM25_Fwd	CACCGCGGCGCAACAGGTCGCGAAC
	gRNA TRIM21_Rev	AAACGTTCGCGACCTGTTGCGCCGC
TRIM26 exon 1 at nucleotide 212	gRNA TRIM26_Fwd	CACCGCATCCGACCCGTGTGGCAAC
	gRNA TRIM26_Rev	AAACGTTGCCACACGGGTCGGATGC
TRIM28 exon 2 at nucleotide 88	gRNA TRIM28_Fwd	CACCGTTCGCATCCTGGGCGTCGG
	gRNA TRIM28_Rev	AAACCCGACGCCCAGGATGCGAAC
TRIM32 CDS complete at nucleotide 1170	gRNA TRIM32_Fwd	CACCGAAGTACTAGTCGCTGACCG
	gRNA TRIM32_Rev	AAACCGGTCAGCGACTAGTACTTC

2.1.10 *Escherichia coli* (*E. coli*) strains

***E. coli* strains**	**Description**
DH5α	This strain was used for transformation with bacterial plasmids.
One Shot™ Stbl3™ Chemically Competent *E. coli* (Stbl3)	Chemically competent bacteria were used for transformation with CRISPR-sgRNA-plasmids. The Stbl3 strain is derived from the HB101 *E. coli* strain. The strain was ordered by Thermo Fisher Scientific (Invitrogen) (10193952).
SW102	The BAC recombineering were done using a modified bacterial strain, SW102. This strain is derived from DY380 and contains the λ prophage recombineering system. The galactose operon has been modified in a way that it is fully functional, except *galK* was deleted (Warming et al., 2005).

2.1.11 Plasmids

Designation	**Description**	**Supplier**
gag-pol psAX2	gag-pol psAX2 is a packing plasmid and used in combination with VSV-G pMD2.G and pLK05.U6.sgRNA (BsmBI,stuffer).EFS.SpCas9.P2A.tageGFP to generate CRISPR/Cas9-mediated knockout cells.	AddGene #12260
pcDNA5/FRT/TO GFP-SQSTM1/p62 abbr: pcGFP-SQSTM1	pcDNA5 FRT/TO GFP-SQSTM1/p62 expresses GFP-SQSTM1/p62.	Lina Herhaus, Institute of Biochemistry II, Goethe University Frankfurt/Main, Germany
pCM1049	Standard cosmid which contains the *UL54* gene of HCMV used for TaqMan® qPCR to determine reference C_T values (cycle threshold).	(Fleckenstein et al., 1982)
pEGFP-N2-UL97	pEGFP-N2-UL97 expresses *UL97* of HCMV and contains the green fluorescent protein *(GFP)* coding sequence.	BioCat GmbH
pEGFP-N2-UL97-as1	pEGFP-N2-UL97-as1 expresses *UL97-as1*, which gene product is an analog-sensitive version of pUL97 (pUL97-as1) of HCMV. Plasmid contains the GFP coding sequence.	BioCat GmbH

Designation	Description	Supplier
pGalK	Encoding the bacterial *galK* gene, required for positive selection in bacteria	(Warming et al., 2005)
pLKO5.U6.sgRNA (BsmBI,stuffer).EFS. SpCas9.P2A.tageGFP	The expression plasmid for gRNA cloning and CRISPR/Cas9-mediated genome editing. The vector includes *GFP* for selection of transduced HFF by flow cytometry.	Dirk Heckl, Martin Luther University, Halle via Melanie Brinkmann, Helmholtz Centre for Infection Research, Braunschweig, Germany
pLKO-based lentiviral vector	pLKO-based lentiviral vector is under control of EF1 alpha promotor. The vector includes an ampicillin resistance cassette for cloning and a geneticin resistance for selection of transduced HFF.	Myriam Scherer, Institute for Virology, University of Ulm, Germany
pLP1	Lentiviral packaging plasmid containing the HIV-1 gag and pol genes, which can be used in combination with pLP2, pVSVg and pLKO-based lentiviral vector.	Myriam Scherer, Institute for Virology, University of Ulm, Germany
pLP2	Lentiviral packaging plasmid containing the HIV-1 rev gene, which can be used in combination with pLP1, pVSVg and pLKO-based lentiviral vector.	Myriam Scherer, Institute for Virology, University of Ulm, Germany
pVSVg	Lentiviral packaging plasmid for expression of the vesicular stomatitis virus G glycoprotein, which can be used in combination with pLP1, pLP2 and pLKO-based lentiviral vector.	Myriam Scherer, Institute for Virology, University of Ulm, Germany
VSV-G pMD2.G	VSV-G pMD2.G is an envelope expressing plasmid and used in combination with gag-pol psAX2 and pLK05.U6.sgRNA(BsmBI,stuffer).EFS.Sp Cas9.P2A.tageGFP to generate CRISPR/Cas9-mediated knockout cells.	AddGene #12259

2.1.12 siRNAs

Designation	Order number	Supplier
CDK1 siRNA (ID: 103821) [1]	AM16708	Thermo Fisher Scientific
CDK1 siRNA (ID: 1440) [2]	AM51331	Thermo Fisher Scientific
GABARAP-L2 siRNA (siGABARAP-L2)		Lina Herhaus, Institute of Biochemistry II, Goethe University Frankfurt/Main, Germany
IRGQ siRNA (siIRGQ)		Lina Herhaus, Institute of Biochemistry II, Goethe University Frankfurt/Main, Germany
Negative control siRNA (siControl) control for siIRGQ and siGABARAP-L2	1027310	QIAGEN GmbH donated by Lina Herhaus, Institute of Biochemistry II, Goethe University Frankfurt/Main, Germany
SignalSilence unconjugated (siControl) control for siCDK1	6568S	Cell Signaling Technology

2.1.13 Bacterial artificial chromosome (BACmid; BAC)

2.1.13.1Externally provided BACmid

BACmid	Description
pBADwt (pAD/Cre)	The HCMV Ad169 genome was cloned into a BAC vector to receive pBADwt (pAD/Cre). The BAC sequence is inserted between the *US28*- and *US29*-gene regions of HCMV and contains a chloramphenicol resistance gene. The BACmid was kindly provided by Thomas Shenk, Princeton University, U.S.A. (Yu et al., 2002).

2.1.13.2 Newly-generated BACmids

BACmids	Description
pHCMV-ΔUL1-6 (pBAD-ΔUL1-6)	pBAD-ΔUL1-6 is based on the parental strain pBADwt. The genes *UL1-UL6* were exchanged by *galK* sequence. The BACmid contains the gene encoding the chloramphenicol acetyltransferase, which confers for chloramphenicol resistance.
pHCMV-SQSTM1-S272A (pBAD-SQSTM1-S272A)	The BACmid pBAD-SQSTM1-S272A is based on pBAD-ΔUL1-6 and the *galK* cassette was replaced by the coding sequence for *SQSTM1* with a substitution of serine (tct) at position 272 to alanine (gca). The BACmid contains the gene encoding the chloramphenicol acetyltransferase. The sequence for *SQSTM1-S272A*, including the MIEP promotor was ordered from Synbio Technologies.

BACmids	**Description**
pHCMV-SQSTM1-S272D (pBAD-SQSTM1-S272D)	The BACmid pBAD-SQSTM1-S272D originates from pBAD-ΔUL1-6 and the *galK* cassette was replaced by the coding sequence for *SQSTM1* with a substitution of serine (tct) at position 272 to aspartate (gac). The BACmid contains the gene encoding the chloramphenicol acetyltransferase. The sequence for *SQSTM1-S272D*, including the MIEP promotor was ordered from Synbio Technologies.
pHCMV-SQSTM1-S272E (pBAD-SQSTM1-S272E)	The BACmid pBAD-SQSTM1-S272E is based on pBAD-ΔUL1-6 and the *galK* sequence was exchanged by the coding sequence for *SQSTM1* with a substitution of serine (tct) at position 272 to glutamate (gag). The BACmid contains the gene encoding the chloramphenicol acetyltransferase. The sequence for *SQSTM1-S272E*, including the MIEP promotor was ordered from Synbio Technologies.
pHCMV-SQSTM1-S272wt (pBAD-SQSTM1-S272wt)	The BACmid pBAD-SQSTM1-S272wt originates from pBAD-ΔUL1-6. The *galK* gene was then replaced by the coding sequence for *SQSTM1* as a control strain. The BACmid contains the gene encoding the chloramphenicol acetyltransferase. The sequence for *SQSTM1-S272wt*, including the MIEP promotor was ordered from Synbio Technologies.
pHCMV-UL97-as1 (pBAD-UL97-as1)	The BACmid pBAD-UL97-as1 is based on pBAD-ΔUL97-galK. The *galK* cassette was replaced by the DNA fragment *UL97-as1*, which encodes the previously deleted nucleotides of *UL97*, but containing a substitution of histidine (cat) of wt *UL97* to a glycine (ggg) on position 411 in the gene. The BACmid contains the gene encoding the chloramphenicol acetyltransferase. The sequence for *UL97-as1* was ordered from Synbio Technologies.
pHCMV-ΔUL97-galK (pBAD-ΔUL97-galK)	Based on the parental strain pBADwt, which has a deletion between nucleotides 1177 and 1286 of *UL97* and instead encodes *galK*. The BACmid contains the gene encoding the chloramphenicol acetyltransferase.

2.1.14 Viruses

HCMV strains	Description
HCMV (BADwt)	HCMV wildtype (wt) strain, encoding the genome of Ad169. After reconstitution of HFF with pAD/cre, the BAC-sequence was removed by recombination (Yu et al., 2002).
HCMV-ΔUL1-6 (BAD-ΔUL1-6)	Derivative of HCMV strain Ad169. The gene region of *UL1-6* was deleted by inserting the *galK* fragment.
HCMV-SQSTM1-S272A (BAD-SQSTM1-S272A)	The mutant, based on HCMV strain BADwt, expressed *SQSTM1-S272A,* resulting in the gene product SQSTM1/p62-S272A, which possessed an amino acid substitution from serine to alanine at position 272. This mutant is no longer phosphorylated at this specific residue.
HCMV-SQSTM1-S272D (BAD-SQSTM1-S272D)	The mutant is based on HCMV strain BADwt. It encodes SQSTM1/p62 with amino acid substitution from serine to aspartate at position 272 to mimic phosphorylation at this specific residue.
HCMV-SQSTM1-S272E (BAD-SQSTM1-S272E)	The mutant is based on HCMV strain BADwt. It encodes SQSTM1/p62 with amino acid substitution from serine to glutamate at position 272 to mimic phosphorylation at this specific residue.
HCMV-SQSTM1-S272wt (BAD-SQSTM1-S272wt)	HCMV strain, based on the HCMV strain BADwt. It expresses the wt sequence of *SQSTM1*, which gene product contains a serine at position 272.
HCMV-UL97-as1 (BAD-UL97-as1)	HCMV mutant, based on HCMV strain BADwt that expresses an analogue sensitive version of the kinase pUL97 (pUL97-as1) that can be inhibited by 3MB-PP1, but still can bind normal ATP.
TB40/E-BAC7 (TB40/E)	Clinical strain of HCMV, which contains a deletion in the *US2-US6* genome region (Sampaio et al., 2017).

2.1.15 Cells

Designation	Description
HEK293T	Human Embryonic Kidney cell line, expressing the gene for the SV40 T-antigen. HEK293T are not permissive for HCMV infection.
HFF	Human foreskin fibroblasts, permissive for productive infection of HCMV
HFF control (control)	HFF control cells, which were lentiviral transduced with an empty pLKO5.U6.sgRNA(BsmBI,stuffer).EFS.SpCas9.P2A.tageGFP
HFF ko-OPTN (ko-OPTN)	Lentiviral transduced HFF, carrying a knockout of *OPTN*

Designation	Description
HFF ko-SQSTM1 (ko-SQSTM1)	Lentiviral transduced HFF, carrying a knockout of *SQSTM1*
HFF ko-TRIM21 (ko-TRIM21)	Lentiviral transduced HFF, carrying a knockout of *TRIM21*
HFF ko-TRIM25 (ko-TRIM25)	Lentiviral transduced HFF, carrying a knockout of *TRIM25*
HFF ko-TRIM26 (ko-TRIM26)	Lentiviral transduced HFF, carrying a knockout of *TRIM26*
HFF ko-TRIM28 (ko-TRIM28)	Lentiviral transduced HFF, carrying a knockout of *TRIM28*
HFF ko-TRIM32 (ko-TRIM32)	Lentiviral transduced HFF, carrying a knockout of *TRIM32*
HFF-GFP-SQSTM1	HFF, lentiviral transduced HFF, permanently expressing *GFP-SQSTM1*.

2.1.16 Software and online tools

Software	Company/ Website
7000 System Sequence Detection Software RQ Study Application V.1.2.3	Applied Biosystems
BioDocAnalyze 2.2 2.67.5.0	Biometra
Clone Manager 7, version 7.04	Sci Ed Software LLC
CorelDraw Graphics Suite X7	Corel Corporation
crisporWebsite, version 5.01	http://crispor.tefor.net/
GraphPad Prism 8, version 8.3.0	GraphPad
Image Studio™ Lite	LI-COR Biotechnology
NanoDrop, version 3.8.1	Thermo Fisher Scientific
STRING database	https://string-db.org/
Universal Protein Knowledge Base (UniProtKB database)	https://www.uniprot.org

2.2 Methods

2.2.1 Gel electrophoresis

To analyze the size of DNA fragments, agarose gels in the range of 0.7-1% agarose were prepared. For this, agarose was dissolved in 1× Tris/Borate/EDTA (ethylene diamine tetra acetic acid) (TBE) buffer and subsequently the solution was supplemented with 5 µL HD-Green/100 mL. Afterwards, the gel was transferred to an electrophoresis chamber. 6× loading dye was added to the samples and peqGold DNA-ladder mix was used as a molecular weight marker. Electrophoresis was usually performed at 8 V/cm.

2.2.2 HCMV mutagenesis in BACmids

The BAC technology was applied for genetic modification of the HCMV genome in bacteria.

2.2.2.1 Amplification of the gene, encoding *galK* (*galK* cassette)

The *galK* cassette was amplified by PCR using the plasmid pGalK as template DNA and the respective primer pairs of interest, see 2.1.9.1. The used master mix is listed in Table 1 and the PCR program is shown in Table 2. The *galK* amplification was verified by gel electrophoresis. To remove the template DNA after the PCR, the purified PCR product was subjected to restriction with the enzyme *Dpn*I at 37 °C for 3 hours. This restriction enzyme degrades methylated template DNA, but not the non-methylated DNA of the PCR products.

Table 1. Master mix for *galK* cassette amplification

Master mix	**Volume**
pGalK (100 ng)	1 µL
Primer galK fwd (20 pmol/µL)	2 µL
Primer galK rev (20 pmol/µL)	2 µL
Puffer (10x)	5 µL
dNTPs (10 mM)	1 µL
ddH_2O	38.25 µL
Taq (Roche, 3.5 U/µL):	0.75 µL
	50 µL

Table 2. PCR program for *galK* cassette amplification

Program	**Temperature**	**Duration**	
Initial Denaturation	94°C	2 min	
Denaturation	94°C	45 sec	30× cycles
Annealing	58°C	45 sec	
Extension	72°C	90 sec	
Extension	72°C	10 min	

2.2.2.2 Recombineering and GalK selection

In a first step, the plasmid DNA containing the gene of interest was extracted from *E. coli* strain DH5α, using the PowerPrep® HP Plasmid Maxiprep System. Then, depending on the restriction sites chosen, the DNA was digested either with both endonucleases *Eco*RI-HF and *Hind*III or only with *Eco*RI-HF at 37 °C for 1 h with shaking at 300 rpm in a thermo mixer. Samples were then subjected to preparative agarose gel electrophoresis (0.7% agarose gels). Fragments of linearized DNA were isolated from the gel, using the QIAquick Gel Extraction Kit DNA. The concentration of the DNA was measured with a NanoDrop ND-1000 Spectrophotometer and the corresponding software NanoDrop V3.8.1. For recombineering, 5 mL LB medium in a test glass under chloramphenicol selection (15 µg/mL) was inoculated with an *E.coli* SW102 culture, containing the BAC vector of interest, and incubated overnight in a shaker at 200 rpm and 32°C. The following day, 1 mL of the culture was diluted in 50 mL LB medium with chloramphenicol selection in a 500 mL conical flask. The bacterial culture was grown to an OD600 of 0.55-0.6 at 32°C in a shaker with 200 rpm. Afterwards, the cells were heat-shocked at 42°C for exactly 15 min in a shaking water bath to generate electro-competent cells. The culture was immediately cooled down on ice, transferred to a cooled 50 mL Falcon tube and pelleted at 5,600 g, 4°C for 6 min. After that, the supernatant was removed and the cell pellet was dissolved in 1 mL ice-cold ddH_2O by swirling the tubes in an ice/water bath slurry. Following that, ice-cold ddH_2O was added until 20 mL and the bacterial suspension was again centrifuged under the same conditions. This step was repeated a second time. After the last washing step, the supernatant was discharged and the cells with remaining water were kept on ice until electroporation. For each electroporation, 30 µL SW102 electro-competent cells and either 150 ng (positive selection) or 300 ng (negative selection) of a gel-purified DNA fragment were mixed and filled into a 0.1 cm cuvette. The transformation was done at 25 µF, 1.75 kV and 200 Ω. The electroporated cells were then either transferred to 1 mL LB medium and incubated at 32°C, 100 rpm for 1h (positive selection) or transferred to a 100 mL conical flask with 10 mL LB medium and incubated at 32°C, 100 rpm for 4.5 h (negative selection). After incubation, 1 mL of the bacterial cells was pelleted at 18,000 g for 15 sec and the supernatant was removed. In a next step, the bacterial culture was washed three times in 1mL M9 medium. After the

last washing step, the supernatant was disposed and cells were resuspended in 500 µL M9 medium. The cells were plated on M63 minimal plates and incubated at 32°C until single clones became visible. Ten clones were picked and streaked out on MacConkey indicator agar plates. The plates were again incubated at 32°C until single colonies became visible.

2.2.2.3 Colony PCR

After the recombination step, clones were picked from MacConkey indicator plates to inoculate 5 mL LB medium with chloramphenicol (15 µg/mL). 1 mL of every overnight culture was pelleted at 27,000 g, RT for 1 min and used for analysis by colony PCR. After centrifugation, the supernatant was removed and cells were resuspended in the remaining medium. 5 µL of each resuspension was mixed with 15 µL ddH_2O in a PCR tube and heated to 99°C for 5 min. Subsequently, the samples were centrifuged at 27,000 g, RT for 2 min. 5 µL of each supernatant was used as template and mixed with 20 µL master mix, respectively, (see Table 3.) Different primer pairs were used to test either for the insertion of the *galK* cassette or the insertion of the sequence of interest, see 2.1.9.2. The used PCR conditions are described in Table 4. To verify the insertion of the sequence of interest, fragments were analyzed by agarose gel electrophoresis. In addition, the amplified fragments, representing the respective insertion of each *SQSTM1-S272* version into a BACmid were sequenced. For this, DNA fragments were purified by using the QIAquick PCR Purification Kit, according to manufacturer's instructions. The fragments were sent to Eurofins Genomics Europe Shared Services GmbH for sequence analysis, using Seq SQSTM1-fwd, Seq UL1-SQSTM1-fwd and Seq SQSTM1-UL7-fwd.

Table 3. Master mix for colony PCR

Master mix	**Volume**
Primer fwd (10 pmol/µL)	1 µL
Primer rev (10 pmol/µL)	1 µL
10× Puffer Complete (incl. Mg^{2+})	2.5 µL
dNTPs (10 mM)	0.5 µL
50% Glycerin	1.25 µL
miTaq only Polymerase	0.5 µL
ddH_2O	13.25 µL
	20 µL

Table 4. Colony PCR program

Step	Temperature	Time	
Initial Denaturation	95°C	3 min	
Denaturation	95°C	1 min	35× Cycles
Annealing	60°C	1 min	
Extension	72°C	30 sec/500 bp	
Extension	72°C	10 min	

2.2.2.4 BAC-Digestion

For restriction enzyme analysis of DNA from BAC clones, SW102 cultures containing the BACmid of interest were grown over night at 32°C and 200 rpm in conical flasks with 20 mL LB medium with chloramphenicol (15 µg/mL) in a shaker. On the next day, bacterial suspensions were centrifuged at 5,400 g for 5 min. Afterwards, the BAC DNA was isolated by using the PowerPrep® HP Plasmid Miniprep System and cleaved by using both restriction enzymes *Bam*HI-HF and *Eco*RI-HF at 37°C. After 5h of incubation, samples were heat-shock inactivated at 65°C for 20 min. DNA fragments were separated and analyzed by agarose gel electrophoresis for 2 h with 2.4 V/cm. The documentation was performed using UV transillumination and the software BioDocAnalyze 2.2 2.67.5.0.

2.2.3 Culture of human cells

Primary human foreskin fibroblasts (HFF) and human embryonic kidney (HEK) 293 cells, expressing the simian virus 40 large t antigen (HEK293T) were cultured in T-175 cm^2 flasks at 37°C, 90% humidity and 5% CO_2. All cell culture experiments were done using sterile instruments under a laminar flow clean bench. HFF were maintained in MEM, supplemented with 10% FCS, 2mM L-Glutamine, 0.5 ng/mL bFGF and 50 mg/L gentamycin. HEK293T cells were cultured in DMEM which was supplemented with 10% FCS, 2mM L-Glutamine, and 50 mg/L gentamycin.

HFF were passaged once a week, HEK293T twice a week. Either 1.8× 10^6 of HFF or 5× 10^6 of HEK293T cells were seeded into a T-175 cm^2 flask for passaging.

2.2.3.1 Seeding and harvesting of cells for experiments

To seed cells, the medium was removed, and the cells were washed with 1× DPBS, then incubated with 1× trypsin/EDTA for 5 min at 37°C. The digestion was stopped by adding the respective medium containing FCS. Afterwards, cells were pelleted at 432 g for five minutes, and the supernatant was discharged. Cells were either resolved in the appropriate medium for maintaining in cell culture or DPBS for further analysis. Next, the cell number was determined. For this, 50 µL of the cell suspension was 1:1 diluted in trypan blue staining

solution and transferred to a Neubauer counting chamber to calculate the cell number per mL. For seeding, the appropriate number of cells was delivered to the respective cell culture dish, and cells were cultured until further use, such as infection or transfection. The cell culture dishes used and the respective cell numbers and media are listed in Table 5. In the case of cell harvesting, a specific number of cells were either solved in DBPS or 2× SDS sample buffer, depending on the following analysis method.

Table 5. Cell amounts and correspond cell culture dishes

Cell line	**Cell culture dishes**	**Seeded cell number**	**Medium volume**	**Amount of DPBS and trypsin/EDTA**
HFF	96-well plate	5× 10^3	50 µL	-
	6-well plate	0.1× 10^6	2 mL	1 mL
	6 cm^2 dish	0.2× 10^6	5 mL	1 mL
	10 cm^2 dish	0.5× 10^6	10 mL	3 mL
	25 cm^2 flask	0.3× 10^6	5 mL	1 mL
	75 cm^2 flask	0.5× 10^6	10 mL	3 mL
	175 cm^2 flask	1.8× 10^6	20 mL	5 mL
HEK293T	10 cm^2 dish	5× 10^6	10 mL	3 mL
	175 cm^2 flask	8× 10^6	20 mL	5 mL

2.2.3.2 Addition of inhibitors

3-methylbenzyl pyrazolopyrimidine (3MB-PP1) was added to HFF once 4 h before cell harvest. HEK283T cells were treated with 3MB-PP1 12 hours before transfection. MG132 was added to HFF once 18 hours before cell harvest. Medium of HFF was supplemented with 200 µM of Bafilomycin A1 4 hours before cell harvest.

2.2.4 Generation of cell lines

2.2.4.1 Generation of autophagy receptor knockout (ko) HFF using CRISPR/Cas9-mediated genome editing

gRNAs were designed to interfere with the respective gene expression of various autophagy receptors by using the website http://crispor.tefor.net/ (Concordet and Haeussler, 2018; Haeussler et al., 2016).

The generated gRNA sequences, including a forward and a reverse sequence, are summarized in 2.1.9.5. First, 1 µg of the lentiviral vector pLKO5.U6.sgRNA(BsmBI, stuffer).EFS.SpCas9.P2A.tagGFP was digested, using 2 µL of 10× FastDigest Buffer, 2 µL of 10

mM DTT and 1 µL FastDigest *Esp3I* in a total volume of 20 µL at 37°C for 30 min. The digested vector was transferred to a 1% agarose gel and gel electrophoresis was performed. The larger band was cut out of the gel and DNA extraction was performed using the QIAquick Gel Extraction Kit DNA according to the manufacture's protocol. Next, the corresponding forward and reverse gRNA sequences were annealed at 85°C for 10 min, afterwards it was cooled until the room temperature (RT) is reached. For ligation, 50 ng of the linearized vector, 1 µL of the 1:200 annealed gRNA in ddH_2O, 2 µL of 5× DNA ligase buffer, 1 µL T4 DNA ligase in a total volume of 10 µL, filled up with dH_2O were used. As a control, dH_2O was used instead of the annealed gRNAs. The ligation mix was incubated at RT for 60 min. Afterwards, 50 µL Stbl3 bacteria were transformed with 2 µL of each ligation by incubating the samples for 1 hour on ice, followed by heat shock for 30 sec at 42°C, and immediate transfer to ice for 2 min. The transformed Stbl3 bacteria were plated onto LB-Ampicillin (Amp) plates and incubated at 30°C. The next day, 5 mL LB tubes with 100 µg/mL Amp were inoculated with individual colonies and incubated at 30°C overnight. Subsequently, DNA was isolated by using the MiniPrep Kit. Successful insertion was verified by DNA sequencing, using the pLKO-U6-Seq-fwd primer. The transduction of HFF with pLKO5 lentiviral supernatant to produce ko and control cells is described in the following section.

First, 5× 10^6 HEK293T cells were seeded in 10 cm^2 dishes, containing 10% DMEM. The next day, cells were transfected. For each lentiviral construct, 14 µg of the pLKO5.U6.sgRNA(BsmBI, stuffer).EFS.SpCas9.P2A.tagGFP of interest, 2.8 µg pMD2.G and 11 µg PAX2 were prepared and mixed in 1.700 mL OpitMEM. In a second tube, 70 µL of Lipofectamine 2000 was added to 1.700 mL OptiMEM and incubated at RT for 5 min. Subsequently, 1.770 mL diluted Lipofectamine was added to each diluted DNA approach and incubated at RT for 20 min. The DNA/Lipofectamine mix was added to the cells, and the dishes were placed into the incubator overnight. In the morning of the next day, the medium was replaced with the lentiviral harvest medium. 36 hours post transfection, the supernatant of the transfected HEK293 was collected and filtered through a 0.45 µm filter into a sterile 50 mL falcon tube. The supernatant was 1:2 diluted with HFF medium. Finally, polybrene was added to a final concentration of 4 µg/mL. Medium of HFF (0.25× 10^6), seeded in 6-well plates the previous day, was removed and replaced with 3 mL lentivirus containing medium in the appropriate wells. Lentiviral transduction/infection was enhanced by a centrifugation step. For this, 6-well plates were centrifugated at 700 g at RT for 90 min. Afterwards, cells were transferred to the incubator. After incubation for 4 hours, the medium was exchanged with HFF medium and incubated for 4 days until Fluorescence-Activated Cell Sorting (FACS). Cells were resolved in FACS-buffer and the successfully transduced cells were sorted by flow cytometry for the GFP signal in the FACS Core Facility of the University Medical Center Mainz. Selected HFF knockout and HFF control were seeded into appropriate cell culture dishes and maintained in cell culture until used for infection experiments.

2.2.4.2 Knockin cells

For the generation of HFF, permanently expressing *GFP-SQSTM1*, a pLKO-based expression vector was used. For this, a nucleotide sequence was designed encoding *SQSTM1* with the *GFP*-coding sequence inserted *in-frame* at the 3'-end (N-terminal GFP-tag). The construct was cloned into the *Esp3*I digested pLKO-based expression vector, similarly as described in 2.2.4. The plasmid was isolated by using the mini-prep kit and a successful insertion was confirmed by DNA sequencing, using the Seq-plKObv-fwd primer.

5× 10^6 HEK293T were seeded in 10× cm^2 dishes, containing 10 mL DMEM, supplemented with 10% FCS. On the next day, the medium was replaced with 5 mL DMEM, including 10% FCS in the absence of antibiotics. 6 hours later, cells were co-transfected with 6 μg of the pLKO-based lentiviral vector encoding GFP-tagged SQSTM1/p62, termed pLKO-GFP-SQSTM1, together with 3 μg each of the three packaging plasmids, pLP1, pLP2 and pLP/VSV-G. For transfection, all plasmids were diluted in 1.5 mL OptiMEM. In a second reaction tube, 36 μL Lipofectamine 2000 transfection reagent was diluted in 1.5 mL OptiMEM. After 5 min, Lipofectamine 2000 complex was added to the plasmid solution, incubated at RT for 20 min, and added dropwise to HFF. Cells were incubated at 37°C overnight. 18 hours after transfection, the medium was replaced with DMEM containing 10% FCS. 48 h post transfection, lentiviral supernatants were collected and cleared through a 0.45 μM filter. One day before transfection, fibroblasts were seeded in 10 cm^2 dishes (0.5× 10^6). The next day, the medium was replaced with lentiviral supernatant, diluted 1:2 in 10% MEM medium containing 7.5 μg/mL polybrene. Cells were incubated at 37°C and on the following day, medium was exchanged with HFF culture medium. The HFF-GFP-SQSTM1 were selected by adding 500 μg/mL geneticin to 10% MEM medium two days after transduction. For the cultivation of HFF-GFP-SQSTM1, medium was permanently supplemented with 500 μg/ mL geneticin.

2.2.4.3 siRNA transfection

0.2× 10^6 HFF were seeded in 6 cm dishes and cultured in 10% MEM without gentamycin. The next day, cells were transfected with 30 pmol of the siRNA of interest or a control siRNA. In the case of a double transfection, 15 pmol per siRNA was used. In each approach, the siRNA was resolved in a total volume of 150 μL OPTI-MEM. In a second tube, 9 μL of Lipofectamine RNAiMAX was supplemented in 141 μL OPTI-MEM. The latter one was added to siRNA-OPTI-MEM mix and incubated at RT for 5 min. Subsequently, 300 μL of the transfection solution siRNA was dropwise added to the cells. The transfection medium was removed after 48 h or, in the case of CDK1-mediated knockdown, the medium was removed 6 hours after transfection. The siRNA-mediated knockdown was verified by Western blot.

2.2.5 Virus

2.2.5.1 Virus reconstitution

For virus reconstitution, 1× 10^5 HFF/well were seeded in 6-well plates in 2 mL 10% MEM. On the next day, 20 µL BACmid DNA, obtained from a BACmid maxi-preparation, were mixed carefully with 80 µL MEM medium without any supplements in a new 1.5 mL reaction tube. Subsequently, 12 µL SuperFect Transfection Reagent was added and the preparation was incubated at RT. After 10 minutes, 600 µL of 10% MEM was added, mixed and the solution was added directly to HFF, which had previously been washed once with 1× DPBS. After incubation at 37°C for 2.5 h, cells were washed two times with 4 mL 1× DPBS and cultured in HFF medium. After three days, the medium was removed, cells were washed two times with 1× DPBS and new HFF medium was added. The cells were passaged until confluence. As soon as an advanced cytopathic effect (CPE) appeared, the cells were further incubated without passage until the majority of the cells were lysed. Then, this first supernatant was collected and newly seeded HFF in 5× T-175 cm^2 flasks were infected with 0.5 mL supernatant, dissolved in a total volume of 5 mL MEM medium to recover the supernatant as a seed stock. This seed stock was used to infect HFF in 5× T-175 cm^2 flasks under the same infection conditions. The third virus supernatant was collected and stored at -80°C until use for experiments.

2.2.5.2 HCMV infection of HFF in culture

A day before infection, a defined number of HFF were seeded in respective cell culture dishes (Table 6). At the next day, cell culture supernatants were removed and cells were infected with the respective HCMV strain at a desired multiplicity of infection (m.o.i.) or genomes/ cell in the corresponding infection volume. After virus adsorption at 37°C for 1.5 hours, respective volume of cell culture medium was added. The cells were further incubated at 37°C and 5% CO_2 until use.

Table 6. Infection volumes in dependence of cell culture dishes

Cell line	Cell culture dishes	Seeded cell number	Infection volume
HFF	96-well plate	5× 10^3	100 µL
	6-well plate	0.1× 10^6	1 mL
	6 cm^2 dish	0.2× 10^6	2 mL
	10 cm^2 dish	0.5× 10^6	3 mL
	25 cm^2 flask	0.3× 10^6	2 mL
	75 cm^2 flask	0.5× 10^6	3 mL
	175 cm^2 flask	1.8× 10^6	5 mL

2.2.5.3 Adjustment of virus concentrations for infection experiments

The concentrations of viruses, released from infected HFF into the culture supernatants differed between experiments and strains. To adjust for these differences in the experimental stocks, two different methods were used.

2.2.5.3.1 TaqMan qPCR

The transfer of viral genomes into cells as a measure of virus concentration in supernatants used for experiments was evaluated by quantitative PCR. The genome copy numbers in 6 h infected cells were determined in serial dilutions. For this, HFF were seeded in 10 cm^2 dishes. On the next day, cells were infected with the supernatants, containing the HCMV strains of interest (10 µL, 50 µL, 100 µL and 500 µL). The total volume was 3 mL in each case. 6 hours post infection (h.p.i.), HFF were washed 2× with DPBS, collected, adjusted to 1× 10^6/mL in 1 ×DPBS and stored at -20°C until usage. The viral DNA was isolated out of 1× 10^5 cells with the High Pure Viral Nucleic Acid Kit according to the instructions of the manufacturer. 5 µL of isolated DNA was mixed with 45 µL master mix per tube for qPCR (Table 7). As a non-template control, ddH_2O was used and serial diluted standard DNA from HCMV cosmid pCM1049 was taken for calibration (3.5× 10^5, 10^4, 10^3, 10^2, 10^1). Three technical replicates were evaluated, using the 7500 Real-Time PCR system from Applied Biosystems. In Table 8 the used PCR program is shown. Genome copies were analyzed by the 7000 System SDS software V.1.2.3. Copy numbers of the viral genome per cell were determined by the mean specific C_T value in relation to the standard serial dilutions.

Table 7. Master mix of TaqMan-based qPCR

Component	**Concentration**	**Volume**
PCR-Buffer (+ 15 mM $MgCl_2$	10×	5 µL
$MgCl_2$	25 mM	2 µL
dNTP-Mix	2 mM	5 µL
TaqMan-CMV probe	1 µM	5 µL
CMV-fwd	3 µM	5 µL
CMV-rev	3 µM	5 µL
HPLC water		17.25 µL
Template DNA		5 µL
Rox	100 µM	0.25 µL
HotStar Taq DNA polymerase	5 units/µl	0.5 µL
		50 µL

Table 8. TaqMan qPCR program

Step	Temperature	Time	Cycles
Hold	95°C	10 min	1×
Denaturation	95°C	15 sec	42×
Annealing/Extension	60°C	60 sec	

2.2.5.3.2 IE1-assay

The release of HCMV viral progeny was analyzed by infecting indicator HFF cultures in serial dilutions of culture supernatants from infected cells. For this, 5×10^3 HFF were seeded into each well of a 96 well plate and incubated over night at 37 °C. The next day, one vial containing the supernatant of the virus of interest was serially diluted (10^{-1} up to 10^{-4} in a total volume of 1 mL, respectively) in a 48 well plate. Afterwards, 100 µL of 10^{-1} up to 10^{-4} dilutions were added to the cells. Both negative (medium) and positive controls (undiluted virus) were carried along. The plate was incubated at 37°C for 2 days. Subsequently, the medium was removed, the cells were washed with 200 µL 1× DPBS per well, and finally fixed with 100 µL $EtOH_{absolute}$ per well at RT. After 20 min, the cells were washed with 1× DPBS and 50 µL of the primary antibody, directed against the viral IE1-protein were added (undiluted). The plate was transferred into a moist chamber and incubated at 37°C for 1h. After that, each well in the plates was washed twice with 200 µL 1× DPBS. Then 50 µL of the secondary antibody, horseradish peroxidase (HRP)-coupled rabbit anti-mouse IgG (H+L) diluted 1:500 in 1× DPBS, was added to each well. The plate was transferred into a moist chamber, incubated at 37°C for 1h again and washed with 1× DPBS. Afterwards, a fresh AEC-staining solution was prepared by diluting AEC-stock solution (4 mg/DMF mL) in acetate buffer in a ratio of 1:20 and filtered via a folded filter (retention range >4 µm) into a fresh flask. In addition, H_2O_2 (30%) was added in a 1:1000 dilution. In every well, 100 µL of the AEC-staining solution was pipetted. The plate was incubated again as done before. Finally, the plate was washed once with 1× DPBS, covered with 200 µL 1× DBPS, and stored at 4°C in the dark until microscopic inspection. For analysis, eight technical replicates were evaluated by counting the viral immediate-early protein 1 (IE1)-positive nuclei, stained in red. The concentration of viral progeny in each supernatant was then calculated. In total, the concentration of the viruses is composed of three IE1-assays each.

2.2.5.4 Purification of virions

For the purification of virions, HFF were seeded in 10-20× 175 cm^2 flasks and infected with 0.5 mL of virus-containing cell culture supernatant. After seven days of incubation at 37°C and 5% CO_2, the culture supernatant was collected, transferred to 50 mL falcon tubes and centrifugated at 1,475 g, RT for 10 min. Afterwards, the supernatant was collected and centrifuged at 95,000 g (70 min; 10°C) in a SW32Ti swing-out rotor or a 45Ti in a Beckman Optima L-90K ultracentrifuge. The supernatant was discharged and the pellets were

resuspended in 2 mL of 1× DPBS. Afterwards, the virions were separated via a glycerol-tartrate density gradient ultracentrifugation step. For this, glycerol tartrate gradients were immediately prepared, as follows: 4 mL of a 35% Na-tartrate solution in 0.04 M Na-phosphate buffer, pH 7.4, and 5 mL of a 15% Na-tartrate–30% glycerol solution in 0.04 M Na-phosphate buffer, pH 7.4, were applied to respective columns of a gradient mixer. The gradients were made by slowly dropping the solutions into Beckman Ultra-clear centrifuge tubes (14 by 89 mm), positioned at an angle of 45°. One mL of the resuspended viral particles was carefully layered on top of the gradients. Ultracentrifugation was done with low deceleration in a Beckman SW41Ti swing-out rotor for 60 min at 90,000× g and 10°C. Subsequently, the particles were illuminated by light scattering. Virions were collected from the gradient by penetrating the centrifuge tube with a hollow needle below the band. Samples were carefully drawn from the tube with a syringe. The particle fraction was washed with 1× DPBS and pelleted in an SW41Ti swing-out rotor for 90 min at 98,000× g and 10°C. After the last centrifugation step, virions were resuspended in 60 µL of 1× DPBS and stored at –80°C until analysis. The protein concentration of the virions was determined with the Pierce BCA Protein Assay Kit.

2.2.5.5 Analysis of HCMV infections

2.2.5.5.1 TaqMan/Kinetics

Quantitative PCR was used to either study HCMV genome replication over time or to analyze viral genome release as a surrogate for progeny release. HFF were seeded in 10% MEM and infected with HCMV strains the next day. For both approaches, cells were infected with a low genome copy number per cell (4 genome copies/cell), and cells and supernatants were collected at various times after infection. The cell culture supernatant was centrifuged at 1,470 g for 10 min, aliquoted to 1 mL and stored at -80°C until analysis. Cells were washed twice with 1× DPBS, adjusted to 1× 10^6 cells/mL in 1× DPBS, and stored at -20°C until use. Subsequently, the viral DNA was isolated out of both 200 µL supernatant or 1× 10^5 cells with the High Pure Viral Nucleic Acid Kit according to the manufacturer's instructions. Genome copies per cell and per 1 mL were measured as described in 2.2.5.3.1.

2.2.5.5.2 Western Blot

Both, infected cell lysates and purified virions were investigated by Western blot analysis. HFF were infected with the desired m.o.i.. Samples were collected at various days post infection (d.p.i.). For the analysis of cell proteins, the lysates were adjusted to 1× 10^5 cells/10 µL 2× SDS sample buffer. For the analysis of viral particles, 30 µg of virions were lysed in 2× SDS sample buffer. All samples were boiled at 99°C for 10 min and subsequently centrifugated at 27,000g for 1 min in a microfuge. 1× 10^5 cells per slot to study protein levels, 2× 10^5 cells per slot to investigate phosphorylation of proteins, or 30 µg of viral particles per slot were loaded onto 10% Bolt™ Bis-Tris Plus gels. The molecular weight marker

PageRuler™ Prestained Protein Ladder was used alongside. The separation of proteins was done by sodium dodecyl sulfate polyacrylamide gel electrophoresis (SDS-PAGE) with 157 V/cm, 400 mA, and 100 Ω. After electrophoresis, the proteins were transferred to a 0.2 µM Immobilon-PSQ PVDF-membrane using a Mini Blot module (Thermo Fisher Scientific), according to the manufacturer's instructions. The transfer was done at 20 V for 1h. Then, the membrane was incubated in blocking solution with Tris buffered saline, containing 0.2% Tween 20 (TBS-T) with either 5% milk powder or 5% BSA. After 1 h, the solution was discarded and the primary antibody solutions were applied to the membranes. The incubation was performed at 4°C on a tilt/roller mixer overnight. The next day, the membrane was washed three times for 10 min in TBS-T. After the last washing step, membranes were incubated with secondary antibodies at RT on an orbital shaker in the dark for 1.5 h. Then, the membranes were washed again in the dark as done before. Signals were analyzed with the Odyssey Infrared Imager CLx (LI-COR Biotechnology), according to the instructions of the manufacturer, and analyzed by using the Image Studio Lite Version 5.0 software.

2.2.5.5.3 Co-immunoprecipitation (Co-IP) experiments

To analyze the interaction of HCMV proteins and different autophagy receptors, Co-IPs with antibodies against the respective receptors were performed. Depending on the following experimental setup, either 1.8×10^6 or 1×10^5 HFF were seeded in the appropriate cell culture dishes. Cells, infected with an m.o.i.=1 were harvested at 3 d.p.i. and resuspended in 1 mL lysis buffer (0.5 M NaCl, 0.05 M Tris-HCl (pH = 8.5), 0.5% NP-40 alternative, 1 mM DTT, 1 complete protease inhibitor cocktail tablet/10 mL and 1 PhosSTOP phosphatase inhibitor cocktail tablet/10 mL in ddH_2O). Afterwards, cell lysates were sonicated by ultrasound (1× 10s and 30% output), using a Branson Sonifier 250. Specific antibodies against either SQSTM1/p62, optineurin, TRIM25 or TRIM26 were added to the cleared cell extracts and samples were rotated at 4°C overnight. The next day, either 30 µL protein-A/G magnetic or 30 µL IgG beads were added to the protein-antibody complexes and incubated in a rotator at 4°C. After 4 hours, magnetic beads were washed 3 times with lysis buffer. Depending on the following experiment, immunoprecipitated samples and lysate controls were either washed two times with the lysis buffer without detergents and send to mass spectrometry, or incubated in 50 µL 2× SDS sample buffer for Western blot, respectively.

For phosphoproteomic studies, HFF-GFP-SQSTM1/p62 (1.8×10^6) were infected with an m.o.i. of 1 with HCMV (BADwt) or left uninfected, harvested 3 d.p.i., centrifuged and resuspended in lysis buffer and sonicated (1× 10s and 30% output). Cells were then washed with lysis buffer and incubated with 30 µL GFP-Trap magnetic beads on a rotating platform at 4°C overnight to perform the GFP-Trap immunoprecipitation. The next day, the beads were washed three times in lysis buffer, supplemented with 8 M urea, and subsequently washed twice with wash buffer without detergents. After validation of the GFP signal by

Western blot, beads were analyzed by mass spectrometry together with our collaboration partners Lina Herhaus and Uxía Gestal Mato, Institute of Biochemistry II, Goethe University Frankfurt/Main, Germany.

For co-transfection experiments, plasmids pEGFP-N2-UL97-as1 and pcDNA5 FRT/TO GFP_SQSTM1/p62 were used. 3× 10^6 HEK293T were seeded in 10 cm^2 dishes. 12 hours before infection, cells were treated with the inhibitor 3MB-PP1 or DMSO as control. After incubation, co-transfection with 9 µg pEGFP-N2-UL97-as1 and 9 µg pcDNA5 FRT/TO GFP_SQSTM1/p62 were performed by mixing both plasmids in 850 µL Opti-MEM. Lipofectamine 2000 transfection reagent was added to the approach in a Lipofectamine:DNA ratio of 3:1. The DNA transfection complex was carefully mixed and incubated at RT for 10 min. 850 µL of the complex solution was dropwise added to HEK293T and gently spread over the cells. The cultures were incubated at 37°C for 24 hours. After incubation, cells were collected and sonicated (1× 10 sec with 30% output). Next, cells were cleared in lysis buffer and GFP-Trap immunoprecipitation was done as described above. Confirmation of successful expression of SQSTM1/p62 and pUL97-as1, the latter one represented by free GFP, was controlled by Western blot analysis, using a GFP-specific antibody. The beads were transferred to mass spectrometry.

One day before the non-radioactive in-vitro kinase assay (IVKA), protein-A/G magnetic beads (25 µL) were prepared in 300 µL lysis buffer without protease inhibitors. An antibody against pUL97 and either an antibody against SQSTM1/p62 or phosphoprotein 65 (pp65) as a positive control were added. Beads were incubated at 4°C overnight on a rotating platform. Co-IP samples for IVKA were generated on the day of analysis as follows: 5-day infected HFF (m.o.i. of 1) were harvested. Uninfected HFF were carried along for control. Cells were centrifuged and the pellets were resolved in 300 µL lysis buffer, ultrasonicated (1× 10 sec with 30% output) and incubated in a rotor at 4°C for 20 min. Subsequently, cells were centrifuged at 14,000 rpm, 10 min at 4°C. During this centrifugation step, beads were washed three times with lysis buffer without DTT. Afterwards, beads and lysates were mixed, incubated on a rotating platform for 1.5h at 4°C again and were used for IVKA.

2.2.5.5.4 IVKA

Following up on the Co-IP for IVKA, beads were washed twice in 500 µL lysis buffer without DTT and subsequently in 500 µL IVKA buffer (20 mM Tris/Cl (pH 7.5), 0.5 mM $MnCl_2$ and 0.5 mM DTT, diluted in 10 mL dH_2O). After the last washing step, the sample was split in three aliquots. 75 µL of the beads were used for immunoprecipitation (IP) control and lysed in 2× SDS sample buffer, while 2× 200 µL of the beads were used for the IVKA reaction. For this, the supernatants of the beads were removed and 30 µL IVKA buffer was added. The buffer was either supplemented with 200 ng ATPγS or, as specificity control, one sample was incubated without ATPγS. Beads were incubated under shaking at 30°C, 1400 rpm for 60 min in a thermo mixer. Afterwards, 1.5 µL of 50 mM p-nitrobenzyl mesylate

(PNBM) was added to the reaction to alkylate thiophosphates. Samples were incubated under shaking at 25°C, 500 rpm for 60 min in a thermo mixer again. Finally, 2× SDS sample buffer was added, and Western blot analysis was performed, detecting phosphorylation of SQSTM1/p62 or pp65 as control via a thioester specific antibody.

2.2.5.5.5 Mass spectrometry (MS) analysis of interaction partners and phosphosites

The experiments were performed similarly as described in (Herhaus et al., 2020). All data are based on three biological samples per experiment.

After Co-IP, the proteins bound to magnetic beads were incubated in SDC-buffer (2% SDC, 1mM TCEP, 4mM chloroacetamide, 50mM Tris pH 8.5) for 30 minutes at 60ºC. Samples were diluted 1:2 with 50 mM Tris pH 8.5 prior to overnight digestion with trypsin, done at 37ºC. Digested peptides were acidified with trifluoroacetic acid (TFA) to inhibit trypsin and peptides were prepared for SDB-RPS StageTip desalting. SDB-RPS StageTips were made by stacking two layers of 3 MEm-pore solid phase extraction SDB membranes into a 200-mL micropipette tip. Acidified peptides were loaded onto the SDB-RPS StageTips and washed with 0.2% (v/v) TFA. Peptides were eluted using a two-step elution with 1.25% ammonium Hydroxide, 80% (v/v) ACN and then dried using a speed-vacuum concentrator (45-75 min at 60 °C). Dried peptides were stored at -20 °C. Peptides were analyzed on an Orbitrap EliteTM or Q Exactive HF mass spectrometer (Thermo Fisher Scientific).

Raw data were analyzed using MaxQuant 1.6.5.0 with standard settings and activated LFQ quantification. The HCMV reference protein database (UniProt) or the human reference protein database (UniProt) was used as the database to identify the viral peptides, and the (false discovery rate) FDR was set at 1% at the protein, peptide spectrum match (PSM) and site-decoy levels. Statistical analysis was done with Perseus 1.6.5. Proteins were defined as interactors if they passed a 5% FDR corrected one sided two-sample Student's t-test with a minimal enrichment factor. For interactors; the matrix of significant hits from the right-sided Student's t-test, was imputed and analyzed for variance between groups through a One-Way ANOVA. Tukey's HSD Post-Hoc test was used to identify significant pairs. Similarly, phosphorylation sites were searched and statistical analysis was done with Perseus 1.6.5. Sites were selected as significant if they showed a $\log2 \geq 1$ and p value ≤ 0.05.

2.2.6 Statistical analysis

The statistical analysis was respectively performed with Prism 8.0 software (Version 8.3.0) from GraphPad.

3 Objectives

Autophagy has been shown to serve both anti-viral and pro-viral functions during viral infections. Generally, cells react to infection by activating selective autophagy in order to remove the invading pathogen. In this context, autophagy receptors are essential as they form a bridge between the cargo and the autophagosomal membranes. Therefore, autophagy receptors are convenient targets for viruses to regulate and manipulate this intrinsic defense mechanism. Indeed, several viruses target autophagy receptors for proteasomal degradation, proteolytic cleavage, or post-translation modifications to functionally deactivate these proteins. Phosphorylation is one important post-translational modification that regulates the selectivity of autophagy receptors towards their cargo and their interaction with autophagic structures.

We have observed a restricting effect of autophagy on HCMV infection and documented the interaction between autophagy receptors and viral structural components. These findings suggested that nascent HCMV particles were subject to autophagosomal degradation. However, HCMV replicates efficiently even in the presence of autophagy. Interestingly, some components of the autophagy machinery are packaged into mature virions. These findings indicate that divergent processes, the activation of autophagy as well as the inhibition of autophagosomal degradation occur in HCMV-infected cells. It was hypothesized that HCMV interferes with autophagy receptors and their recognition of viral cargo by manipulating their selectivity via changes in their phosphorylation status and converting the autophagic process by incorporating autophagy components into viral particles. In this work, the impact of autophagy receptors on HCMV infection was analyzed. A particular focus on clarifying whether phosphorylation is used as a regulatory modification and if it has an effect on viral replication was set.

The following major questions were addressed:

1. Which autophagy receptors, incorporated into HCMV particles, interact with HCMV components?
2. How do autophagy receptors and their phosphorylation status impact HCMV infection?
3. Does HCMV use phosphorylation to regulate the interaction between autophagy receptors and their cargo?
4. What is the role of the HCMV kinase pUL97 on autophagy receptor phosphorylation?

This study aimed to analyze the interplay between autophagy receptors and HCMV, thereby providing a better understanding of virus-host interactions and promoting the use of substances that regulate autophagy for treatment of HCMV infection.

4 Results

4.1 Impact of autophagy receptors SQSTM1/p62 and optineurin on HCMV infection and autophagy in HCMV-infected cells

Autophagy has been shown to function as an antiviral defense mechanism by selectively degrading viral and cellular cargo (Jordan and Randall, 2012; Paul and Münz, 2016; Richetta and Faure, 2013). In this process, autophagy receptors take a special role by linking the cargo to the autophagy machinery (Gubas and Dikic, 2022; Stolz et al., 2014). Autophagy has been shown to restrict HCMV infection (Zimmermann, Krämer et al., 2021). A surprising result in this context was that several autophagy receptors, including SQSTM1/p62 (Zimmermann, Krämer et al., 2021) and optineurin (Zimmermann, unpublished) were found to be incorporated into newly-synthesized viral particles, suggesting that HCMV may package autophagy receptors in order to evade degradation of viral particles during morphogenesis. One goal in this section was to verify the packaging of autophagy receptors. As a major part, the viral interaction partners of SQSTM1/p62 and optineurin should be identified, and the role of these receptors in HCMV infection should be addressed.

4.1.1 SQSTM1/p62 interacts with several viral proteins

Previously, MS analyses had revealed that both SQSTM1/p62 and optineurin were detectable in purified extracellular HCMV virions (Zimmermann, unpublished; Zimmermann et al., 2021). To confirm these data, purified viral particles, obtained from HFF, infected with the different HCMV laboratory strains BADwt, HB15, and TowneBAC were analyzed for the presence of both SQSTM1/p62 and optineurin by Western blot. For this, HFF were infected with the respective HCMV strains. Cell-culture supernatants were harvested at 7 d.p.i. for virion purification by density gradient ultracentrifugation. The respective virion samples were subjected to SDS-PAGE, followed by Western blot analysis. A BADwt-infected cell lysate, harvested at 6 d.p.i. was used as a control for HCMV infection. The Western blot showed that both SQSTM1/p62 and optineurin were present in virions, confirming the MS data (Figure 3). The proteins major capsid protein (MCP) and phosphoprotein 28 (pp28), were probed as an infection control.

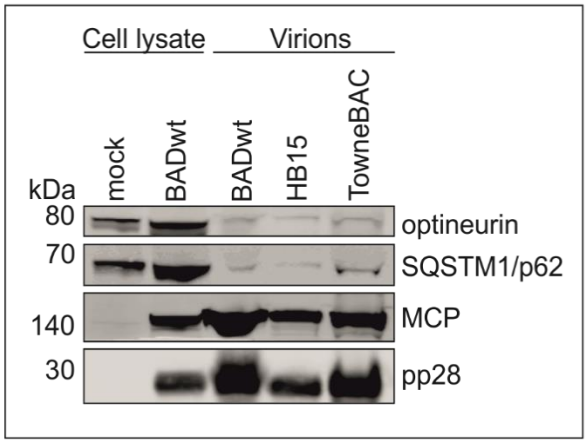

Figure 3. Western blot analysis of the packaging of autophagy receptors SQSTM1/p62 and optineurin into HCMV virions. Proteins from gradient-purified virions of HCMV strains BADwt, HB15, and TowneBAC were separated by SDS-PAGE, blotted and probed with antibodies against SQSTM1/p62 and optineurin, respectively. Cell lysates from 6-day BADwt-infected HFF and uninfected cells (mock) were taken along as control. Antibodies directed against the viral major capsid protein (MCP) and the phosphoprotein 28 (pp28) served as infection controls.

The laboratory HCMV strain BADwt was primarily used for the following experiments and was thus designated as HCMV. In the case when other HCMV strains were used, they were mentioned separately.

To confirm the interaction of SQSTM1/p62 with viral proteins, as published by Zimmermann, Krämer et al., 2021 and to determine, whether optineurin also interacted with HCMV proteins, Co-IP experiments were performed on lysates of infected cells, using an antibody directed against either receptor. Both precipitation samples were analyzed by MS in order to identify viral interaction partners. Briefly, HFF were infected with HCMV, using a m.o.i. of 1. Cells were collected at 3 d.p.i., lysed and incubated with antibodies directed either against SQSTM1/p62 or optineurin or, as a control, against IgG. The antibody-bait protein complexes were precipitated using protein A/G magnetic beads. MS was performed in collaboration with the group of Lina Herhaus and the MS platform located at the Institute of Biochemistry II (IBC2) of the Goethe University Frankfurt/Main, Germany. In the raw data set analysis before statistical evaluation, a total of 43 virus proteins were detected with SQSTM1/p62-specific antibodies and 41 virus proteins were identified upon Co-IP with optineurin-specific antibodies (Figure 4). To determine the proteins that significantly co-precipitated with each receptor, the raw data was analyzed by a one-sided two-sample Student's t-test with 5% false discovery rate (FDR) in comparison to IgG IP.

Using these criteria, 16 HCMV proteins were classified as *bona-fide* interaction partners of SQSTM1/p62, representing capsid-, tegument-, or envelope proteins. SQSTM1/p62 precipitated with almost all capsid proteins, confirming our previous findings (Zimmermann, Krämer et al., 2021). The analysis also revealed that the receptor precipitated with a smaller number of proteins as previously reported (Zimmermann, Krämer et al., 2021). This may be related to a different type of labeling for MS analysis. Interestingly, optineurin co-precipitated with only one viral protein, namely pUL84, which also co-precipitated with SQSTM1/p62.

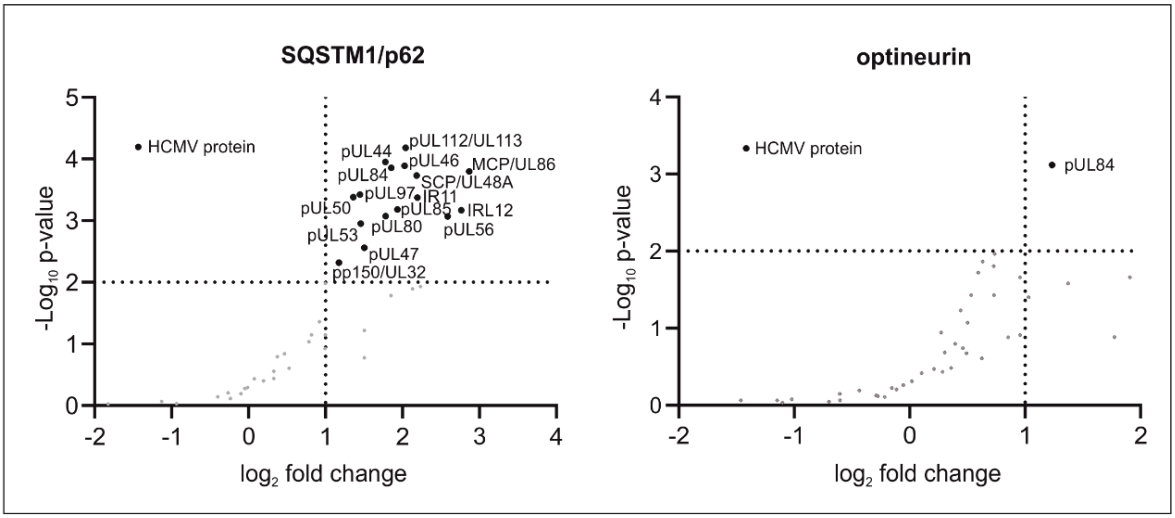

Figure 4. MS analysis of the interaction of SQSTM1/p62 and optineurin with HCMV proteins. HFF, infected with HCMV (m.o.i.= 1) were incubated with protein A/G magnetic beads and specific antibodies against either SQSTM1/p62 or optineurin or, IgG, as control were used. Precipitates were analyzed and quantified by mass spectrometry (MS). Matching the following conditions, they were considered as being significant: one-sided two-sample Student's t-test with a minimal enrichment factor of 2 ($\log_2(2) = 1$), showing the $\log_2$ fold change and $p < 0.01$ ($-\log_{10}(0.01) = 2$). Horizontal dotted lines represent the difference and the vertical dotted lines represent the p-value. Black data points show significantly co-precipitated viral proteins, whereas grey data points represent proteins that were excluded because of their failure to match the criteria. HCMV proteins are viral proteins and are structural and non-structural such as phosphoprotein 150 (pp150)/UL32, pUL97 and MCP/UL86.

The interaction of SQSTM1/p62 and optineurin with HCMV proteins was validated as part of a master thesis by Ahmad Afifi (Afifi, 2021, unpublished). Here Co-IPs against either the respective receptor or different HCMV proteins such as MCP and glycoprotein B (gB) with subsequent Western blot analysis was performed. Again, SQSTM1/p62 showed an interaction with MCP, gB and pUL84, whereas optineurin only interacted with pUL84. As part of the master thesis, the co-localization of both autophagy receptors with several HCMV proteins was studied, showing that SQSTM1/p62 but not optineurin co-localized with HCMV proteins. Taken together, these data showed that SQSTM1/p62 interacted with a subset of HCMV proteins.

4.1.2 Absence of SQSTM1/p62 leads to an enhanced viral progeny release

In a next step, the impact of both SQSTM1/p62 and optineurin on HCMV replication and particle release was investigated. For this, both SQSTM1/p62- and optineurin-deficient HFF cell lines, termed ko-SQSTM1 or ko-OPTN were generated, using the CRISPR/Cas9 technology (Figure 5A). The guide RNAs (gRNA) either targeted the second exon of *SQSTM1* or the first exon of *OPTN,* respectively, thereby affecting their expression. To verify the efficacy of the genome editing, lysates of the cell lines were analyzed by Western blot. Both SQSTM1/p62 and optineurin were undetectable, confirming that the genome editing was successful (Figure 5B). An HFF cell line with a non-targeting gRNA was also generated which was used as control.

The influence of both SQSTM1/p62 and optineurin on viral growth was addressed by infecting either ko-SQSTM1, ko-OPTN or control cells with HCMV, using an infectious dose of 4 genome copies/cell. Both infected cells and cell culture supernatants were collected from 6 h.p.i. on up to 8 d.p.i.. Subsequently, viral DNA was isolated from both cells and supernatants to determine genome copies per cell and genome copies per mL supernatant. The TaqMan qPCR analysis showed that the HCMV genome replication was not affected by the absence of SQSTM1/p62 or optineurin, compared with infected control cells (Figure 5C). The release of viral genomic DNA also remained unaltered in the absence of either autophagy receptor (Figure 5D). Because the quantification of extracellular viral DNA does not necessarily reflect release of infectious progeny, an IE1-assay was performed, staining against the viral protein IE1. For this, HFF cells were once again infected, using an m.o.i. of 0.5. A possible impact on HCMV progeny release was expected between 4 and 6 d.p.i. as seen in experiments performed in the past. Hence, the supernatants were collected at the respective time points and transferred onto newly seeded HFF in a serial dilution to perform the IE1-assay (Andreoni et al., 1989; Chou and Scott, 1988). The results showed that the depletion of *OPTN* had no impact on the HCMV progeny release, reflecting the results of the qPCR analyses (Figure 5E). Interestingly, the absence of SQSTM1/p62 led to a two-fold increase of IE1-positive cells in samples from 4 d.p.i., showing a significant increase in viral progeny release. At 6 d.p.i., the release of progeny from ko-SQSTM1-infected cells was similar to that from control-infected cells. To finally test, if SQSTM1/p62 had an influence on the expression kinetics of viral proteins, Western blot analysis was performed, using antibodies against selected HCMV proteins. Control and ko-SQSTM1 cells were infected with HCMV. Cell lysates obtained at 1, 3 and 6 d.p.i., respectively, were subjected to the analysis. The membrane was probed with antibodies against MCP, the pp150, pp28 and small capsid protein (SCP). In contrast to DNA replication, reduced levels of these proteins were found in infected ko-SQSTM1 cells compared with infected control HFF (Figure 5F). This effect was only observed at 6 d.p.i..

Taken together, these results showed that the deletion of SQSTM1/p62 had little impact on HCMV genome replication but enhanced the release of infectious progeny. This was

interestingly accompanied by reduced viral structural protein levels in the cell. As there is no evidence for an influence of SQSTM1/p62 on viral gene expression, this indicates that there is enhanced protein turnover in the absence of the receptor, e.g., by cellular sensing of SQSTM1/p62 deficiency and induction of proteasomal degradation. The absence of optineurin had no impact on both viral genome replication and progeny release, indicating that this receptor bears no antiviral function in fibroblast cells.

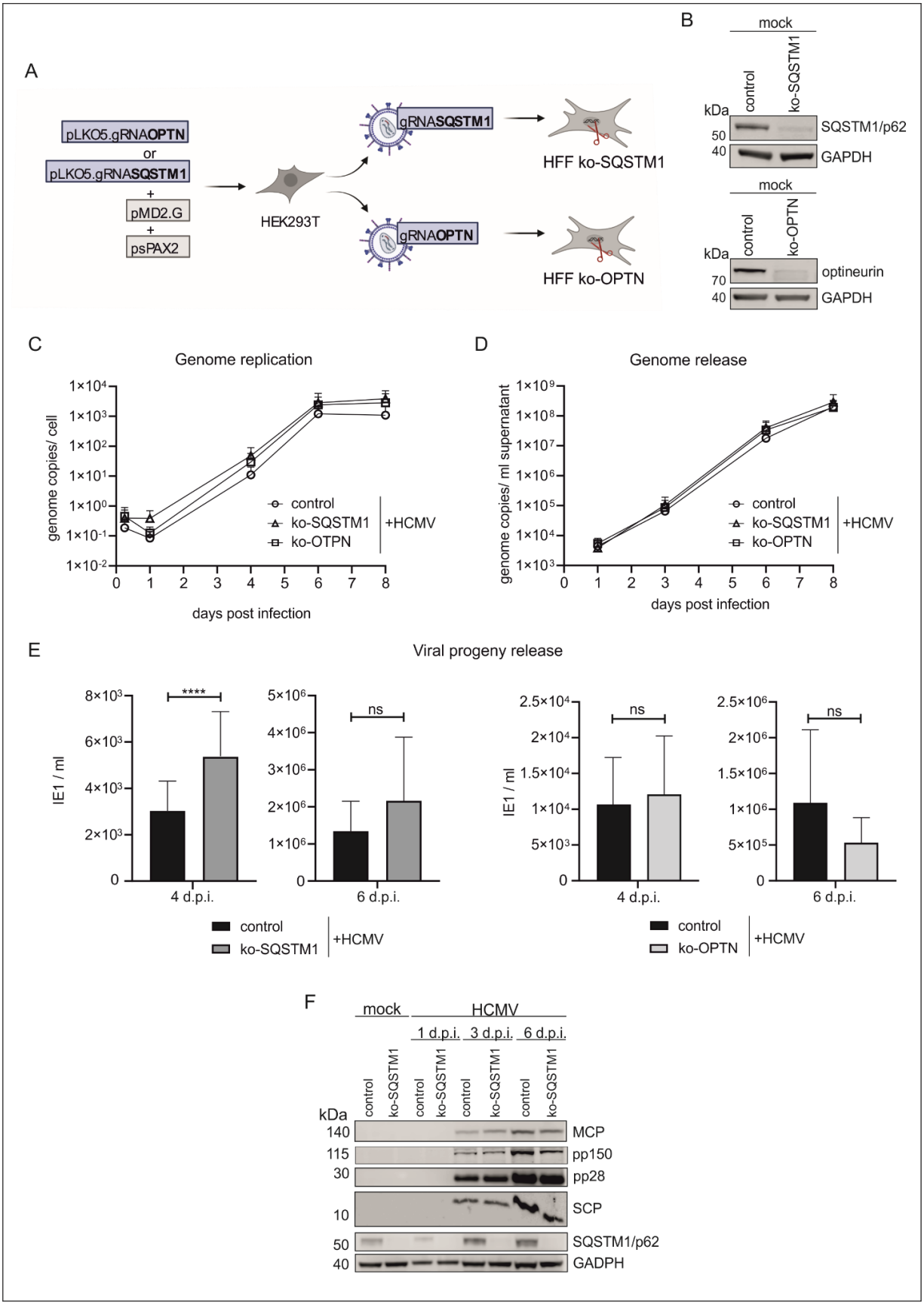
A
pLKO5.gRNAOPTN
or
pLKO5.gRNASQSTM1
+
pMD2.G
+
psPAX2
HEK293T
gRNASQSTM1
gRNAOPTN
HFF ko-SQSTM1
HFF ko-OPTN
B
mock
control
ko-SQSTM1
kDa
50
40
SQSTM1/p62
GAPDH
mock
control
ko-OPTN
kDa
70
40
optineurin
GAPDH
C
Genome replication
genome copies/ cell
days post infection
control
ko-SQSTM1
ko-OTPN
+HCMV
D
Genome release
genome copies/ ml supernatant
days post infection
control
ko-SQSTM1
ko-OPTN
+HCMV
E
Viral progeny release
IE1 / ml
****
ns
4 d.p.i.
6 d.p.i.
control
ko-SQSTM1
+HCMV
control
ko-OPTN
+HCMV
F
mock
HCMV
1 d.p.i.
3 d.p.i.
6 d.p.i.
control
ko-SQSTM1
kDa
140
115
30
10
50
40
MCP
pp150
pp28
SCP
SQSTM1/p62
GADPH

Figure 5. Impact of SQSTM1/p62 and optineurin on HCMV. (A) Workflow of the generation of ko-SQSTM1 cells (SQSTM1/p62) and ko-OPTN cells (optineurin), using the CRISPR/Cas9 method. HEK293T were co-transfected with the lentiviral vector pLKO5.gRNA.OPTN or pLKO5.gRNA.SQSTM1, respectively, as well as with plasmids pMD2.G (VSV-G envelope expressing plasmid) and psPAX2 (packaging plasmid). Lentiviruses released from the co-transfected HEK293T were used to transduce HFF in order to obtain the desired HFF knockout cell lines ko-SQSTM1 cells and ko-OPTN cells. This workflow was created with BioRender.com. (B) The knockout of both genes was confirmed by Western blot, using specific antibodies against both SQSTM1/p62 and optineurin. (C) Viral DNA replication in dependence on *SQSTM1* or *OPTN* was investigated. ko-SQSTM1 cells, ko-OPTN cells and control cells were infected with HCMV (4 genome copies/cell), and collected at the indicated time points post infection. Genome copies of the isolated viral DNA were determined by TaqMan qPCR and are shown for each cell line and the corresponding time point in a diagram. Each value represents the mean of triplicate determinations from three independent experiments. The corresponding standard deviation (SD) is represented as an error bar. (D) Determination of HCMV genome copies, released from infected cells at 4 and 6 d.p.i. Viral DNA was purified and analyzed by qPCR. The graphic shows the mean values + SD of triplicate determinations from three independent experiments for each knockout cell line and time point. (E) HCMV progeny release in the absence of either SQSTM1/p62 or optineurin, measured by IE1-assay. The cell culture medium of HCMV-infected ko-SQSTM1, ko-OPTN and control cells were collected at 4 and 6 d.p.i. Infectivity of viral progeny was analyzed by counting IE1-positive cells in serial dilutions of the supernatants on indicator HFF. The data represent mean values + SD of eight technical replicates from four (ko-SQSTM1) or three (ko-OPTN) individual experiments for each cell line and the corresponding time point. The statistical analysis was performed by utilizing Welch's t-test, not significant (ns): $p>0.05$ and ****: $p\leq0.0001$. (F) Western blot analysis of the intracellular levels of selected viral proteins following infection of ko-SQSTM1 cells and control HFF with HCMV (m.o.i.= 0.5). Cells were harvested at 1, 3, and 6 d.p.i., lysed, and probed by Western blot, using antibodies against selected HCMV proteins MCP, pp150, pp28 and small capsid protein (SCP). The levels of glyceraldehyde 3-phosphate dehydrogenase (GAPDH) were used as loading control. Shown is one representative Western blot out of two experiments.

To exclude an HCMV strain-specific impact on viral progeny release by SQSTM1/p62 or optineurin, the analyses were repeated, using an HCMV strain, TB40/E, which, in its composition, is closely related to clinical HCMV isolates. The same experimental setup was used, infecting cells with an m.o.i. of 0.5 and collecting supernatants at 4 and 6 d.p.i. from both autophagy receptor knockout cell lines and control cells. First, the extracellular DNA levels of the supernatants were determined by analyzing HCMV genome copies by quantitative PCR (Figure 6A). As with BADwt, similar viral DNA levels were released from the ko-cells, infected for 4 and 6 days with the strain TB40/E in comparison with the release from control cells. The progeny release from infected ko-SQSTM1 cells in comparison to control cells was as also elevated at 4 d.p.i., also confirming the results obtained with the HCMV strain BADwt (Figure 6B). The absence of optineurin, again, had no impact on HCMV progeny release when using the strain TB40/E. Lastly, it was investigated if the detected expression kinetics of viral proteins was as well altered in TB40/E infected ko-

SQSTM1 cells compared with control cells. Again, Western blot analysis was performed on the lysates of infected cells (m.o.i. of 0.5), obtained at 1, 3 and 6 d.p.i., respectively Figure 6C). Several HCMV proteins were tested, including MCP, pp150, pp28, and SCP. As before, viral protein levels were notably decreased in the absence of SQSTM1/p62 and the effect was already clearly visible already at 3 d.p.i.

Taken together, these data confirm the results obtained with the HCMV laboratory strain BADwt.

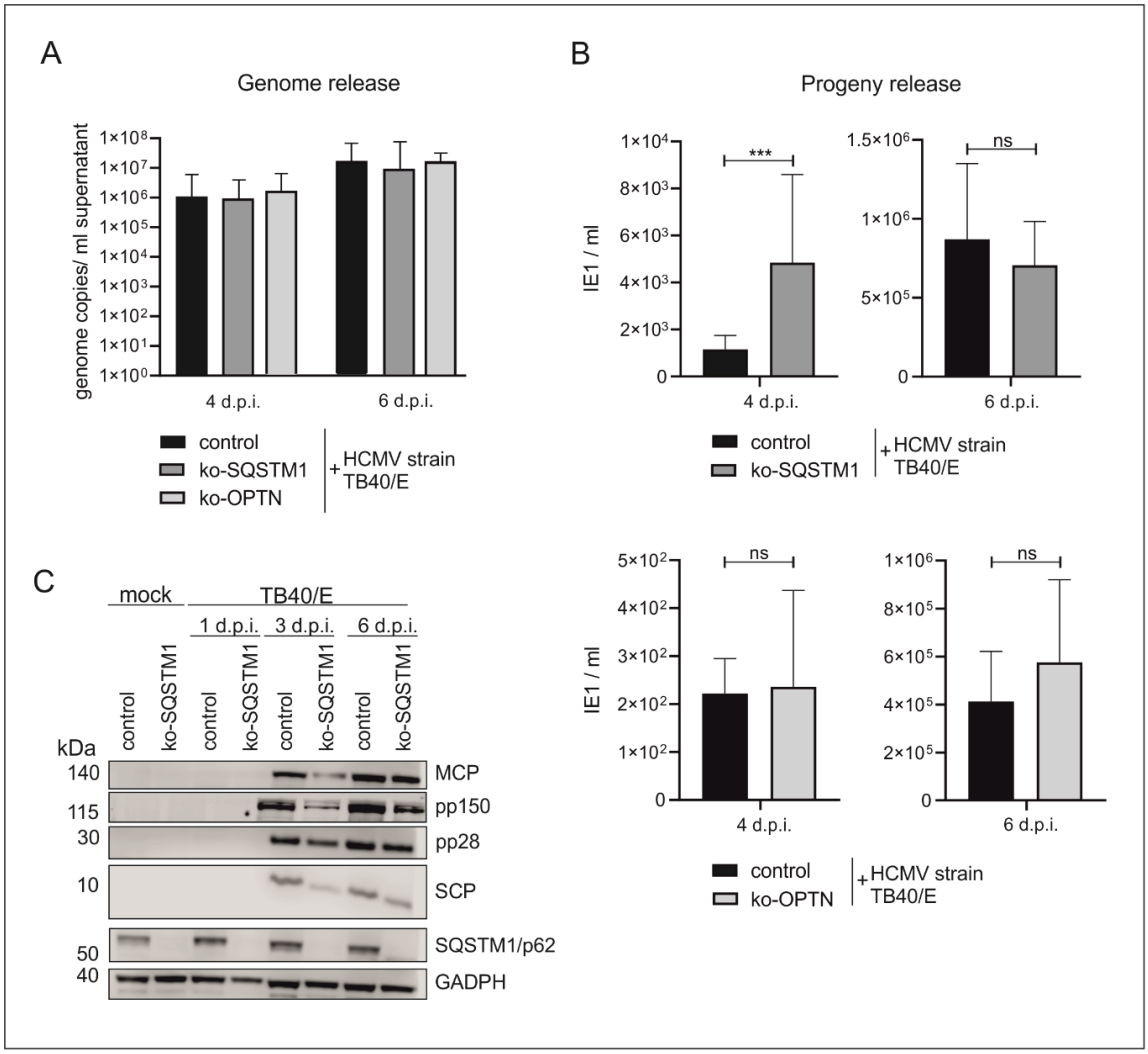

Figure 6. Impact of SQSTM1/p62 and optineurin on HCMV, using the clinical HCMV strain TB40/E for infection. (A) Determination of HCMV genome copies per ml supernatant, released from ko-SQSTM1, ko-OPTN and control cells, infected with the HCMV clinical strain TB40/E for 4 and 6 days. The isolated viral DNA was analyzed by quantitative PCR. The mean values of three technical replicates are shown as a bar graph with the corresponding SD as error bars. (B) HCMV progeny release in the absence of either SQSTM1/p62 or optineurin, measured by IE1-assay. The cell culture medium of TB40/E infected (m.o.i.= 0.5) ko-SQSTM1, ko-OPTN and control cells was respectively collected at 4 and 6 d.p.i. and analyzed by counting IE1-positive cells. The titer of infectious virus is shown in bar charts and the data represent mean values + SD of eight technical replicates from three individual experiments for each cell line and the corresponding time point. The

statistical analysis was performed by utilizing Welch's t-test (not significant (ns): $p>0.05$ and ***: $p\leq0.001$. (C) Western blot analysis of the intracellular levels of selected viral proteins, following infection of ko-SQSTM1 cells and control cells (TB40/E; m.o.i.= 0.5). Cells were collected at 1, 3, and 6 d.p.i., lysed and analyzed by Western blot, using antibodies against selected HCMV proteins (MCP, pp150, pp28 and SCP). The levels of GAPDH were used as loading control. Shown is one representative Western blot out of two experiments.

4.1.3 SQSTM1/p62 and optineurin do not affect autophagy in HCMV-infected cells

The absence of SQSTM1/p62 enhanced HCMV progeny release. One possible explanation for this was that the absence of the autophagy receptor impaired the autophagy process as a whole, thus also impairing degradation of nascent HCMV virions and enhancing virion release. SQSTM1/p62 and optineurin can form an autophagy receptor complex and thereby activating autophagy and the autophagic flux (Liu et al., 2014). Wu et al., showed that the overexpression of SQSTM1/p62 can induce autophagy in carcinoma cells, while optineurin can also regulate autophagy induction and autophagosome formation (Bansal et al., 2018; Wu et al., 2020a; Ying and Yue, 2016). To exclude that the observed effect was due to a negative impact on autophagy, the intrinsic defense mechanism was analyzed, using microtubule-associated protein 1 light chain 3 beta (LC3B) as a marker of autophagosomal membranes and to monitor autophagy (Kabeya et al., 2004; Tanida et al., 2008). Two forms of LC3B are detectable upon Western blot analysis: the cytosolic form, LC3BI, and the autophagosomal membrane-bound form, LC3BII. During autophagosomal membrane formation, pro-LC3B is cleaved to LC3BI, which is then conjugated to phosphatidylethanolamine (PE) to LC3BII (Kabeya et al., 2004; Tanida et al., 2008; Weidberg et al., 2010). The latter form is covalently bound to autophagic membranes and mediates membrane elongation (Tanida et al., 2008). Thus, the turnover from LC3BI to LC3BII represents the autophagosome formation and autophagy activity levels (Tanida et al., 2005). In order to study the impact of SQSTM1/p62 and optineurin, respectively, on autophagy, LC3BII levels were analyzed by Western blot analyses, using an anti-LC3B-specific antibody. Ko-SQSTM1 cells and ko-OPTN cells were infected with HMCV (m.o.i.=0.5), collected at 1, 3 and 6 d.p.i. and submitted to Western blot analysis (Figure 7A). Infected control cells were carried along. The analysis showed that autophagy was induced in both autophagy receptor knockout cell lines upon HCMV infection (1 d.p.i.) in a way comparable to control cells, represented by the elevated LC3BII levels. LC3BII levels were also comparable in uninfected ko-SQSTM1 cells, ko-OPTN cells, and control cells, as seen by the quantification of the LC3BII levels (Figure 7B). This indicated that the absence of either receptor had also no impact on autophagy in the absence of infection.

Thus, the induction of autophagy was unaffected by the knockout of *SQSTM1* or *OPTN* in infected cells. These findings indicated that the impact of SQSTM1/p62 on HCMV infection was independent of the role of the protein in autophagy regulation.

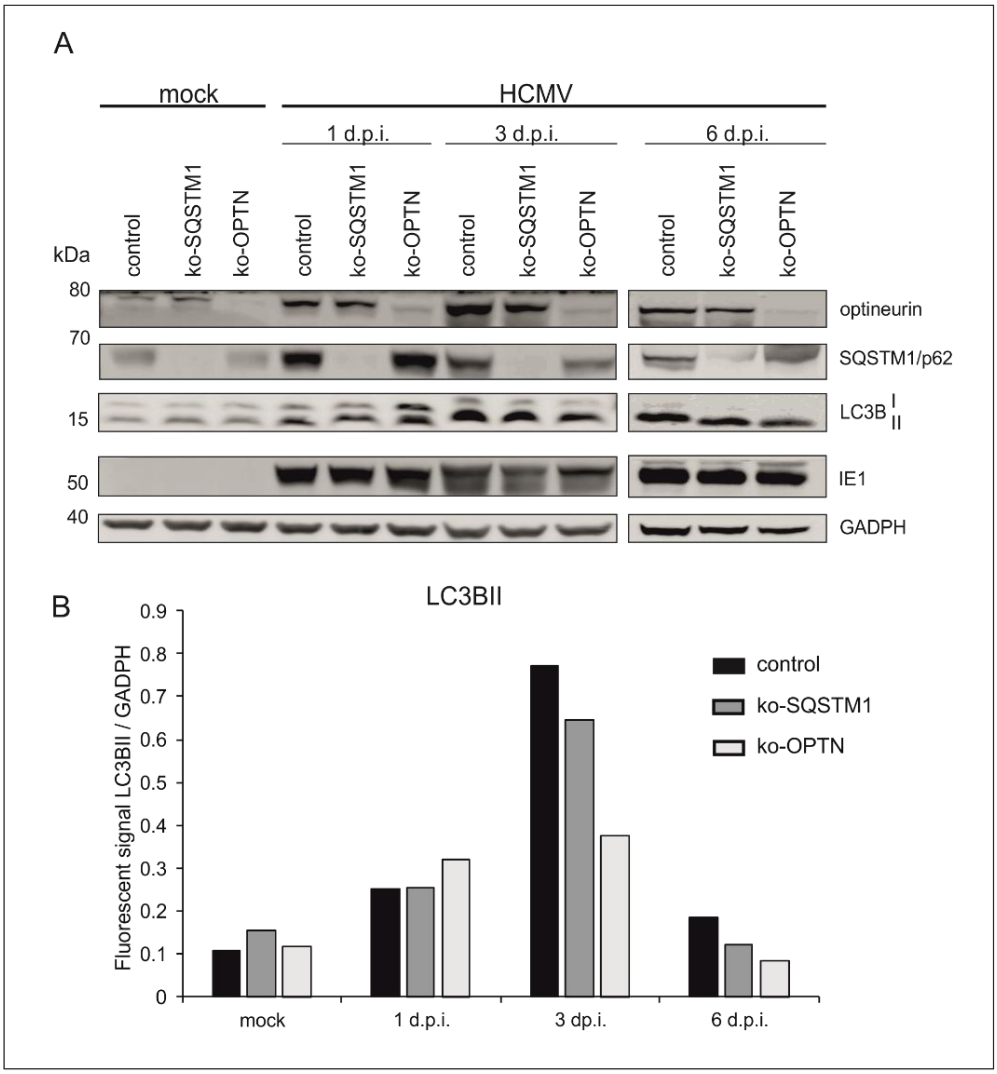

Figure 7. Western blot analysis of the influence of SQSTM1/p62 and optineurin on autophagy. (A) ko-SQSTM1, ko-OPTN, and control cells were infected with HCMV, using an m.o.i. of 0.5. At 1, 3 and 6 d.p.i., cells were collected and autophagy was analyzed by Western blot. As an indicator for autophagy functions, LC3B was used. The turnover of the cytosolic form (LC3BI) to the autophagosomal membrane associated from (LC3BII) was detected with a LC3B-specific antibody. Antibodies against SQSTM1/p62 and optineurin were applied for control. Detection of the viral IE1 protein served as control for HCMV infection. The levels of GAPDH were used as loading control. Shown is a representative Western blot out of four experiments. (B) The fluorescence intensity band ratios of LC3BII to GAPDH were determined and plotted for each cell line and each time point of the Western blot shown in A.

4.1.4 SQSTM1/p62 negatively regulates the levels of selected ISG products in HCMV-infected cells

HCMV replication is highly sensitive to interferon β (IFN-β) and the induction of interferon stimulated genes (ISGs). On the other hand, SQSTM1/p62 is linked to the IFN-I pathway by mediating the degradation of several involved proteins such as the DNA sensor cyclic GMP-AMP synthase (cGAS) or the adaptor protein stimulator of IFN genes (STING) (Chen et al., 2016; Prabakaran et al., 2018). To investigate, whether the impact of SQSTM1/p62 on HCMV infection could be based on an altered IFN-signaling pathway, we analyzed the expression levels of selected ISGs, the interferon induced GTP-binding protein Mx1 (Mx1), and interferon-stimulated gene 15 (ISG15). Both ISG products are well known to be upregulated during HCMV infection (Ashley et al., 2019). Ko-SQSTM1 cells and control cells were infected with HCMV (m.o.i. 0.5) and were collected at 1, 3 d.p.i. and 6 d.p.i.. Cell lysates were subjected to Western blot analysis. The results showed that Mx1 and ISG15 were induced in both cell lines after infection (Figure 8A). Interestingly, the protein levels of both ISGs were higher in infected ko-SQSTM1 cells than in comparison to control cells, which was illustrated by the quantification of Mx1 (Figure 8A and B).

This indicates that the presence of SQSTM1/p62 in HCMV-infected cells restricts interferon signaling and the expression of ISGs, such as Mx1 and ISG15.

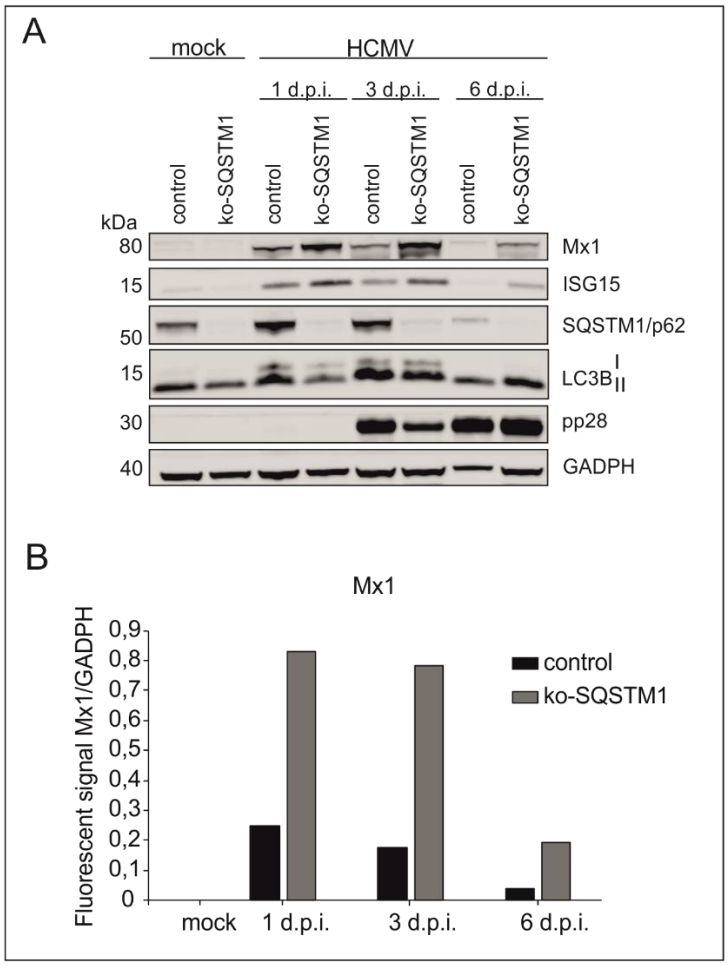

Figure 8. ISGs protein levels in dependence of SQSTM1/p62 in HCMV-infected cells. (A) ko-SQSTM1 and control cells were infected with HCMV, using an m.o.i. of 0.5. At 1, 3 and 6 d.p.i., cells were collected to detect ISG protein levels by Western blot. The membrane was probed with antibodies against ISGs Mx1 and ISG15. Antibodies against LC3B and SQSTM1/p62 were used as controls. Detection of pp28 served as a control for HCMV infection. The levels of GAPDH were used as loading control. Shown is a representative Western blot of four analyses. (B) The fluorescence intensity band ratios of Mx1 to GAPDH were determined and plotted for each cell line and each time point of the Western blot shown in A.

4.2 Analysis of SQSTM1/p62 phosphorylation during HCMV infection

Phosphorylation of autophagy receptors can regulate their ability to bridge the cargo and the autophagic machinery (Farré et al., 2013; Lim et al., 2015; Rogov et al., 2017). For most parts, the phosphorylation regulates binding to LC3 and GABARAP proteins, attached to autophagosomal membranes (Rogov et al., 2017; Wild et al., 2011). However, it also regulates the receptor affinity for ubiquitin chains and facilitates dimer to monomer transition (Gubas and Dikic, 2022; Lim et al., 2015). Thus, the selectivity of autophagy receptors towards cargo is, at least in part, influenced by phosphorylation (Gubas and Dikic, 2022). SQSTM1/p62 has been identified as an autophagy receptor in HCMV-infected fibroblasts that interacts with viral proteins. Thus, the hypothesis was that the phosphorylation status of SQSTM1/p62 changes upon HCMV infection, regulating the ability of SQSTM1/p62 to bind and deliver cargo to the autophagic machinery.

Several questions were addressed:

1. Does the phosphorylation status of SQSTM1/p62 change upon HCMV infection?

2. What is the impact of the phosphorylation status on HCMV infection and autophagy?

3. Does the phosphorylation status regulate the selectivity of SQSTM1/p62 towards its cargo?

4.2.1 Investigation of SQSTM1/p62 phosphorylation status in dependence on HCMV

In this section, the hypothesis that the phosphorylation status of SQSTM1/p62 was altered in HCMV-infected cells was investigated. The aim was to examine the phosphorylation level of SQSTM1/p62 by comparing infected and uninfected cells, using MS analyses. The amount and purity level of endogenous SQSTM1/p62 was not sufficient for phosphoproteomic analysis. To be able to perform these experiments, an HFF cell line stably expressing *GFP-SQSTM1* (HFF-GFP-SQSTM1) was generated (Figure 9A). To obtain this cell line, the lentiviral transduction system was used by inserting *GFP-SQSTM1* into an pLKO5 based vector. A sequence was designed that encoded SQSTM1 with the GFP-coding sequence inserted *in-frame* at the 3'-end. For phosphoproteomic analysis, HFF-GFP-SQSTM1 were infected with HCMV, using an m.o.i.=1. Both, infected as well non-infected cells were harvested at 3 d.p.i.. Co-IP was performed with an antibody directed against GFP, which was N-terminal tagged to SQSTM1/p62. The phosphorylation status of SQSTM1/p62 was investigated by MS in three biological replicates in collaboration with Lina Herhaus at the Institute of Biochemistry II of the Goethe University Frankfurt/Main, Germany. The results revealed that the phosphorylation of only one phosphosite of SQSTM1/p62, namely at serine at position 272 (S272), was significantly altered upon HCMV

infection (Figure 9B). The phosphorylation at S272 was enhanced following HCMV infection, compared to the phosphorylation level in non-infected cells. Phosphorylation of SQSTM1/p62 was found at other locations, but no significant differences between infected versus non-infected cells were seen.

To confirm the result, Western blot analyses were performed. For this, HFF were infected with HCMV (m.o.i. of 1) and cell lysates were collected at 1, 3 and 6 d.p.i.. The phosphorylation status of SQSTM1/p62 was evaluated by using a phospho-specific antibody against S272. Indeed, an increased phosphorylation of SQSTM1/p62 at S272 upon HCMV infection was observed (Figure 9C). The ratio of phosphorylated SQSTM1/p62 at S272 versus the total protein level was calculated (Figure 9D). The Western blot experiment thus corroborated the MS analyses. Interestingly, the phosphorylation level decreased at 6 d.p.i., indicating that this post-translational modification was regulated during HCMV infection.

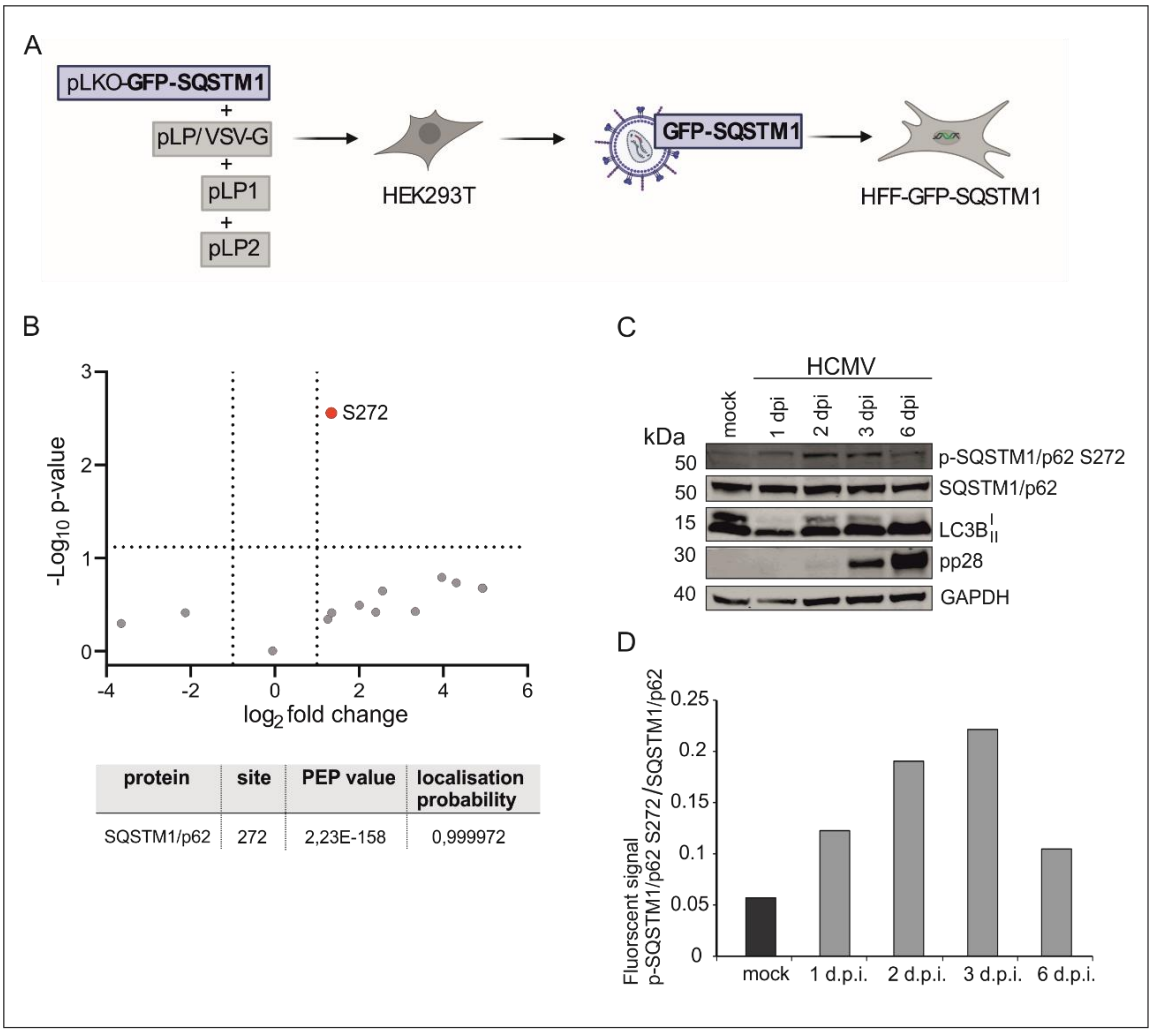

Figure 9. Determination of the phosphorylation status of SQSTM1/p62 during HCMV infection (A) Schematic drawing of the workflow to obtain HFF-GFP-SQSTM1 by lentiviral transduction. HEK293T were transfected with pLKO-GFP-SQSTM1 together with three packaging plasmids pLP1 pLP2 and the pLP/VSV-G plasmid to produce lentiviruses carrying GFP-SQSTM1. Lentiviral supernatant was used to transduce HFF in order to obtain stably expressing HFF-GFP-

SQSTM1. This workflow was created with BioRender.com. (B) MS analysis of the phosphorylation status of SQSTM1/p62 in HCMV-infected versus non-infected HFF-GFP-SQSTM1. The detected phosphorylation sites of SQSTM1/p62 of three biological replicates are displayed in a volcano plot, showing the fold change (x-axis) and significance as $-\log_{10}$ p-value (y-axis). The phosphorylation sites are shown as single data points. Changes in the phosphorylation status at S272 (colored dot) in infected versus non-infected cells reached significance over the threshold for the fold change of $\log_2 \geq 1$ and p-value-$\log_{10} \leq 0.05$, represented by the vertical and horizontal dotted lines, respectively. Phosphorylation sites that were detected but showed no significant differences are shown as gray data points. In order to assess the confidence of identification, the posterior error probability (PEP) and modification localization probability were estimated, and are depicted in the table below. PEP represents the probability that an observed eptide spectrum match (PSM) is incorrect, thus, the lower the value the higher the confidence. Similarly, the modification localization probability (also called false localization rate), represents the probability that a specific residue is carrying the identified modification; values above 75% (0.75) are considered as high confidence. (C) Validation of the phosphoproteomic data in B was performed by Western blot, using a phospho-specific antibody against SQSTM1/p62 S272. Lysates of HCMV-infected normal HFF cells were submitted to SDS-PAGE, followed by Western blot analysis. The phosphorylation level of SQSTM1/p62 at S272 was analyzed at 1, 3, and 6 d.p.i.. The levels of GAPDH were used as loading control. One Western blot of two individual analyses is shown. (D) The relative fluorescence signal of p-SQSTM1/p62 S272 versus the total protein SQSTM1/p62 was determined for different periods of HCMV infection. The ratios were calculated from the Western blot shown in C and the respective ratios of mock and 1, 3, and 6 d.p.i. were plotted on a bar graph.

4.2.2 Cloning of HCMV-SQSTM1-mutants, containing SQSTM1/p62 with amino acid substitutions at position 272

In a next step, the question was addressed, whether the phosphorylation at residue S272 of SQSTM1/p62 had a direct impact on HCMV infection. For this, HCMV mutants were generated by the BAC-technology that expressed different S272-variants of SQSTM1/p62 (Figure 10). Either the wild-type *SQSTM1* gene or mutants thereof at S272 were inserted into the HCMV genome. In these mutant versions, the serine (S) of S272 was replaced by either alanine (A), aspartate (D) or glutamate (E). Alanine cannot be phosphorylated, thus resulting in a mutant that permanently lacks a phosphoresidue at position S272. The replacement of serine by negatively charged amino acids, such as aspartate or glutamate mimics phosphorylation. A BACmid containing the complete genomic sequence of the HCMV strain BADwt was used for mutagenesis. First, the non-essential gene region *UL1-6* of the HCMV genome was deleted from this BACmid by inserting the bacterial *galK* gene (Borst and Messerle, 2005; Van Damme and Van Loock, 2014), using positive selection (Warming et al., 2005). To initially exclude that the deletion of the non-essential gene region *UL1-6* resulted in an HCMV replication deficit, the BACmid pHCMV-ΔUL1-6 was reconstituted in HFF, thereby generating the strain HCMV-ΔUL1-6. The genome replication of this virus was compared to wild-type virus by performing quantitative PCR using virus-specific primers. The results showed that the absence of UL1-6 had no impact on HCMV infection (Figure 11) and thus the BACmid pHCMV-ΔUL1-6 was used for

further mutagenesis. In a second step, *galK* was replaced by the coding sequences of SQSTM1/p62 with either an alanine, aspartate, glutamate or serine (wt-version) at position 272, using negative selection (Figure 10) (Warming et al., 2005). For gene expression, the major immediate early promotor (MIEP) of HCMV containing a non-functional cis repressive sequence (crs) was inserted upstream, allowing for permanent expression throughout infection (Isomura et al., 2008; Lang and Stamminger, 1993). The correct integration of the *SQSTM1* sequences into the HCMV genome was confirmed by nucleotide sequencing. Upon reconstitution of the BACmids in HFF, the following HCMV-SQSTM1-phosphomutants were generated: HCMV-SQSTM1-S272wt, HCMV-SQSTM1-S272A, HCMV-SQSTM1-S272D and HCMV-SQSTM1-S272E. The mutant viruses and their associated features are summarized in Table 9.

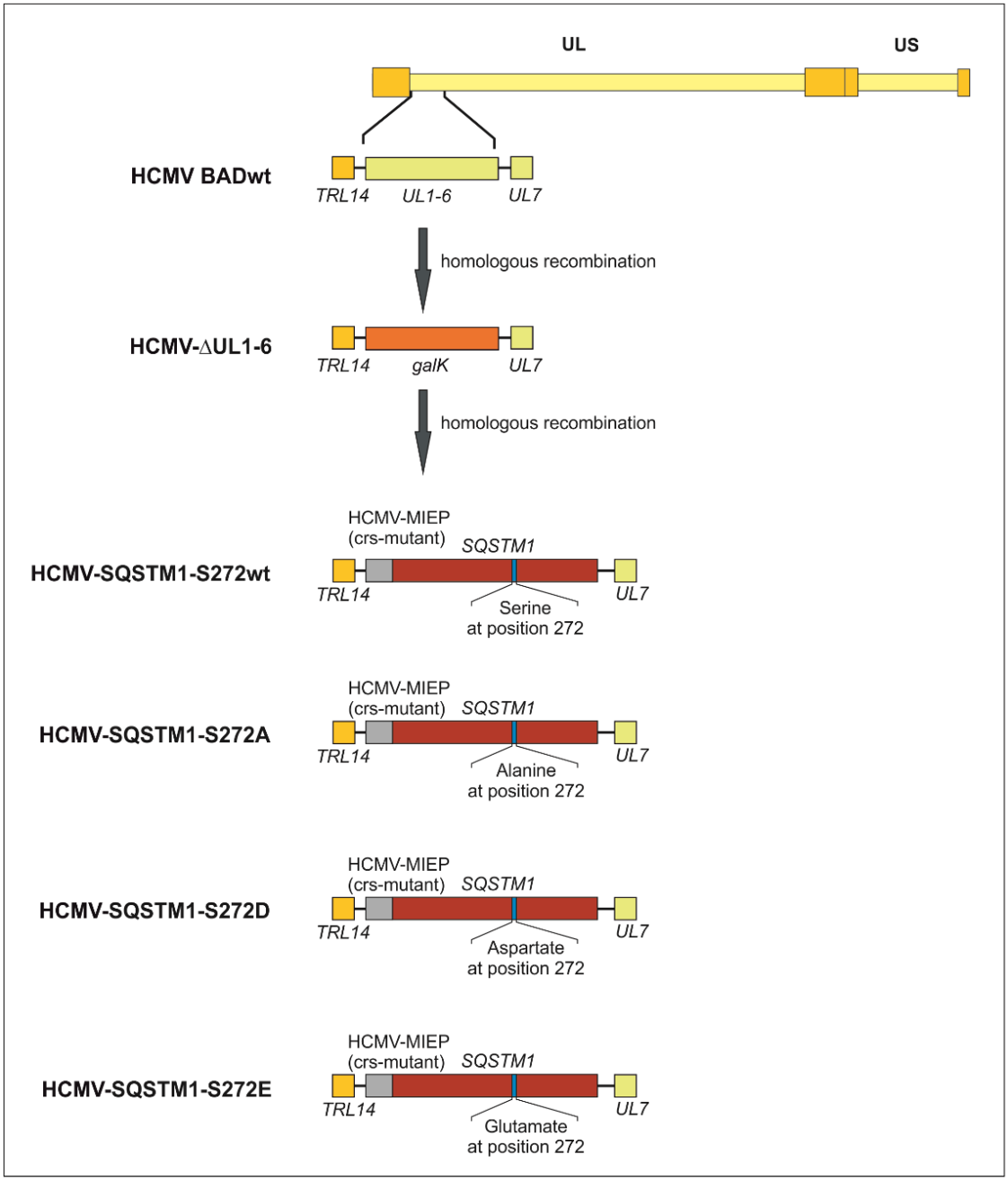

Figure 10. Construction of different HCMV-SQSTM1-S272 strains. All HCMV-SQSTM1-S272 mutants were based on the HCMV parental strain BADwt, which consist of unique long and short genomic segments (UL, US). For generation of mutant strains, the BAC technology was used. In a first step, the gene region *UL1-6* of the parental strain, located between *Terminal Repeat Long 14* (*TRL14*) and *UL7*, was replaced by the *galactokinase* gene (*galK)* to obtain the BACmid HCMV-ΔUL1-6. Reconstitution of this BACmid resulted in the virus HCMV-ΔUL1-6, which served as a control for the deleted gene region. In a second step, *galK* was replaced by DNA-sequences of the *SQSTM1* gene, encoding the different mutations at the position 272 of SQSTM/p62 [serine (wt), alanine (A), aspartate (D) or glutamate (E)]. The BACmids were reconstituted, resulting in the viruses HCMV-SQSTM1-S272wt, HCMV-SQSTM1-S272A, HCMV-SQSTM1-S272D and HCMV-SQSTM1-S272E. In all strains, *SQSTM1* is driven by the modified HCMV major immediate-early promotor (MIEP), which has a nonfunctional cis repressive sequence (crs) to allow a permanent expression of the respective *SQSTM1* sequences in infected cells.

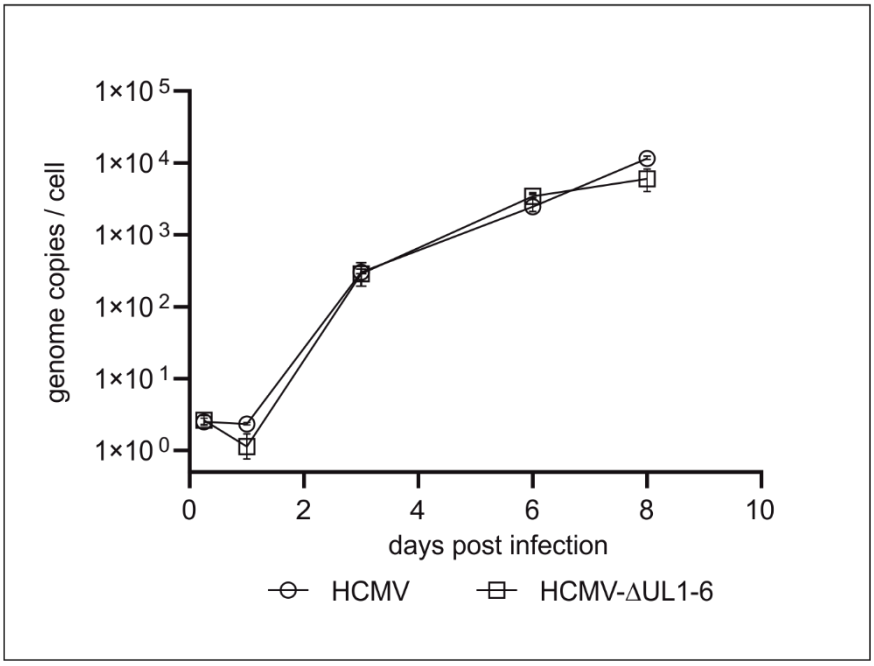

Figure 11. Analysis of viral genome replication of HCMV-ΔUL1-6 in comparison to its parental strain HCMV. HFF were infected with HCMV and HCMV-ΔUL1-6, respectively, using 4 genome copies/cell. Cells were collected at the indicated time points, viral DNA was purified and analyzed by quantitative PCR analysis. The mean values of three technical replicates and the corresponding SD are shown for each virus and the respective time point.

Table 9. HCMV-SQSTM1-S272 strains

HCMV-SQSTM1-S272 strains	**Amino acid at position 272**	**Function**
HCMV-SQSTM1-S272wt	Serine (S)	Can be phosphorylated upon infection
HCMV-SQSTM1-S272A	Alanine (A)	Cannot be phosphorylated upon infection
HCMV-SQSTM1-S272D	Aspartate (D)	Phosphomimicking
HCMV-SQSTM1-S272E	Glutamate (E)	Phosphomimicking

To initially verify the expression of SQSTM1/p62 by each of the reconstituted HCMV-SQSTM1-S272 mutants, the SQSTM1/p62 deficient cell line was infected (m.o.i.=0.5) with the respective viruses. Uninfected ko-SQSTM1 cells and wt cells infected with the parental HCMV strain served as controls. At 5 d.p.i., cells were harvested and analyzed for SQSTM1/p62 expression by Western blot. SQSTM1/p62 was expressed by each of the recombinant viruses, indicating that the mutagenesis of this autophagy receptor was successful (Figure 12A). Increased levels of SQSTM1/p62 were detected after infection of ko-SQSTM1 cells with the mutant viruses, compared to wt HCMV infection in wt HFF. This was expected due to the constitutive overexpression of SQSTM1/p62, driven by the HCMV MIEP. Surprisingly, only a subtly higher protein level was seen in SQSTM1/p62-S272A-infected cells, compared to infected wt HFF.

The phosphorylation status of each HCMV-SQSTM1-S272 mutant was determined by immunoblotting with a phospho-specific antibody against p-SQSTM1/p62-S272. A specific band for SQSTM1/p62 was detectable in HCMV-SQSTM1-S272wt-infected cells, showing that the recombinant protein retained its ability to be phosphorylated (Figure 12B). As expected, no signal was detected when probing lysates from cells, infected with the SQSTM1/p62 mutant viruses, as the used antibody was specific for phosphorylated serine.

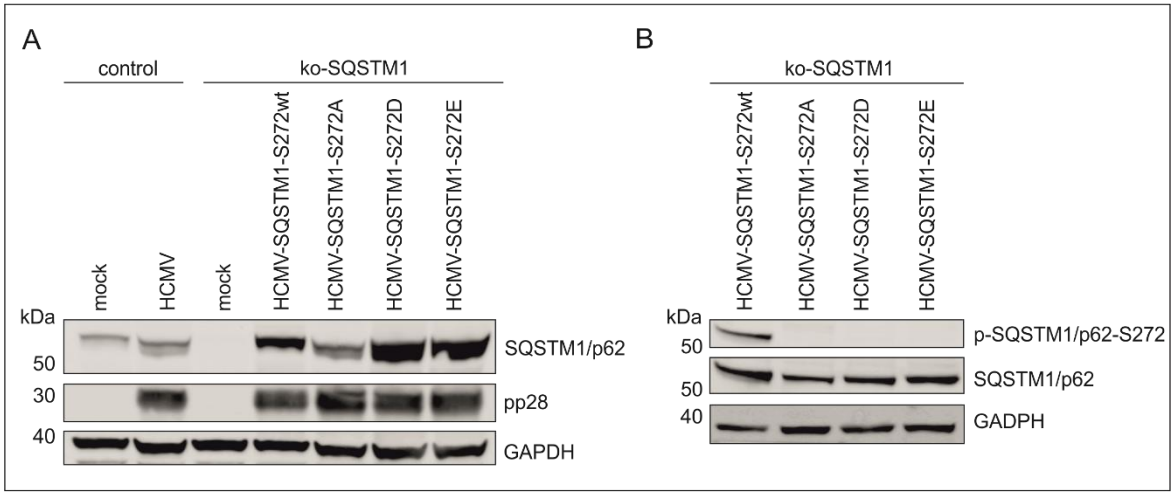

Figure 12. Western blot analysis of the SQSTM1/p62 levels in ko-SQSTM1 cells infected with different HCMV-SQSTM1-S272 strains. (A) Analysis of SQSTM1/p62 levels in ko-SQSTM1 cells, infected with the different HCMV-SQSTM1-S272 strains (wt/ A/ D/ E). HCMV-infected wildtype (wt) HFF were taken as a control for SQSTM1/p62. Lysates of 5 d.p.i. infected cells were collected and analyzed by Western blot with an antibody directed against SQSTM1/p62. The levels of the viral pp28 were used as infection control, the levels of GAPDH were used as loading control. Shown is one representative Western blot out of two analyses. (B) Analysis of the levels of phosphorylation of SQSTM1/p62 at position 272, following infection of ko-SQSTM1 cells. Cells were infected as in A and harvested at 3 d.p.i.. Samples were probed for the phosphorylation level of SQSTM1/p62 at position 272, using a phospho-specific antibody. Shown is a representative Western blot of two analyses.

4.2.3 Impact of the phosphorylation status of SQSTM1/p62 at S272 on HCMV infection

Based on the findings that the autophagy receptor SQSTM1/p62 is hyperphosphorylated at S272 upon HCMV infection, the question arose whether this had implications for viral DNA replication and viral progeny release. In a first attempt to answer this, ko-SQSTM1 cells were infected with HCMV-SQSTM1-S272 mutants, using an m.o.i. of 0.1, representing a low infection rate. Cells were harvested at 6 hours up to 8 d.p.i. for replication analysis and supernatants were collected at 3 and 6 d.p.i. for the analysis of progeny release in the IE1-assay. The DNA that was isolated from the cells was quantified by TaqMan qPCR. There was a delay in viral genome replication for HCMV-SQSTM1-S272D and HCMV-SQSTM1-S272wt (Figure 13A). This indicated that viral genome replication was slightly impaired by phosphorylation of SQSTM1/p62 at S272. In a next step, progeny release from infected cells was analyzed by the IE1-assay. Levels of virus release from HCMV-SQSTM1-S272wt and HCMV-SQSTM1-S272D-infeced cells were comparable (Figure 13B). Progeny release from cells, infected with HCMV-SQSTM1-S272A was increased relative to HCMV-SQSTM1-S272wt-infeced cells. This indicated that phosphorylation at S272 reduced the efficiency of HCMV progeny production. Virus release was also enhanced from HCMV-SQSTM1-

S272E-infected cells. This was surprising as the phenotypes of HCMV-SQSTM1-S272E and HCMV-SQSTM1-S272D should match. It is however well established that replacement of phosphosites by acidic acids not always results in correct mimicking. Therefore, further analyses focused on HCMV-SQSTM1-S272D and the phenotype of HCMV-SQSTM1-S272E was not further evaluated.

To address the impact of S272 phosphorylation on the expression of HCMV late proteins, Western blot analyses were performed. Infection with HCMV-SQSTM1-S272A led to an increase in the levels of all late viral proteins tested, compared to SQSTM1-S272D and SQSTM1-S272wt (Figure 13C). In the same samples, the levels of SQSTM1-S272A were reduced compared the levels of the receptor seen with the other viruses. This showed that the levels of the receptor inversely correlated with the levels of expression of viral structural proteins.

The replacement of S272 by alanine resulted, in summary, in reduced levels of the receptor in infected cells and this correlated with increased viral late protein expression and progeny release.

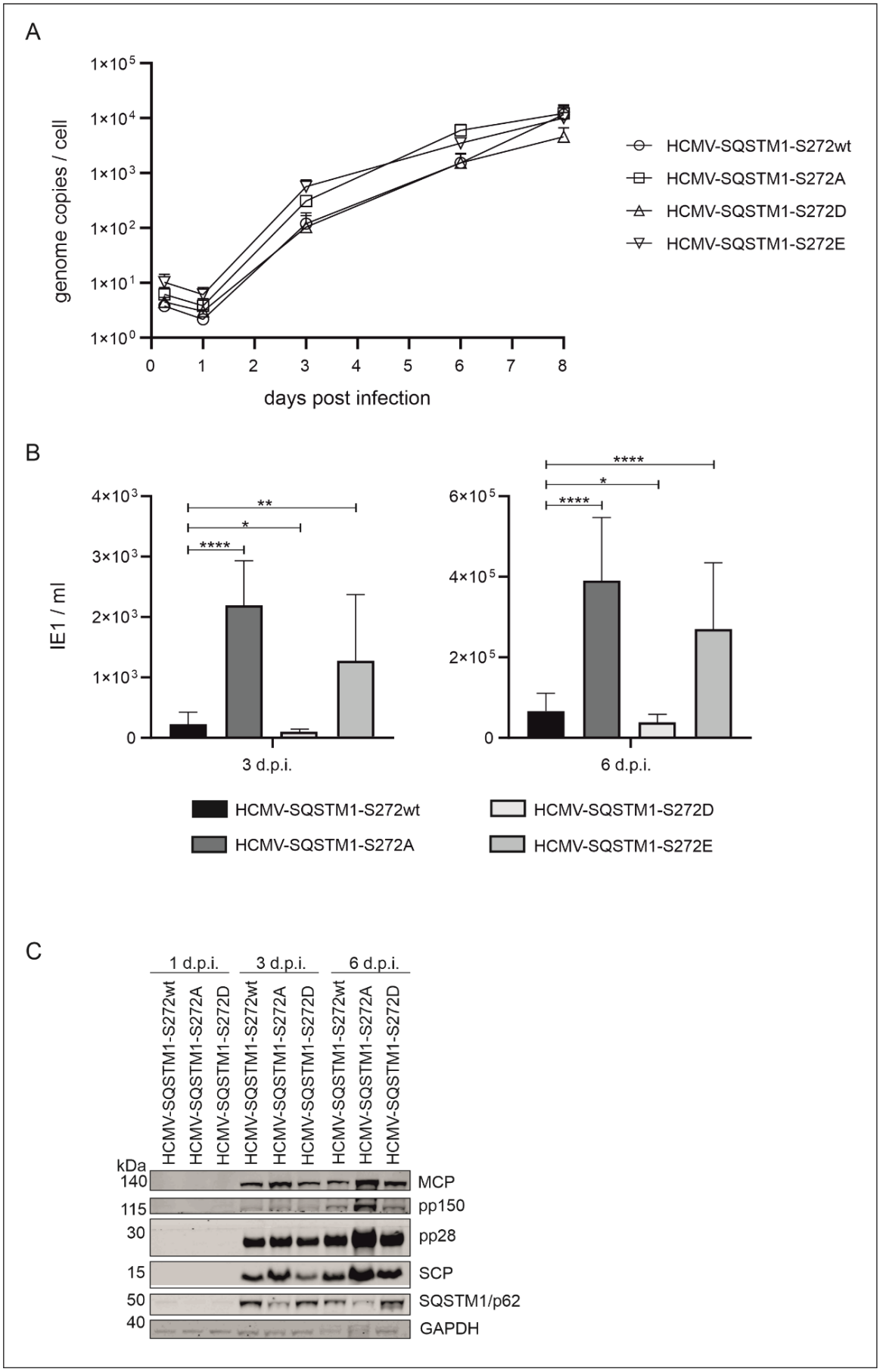
A
genome copies / cell
1×10^5
1×10^4
1×10^3
1×10^2
1×10^1
1×10^0
0 1 2 3 4 5 6 7 8
days post infection
HCMV-SQSTM1-S272wt
HCMV-SQSTM1-S272A
HCMV-SQSTM1-S272D
HCMV-SQSTM1-S272E
B
IE1 / ml
4×10^3
3×10^3
2×10^3
1×10^3
0
**
*
****
3 d.p.i.
6×10^5
4×10^5
2×10^5
0
****
*
****
6 d.p.i.
HCMV-SQSTM1-S272wt
HCMV-SQSTM1-S272A
HCMV-SQSTM1-S272D
HCMV-SQSTM1-S272E
C
1 d.p.i.
3 d.p.i.
6 d.p.i.
HCMV-SQSTM1-S272wt
HCMV-SQSTM1-S272A
HCMV-SQSTM1-S272D
kDa
140
115
30
15
50
40
MCP
pp150
pp28
SCP
SQSTM1/p62
GAPDH

Figure 13. Analysis of viral genome replication and progeny production in dependence on SQSTM1/p62-272 phosphorylation. (A+B) ko-SQSTM1 cells were infected with HCMV-SQSTM1-S272wt, HCMV-SQSTM1-S272A, HCMV-SQSTM1-S272D, and HCMV-SQSTM1-S272E strains, respectively, using an m.o.i. of 0.1. Cells and cell culture supernatants were collected at the indicated time points. The results of three biological replicates are respectively shown. (A) The viral DNA was purified from the cells and subjected to quantitative PCR analysis. The mean values of three technical replicates from three independent experiments are shown for each virus and time point. The corresponding SD is displayed as error bars. (B) Supernatants from 3 and 6 d.p.i. were analyzed by the IE1-assay. The graph represents mean values of eight technical replicates from three independent experiments for each virus and time point. The mean values and corresponding SD are represented in a bar chart with error bars. Statistical analysis was performed utilizing Welch's t-test (not significant (ns): $p>0.05$; *: $p<0.05$; **: $p<0.01$; and ****: $p<0.0001$). (C) Western blot analysis of the intracellular levels of selected viral proteins following infection of ko-SQSTM1 with HCMV-SQSTM1-S272wt, -S272A, and -S272D (m.o.i.=0.1). Cells were harvested at 1, 3, and 6 d.p.i., lysed, and probed by Western blot, using antibodies against HCMV proteins MCP, pp150, pp28 and SCP. The levels of GAPDH were used as loading control. One out of two individual experiments is shown.

4.2.4 Phosphorylation of SQSTM1/p62 at S272 prevents the receptor from proteasomal degradation HCMV-infected cells

SQSTM1/p62 protein levels were reduced in HCMV-SQSTM1-S272A-infeced cells, compared to the levels seen after infection with the other mutant viruses. Nucleotide sequencing had not revealed any unintentional mutations within the promotor region of *SQSTM1*, thus rendering altered gene expression as the reason for different protein levels unlikely. This indicated that of the amount of SQSTM1/p62-S272A was regulated on the protein level and that the phosphorylation at position 272 was important for the SQSTM1/p62 protein stability in infected cells.

To investigate, if the absence of S272 phosphorylation resulted in increased protein degradation, ko-SQSTM1 cells were infected with the different HCMV-SQSTM1-S272 strains. Proteasomal degradation was addressed by adding the inhibitor MG132 to the cultures. To block lysosomal degradation of autophagosomes, Bafilomycin A1 was added. In both approaches, DMSO was added as control. Cell lysates were probed for SQSTM1/p62 levels by Western blot. Addition of MG132 restored SQSTM1/p62-272A to wt levels, indicating that the phosphorylation of SQSTM1/p62 at serine 272 had an impact on its proteasomal degradation (Figure 14A). The prevention of lysosomal degradation did not affect the SQSTM1/p62 level (Figure 14B).

In an attempt to equilibrate the SQSTM1/p62 protein levels, the m.o.i. for HCMV-SQSTM1-S272wt was reduced in order to reach equal proteins levels. Ko-SQSTM1 cells were infected with either HCMV-SQSTM1-S272A with an m.o.i. of 0.2 or with HCMV-SQSTM1-S272wt with an m.o.i. of 0.2, 0.1, and 0.05, respectively. Cells were harvested after 6 d.p.i., and SQSTM1/p62 levels were analyzed by Western blot. The analysis showed that

infection with even low levels of HCMV-SQSTM1-S272wt did not result in low protein levels of SQSTM1/p62 comparable to those after SQSTM1-p62-S272A infection (Figure 14C). This confirmed the finding that the protein stability of SQSTM1/p62 in HCMV-infected cells is dependent on the phosphorylation status at residue S272 and that the lack of a phosphate residue at this position markedly reduced the stability of the protein. Furthermore, this corroborated the notion that low levels of SQSTM1/p62 lead to enhancement of viral infection, represented by the levels of the late viral protein pp28 in cells, infected with the same m.o.i. (here 0.2).

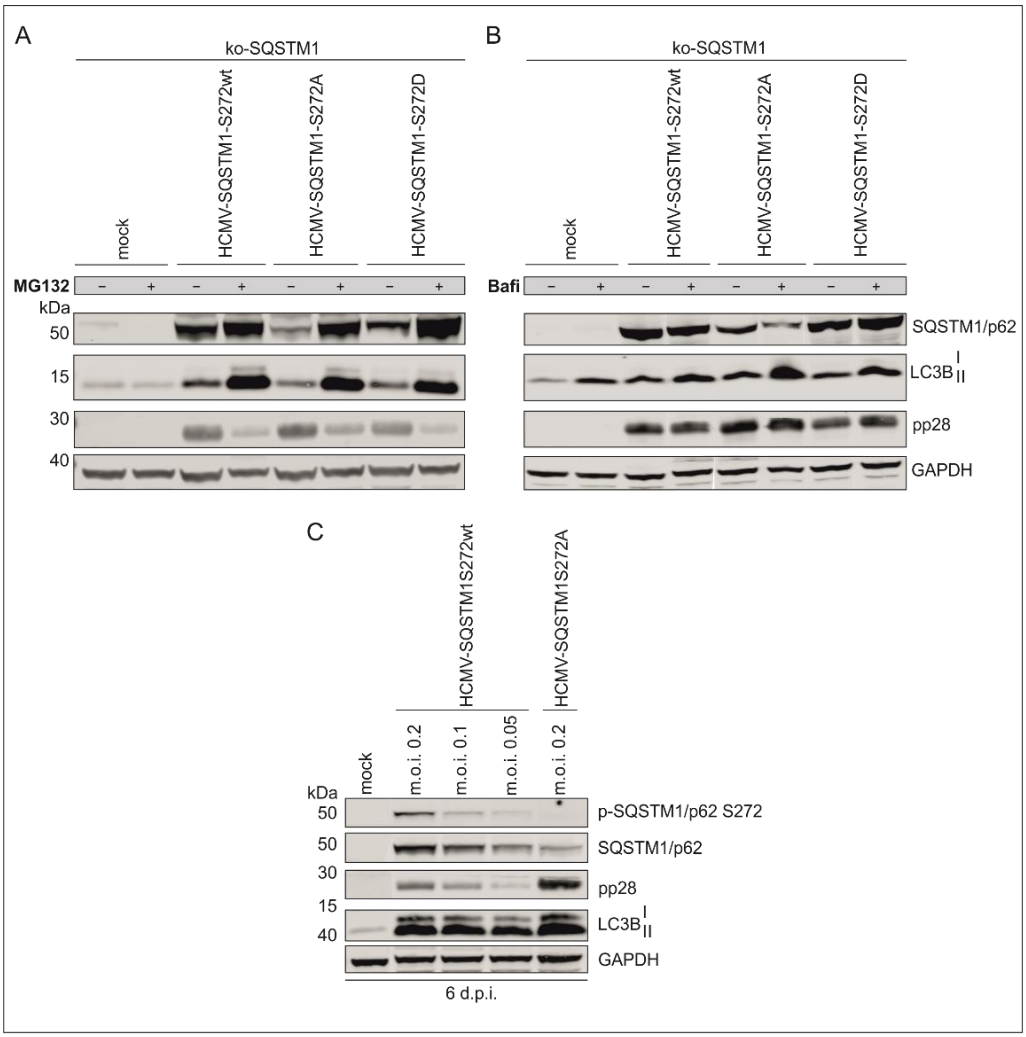

Figure 14. Western blot analysis of the impact of p272-phosphorylation on proteasomal and lysosomal degradation of SQSTM1/p62 (A) Western blot analysis of SQSTM1/p62-levels following 5-day infection of ko-SQSTM1 cells with respective HCMV-SQSTM1-S272 strains (wt/ D/ A) using an m.o.i. of 0.2. Cells were treated with 10 µM of the proteasomal inhibitor MG132 18 hours before sample collection. One of two individual experiments is shown. (B) Western blot analysis of SQSTM1/p62-levels using 200 µM of the lysosomal inhibitor Bafilomycin (Bafi) 4 hours before cell harvest, n=1. (C) Western blot analysis of SQSTM1/p62-levels of HCMV-SQSTM1-S272wt and HCMV-SQSTM1-S272A infected ko-SQSTM1 cells at 6 d.p.i. Different m.o.i. of HCMV-SQSTM1-S272wt were used (0.2, 0.1 and 0.05), n=1. (A, B, C) Cell lysates were probed with antibodies against SQSTM1/p62, p-SQSTM1/p62 S272, pp28 (virus control), GAPDH (loading control), LC3B served as control for inhibition of both degradation processes.

4.2.5 The phosphorylation status of SQSTM1/p62 at its residue 272 does not affect induction of autophagy in HCMV-infected cells

Linares and colleagues previously showed that phosphorylation of SQSTM1/p62 at S272 activates a cellular complex that restricts autophagy (Linares et al., 2015). Thus, the question was asked if the same was true in HCMV-infected cells. Ko-SQSTM1 cells were infected with HCMV-SQSTM1-S272wt, HCMV-SQSTM1-S272A and HCMV-SQSTM1-S272D (m.o.i. 0.2). Infected cells were collected at 1, 3 and 6 d.p.i.. The induction of autophagy in these cells was analyzed by Western blot by measuring the levels of LC3BII. Different controls were carried along, including non-infected ko-SQSTM1 cells and HFF, either uninfected or infected with HCMV. As expected, Western blot analysis showed an induction of autophagy in ko-SQSTM1 cells, infected with HCMV-SQSTM1-S272wt and the -S272A or -272D mutants at 3 and 6 d.p.i., as indicated by increased LC3BII levels in comparison to uninfected cells (Figure 15A). No differences in the LC3BII levels were, however, found at all investigated time points between the respective HCMV-SQSTM1-S272 mutants. The analysis showed that the phosphorylation status of SQSTM1/p62 at S272 does not regulate autophagy in HCMV-infected cells. Interestingly, LC3BII levels were similar in all infected cells, indicating that neither the phosphorylation status of SQSTM1/p62 at S272 nor the protein level of this receptor had an impact on autophagosome formation during HCMV infection. This was illustrated by the quantification of the respective LC3BII levels (Figure 15B).

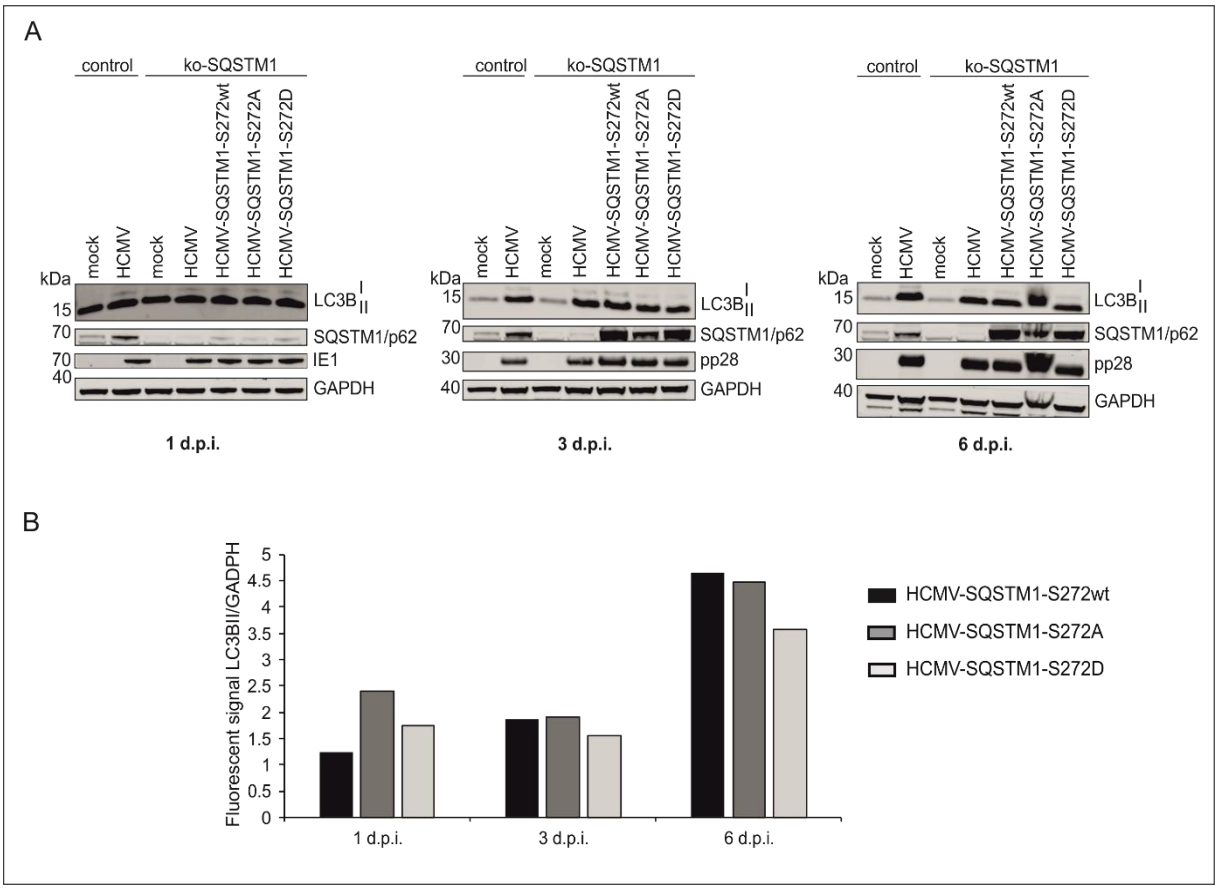

Figure 15. Western blot analysis of the impact of phosphorylation at S272 of SQSTM1/p62 on autophagy. (A) ko-SQSTM1 cells were infected with an m.o.i. of 0.2 of the indicated strains. Cells were harvested at 1, 3, and 6 d.p.i.. Western blot analysis was performed to detect the autophagic marker LC3BII, representing the induction of autophagy, using antibodies against LC3B (autophagy control), SQSTM1/p62, IE1 and pp28 (virus control), and GAPDH (loading control). One representative Western blot out of three individual analyses is shown. (B) The fluorescence intensity ratios of the bands for LC3BII versus GAPDH were calculated of a representative Western blot. Evaluation of the analyzed time points (1, 3, and 6 d.p.i.) was plotted in a bar diagram.

4.2.1 Phosphorylation of SQSTM1/p62 at S272 positively correlates with ISG-expression in HCMV-infected cells

SQSTM1/p62 influences a number of cellular processes. One of these relates to the control of the IFN-I pathway. This is mediated by the degradation of STING or cGAS, leading to reduced IFN-I production and reduced induction of ISGs (Chen et al., 2016; Prabakaran et al., 2018). In this work, the impact of SQSTM1/p62 on the induction of ISGs in HCMV-infected cells was investigated, showing that the deletion of the receptor led to increased ISG protein levels of Mx1 and ISG15 (Figure 8). To investigate if the phosphorylation at the site 272 of SQSTM1/p62 had also an influence on the IFN-I signaling pathway, ISG protein levels were analyzed. For this, ko-SQSTM1 cells were infected with the different HCMV-SQSTM1-S272 mutants. The cells were collected at 1, 3, and 6 d.p.i. and subjected to Western

blot analysis. Interestingly, the protein levels of the ISGs were distinctly reduced in ko-SQSTM1 cells, infected with HCMV-SQSTM1-S272A, compared to infection with HCMV-SQSTM1-S272wt and HCMV-SQSTM1-S272D (Figure 16A and B). As HCMV replication is impeded by ISG-induction (Schoggins, 2019; Schoggins and Rice, 2011), the decreased Mx1 and ISG15 levels might thus also explain the elevated progeny release from HCMV-SQSTM1-S272A-infected cells. Interestingly, as SQSTM1/p62 levels were comparable in HCMV-SQSTM1-S272D- and HCMV-SQSTM1-S272A-infected cells at 3 d.p.i., differences in the amount of receptor proteins cannot account for the differences in ISG induction. Thus, these results indicate that the phosphorylation at S272 enhances the interferon response in HCMV-infected cells.

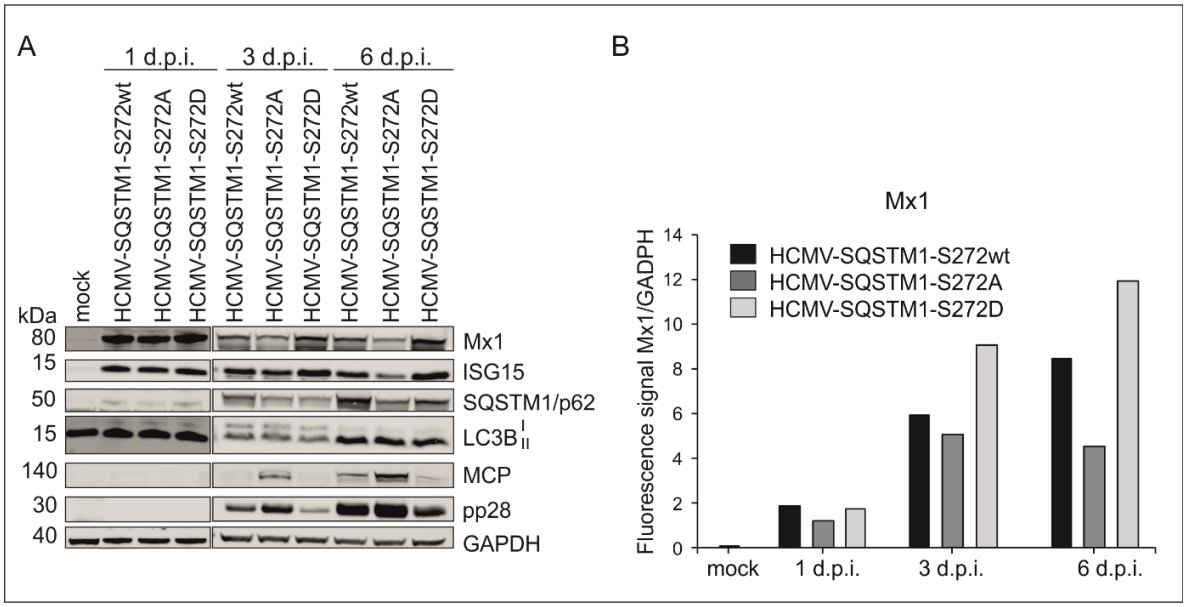

Figure 16. Western blot analysis of the impact of HCMV-SQSTM1-S272 mutants on ISG protein levels in infected cells. Ko-SQSTM1 cells were infected at an m.o.i. of 0.2 with the different HCMV-SQSTM1-S272 strains (wt/ A/ D). Cells were harvested 1, 3, or 6 d.p.i.. Cell lysates were subjected to Western blot analysis. Membranes were probed against ISGs Mx1 and ISG15. Antibodies against SQSTM1/p62, LC3B (autophagy induction), pp28 (virus control), and GAPDH (loading control) were used for control. One representative Western blot out of three individual analyses is shown. (B) The fluorescence intensity ratios of the band for Mx1 versus GAPDH were calculated of the represented Western blot, shown in A. Evaluation of the analyzed time points (1, 3, and 6 d.p.i.) and mock were plotted in a bar diagram.

4.2.2 Impact of SQSTM1/p62 phosphorylation at position 272 on its interaction with other proteins

The phosphorylation of autophagy receptors is known to regulate their affinity for their cargo and their interaction with autophagy machinery components (Gubas and Dikic, 2022). Thus, the hypothesis was tested that the phosphorylation of SQSTM1/p62 at S272 regulated the binding of the autophagy receptor to both viral and cellular proteins. This was analyzed by MS. Ko-SQSTM1 cells were infected with HCMV-SQSTM1-S272wt, HCMV-SQSTM1-S272A, and HCMV-SQSTM1-S272D, respectively, using an m.o.i. of 0.5. Cells were collected at 3 d.p.i.. SQSTM1/p62 was co-immunoprecipitated using a receptor-specific antibody. The amount of SQSTM1/p62 used for IP was adjusted to control for reduced steady-state levels of HCMV-SQSTM1-S272A-infected cells by using twice the number of lysed cells for IP against SQSTM1-S272A, compared to SQSTM1-S272wt or SQSTM1-S272D. Samples were analyzed in collaboration with Lina Herhaus, the Institute of Biochemistry II of the Goethe University Frankfurt/Main, Germany.

The aim was to identify the target proteins of SQSTM1/p62-S272wt, SQSTM1/p62-S272A, and SQSTM1/p62-S272D, respectively, and to elaborate whether the phosphorylation status had an impact on the binding preferences of these receptors. This required two main steps: first, proteins that significantly co-precipitated with the respective receptors had to be determined by analyzing the precipitates against SQSTM1/p62 of the three receptor mutants against the IgG control precipitates. Significantly co-precipitated proteins were identified using a right-sided t-test, which provided the log2-fold change values (raw data). Second, since the levels of SQSTM1/p62 after precipitations were still slightly different, the raw data set of each precipitation was normalized to the respective SQSTM1/p62 levels. The normalization eliminated possible false positives coming from just a higher abundance of SQSTM1/p62.

An unusually high number of proteins were identified in the precipitates with the different SQSTM1/p62-S272 mutants. This was especially true for SQSTM1/p62-S272A. After t-test analysis and normalization, 181 cellular proteins overall significantly co-precipitated with at least one receptor version of SQSTM1/p62-S272. The normalized log2 fold change values for each protein are shown in a heat map as a color gradient (Figure 17A). The respective p-values and log2 fold change values are shown in a table in the appendix (A1).

According to these criteria, SQSTM1/p62-S272wt interacted with 28 cellular proteins. The same set of proteins interacted with SQSTM1/p62-S272A, and a subset of 20 of these also precipitated with SQSTM1/p62-S272D. These results suggested that the association of these 20 proteins with SQSTM1/p62 was independent of the phosphorylation status of the receptor at S272.

103 cellular proteins were found in SQSTM1/p62-S272D precipitate samples. As alluded to above, 20 of these proteins were also found in the SQSTM1/p62-S272wt samples, whereas

8 of those, found with the latter version of the receptors did not precipitate with SQSTM1/p62-S272D. This might indicate that the interaction of these 8 proteins was dependent on the S272-phosphorylation status of the receptor. However, as the precipitate samples of SQSTM1/p62-S272A also contained these proteins, a role of S272 phosphorylation for the interaction with these 8 proteins appears questionable.

The phosphomimicking variant of the receptor SQSTM1/p62-S272D precipitated several further cellular proteins which were not found in SQSTM1/p62-S272wt samples. This might lead to the assumption that the permanent phosphorylation at S272 of SQSTM1/p62 affects the affinity to cellular target proteins. However, SQSTM1/p62-S272A samples contained the same set of proteins as the SQSTM1/p62-S272D samples, though in different amounts. This renders an impact of S272 phosphorylation in the interaction with these proteins unlikely.

179 cellular proteins in total were found in co-precipitates with SQSTM1/p62-S272A. This number of possible interactors appeared to be unreasonably high. We noticed that a twofold higher amount of cell lysates from SQSTM1/p62-S272A-infected cells had to be used to reach an equal amount of receptor precipitated for analysis. Thus, the most likely explanation for the high number of detected proteins are the increased amounts of cellular proteins in the sample, despite the efforts to normalize the samples to SQSTM1/p62 levels. Thus the proteins that were exclusively found in the SQSTM1/p62-S272A samples were considered to be unspecific interactors and are not shown in the heatmap in Figure 17A, but can be found in a table in the appendix (A2). Only those proteins that were also found in samples of SQSTM1/p62-S272D-infected cells are shown in the heatmap.

In summary, the MS analysis provided a set of possible cellular interactors of SQSTM1/p62, some of which may depend on the phosphorylation status of the receptor at position S272.

Such data, however, have to be confirmed by an independent method. In order to validate some of these interactions, both infection and IP were repeated under the same experimental setup to investigate cellular interaction partners of SQSTM1/p62 in dependence on its phosphorylation status at S272 by Western blot. Possible interacting proteins were selected for analysis before SQSTM1/p62 normalization by their high log2 fold-change value, at least ($\log_2(4) = 2$), and a low p-value, at most ($-\log_{10}(0.03) = 1.5$). These criteria indicated that these proteins were true interaction partners of SQSTM1/p62. They were also selected according to whether they co-precipitated with either all or only some of the SQSTM1/p62-S272 mutants in order to display the interaction depending on the phosphorylation status at 272. The following proteins were analyzed: nuclear envelope pore membrane protein POM 121 (POM121), TATA-binding protein-associated factor 2N (TAF15), ADP-ribosylation factor-like protein 6-interacting protein 1 (ARL6IP1), translocating chain-associated membrane protein 1 (TRAM1), ADP-ribosylation factor 6 (ARF6) and gamma-glutamyl hydrolase (GGH). According to the MS results, only POM121 and GGH should interact with all SQSTM1/p62-S272 mutants, while ARL6IP1 and TAF15 should be co-precipitated by both SQSTM1/p62-S272wt and SQSTM1/p62-S272A. ARF6 should only interact with

SQSTM1/p62-S272wt and TRAM1 should be co-precipitated by SQSTM1/p62-S272A and SQSTM1/p62-S272D, respectively. The respective p-values and log2 fold change values for these proteins are listed in a table in the appendix (A3). The Western blot analysis confirmed the interaction of POM121 with SQSTM1/p62-S272wt and SQSTM1/p62-S272A, but not for SQSTM1/p62-S272D (Figure 17B). As there was less POM121 in the input for the IP with the S272D mutant, it is unclear, if this mutant truly failed to interact with POM121. All other tested proteins could not be detected in the precipitated samples. These experiments confirmed the interaction of POM121 with SQSTM1/p62, and this interaction appeared to be independent of its phosphorylation status at S272.

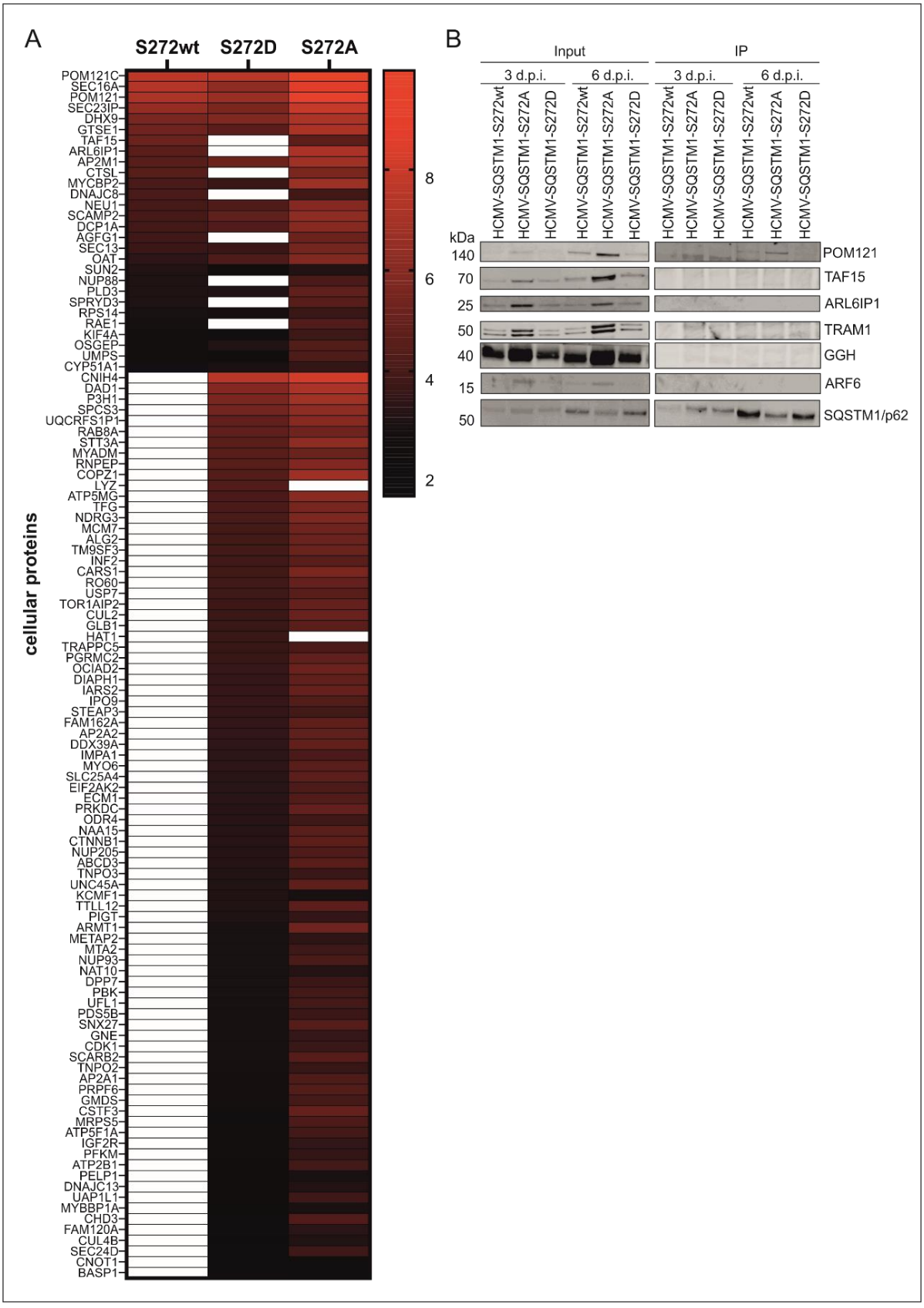
A
S272wt
S272D
S272A
cellular proteins
POM121C
SEC16A
POM121
SEC23IP
DHX9
GTSE1
TAF15
ARL6IP1
AP2M1
CTSL
MYCBP2
DNAJC8
NEU1
SCAMP2
DCP1A
AGFG1
SEC13
OAT
SUN2
NUP88
PLD3
SPRYD3
RPS14
RAE1
KIF4A
OSGEP
UMPS
CYP51A1
CNIH4
DAD1
P3H1
SPCS3
UQCRFS1P1
RAB8A
STT3A
MYADM
RNPEP
COPZ1
LYZ
ATP5MG
TFG
NDRG3
MCM7
ALG2
TM9SF3
INF2
CARS1
RO60
USP7
TOR1AIP2
CUL2
GLB1
HAT1
TRAPPC5
PGRMC2
OCIAD2
DIAPH1
IARS2
IPO9
STEAP3
FAM162A
AP2A2
DDX39A
IMPA1
MYO6
SLC25A4
EIF2AK2
ECM1
PRKDC
ODR4
NAA15
CTNNB1
NUP205
ABCD3
TNPO3
UNC45A
KCMF1
TTLL12
PIGT
ARMT1
METAP2
MTA2
NUP93
NAT10
DPP7
PBK
UFL1
PDS5B
SNX27
GNE
CDK1
SCARB2
TNPO2
AP2A1
PRPF6
GMDS
CSTF3
MRPS5
ATP5F1A
IGF2R
PFKM
ATP2B1
PELP1
DNAJC13
UAP1L1
MYBBP1A
CHD3
FAM120A
CUL4B
SEC24D
CNOT1
BASP1
8
6
4
2
B
Input
IP
3 d.p.i.
6 d.p.i.
HCMV-SQSTM1-S272wt
HCMV-SQSTM1-S272A
HCMV-SQSTM1-S272D
kDa
140
70
25
50
40
15
50
POM121
TAF15
ARL6IP1
TRAM1
GGH
ARF6
SQSTM1/p62

Figure 17. Analysis of cellular interactors of SQSTM1/p62, depending on the phosphorylation status at S272. (A) MS analyses of proteins, precipitated with SQSTM1/p62-specific antibodies from mutant-virus infected ko-SQSTM1 cells. Cells were infected with the different HCMV-SQSTM1/p62-S272 mutants (wt/ A/ D). Cell lysates were harvested at 3 d.p.i., subjected to Co-IP and analyzed by MS. A right-sided t-test with a minimal enrichment factor of 2 ($log_2(2) = 1$), showing the difference, and $p < 0.05$ ($-log_{10}(0.05) = 1.3$) was performed. The log2 fold change of each precipitation (wt/ D/ A) was normalized to the respective SQSTM1/p62-S272 mutant protein level. The respective normalized log2 fold change values are plotted in the heat map with a color gradient. Proteins that co-precipitated only with SQSTM1/p62-S272A are not shown. Cellular proteins were sorted by SQSTM1/p62-S272wt from highest to lowest log2 fold change values, except those with no log2 fold change value for SQSTM1/p62-S272wt. These proteins were sorted by SQSTM1/p62-S272D from highest to lowest log2 fold change values. Shown are the log2 fold change values of three biological samples for each mutant. (B) Validation of selected, co-precipitated cellular proteins after t-test analysis by Western blot. Cells were infected and precipitated with a SQSTM1/p62 antibody as in A. Both lysate (input) and immunoprecipitation (IP) samples were analyzed by Western blot, using the antibodies against the following proteins: nuclear envelope pore membrane protein POM 121 (POM121), TATA-binding protein-associated factor 2N (TAF15), ADP-ribosylation factor-like protein 6-interacting protein 1 (ARL6IP1), translocating chain-associated membrane protein 1 (TRAM1), ADP-ribosylation factor 6 (ARF6) and gamma-glutamyl hydrolase (GGH). Antibodies against SQSTM1/p62 and pp28 (virus control) were used for respective controls, n=1.

In summary, a wide array of proteins was detected in the IP samples by MS. From a selected set of these, POM121 could be confirmed as *bona-fide* SQSTM1/p62 interactor in Western blot analyses. Further testing of other proteins by Western blot could not be performed, considering the number of possible interactors and the lack of specific antibodies. To further evaluate the data set, a gene ontology (GO)-analysis was performed by using the Search Tool for the Retrieval of Interacting Genes (STRING) database (http://string-DBs.org). This analysis provides an overview how, the co-precipitated proteins are related and if they are associated with particular biological processes. These processes were listed according to their lowest to the highest false discovery rate. The number of detected genes belonging to one particular process was plotted in the bar chart for each receptor (Figure 18). The GO analysis revealed a striking similarity of the biological processes to which the putative interactors for the SQSTM1/p62-variants could be assigned to. Most of these proteins fell into categories intracellular transport processes, metabolic processes and macromolecule localization. Moreover, the analyses suggest, that the phosphorylation status at S272 is not a major determinant of the general interaction of SQSTM1/p62 with other cellular proteins.

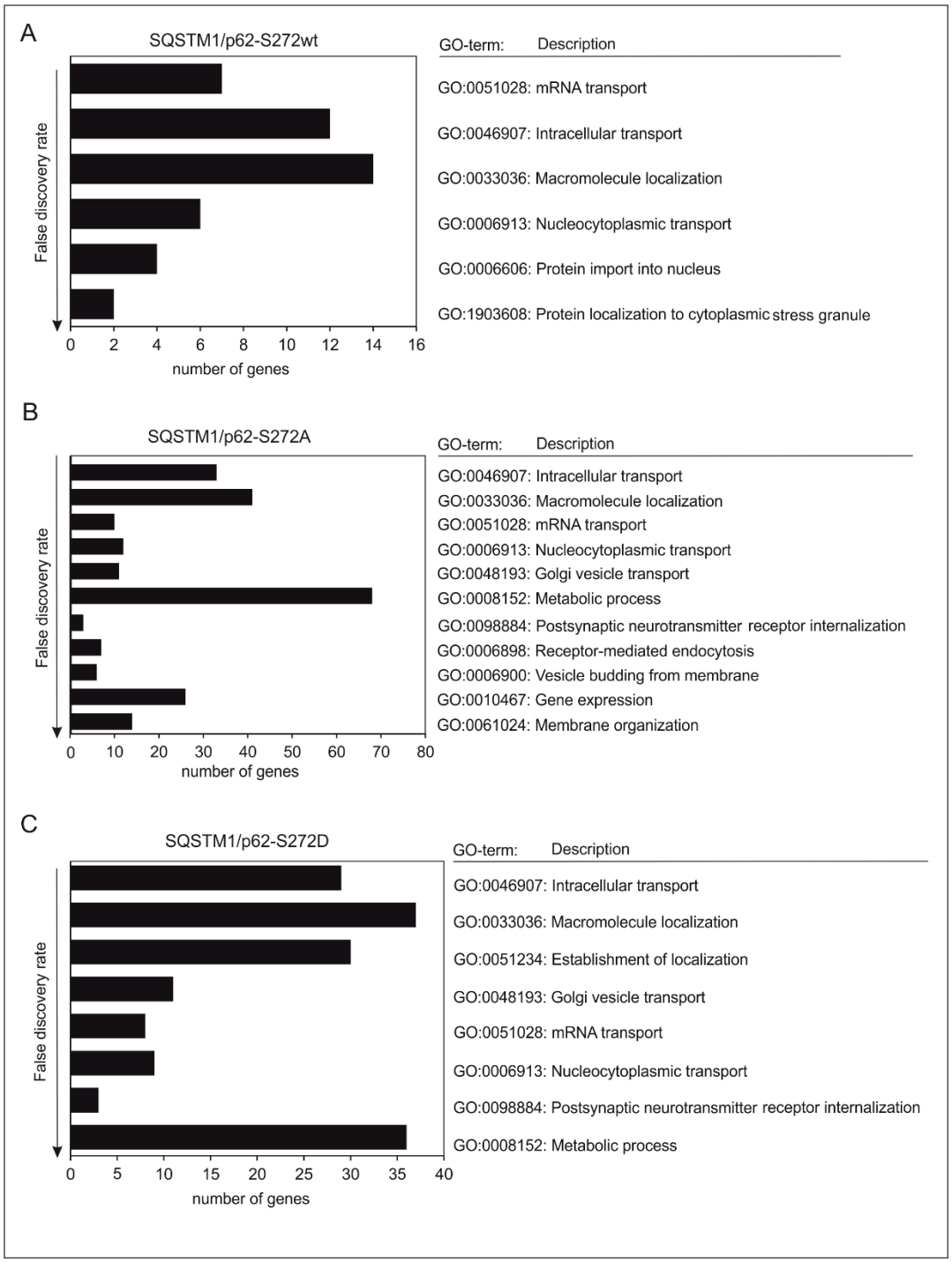

Figure 18. Biological processes of the cellular interactors of SQSTM1/p62 in dependence on the phosphorylation status at S272. Samples obtained from cells infected with either HCMV-SQSTM1-S272wt, -S272A or -S272D and immunoprecipitated with SQSTM1/p62-specific antibodies were analyzed by MS. Co-precipitated proteins, shown in Figure 17, were grouped into biological process, based on the Gene Ontology (GO) analysis using the STRING network database. Results are presented in bar charts. The categories of the biological processes are displayed. The y-axis represents biological process categories sorted from the lowest to the highest false discovery rate, while the x-axis indicates the number of genes involved in each category. The precipitation with SQSTM1/p62-S272wt is shown in (A), the precipitation with SQSTM1/p62-S272A is presented in (B) and the precipitation with SQSTM1/p62-S272D is shown in (C).

To further display functional interactions, a predicted protein-protein interaction analysis was performed by again using the STRING database (http://string-DBs.org) (Figure 19). Protein-protein interaction analysis was done for precipitation from HCMV-SQSTM1-S272wt-, -S272A-, and -S272D-infected cells. Only proteins that interacted with at least two further proteins are shown in the protein-protein-interaction network. Most proteins that were identified in Co-IP experiments did not meet the above-mentioned criterion and could thus not be integrated into an interaction network. The grey-colored proteins in each network analysis belong to unspecific clusters such as metabolic process or intracellular transport.

Interestingly, one cluster related to the functional category of nucleocytoplasmic transport was identified for each receptor variant and this is highlighted in red colors. This is concordant with the known role of SQSTM1/p62 in nucleocytoplasmic transport processes (Pankiv et al., 2010; Thakar et al., 2013) and indirectly confirms the validity of the data set, obtained by MS. The network analysis also showed that SQSTM1/p62-S272A and SQSTM1/p62-S272D shared two further clusters, i.e., the Golgi vesicle transport (green) and the postsynaptic neurotransmitter receptor internalization (purple). This similarity was rather unexpected, considering that those two receptors represent the largest difference regarding their phosphorylation status at S272. Thus, the STRING analysis confirms that the interaction of SQSTM1/p62 with other cellular proteins is overall independent of the phosphorylation status at S272. This is also supported by the finding that, although SQSTM1/p62-S272A interacted with more cellular proteins than the other variants, no further biological clusters were identified for this receptor. All of this, however, cannot exclude, that individual protein-protein interactions are regulated by S272 phosphorylation.

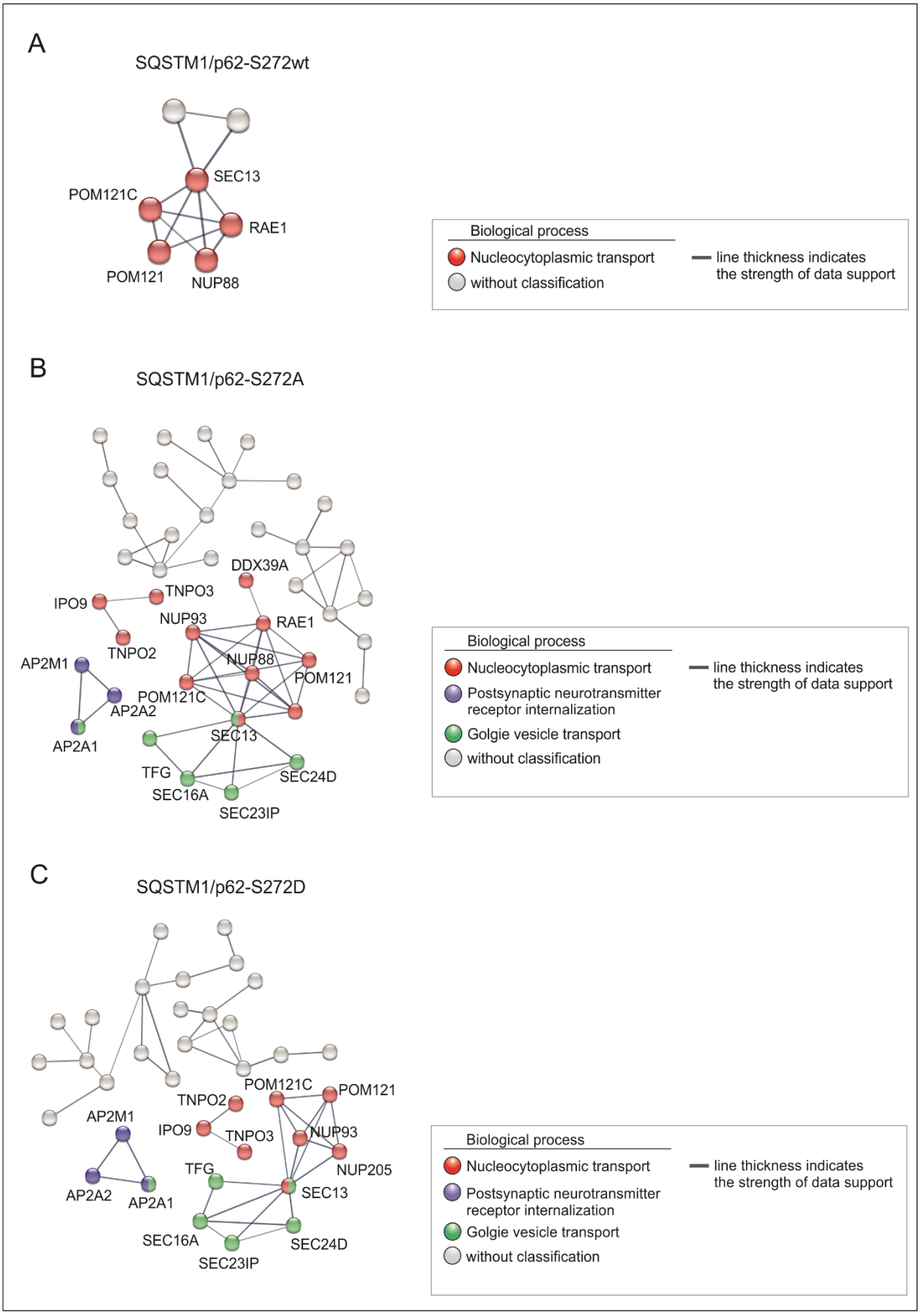
A
SQSTM1/p62-S272wt
SEC13
POM121C
RAE1
POM121
NUP88
Biological process
Nucleocytoplasmic transport
without classification
line thickness indicates the strength of data support
B
SQSTM1/p62-S272A
DDX39A
TNPO3
IPO9
NUP93
RAE1
TNPO2
AP2M1
NUP88
POM121
POM121C
AP2A2
AP2A1
SEC13
TFG
SEC24D
SEC16A
SEC23IP
Biological process
Nucleocytoplasmic transport
Postsynaptic neurotransmitter receptor internalization
Golgie vesicle transport
without classification
line thickness indicates the strength of data support
C
SQSTM1/p62-S272D
POM121C
POM121
TNPO2
AP2M1
IPO9
TNPO3
NUP93
NUP205
TFG
SEC13
AP2A2
AP2A1
SEC16A
SEC24D
SEC23IP
Biological process
Nucleocytoplasmic transport
Postsynaptic neurotransmitter receptor internalization
Golgie vesicle transport
without classification
line thickness indicates the strength of data support

Figure 19. Protein-protein interaction network of the cellular interactors of SQSTM1/p62 in dependence on the phosphorylation status at S272. The results of the data shown in Figure 17 are graphically displayed as interaction networks, again using the STRING database (http://string-DBs.org). Each node represents a protein and the colored nodes were assigned to a biological cluster, as shown in the insert. The interaction network was generated with a high confidence interaction score (0.7). Networks of proteins that co-precipitated with SQSTM1/p62-S272wt are shown in (A), those co-precipitated with SQSTM1/p62-S272A are shown in (B), and those co-precipitated with SQSTM1/p62-S272D are shown in (C).

In a further approach, the specificity of SQSTM1/p62 for viral proteins was investigated. The data sets used for the MS analyses of cellular interactors (Figure 17) were analyzed with respect to viral proteins. The respective co-precipitated viral proteins and their corresponding p-values and log2 fold change values are listed in a table in the appendix (A4). Again, proteins that exclusively precipitated with SQSTM1/p62-S272A are not shown, as these precipitates could be due to the higher protein amount in the input. However, they can be found in a table in the appendix (A5).

The results showed that some HCMV proteins precipitated significantly with SQSTM1/p62 (Figure 20). Of note, the number of precipitated viral proteins was enhanced when cells were infected with of HCMV-SQSTM1/p62-S272A. As detailed above, however, twice the number of infected cells was used in the analysis of the SQSTM1/p62-S272A mutant virus, thus challenging the results for viral proteins, only found with this variant. Interestingly, SQSTM1/p62-S272D and SQSTM1/p62-S272wt precipitated a comparable number of viral proteins. Again, viral structural proteins like the capsid vertex component 1 (CVC1, pUL93), the capsid vertex component 2 (CVC2, pUL77) and the large protein pp150 (UL32) were among those that were precipitated together with SQSTM1/p62. The capsid protein MCP was only precipitated by SQSTM1/p62-S272wt and SQSTM1/p62-S272A. The abundant protein pp65 was not detected. As this protein is known to nonspecifically bind to unrelated proteins, it may serve as a control here that validates the precipitation protocol used. In conclusion, the interaction of SQSTM1/p62 with viral proteins appears to be independent of the phosphorylation status at S272. Still the data should again be viewed as preliminary, as validation by Western blot is still pending.

In conclusion, these analyses showed that SQSTM1/p62 binds to an array of cellular and a subset of viral proteins. The interactions seem to be unaffected by the phosphorylation status at S272. Further experiments are mandatory to confirm this and to investigate the regulatory role of phosphorylation at S272 for its binding to other proteins and its role in HCMV infection.

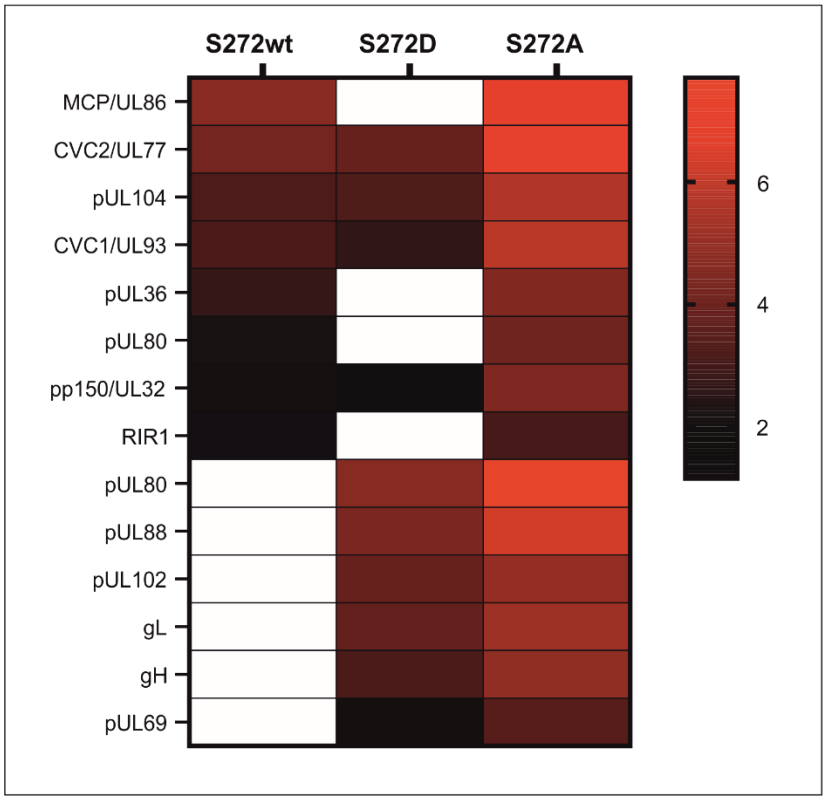

Figure 20. **Heat map of MS analysis of viral interactors with SQSTM1/p62 in dependence on the phosphorylation status at S272**. MS analyses of proteins, precipitated with SQSTM1/p62-specific antibodies from mutant-virus infected ko-SQSTM1 cells. Cells were infected with the different HCMV-SQSTM1/p62-S272 mutants (wt/ A/ D). Cell lysates were harvested at 3 d.p.i., subjected to Co-IP and analyzed by MS. A right-sided t-test with a minimal enrichment factor of 2 ($\log_2(2) = 1$), showing the difference and $p < 0.05$ ($-\log_{10}(0.05) = 1.3$) was performed. The log2 fold change values from each precipitation experiment (wt/ D/ A) were normalized to the respective SQSTM1/p62-S272 mutant protein level and plotted in a heat map with a color gradient. Proteins co-precipitated only from SQSTM1/p62-S272A-infected cells are not shown. Viral proteins were sorted by SQSTM1/p62-S272wt from highest to lowest log2 fold change values. Viral proteins, which were not precipitated by SQSTM1/p62-S272wt, were sorted by SQSTM1/p62-S272D from highest to lowest log2 fold change values.

4.3 Analysis of the kinases involved in the phosphorylation of SQSTM1/p62 at S272 in HCMV-infected cells

SQSTM1/p62 at S272 is hyperphosphorylated upon HCMV infection (Figure 9). It was unclear, whether a cellular kinase is activated upon viral infection or if the HCMV kinase pUL97 was involved in this post-translational modification. Thus, in the next section, the role of pUL97 in the phosphorylation of SQSTM1/p62 at S272 was addressed.

4.3.1 Cloning and characterization of the HCMV mutant HCMV-UL97-as1

The kinase pUL97 is the only viral kinase expressed by HCMV. Its protein synthesis occurs early upon infection and impacts both early and late stages of the viral life cycle (van Zeijl et al., 1997). It has been identified as a viral cyclin-dependent kinase (CDK) ortholog of human CDKs (vCDK) which alters the phosphorylation dynamics of HCMV-infected cells by phosphorylation of both viral and cellular proteins (Schütz et al., 2021; Steingruber and Marschall, 2020). Examples of viral target proteins are the tegument proteins pUL44 and pp65. pUL97 also phosphorylates host proteins including the retinoblastoma protein (Rb), lamin A/C, RNA polymerase II and the intrinsic immune restriction factor interferon gamma inducible protein 16 (IFI16) (Baek et al., 2004; Becke et al., 2010; Dell'Oste et al., 2014; Hume et al., 2008; Kuny et al., 2010; Marschall et al., 2003; Milbradt et al., 2010). While the phosphorylation of lamin A/C facilitates the nuclear egress of virus capsid proteins, the phosphorylation of Rb promotes changes in the cell cycle (Hamirally et al., 2009; Iwahori and Kalejta, 2017; Iwahori et al., 2017; Milbradt et al., 2010). pUL97 has a crucial role in HCMV replication as the reduction or deletion of pUL97 leads to severe replication deficits (Prichard et al., 2005; Prichard et al., 1999; Wolf et al., 2001). To be able to study the function of pUL97 in HCMV-infected cells and to minimize replication deficits, a novel approach for conditional regulation of pUL97 activity was chosen. For this, an HCMV mutant expressing an analogue-sensitive version of the pUL97, called pUL97-as1 was generated (Krämer et al., 2022). The mutation to obtain pUL97-as1 was originally published by Umaña and colleagues (Umaña et al., 2018) and used for transient plasmid transfections. The pUL97-as1 protein carries a mutation at position 411 (S411G), leading to an enlarged ATP binding pocket. This mutation allows the binding of a non-phosphorylatable ATP-orthologue (3MB-PP1), thereby suppressing pUL97 catalytic activity. In the absence of the inhibitor, pUL97-as1 can still bind ATP and shows normal kinase activity (Krämer et al., 2022; Umaña et al., 2018). Thus, the virus can be grown in the absence of the inhibitor, while pUL97 activity can be blocked for investigation.

The cloning and characterization of the HCMV mutant is described in the inserted publication in the appendix, see A6 (Krämer et al., 2022).

4.3.2 The viral HCMV kinase pUL97 is involved in the phosphorylation of SQSTM1/p62 at S272

Based on the increased phosphorylation of SQSTM1/p62 at S272 in HCMV-infected cells, the question arose whether the HCMV kinase pUL97 plays a role in this modification. To investigate this, the approach taken was to inhibit the viral kinase in order to study the phosphorylation status of SQSTM1/p62 at S272 by Western blot, using a phospho-specific antibody. For this, the HCMV mutant BAD-UL97-as1 (Krämer et al., 2022), herein termed HCMV-UL97-as1, was used to infect HFF with 4 genome copies/cell. For inhibition of pUL97-as1, the ATP-orthologue 3MB-PP1 was added 4 hours before the cells were collected. In a parallel control, the cell culture medium was supplemented with DMSO instead. Cells were harvested at 1, 2, 3 and 6 d.p.i., respectively and probed in a Western blot to detect the phosphorylation status of SQSTM1/p62 at S272. Inhibition of pUL97-as1 activity by 3MB-PP1 resulted in reduced SQSTM1/p62 phosphorylation at S272 in comparison to control cells (Figure 21A). To visualize the difference, the ratio of p-SQSTM1/p62 S272 versus the total protein is displayed in a bar chart. The data indicated that the phosphorylation of SQSTM1/p62 at its residue S272 is dependent on pUL97 (Figure 21B). SQSTM1/p62 S272 phosphorylation was enhanced at early time points after infection but declined to the level of uninfected cells at 6 d.p.i.. The inhibition of pUL97-as1 was controlled by analyzing the pUL97 target protein Rb and its phosphorylation at amino acids 807/811. Rb phosphorylation was already sensitive to the pUL97-as1 inhibition at 1 d.p.i. (3MB-PP1 sample). The phosphorylation of the autophagy receptor by active pUL97-as1 was most prominent during early stages of infection, whereas the strongest inhibition of pUL97-as1 was observed at 6 d.p.i., as seen by the reduced phosphorylation of Rb. Together these analyses revealed that the inhibition of pUL97-as1 leads to a decreased phosphorylation level of SQSTM1/p62 at S272 in HCMV-infected cells.

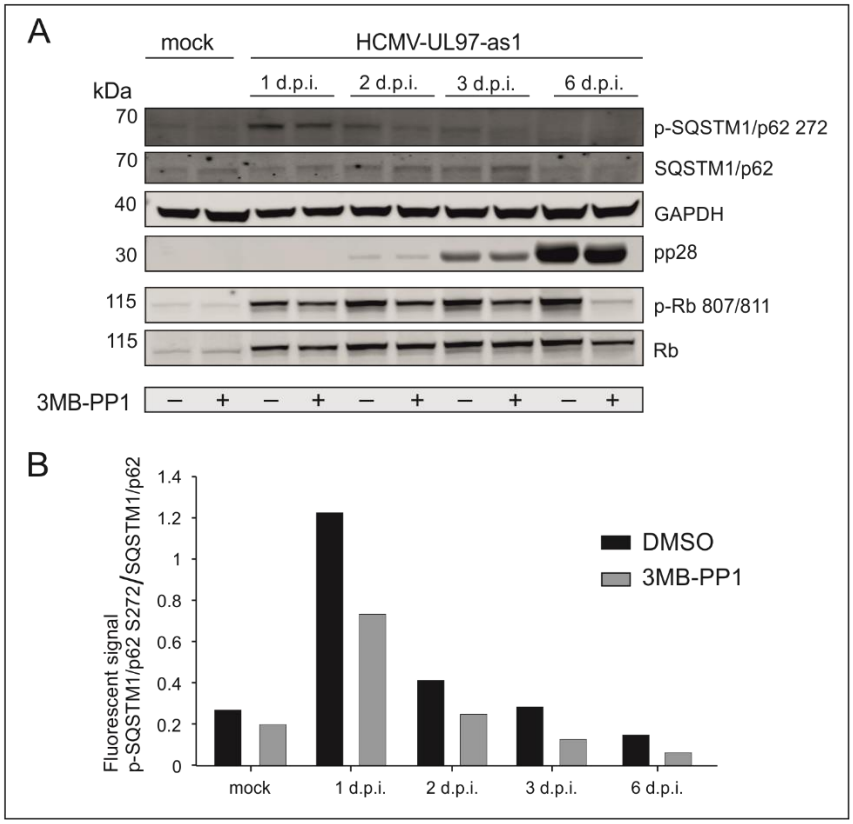

Figure 21. Western blot analysis of the role of the HCMV kinase pUL97 in SQSTM1/p62-S272 phosphorylation in infected cells. (A) Cells were infected with HCMV-UL97-as1 for the indicated times. 4 hours before harvest, the cells were incubated with the inhibitor ATP orthologue 3MB-PP1 (40 μM). A phospho-specific antibody against S272 of SQSTM1/p62 was used to investigate the phosphorylation status of SQSTM1/p62. Antibodies against SQSTM1/p62 (control for SQSTM1/p62 levels), GAPDH (loading control), pp28 (virus control), p-RB 807/811 (control for pUL97-kinase activity) and Rb (control for Rb levels) were carried along. This result was validated in a second experiment. (B) The fluorescence intensity ratios of the band for p-SQSTM1/p62 S272 versus SQSTM1/p62 were calculated of the represented Western blot, shown in A. Evaluation of the analyzed time points (1, 2, 3, and 6 d.p.i.) and mock were plotted in a bar diagram.

To evaluate the data and to exclude an impact of other viral factors, these results were confirmed in a transfection experiment. A particular focus laid on regulated phosphorylation sites of SQSTM1/p62 independent of HCMV infection but dependent on pUL97-as1. For this, a co-transfection experiment in the absence of infection was performed, using expression vectors for both pEGFP-N2-UL97-as1 and pGFP-SQSTM1, followed by MS analysis (Figure 22A). pGFP-SQSTM1 encodes *GFP* in fusion with *SQSTM1* whereas the plasmid pEGFP-N2-UL97-as1 encodes unfused *GFP* from a separate gene. HEK293T were pre-incubated with either 3MB-PP1 or DMSO as control and co-transfected with both plasmids. Cells were harvested 24 hours post transfection and IP against GFP was performed to obtain GFP-SQSTM1/p62 co-precipitates. Successful transfection was verified by analyzing the GFP levels, showing either GFP-SQSTM1/p62 from pcGFP-SQSTM1 or free GFP from pEGFP-N2-UL97-as1 by Western blot (data not shown). Three biological

replicate samples from each of the two individual experiments were sent for MS analyses, again, in collaboration with Lina Herhaus at the Institute of Biochemistry II of the Goethe University Frankfurt/Main, Germany. S272 was the only site that showed significant regulation in its phosphorylation status in both experiments (Figure 22A). S272 was hypophosphorylated in pEGFP-N2-UL97-as1 and pcGFP-SQSTM1 co-transfected cells, treated with 3MB-PP1, compared to DSMO controls. Thus, these experiments confirmed the finding that pUL97 contributes to the phosphorylation status of SQSTM1/p62-S272. To corroborate this, a similar experimental setup was chosen, using a phospho-specific antibody in Western blot analyses. HEK293T were pre-incubated with either 3MB-PP1 or DMSO as control for 12 hours. Cells were either again co-transfected with plasmids pEGFP-N2-UL97-as1 and pcGFP-SQSTM1 or co-transfected with plasmids, expressing the wt kinase, *UL97,* and pcGFP-SQSTM1. The plasmid pEGFP-N2-UL97 encodes unfused GFP from a separate gene. In addition, pcGFP-SQSTM1was transfected alone for control. 24 hours after transfection, cells were collected, lysed and the phosphorylation level of SQSTM1/p62 S272 was examined in a Western blot analysis. The expression of, pUL97 and pUL97-as1, as well as GFP-SQSTM1/p62 were visualized by a GFP antibody, detecting either free GFP from the respective kinase expressing plasmid or pcGFP-SQSTM1. The ratio of the phosphorylation signal of p-SQSTM1/p62 S272 versus the total protein was quantified and is shown here as a bar diagram. Western blot analysis showed that S272 phosphorylation of SQSTM1/p62 decreased when pUL97-as1 was inhibited, confirming the MS data (Figure 22B). As expected, the phosphorylation level of SQSTM1/p62 stayed unaffected in cells transfected with pEGFP-N2-UL97 and treated with 3MB-PP1 compared to DMSO-treated controls. This confirmed that the phosphorylation of SQSTM1/p62 S272 by pUL97 was specific for the activity of the kinase and not a secondary effect mediated by 3MB-PP1. Surprisingly, the Western blot showed that cells transfected only with pcGFP-SQSTM1 revealed a reduced phosphorylation status at S272 of SQSTM1/p62 in the presence of 3MB-PP1.Yet, the ratio of p-SQSTM1/p62 S272 versus SQSTM1/p62 established that this effect is rather based on a reduced protein level of SQSTM1/p62 than on an inhibition of a cellular kinase (Figure 22C). The free GFP-level should have served as a control for both pUL97-as1 and pUL97. However, the Western blot analysis revealed, that free GFP was detected in all samples, even in those, which only expressed *GFP* tagged to *SQSTM1*. The cause for this is unclear. For this reason and due to the lac of pUL97-specific antibody, the levels of pUL97 after transfection could not be evaluated. Nevertheless, the data showed a decreased phosphorylation level of SQSTM1/p62 at S272 when the viral kinase was inhibited by 3MB-PP1. This indicates that the viral kinase pUL97 is involved, directly or indirectly, in the phosphorylation of the autophagy receptor at its residue 272.

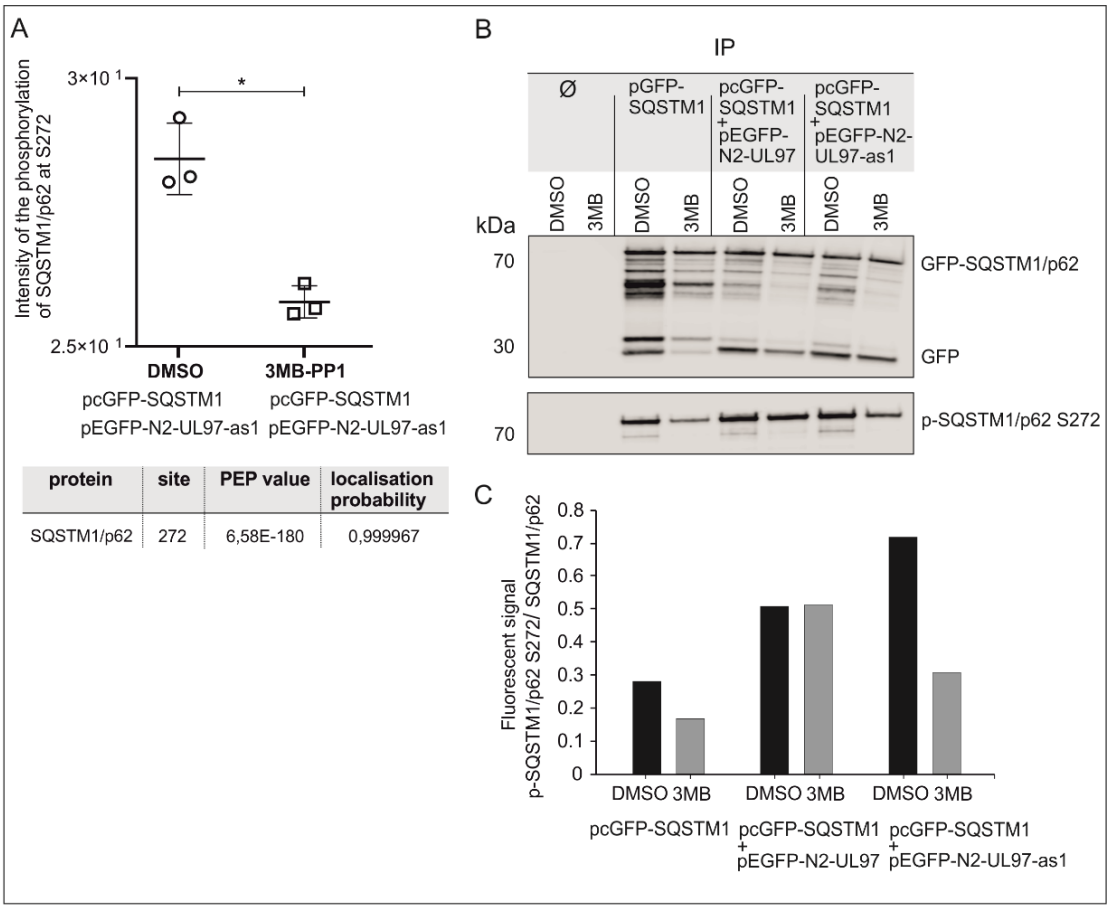

Figure 22. Analysis of the phosphorylation of SQSTM1/p62 at S272 by pUL97 in co-transfected HEK293T. (A) Cells were either pre-treated with 3MB-PP1 (3MB) or with DMSO and co-transfected with plasmids expressing pcGFP-SQSTM1 and pEGFP-N2-UL97-as1, respectively. Cells were harvested 24h after transfection and Co-IPs using GFP-Trap magnetic Dynabeads were performed. The results of three biological replicates of one MS analysis are shown. Only S272 was found to be hypophosphorylated under 3MB-PP1 treatment and thus, only the results for this site are shown. The results fulfill both probability value criteria, i.e., PEP that the detected total number of identified peptide sequences for the protein is incorrect, which should be close to 0, and the localization probability, representing that the correct phosphorylation residue is detected and should be close to 1. Statistical analysis between DMSO and 3MB-PP1 treated samples was performed utilizing the Welch's t-test (*: $p<0.05$). pcGFP-SQSTM1, plasmid encoding *SQSTM1*, fused to *GFP*. pEGFP-N2-UL97-as1, plasmid expressing the 3MB-PP1-sensitive mutant of pUL97, which is pUL97-as1*,* and, from a separate reading frame, *GFP*. This result was validated in a second experiment. (B) HEK293T cells were treated as in A and co-transfected with plasmids, expressing pcGFP-SQSTM1 and pEGFP-N2-UL97-as1 or pEGFP-N2-UL97, respectively, or transfected with pcGFP-SQSTM1 only as a secondary control to detect the phosphorylation status of SQSTM1/p62 at S272 in Western blot analysis. 24h post transfection, cells were collected and probed by Western blot, using a phospho-specific antibody against S272 of SQSTM1/p62. Antibodies directed to the full-length protein of SQSTM1/p62 and GFP were carried along. This result was validated in a second experiment. (C) The fluorescent signal of p-SQSTM1/p62 S272 about GFP-SQSTM1/p62 was determined based on the presence of 3MB-PP1 in transfected cells without infection. The ratio was calculated from the Western blot shown in B. The signals for DMSO or 3MB-PP1 treated cells were plotted on a bar graph.

The results obtained in infected and transfected cells could not discriminate between direct or indirect phosphorylation of SQSTM1/p62 S272 by pUL97. To address this, a Co-IP-based IVKA was performed. HFF were infected with HCMV, using an m.o.i. of 0.5. Cells were collected at 3 d.p.i. and lysates were subjected to IP using antibodies against pUL97 or SQSTM1/p62. Subsequently, IVKA was performed. For this, ATPγS was added for the phosphorylation of the target proteins, which was subsequently detected by a thiophosphate-specific antibody. As a positive control, one of the major pUL97 substrates, the HCMV protein pp65, was analyzed. Interestingly, no phosphorylation of SQSTM1/p62 was observed upon HCMV infection and incubation with ATPγS (Figure 23). As expected, pp65 was phosphorylated by pUL97. Phosphorylation-specific bands were determined by re-staining of the IVKA Western blot membranes using antibodies directed against SQSTM1/p62 and pp65, respectively. It should be noted that that staining against SQSTM1/p62 was weaker than against pp65, suggesting that fewer precipitated SQSTM1/p62 amounts were available for phosphorylation analysis. Thus, phosphorylation of SQSTM1/p62 at S272 is dependent on pUL97 kinase activity but, from *in-vitro* analyses, there was no evidence obtained that pUL97 directly phosphorylates the receptor.

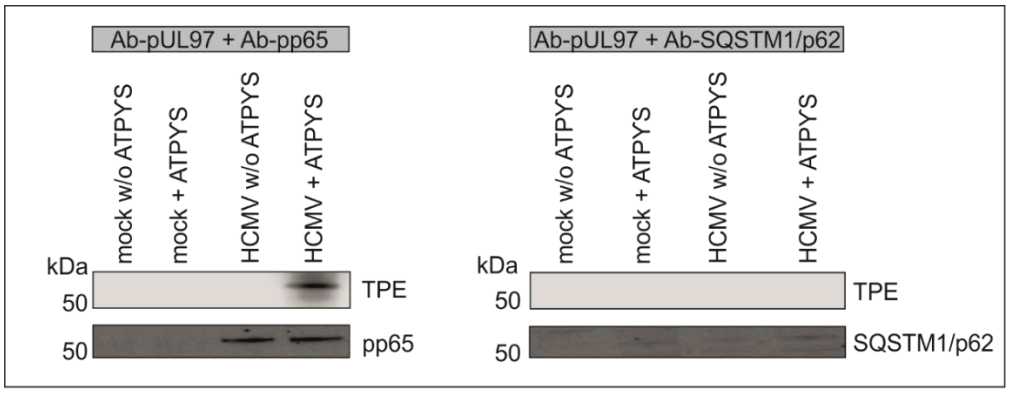

Figure 23. In-vitro kinase assay (IVKA) to assess the phosphorylation of SQSTM1/p62 by pUL97. HFF were infected with HCMV at an m.o.i. of 1. At 3 d.p.i., cells were harvested, lysed and ultrasonicated to analyze the phosphorylation of SQSTM1/p62 by pUL97 via an IVKA. pUL97 was immunoprecipitated together with SQSTM1/p62 or as control with pp65, using specific antibodies. Co-immunoprecipitated proteins were used to perform an IVKA, using ATPγS, which is utilized by kinases to thiophosphorylate their targets. Samples were treated with p-nitrobenzyl mesylate to allow the alkylation of thiophosphorylated substrates to obtain thiophosphate esters (TPE). Phosphorylation was assessed with a specific thiophosphate antibody, and protein levels of pp65 and SQSTM1/p62 were also detected by Western blot.

4.3.3 Determination of the involvement of cellular kinase CDK1 on the phosphorylation of SQSTM1/p62 at S272 upon HCMV infection

The experiments revealed that the phosphorylation status of SQSTM1/p62 at S272 is regulated by the HCMV kinase pUL97. A direct phosphorylation could not be detected in *in-vitro* experiments. Thus, the hypothesis was addressed that a cellular kinase was involved in pUL97-mediated S272-phosphorylation. The focus lied upon the cyclin-dependent kinase 1 (CDK1) (Malumbres, 2014). CDK1 is associated with the phosphorylation of SQSTM1/p62 at S272 (Linares et al., 2011). The kinase is also induced upon HCMV infection, as it plays an essential role in HCMV replication (Bigley et al., 2015). In addition, pUL97 is a viral CDK ortholog and modifies CDK1 to promote virus replication (Gill et al., 2012).

For this, CDK1 was knocked-down and the phosphorylation status of SQSTM1/p62 after HCMV infection was examined by Western blot. HFF were transfected with a siRNA pool consisting of two siRNAs ([1] + [2]), both directed against CDK1 (siCDK1). As control, cells were transfected with an unrelated siRNA (siControl). After transfection, cells were infected with HCMV (m.o.i. = 0.5) and collected at 1, 2 and 3 d.p.i. Cell lysates were subjected to Western blot and the phosphorylation level was investigated by a phospho-specific antibody against SQSTM1/p62 S272. The result for CDK1 was not clear (Figure 24). On the one hand, at 2 d.p.i., a reduced phosphorylation level of SQSTM1/p62 compared to control transfected cells was observed after knockdown. On the other hand, the opposite was seen in non-infected cells and at 1 d.p.i., contrary to the described function of CDK1. Thus, the data are not conclusive and the experiment has to be repeated to determine the role of CDK1 on SQSTM1/p62 S272 phosphorylation.

In conclusion, the phosphorylation of SQSTM1/p62 at S272 is dependent on pUL97 kinase activity, still a direct phosphorylation of the receptor by the cellular enzyme could not be detected.

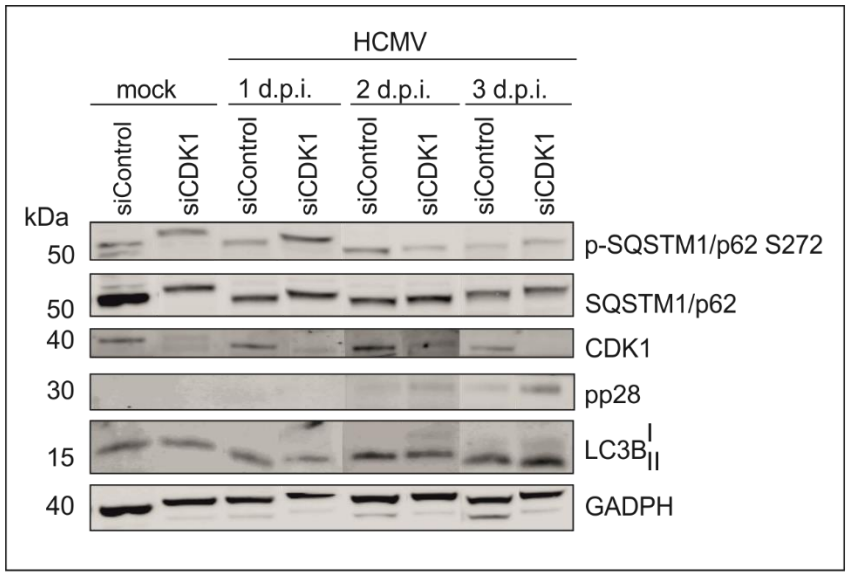

Figure 24. Involvement of the cellular kinase CDK1 in the phosphorylation of SQSTM1/p62 at its residue S272. HFF were transfected with a siRNA pool of two siRNAs directed against CDK1 (siCDK1), or an unrelated siRNA (siControl), using 30 pmol, respectively. 6 hours after transfection, cells were infected with HCMV with an m.o.i. of 0.5. At early points post infection (1, 2 and 3 d.p.i.), cells were harvested, lysed and transferred to SDS-PAGE, followed by Western blot analysis. The membrane was probed with antibodies directed against SQSTM1/p62, p-SQSTM1/p62-S272 and CDK1, respectively. Antibodies against LC3B (autophagy control), pp28 (virus control), and GAPDH (loading control) were also used, n=1.

4.4 Analysis of TRIM proteins as potential autophagy receptors and their impact on HCMV infection and autophagy

Members of the TRIM protein family have multiple antiviral activities including the regulation of autophagy (Di Rienzo et al., 2020; Kimura et al., 2017a). Furthermore, some TRIM proteins have been described as being autophagy receptors, such as TRIM5α, which recognizes and targets the capsid protein of HIV-I for autophagosomal degradation (Mandell et al., 2014b).

Interestingly, in a previous MS analysis in our laboratory some TRIM proteins, namely TRIM25, TRIM26, and TRIM32 were found in extracellular HCMV particles (Zimmermann, unpublished). This led to the hypothesis that these TRIM proteins might play a role during HCMV infection by functioning as autophagy receptors and/or by regulating virus-restricting mechanisms, such as autophagy. Indeed, TRIM32 has been connected to the regulation of the autophagic process in different cellular scenarios. TRIM32 is able to induce autophagy by activating Unc-51 like autophagy activating kinase 1 (ULK1) (Di Rienzo et al., 2019). In addition, the autophagic downregulation of Toll-like receptor signaling is dependent on TRIM32 (Di Rienzo et al., 2019; Overå et al., 2019; Yang et al., 2017). Also, TRIM21 and TRIM28 were investigated for their function as autophagy receptors in HCMV infected cells, as they are known regulators of autophagy. TRIM21 is required for the induction of autophagy by several viruses (Sparrer et al., 2017). It also induces autophagy upon IFN-γ treatment and is involved in autophagosomal degradation of active inhibitor of nuclear factor kappa-B kinase subunit beta (IKKβ) during human T-lymphotropic virus type 1 (HTLV-1) infection (Kimura et al., 2015; Niida et al., 2010). Moreover, TRIM21 has been shown to function as an autophagy receptor by recruiting the interferon regulatory factor 3 (IRF3) to autophagic machinery to execute its degradation (Kimura et al., 2015). In the case of TRIM 28, it both induces and inhibits autophagy under different conditions (Barde et al., 2013; Pineda et al., 2015; Yang et al., 2013).

So far, however, none of these detected TRIM proteins have been described as autophagy receptors upon virus infection.

Thus, the following questions were addressed:

1. Do TRIM proteins function as autophagy receptors during HCMV infection?
2. What is the impact of TRIM proteins on HCMV infection and autophagy?

4.4.1 TRIM25 interacts with selected HCMV proteins

To address, whether members of the TRIM family serve as potential autophagy receptors, their interaction with HCMV proteins was examined. This aspect was already partly addressed in our group (Afifi, 2021, unpublished). Here TRIM21 and TRIM28 but not TRIM32 co-precipitated with some viral proteins, such as MCP. To complete the analysis, an Co-IP experiment with antibodies against TRIM25 and TRIM26, respectively, was

performed. For this, HFF were infected with HCMV at an m.o.i. of 1. Cells were collected at 3 d.p.i. and lysed. TRIM25 or TRIM26 were precipitated with specific antibodies, followed by Western blot. Antibodies against several viral proteins such as pp150, MCP, pp28 and SCP were used to identify possible interaction partners. TRIM25 co-precipitated with almost all of the analyzed viral proteins, whereas TRIM26 did not precipitate with any of them (Figure 25). A summary of both, these data and the data obtained previously, are shown in Table 10. Interestingly, only some of the incorporated members of TRIM family co-precipitated with HCMV proteins. These experiments showed that TRIM21, TRIM25, and TRIM28 interacted with viral structural proteins, thus bearing the potential to act as autophagy receptors in HMCV infection.

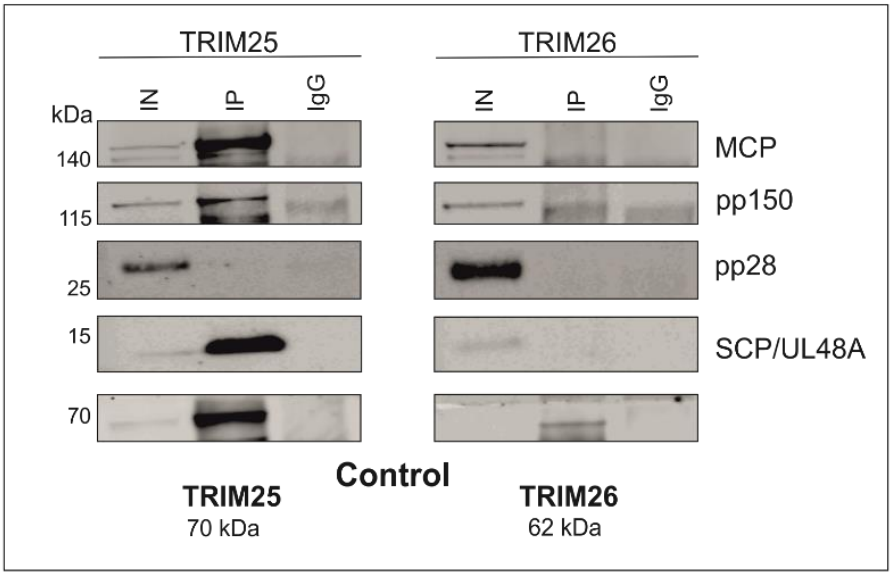

Figure 25. Co-IP analysis of the interaction of TRIM25 and TRIM26 with viral proteins in HCMV infected cells. HCMV-infected cells were collected at 3 d.p.i.. Lysates were precipitated with antibodies against TRIM25, TRIM26, and or IgG as control. Samples and cell lysates were analyzed by Western blot, using antibodies against TRIM25, TRIM26, and the several HCMV proteins MCP, pp150, pp28 and SCP/UL48A.

Table 10. Overview of the TRIM proteins precipitated with HCMV proteins, analyzed in this and a previous work

TRIM proteins	**Precipitation with viral proteins (MCP, pp150, pp28, gB and SCP)**	**Shown in this work**
TRIM21	MCP, pp150	Afifi, Master thesis (Afifi, 2021, unpublished)
TRIM25	MCP, pp150, SCP	This work
TRIM26	None of the tested	This work
TRIM28	MCP	Afifi, Master thesis (Afifi, 2021, unpublished)
TRIM32	None of the tested	Afifi, Master thesis (Afifi, 2021, unpublished)

4.4.2 The role of TRIM proteins in HCMV infection

To study the respective roles of TRIM21, TRIM25, TRIM26, TRIM28 and TRIM32 in HCMV infection, knockout HFF were generated from each TRIM. Ko-TRIM cell lines were obtained by the CRISPR/Cas9 method (2.2.4.1). The schematic process is illustrated in Figure 26A. The successful knockout of each TRIM protein was verified in comparison to control HFF by Western blot, using the corresponding antibodies (Figure 26B). A complete knockout of *TRIM26*, *TRIM28* and *TRIM32* were obtained. In the case of *TRIM21* and *TRIM25*, a significant reduction of the proteins was detected.

To study the impact of TRIM protein knockout on HCMV infection, individual ko-TRIM cells or control HFF were infected with HCMV, using an m.o.i. of 0.5. At 4 and 6 d.p.i., supernatants were collected to perform the IE1-assay. Interestingly, ko-TRIM21, ko-TRIM25, ko-TRIM26 and ko-TRIM32 cells showed increased progeny release at 4 d.p.i. (Figure 26C). This effect was sustained until at 6 d.p.i. for ko-TRIM25 cells and ko-TRIM32 cells, whereas progeny release fell to control-levels in ko-TRIM21- and ko-TRIM26 cells at this time point. The deletion of *TRIM28* had no effect on HCMV progeny release.

These results indicated that the absence of TRIM21, TRIM25, TRIM26 and TRIM32, but not of TRIM28 was supportive for HCMV infection. The deletion of *TRIM25* and *TRIM32* had the strongest impact on HCMV progeny release. Thus, some TRIM proteins indeed seemed to function in the cellular defense against HCMV infection.

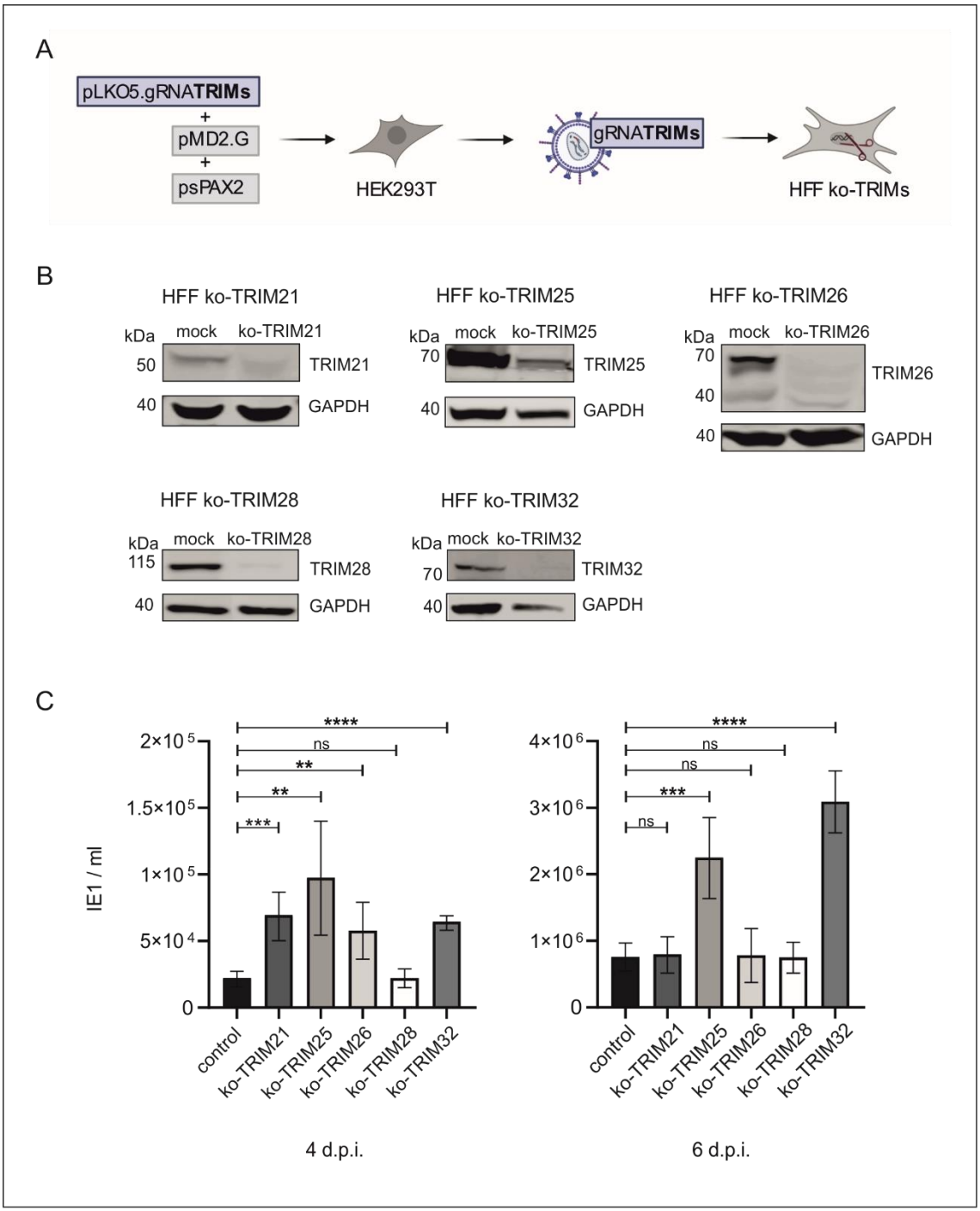

Figure 26. Generation of TRIM knockout HFF and analysis of HCMV progeny release. (A) Several TRIM knockout cell lines were generated by CRISPR/Cas9 technology. HEK293T were co-transfected with the lentiviral vector pLKO5.gRNATRIMs, carrying the gRNA for the genes *TRIM21*, *TRIM25*, *TRIM26*, *TRIM28* or *TRIM32*, respectively, as well as with plasmids pMD2.G (VSV-G envelope expressing plasmid) and psPAX2 (packaging plasmid). Lentivirus-containing culture supernatants of the corresponding HEK293T were used to transduce HFF in order to obtain the desired TRIM knockout cell lines ko-TRIM21, -TRIM25, -TRIM26, -TRIM28, and -TRIM32, respectively. This workflow was created with BioRender.com. (B) Cell lysates of each TRIM knockout cell line and mock cells were subjected to Western blot and analyzed for knockout of each TRIM protein. (C) TRIM knockout cell lines (-21, -25, -26, -28, and -32) and control cells

were infected with HCMV with an m.o.i. of 0.5. Supernatants, collected at 4 and 6 d.p.i. were analyzed for HCMV progeny release, using the IE1-assay. The data show mean values of eight technical replicates from three independent experiments for each cell line and time point. The corresponding SD is represented as error bars. The statistical analysis was determined using Welch's t-test (not significant (ns): $p>0.05$, **: $p\leq0.01$, ***: $p\leq0.001$, and ****: $p\leq0.0001$.

4.4.3 Effect of TRIMs on HCMV replication by analyzing the impact on autophagy and ISG protein products

The molecular mechanisms how TRIM proteins affected HCMV infection were unclear at this stage. Members of the TRIM family execute a well-established role in regulating the IFN-I signaling pathway (Giraldo et al., 2020; Ozato et al., 2008). In addition, it is well established that HCMV replication is highly sensitive to IFN-β and the induction of ISGs. We thus investigated, whether the impact of TRIMs on HCMV replication could be based on an altered IFN-I-signaling pathway by exemplarily analyzing the expression levels of selected ISGs. For this, cell lysates from infected cells were analyzed by Western blot for ISG expression. ISG levels from infected HFF were compared to those of infected TRIM knockout cells. The results showed that Mx1 and ISG15 were induced in all ko-TRIMs cells as well as in control cells upon HCMV infection (Figure 27A). Interestingly, at 4 d.p.i. and partly at 6 d.p.i. both ISG products were elevated in ko-TRIM cells compared to control cells. The respective Mx1 levels in infected ko-TRIM26 and ko-TRIM28 cells, thereby, were the highest compared to the other ko-TRIM cells at 4 d.p.i., which was illustrated by a quantification of the Mx1 levels (Figure 27B). Based on Mx1 and ISG15 levels, this finding indicated an increase of an antiviral environment in the respective ko-TRIM cells. However, this result did not explain the difference in HCMV progeny production in ko-TRIM25 cells and ko-TRIM32 cells, compared to the control cells, suggesting that the interferon pathway was not the level on which TRIMs interfered with HCMV infection.

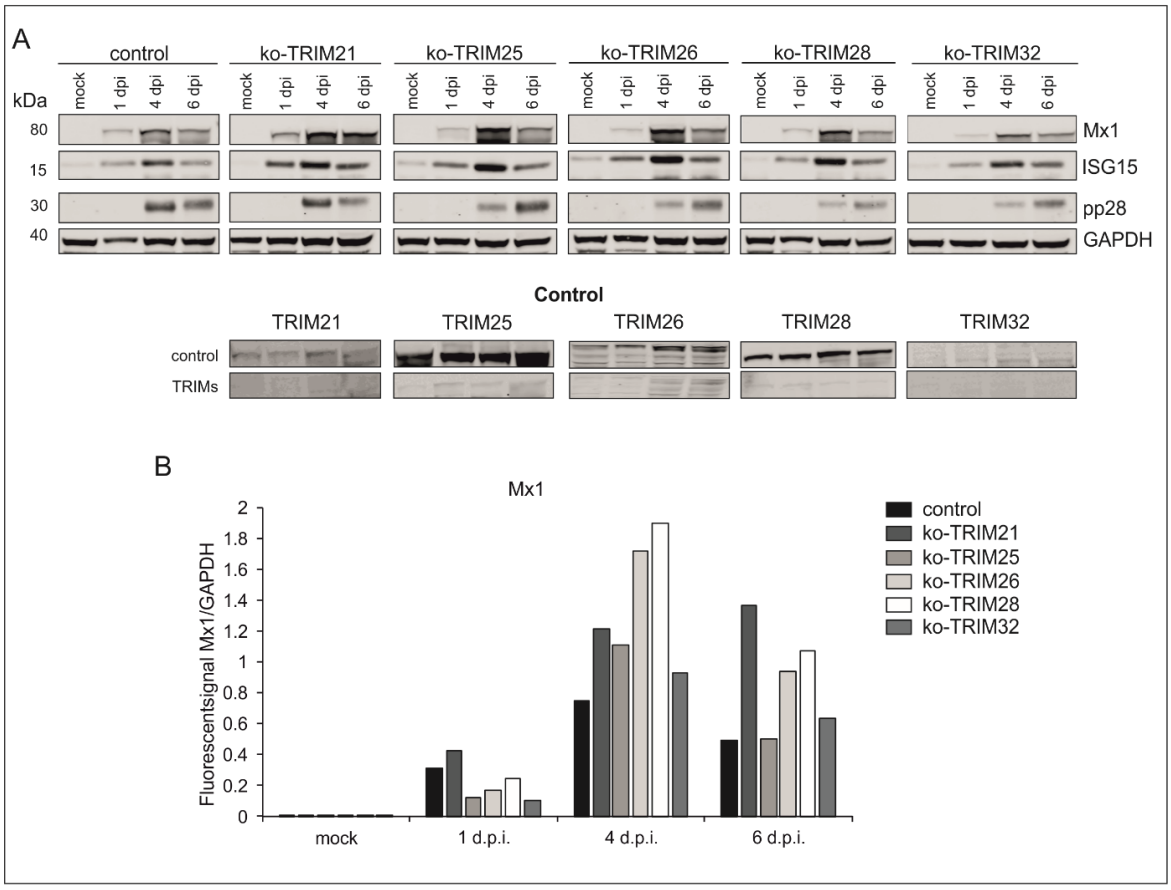

Figure 27. Western blot analysis of the impact of TRIM proteins on ISG protein levels during HCMV infection. (A) ko- TRIM21, -TRIM25, -TRIM26, -TRIM28, and -TRIM32 and control HFF were infected with HCMV (m.o.i. 0.5). At 1, 4, and 6 d.p.i. cells were harvested and cell lysates were investigated for ISG protein levels, using antibodies against Mx1 and ISG15. Antibodies against pp28 (virus control) and GAPDH (loading control) were carried along. These results were validated in a second experiment. (B) The fluorescent signals of Mx1 about GAPDH were determined for each cell line and time points after infection. The ratio was calculated from the Western blot shown in A. The signals were plotted on a bar graph.

Some members of the TRIM family are important player in regulating autophagy. Most of them act as regulators in the upstream autophagy signaling pathways, but they can also impact the autophagic core machinery (Di Rienzo et al., 2020; Mandell et al., 2014a). Moreover, some TRIM proteins can mediate the degradation of autophagy receptors (Wang et al., 2022). Based on the findings that the knockout of some of the TRIM proteins promoted HCMV infection, the question arose whether this effect was due to an impairment of autophagy and/or to reduced autophagy receptor levels. To address this, the TRIM knockout cells were analyzed by Western blot for induction of autophagy, using LC3B as a marker, and for levels of both autophagy receptors SQSTM1/p62 and optineurin. Interestingly, in all TRIM knockout cells, the LC3BII was elevated in a way similar to control infected cells at 1 and 4 d.p.i. (Figure 28A). Only at 6 d.p.i., the LC3BII level was increased in ko-TRIM21, ko-TRIM28 and ko-TRIM32 compared to control HFF. This was visualized by a quantification

of the LC3BII levels (Figure 28B). According to this experiment, the knockout of *TRIM21*, *TRIM28*, and *TRIM32* led to increased autophagy induction, but only at the late stages of HCMV infection. Moreover, this preliminary data indicated that the knockout of *TRIM25* and *TRIM26* did not impact the LC3BII levels and thus the induction of autophagy in HCMV-infected cells. These preliminary data have to be validated in further experiments.

The levels of the autophagy receptor optineurin were unaffected in all ko-TRIM cell lines, either with or without HCMV infection, compared to controls (Figure 28A). In contrast, the SQSTM1/p62 levels were reduced in the absence of either TRIM25 or TRIM32, compared to control cells (Figure 28A). This effect was not seen in the absence of any of the other TRIMs. In addition, HCMV infection of ko-TRIM25 cells or ko-TRIM32 cells did not increase SQSTM1/p62 levels. These results showed that SQSTM1/p62 levels are partly dependent on the presence of TRIM25 and TRIM32. Further experiments will have to be performed to reveal the exact nature of this interaction.

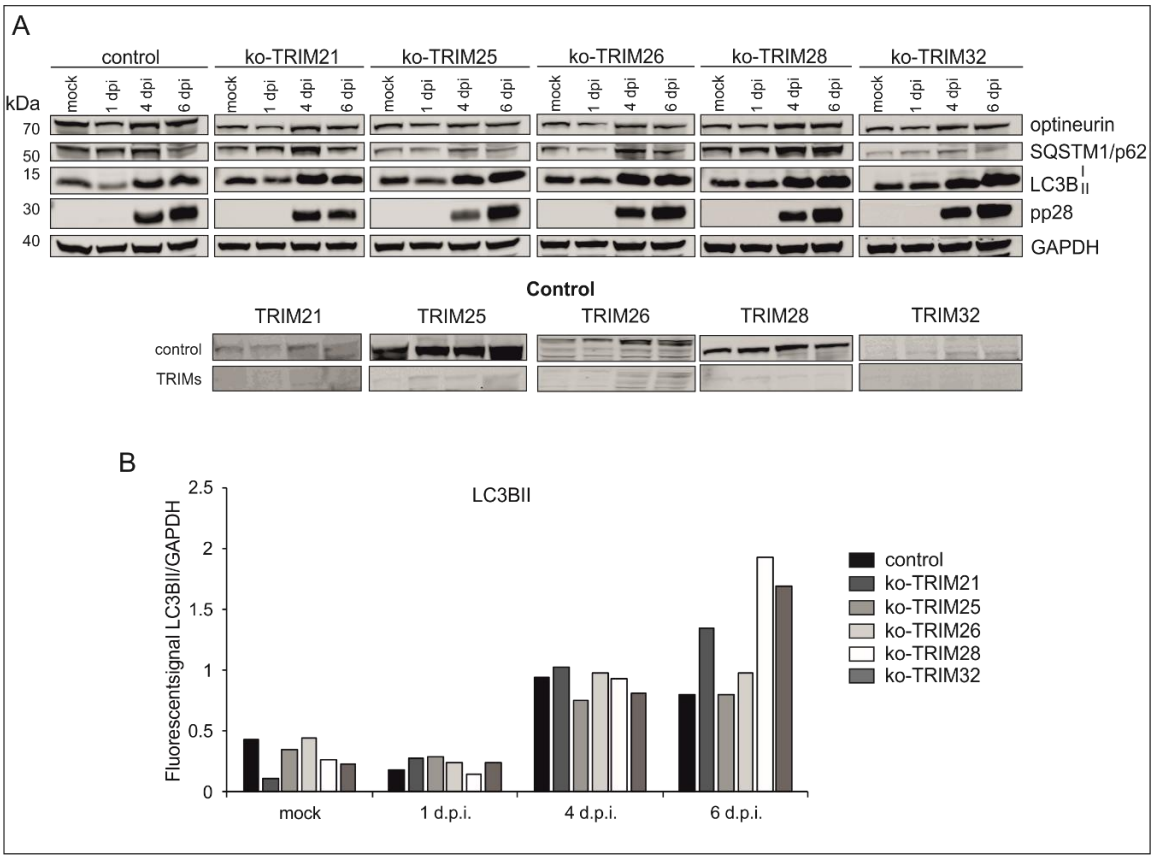

Figure 28. Western blot analysis of the impact of TRIM proteins on autophagy and autophagy receptors in infected cells. (A) HFF knockout cells of *TRIM21, TRIM25, TRIM26, TRIM28*, and *TRIM32* and control cells were infected with HCMV (m.o.i. = 0.5). Cells were harvested at 1, 4, and 6 d.p.i. Autophagy, monitored by the autophagic marker LC3B and levels of both autophagy receptors SQSTM1/p62 and optineurin were analyzed by Western blot, using antibodies against LC3B, SQSTM1/p62 and optineurin. Antibodies against pp28 (virus control) and GAPDH (loading control) were carried along, n=1. (B) The fluorescence intensity band ratios of LC3BII to GAPDH were determined and plotted for each cell line and each time point of the Western blot shown in A.

4.5 IRGQ, a novel autophagy-associated factor, impairs HCMV infection

In the context of our collaboration with the group of Dr. Lina Herhaus we became interested in the role of the immunity related GTPase Q protein (IRGQ). IRGQ had been identified by Herhaus and colleagues as a novel player in autophagy (Herhaus unpublished). They found that IRGQ interacts with members of the LC3/GABARAP family, specifically with GABARAP-L2 and LC3B and that the interaction with GABARAP-L2 is modulated by phosphorylation during infection with *Salmonella*. Thus, IRGQ has been uncovered as a novel player in bacterial clearance (Herhaus unpublished). We thus wished to address the question, if IRGQ is also an effector during viral infection.

4.5.1 Knockdown of IRGQ promotes HCMV progeny production

To investigate whether IRGQ had an impact on HCMV infection, the IRGQ was down-regulated by siRNA knockdown. In an initial experiment, the knockdown of IRGQ was verified in uninfected HFF at different time points after transfection. For this, 2×10^5 HFF were seeded in 6 cm plates, respectively, and transfected with either a siRNA against IRGQ (siIRGQ) or a control siRNA (siControl). Cells were collected at 2, 3 or 6 days post transfection (d.p.t.) and analyzed by Western blot. A distinct knockdown of IRGQ was detectable at all times after transfection tested (Figure 29).

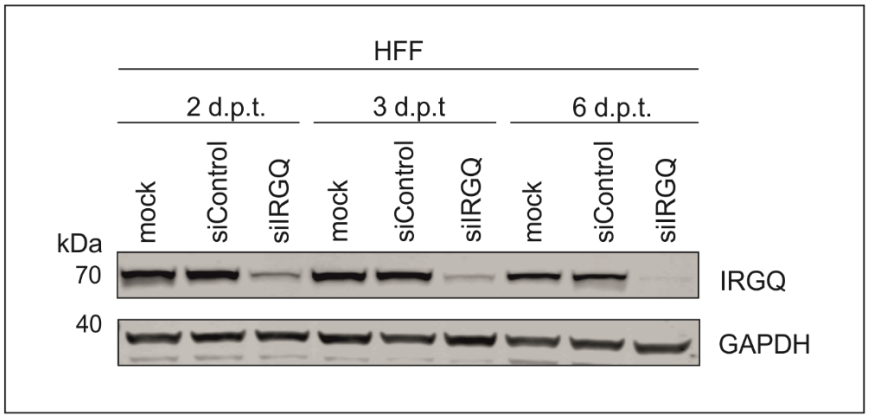

Figure 29. Western blot analysis of the knockdown of IRGQ in HFF. HFF were transfected with 30 pmol of siRNA against IRGQ (siIRGQ). As a control, cells were either transfected with a control siRNA (siControl) or were left untreated (mock). At 2, 3, and 6 d., HFF were harvested and analyzed for the IRGQ level by Western blot. An antibody against GAPDH was used as loading control.

To analyze whether IRGQ would affect HCMV infection, both viral genome replication and progeny production were addressed. For this, HFF were transfected with siIRGQ or siControl, (30 pmol), respectively. Cells were subsequently infected with HCMV (4 genome copies/cell) at 2 d.p.t. Both cells and culture supernatants were harvested at the indicated time points after infection. Viral DNA was isolated and the number of genome copies per cell was quantified by TaqMan qPCR. Comparable viral DNA levels were found in siRNA-IRGQ-transfected and control-transfected cells, indicating that the knockdown of IRGQ had no influence on HCMV genome replication (Figure 30A). For the determination of viral progeny release, the IE1-assay was used. Interestingly, the number of IE1-positive cells was significantly enhanced in supernatants from siIRGQ-transfected cells (Figure 30B), compared to siControl-transfected cells. At 4 and 6 d.p.i., progeny release increased up to 10-fold. In accordance with this, expression levels of the viral proteins IE1 and pp28 were markedly enhanced in siIRGQ-transfected cells in the course of infection (Figure 30C). These data indicated that the expression of *IRGQ* does not interfere with HCMV genome replication but impedes HCMV progeny production.

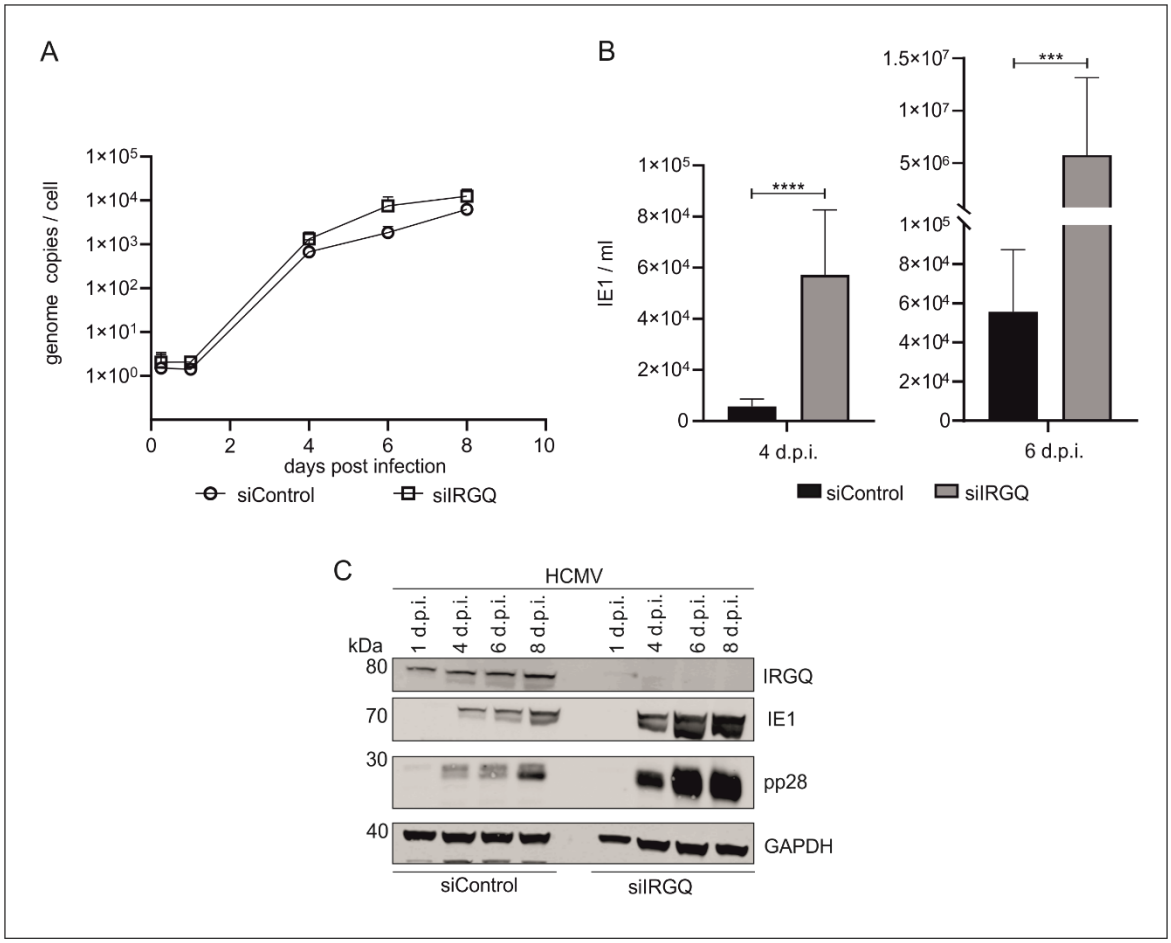

Figure 30. Analysis of the impact of IRGQ on HCMV infection. (A) HFF were transfected with either siIRGQ or siControl and infected with HCMV (4 genome copies/cell) at 2 days after transfection. At different time points post infection, both cells and supernatants were collected. (A) Quantitative PCR analysis of the genome replication of HCMV in HFF, transfected with siIRGQ.

DNA was isolated and viral genomes were quantified by TaqMan-based qPCR. The mean values + SD of three technical replicates from two individual experiments are shown for each siRNA transfection and respective time point. (B) The cell culture supernatant of 4 and 6 days after infection was analyzed for HCMV progeny production by IE1-assay. The mean values + SD of eight technical replicates from three individual experiments are shown for each siRNA transfection and respective time point. Statistical analysis was performed using Welch's t-test: ***: $p < 0.001$; ****: $p < 0.0001$. (C) Western blot analysis of the expression levels of viral proteins IE1 and pp28 in knockdown versus control transfected cells. The knockdown of IRGQ was verified using specific antibody. GAPDH was probed as loading control. A representative Western blot of two analysis is shown.

4.5.2 Knockdown of GABARAP-L2 partially abrogates the enhanced HCMV progeny production in IRGQ down-regulated cells

IRGQ has been identified as an interactor with GABARAP-L2 proteins (Herhaus, unpublished), which decorate autophagosomal membranes, supporting autophagosome formation and recruiting autophagy receptors (Kabeya et al., 2004; Weidberg et al., 2010). The interaction of both proteins has been shown, in addition, to enhance autophagosomal degradation in *Salmonella* infection (Herhaus unpublished). We thus asked whether the two proteins cooperate in a way to reduce HCMV progeny production. For this we concomitantly knock both IRGQ and GABARAP-L2 down. HFF were transfected with the respective siRNAs against either IRGQ, GABARAP-L2 (siGABARAP-L2) or both. Cells transfected with a control siRNA were used as control. 48 hours post transfection, part of the samples was collected and analyzed by Western blot to verify the knockdown (Figure 31A). Like before, the parallel cell samples were infected with the HCMV, using 4 genome copies/cell. Both, supernatants and cells were collected at the different time points after infection. Purified viral DNA from cells was used for qPCR to monitor viral genome replication. As expected, the levels of viral genomes of both, siIRGQ and siControl-transfected HFFs were comparable (Figure 31B). Interestingly, the knockdown of GABARAP-L2, or in combination with the knockdown of IRGQ, also did not affect viral genome replication. The culture supernatants, collected in parallel were tested by the IE1-assay. Again, the downregulation of IRGQ led to a significantly increased HCMV-progeny release rate at 4 and 6 d.p.i. compared to the control samples (Figure 31C). The knockdown of GABARAP-L2 resulted in enhanced progeny release at 4 d.p.i. but not at 6 d.p.i.. Surprisingly, when both IRGQ and GABARAP-L2 were downregulated, the significant effect of IRGQ on HCMV infection was abrogated at both time points tested. The viral titers were similar to the knockdown of GABARAP-L2. Knockdowns of IRGQ and GABARAP-L2 were monitored throughout the period by Western blot (Figure 31D). The data show that the antiviral effect of IRGQ depends on the presence of GABARAP-L2.

The interesting findings shown here provide preliminary evidence that IRGQ interferes with HCMV infection. The molecular analysis of this exceeds the time frame of this thesis and will have to be addressed in further studies.

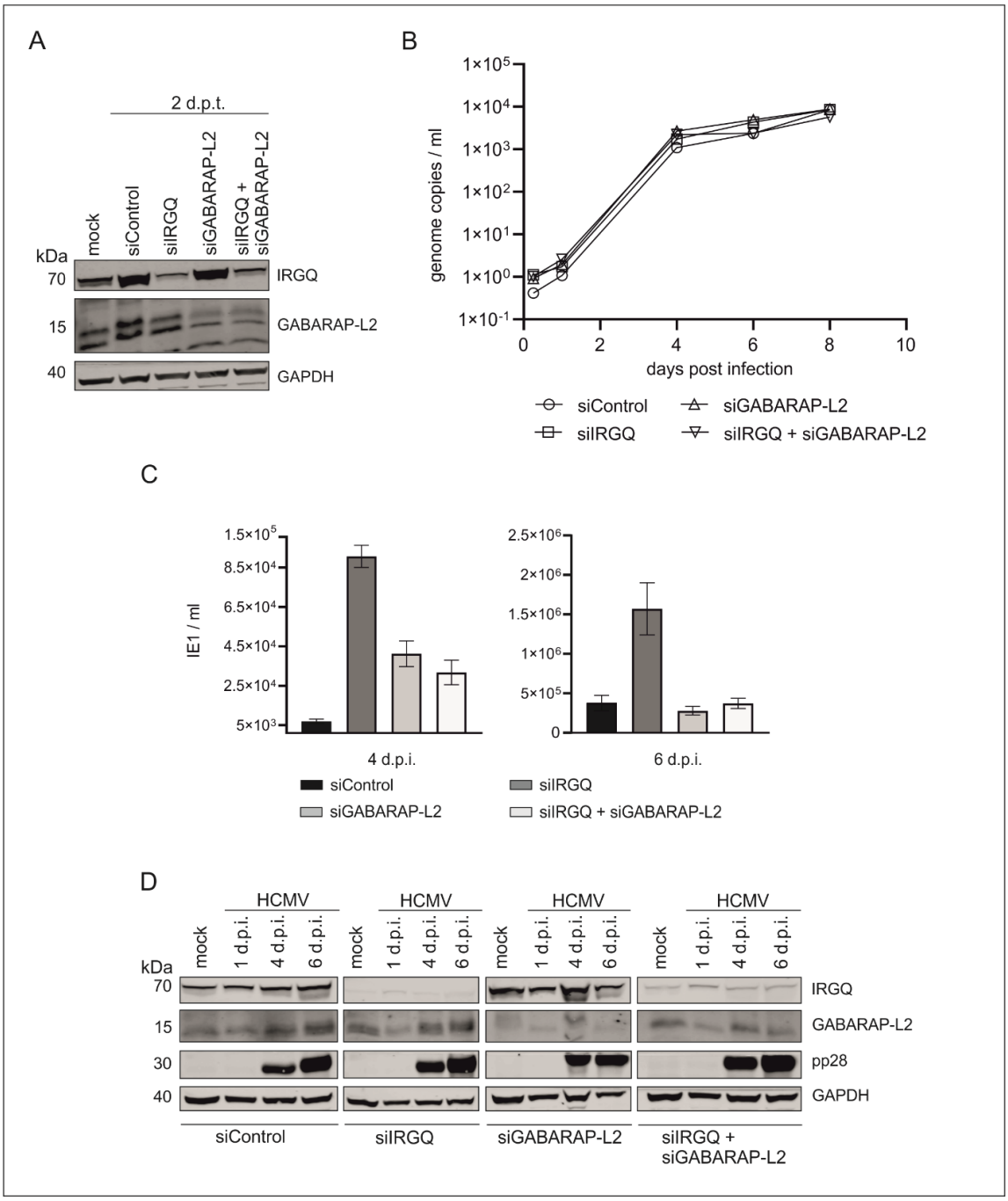

Figure 31. Analysis of the impact of a concomitant knockdown of both IRGQ and GABARAP-L2. (A) Western blot analysis of the efficiency of the concomitant knockdown of IRGQ or GABARAP-L2. HFF were transfected with the indicated siRNAs. At 2 d.p.t., HFF were harvested and the levels of both IRGQ and GABARAP-L2 were investigated by Western blot. GAPDH was probed as loading control, n=1. (B, C, and D) Cells were transfected as described in A and infected 48 hours post transfection with HCMV (moi 0.5). Cells and supernatants were collected at the indicated time points. (B) Viral DNA was isolated from 1× 10^5 cells and DNA replication was analyzed by TaqMan qPCR. The mean values and the corresponding SD are shown from three technical replicates from one biological experiment. (C) Analysis of the release of progeny virus into the culture supernatant by serial dilution and staining for IE1 protein expression on indicator cells in eight technical replicates for each dilution. Viral progeny release is shown in the bar chart. The data

represent mean values + SD of eight technical replicates from one biological experiment. (D) Collected cell samples were analyzed for the knockdown of IRGQ and GABARAP-L2 respectively, during HCMV infection by Western blot, using specific antibodies. Antibodies against pp28 (virus control) and GAPDH (loading control) were also used.

5 Discussion

In selective autophagy, autophagy receptors act as a bridge between cargo and developing autophagosomes. The receptors thereby selectively recognize their cargo, such as viruses, to deliver it to the autophagosomes for lysosomal degradation (Kirkin and Rogov, 2019; Stolz et al., 2014; Viret et al., 2021). The interaction with both the cargo and the autophagic machinery is partly regulated by phosphorylation. In viral infections, several autophagy receptors have come into focus as crucial players, such as SQSTM1/p62 and optineurin (Ames et al., 2021; Mohamud et al., 2019; Orvedahl et al., 2010). Also, some members of the TRIM protein family have been found to serve as autophagy receptors during viral infections (Mandell et al., 2014b). However, the role of SQSTM1/p62, optineurin and several TRIMs and their regulation in HCMV infection remained unclear.

5.1 Interaction of SQSTM1/p62 with viral proteins of HCMV

Both SQSTM1/p62 and optineurin serve as autophagy receptors during viral infections. In HCMV infection, their role remains poorly understood. A first promising result was recently published by our group, showing that SQSTM1/p62 interacts with a number of viral structural and non-structural proteins upon HCMV infection (Zimmermann, Krämer et al., 2021). SQSTM1/p62 and optineurin were found in purified HCMV particles, which might mean that the receptors are intentionally packaged into released progeny and, upon infection delivered into cells, thereby influencing HCMV replication immediately after infection (Taisne et al., 2019), Zimmermann, Krämer et al., 2021) (Figure 3).

The interaction of SQSTM1/p62 with HCMV proteins, previously published by our group (Zimmermann, Krämer et al., 2021) could be confirmed in this work (Figure 4). Remarkably, again major components of the viral capsid could be identified as SQSTM1/p62 interactors. Binding of SQSTM1/p62 to viral capsid proteins has also been reported for Sindbis- and Chikungunya virus, respectively. In both cases, this interaction leads to virophagy by targeting capsids to autophagosomes (Judith et al., 2013; Orvedahl et al., 2010). In analogy with Sindbis virus and Chikungunya virus infection, the interaction of SQSTM1/p62 with viral capsid components might drive nascent HCMV particles into autophagosomal degradation. An examination of the content of autophagosomes from HCMV-infected cells was attempted by FACS analysis. However, it could not provide any information because it was not clearly distinguishable between viral particles and autophagosomes, according to the sort against LC3B, which is present in both structures (data not shown).

5.2 The impact of SQSTM1/p62 on HCMV infection

The role of SQSTM1/p62 in the course of HCMV infection was studied in HFF-ko cells (Figure 5A and B). No significant impact of *SQSTM1* knockout on viral genome replication was found upon HCMV infection of these cells, compared to control HFF (Figure 5C). Thus, although SQSTM1/p62 was packaged into viral particles and presumably introduced into cells during infection, this apparently did not influence the early events leading to HCMV genome replication. A moderate increase in viral progeny release from infected ko-SQSTM1 cells was detected compared to infected HFF control cells, using a biological assay (Figure 5E). In contrast, there was no impact found on viral genome release from infected cells, measured by qPCR (Figure 5D). The latter kind of analysis is frequently used as a surrogate marker for progeny production. These results may indicate that the genome-to-infectivity ratio of particles released from ko-SQSTM1 cells was slightly lower than that of particles released from control-HFF, meaning that more DNA-containing, infectious virions were released from the former cells. This suggests that, although the amount of genomic DNA released was similar, more genomes were packaged into infectious virions released from ko-SQSTM1 cells. These results were obtained using the HCMV strain BADwt and were confirmed, using the clinical HCMV strain TB40/E (Figure 6).

A recent publication by König and colleagues showed that siRNA-mediated knockdown of SQSTM1/p62 had no influence on viral gene expression, confirming our results with the knockout cells (König et al., 2021). Contrary to our results, a reduction in viral genome release but no impact on IE1-level in Western blot analyses were found following SQSTM1/p62 knockdown. The reason for this discrepancy is unclear at this point. In line with their results, a subtle reduction in the levels of late viral proteins important for progeny morphogenesis was found in HCMV-infected ko-SQSTM1 cells, compared to control HFF (Figure 5F and Figure 6C). However, this was also accompanied by a slightly reduced level of the marker protein GAPDH. Of note, the knockout cells showed enhance cytopathic changes upon infection, compared to control-HFF (data not shown). Thus, considering the moderate effects that were observed, the differences might well be explained by effects on cell homoeostasis, afforded by the complete absence of SQSTM1/p62. This is supported by reports showing that, besides its role as autophagy receptor, SQSTM1/p62 may have other functions such as controlling apoptosis or involvement in several signal transduction cascades upon HCMV infection (Fan et al., 2018; Kumar et al., 2022; Orvedahl et al., 2010; Sanz et al., 1999).

These divergent results obtained in studying SQSTM1/p62 may be based on its multifunctional roles, regulating cellular processes with divergent outcomes. An assumption would be that, on the one hand, the capsids or capsid proteins of HCMV are specifically targeted by SQSTM1/p62 and are favorably directed for autophagolysosomal degradation. Consequently, in control HFF, capsid morphogenesis is controlled or impaired by SQSTM1/p62, leading to an elevated release of non-functional virus particles and thus a

higher genome-to-infectivity ratio, compared to the ko-SQSTM1. A concordant result was obtained in our recent publication, where the impairment of autophagy using an HCMV mutant expressing a dominant-negative version of the autophagy regulator ATG4B led to enhanced release of infectious virus (Zimmermann, Krämer et al., 2021). On the other hand, SQSTM1/p62 is involved in cellular transport and in regulating the interferon responses (Chen et al., 2016; Liu et al., 2016; Prabakaran et al., 2018; Seibenhener et al., 2004). Thus, the different effects seen in this work and in the work from other laboratories are likely subject to variation, depending on the methodologies and the cell lines used for analyses.

Interestingly, although SQSTM1/p62 is described to control autophagy via its expression level in different cell lines (Liu et al., 2016), an altered autophagosome formation was not observed in this work in both uninfected and infected ko-SQSTM1 cells (Figure 7). This indicates that SQSTM1/p62 does not regulate autophagy in fibroblasts and, more interestingly, the impact of SQSTM1/p62 on HCMV infection is independent of its role in autophagy regulation.

Knockout of *SQSTM1* resulted in increased levels of the ISGs Mx1 and ISG15 upon HCMV infection (Figure 8). This indicates that the interferon response was controlled by SQSTM1/p62 in HCMV-infected cells. Similar results were reported by Prabakaran and colleagues in murine cytomegalovirus (MCMV)-infected cells. They showed that, upon MCMV infection, active STING was targeted by SQSTM1/p62 to autophagosomal degradation, leading to an enrichment of ISG protein levels. They suggested that degradation of STING was mediated by SQSTM1/p62 as a control mechanism to prevent sustained IFN-I pathway signaling and excessive ISG synthesis (Prabakaran et al., 2018). The mechanisms that are operative are unclear at this point, but SQSTM1/p62 appears to be involved in IFN regulation also in HCMV-infected cells.

Ko-SQSTM1 cells, infected with either the BADwt or the TB40/E strain showed reduced expression levels of late, structural HCMV proteins, concordant with the idea that an overexpression of ISGs limits viral gene expression. Surprisingly, the release of viral progeny from ko-SQSTM1 cells was concomitantly enhanced. The reason for this discrepancy is not immediately clear. Results of our previous work had suggested that HCMV particles are targeted to autophagosomes at late stages of infection. The fact that SQSTM1/p62 interacts with viral structural proteins indicates that this molecule is a key receptor to mediate virophagy in HCMV infection. Thus, the lack of SQSTM1/p62 in the late stages of HCMV infection likely leads to an enhanced number of fully infectious virions that escape degradation and are released from cells into the culture supernatant.

It thus appears that SQSTM1/p62 has a balancing role during HCMV infection, limiting excessive interferon responses and subsequently limiting viral progeny production by targeting nascent virions to autophagy.

5.3 The role of optineurin in HCMV infection and autophagy regulation

Optineurin was described to act in virophagy by targeting two proteins of HSV-1 to the autophagy machinery (Ames et al., 2021). Surprisingly, optineurin poorly interacted with HCMV proteins, questioning its role as an autophagy receptor during HCMV infection (Figure 4). One scenario to explain this might be that optineurin is a supportive autophagy receptor that targets viral proteins in the absence of SQSTM1/p62. This could however not be verified as optineurin was unsuitable to complement SQSTM1/p62 in its capacity to bind to viral proteins upon HCMV infection (Afifi, 2021, unpublished). In addition, the lack of optineurin did not alter autophagy in uninfected and infected HCMV cells (Figure 7). Thus, optineurin does not appear to have a role as an autophagy regulator in HCMV infection.

The packaging of optineurin into HCMV particles indicates that its function goes beyond its role of an autophagy receptor in HCMV-infected cells (Figure 3). This is supported by the fact that several other autophagy receptors were undetectable in HCMV particles, leading to the assumption that optineurin was intentionally incorporated. In addition, pUL84 was the only HCMV protein that was found to interact with optineurin (Figure 4). This protein is required for DNA replication and is essential in regulating viral gene expression (Pari, 2008; Xu et al., 2004a; Xu et al., 2004b). Interestingly, pUL84 was also found in the array of proteins that interacted with SQSTM1/p62. Thus, the interaction of both SQSTM1/p62 and optineurin with pUL84 suggests that the function of this particular viral protein is regulated by both molecules and that their availability immediately after infection by passive introduction into the cells by infecting viral particles was important for the early events of HCMV infection. However, the lack of optineurin neither impaired viral DNA replication, nor DNA- or viral progeny release (Figure 5 and Figure 6). These findings were obtained by using either the HCMV laboratory strain BADwt or the clinical strain TB40/E. More detailed analyses on the role of the optineurin-pUL84 interaction and a possible impact of the cell type with regard to HCMV infection will be necessary to address this issue.

5.4 Phosphorylation of SQSTM1/p62 at S272 and its impact on viral HCMV infection

The ability of autophagy receptors to bridge the cargo with the autophagy machinery is partly controlled by phosphorylation, which either facilities or impedes the interactions (Farré et al., 2013; Gubas and Dikic, 2022; Rogov et al., 2017).

This work demonstrated that the phosphorylation site S272 of SQSTM1/p62 was hyperphosphorylated upon HCMV infection (Figure 9B). Interestingly, the enhanced phosphorylation at this site was only detectable between 1 to 3 d.p.i., whereas the phosphorylation returned to mock levels at 6 d.p.i. (Figure 9C and D). It is not yet clear why the phosphorylation appeared in a specific time window during infection. The phosphorylation at S272 of SQSTM1/p62 is often accompanied by the regulation of the neighboring residue T269 in uninfected cells (Linares et al., 2011; Zhang et al., 2022). Interestingly, the phosphorylation at T269 was unaltered in HCMV-infected cells. This suggested that only the phosphorylation at S272 of SQSTM1/p62 was important during HCMV infection. Consequently, the impact of the phosphorylation status of SQSTM1/p62 at S272 was further investigated by using HCMV mutants expressing SQSTM1/p62 with a different phosphorylation status at position 272 (Figure 10 and Figure 12). Viral genome replication was widely unaltered irrespective of the phosphorylation status of SQSTM1/p62 at 272, with a slight tendency of increased viral DNA replication upon infection with the non-phosphorylatable version of SQSTM1/p62 at 272 (S272A) and the phosphomimicking mutant (S272E) (Figure 13A). Thus, the assumption was that the effect of this phosphorylation occurs downstream of genome replication. A distinct finding was that the progeny release from cells infected with either the wt or the phosphomimicking (S272D) strain was significantly lower compared to cells infected with S272A mutant (Figure 13B), accompanied by elevated viral protein levels upon infection with this non-phosphorylatable mutant (Figure 13C). This indicated that S272 phosphorylation conferred an antiviral effect on HCMV progeny production. Surprisingly, the second phosphomimicking mutant (S272E) did not show the same phenotype as wt and S272D. The most likely explanation for this was that the replacement of this phosphosite with aspartate did not result in the correct mimicking, which is a well-established effect when using phosphomimicking mutants.

The protein levels of SQSTM1/p62 were reduced in S272A-infected cells, compared to wt and S272D (Figure 12). In addition, viral progeny release from S272A infected cells was up to 5-10 higher, compared to wt or S272D infected cells (Figure 13B). Thus, the differences in progeny production could be related to the amount of SQSTM1/p62 in the cell rather than to the phosphorylation status. However, in contrast, the knockout of the endogenous *SQSTM1* led to only a 1.5 to 2 increased release of progeny (Figure 5), arguing against protein levels as the sole determinant of the impact of SQSTM1/p62 on HCMV infection. Rather, viral progeny release in HCMV-infected cells appears to be, at least in part, dependent on the phosphorylation status at S272 of SQSTM1/p62.

5.4.1 Impact of the phosphorylation of SQSTM1/p62 at S272 on its proteasomal degradation

Protein levels of SQSTM1/p62 were reduced in HCMV-SQSTM1-S272A-infeced cells, compared to the levels seen after infection with the other mutant viruses. In addition, the infection with HCMV-SQSTM1-S272wt with a fourfold lower infection rate still resulted in higher protein levels of SQSTM1/p62, compared to the HCMV-SQSTM1-S272A infection (Figure 14C). The nucleotide sequence analyses of the respective BACmids did not reveal any mutations in the coding region or the promotor of *SQSTM1*. This indicated that the amount of SQSTM1/p62-S272A was regulated on the protein level and that the phosphorylation at residue 272 contributed to protein stabilization. The results further showed that the phosphorylation at S272 protects the receptor from proteasomal degradation but that this modification does not drive lysosomal degradation (Figure 14A and B). The residue 272 is positioned in one of the two PEST domains of SQSTM1/p62, a region rich in proline (P), glutamic acid (E), serine (S) and threonine (T) (Liu et al., 2016; Rogers et al., 1986). In general, PEST domains function as a proteolytic signal, enabling rapid protein turnover (Rechsteiner and Rogers, 1996). Although a PEST domain is permanently present, the protein has to be marked for degradation, for example by phosphorylation of this motif, resulting in proteasomal degradation (Rechsteiner, 1990). In the case of SQSTM1/p62, however, the phosphorylation of SQSTM1/p62 at S272 protected the receptor from degradation by the proteasome upon HCMV infection (Figure 14A). Interestingly, a similar effect was also seen for the vascular endothelial growth factor receptor 2 (VEGFR-2), where the phosphorylation of a PEST domain-like sequence attenuated the degradation of the protein (Meyer et al., 2011).

Interestingly, Linares and colleagues found that phosphorylation at positions 269 and 272 of SQSTM1/p62 made the receptor more susceptible to degradation during mitotic exit (Linares et al., 2011). This is in contrast to the findings reported here. The reason for this is unclear at this point. One explanation might be that both 269 and 272 needed to be phosphorylated to mediate degradation of SQSTM1/p62, opposed to the phosphorylation at S272, seen in HCMV-infected cells. In addition, other small molecules might be involved in modifying SQSTM1/p62 in HCMV-infected cells. It is well established that such molecules like ubiquitin or sumo are used by the virus to regulate protein stability in infected cells (Gu and Jan Fada, 2020; Imbert et al., 2022; Le-Trilling et al., 2020). Thus, the regulation of SQSTM1/p62 stability in HCMV-infected cells might be subject to multiple levels of regulation with the phosphorylation at S272 in the PEST-domain being an essential switch.

5.4.2 Impact of the phosphorylation status of SQSTM1/p62 at its residue 272 on autophagy and ISG protein levels in HCMV-infected cells

The mechanism how the phosphorylation of SQSTM1/p62 at S272 affects HCMV infection was part of the analysis by investigating autophagy and IFN-I pathway. According to Linares and colleagues, phosphorylation at both S272 and T269 of SQSTM1/p62 is required for the activation of the mammalian target of rapamycin complex 1 (mTORC1), an inhibitor of autophagy in response to nutrient availability (Linares et al., 2015). Thus, given their results, one might have expected a downregulation of autophagy in cells infected with HCMV-SQSTM1-S272wt or HCMV-SQSTM1-S272D. The analysis however showed that the levels of the autophagic marker LC3BII were similar in cells, infected with all HCMV-SQSTM1-S272-mutants, indicating that autophagosome formation was not influenced by the phosphorylation status of SQSTM1/p62 at S272 (Figure 15). In addition, we did not observe impairment of LC3BII levels in SQSTM1/p62 knockout cells (displayed in Figure 7). Together, this indicates that, at least in HCMV-infected cells, SQSTM1/p62 is not essential for autophagosome formation and that other factors might supplement its function in the process of autophagy regulation.

Lack of SQSTM1/p62 in HCMV-infected cells resulted in increased ISG protein levels, whereas the infection of knockout cells with a SQSTM1/p62-expressing mutant resulted in suppression of ISGs. Thus SQSTM1/p62 was identified as a negative regulator of ISG protein levels upon HCMV infection. This is in line with the finding of Prabakaran and colleagues who showed that the receptor recruits STING to the autophagosome for degradation, resulting in a control of ISG protein levels upon MCMV infection (Prabakaran et al., 2018). The ability of SQSTM1/p62 to degrade STING and to control ISG-production depended on the phosphorylation of the receptor at position S403, as evidenced by a S403A mutant which did not confer control. The authors conclude that SQSTM1/p62 was essential for executing degradation of STING and attenuation of interferon signaling after infection. Interestingly we found that cells infected with the S272A mutant of SQSTM1/p62 displayed lower ISG protein levels, compared to S272wt- and S272D-infected cells (Figure 16). This suggests that, opposed to the phosphorylation at S403, the phosphorylation at S272 attenuates the control function of SQSTM1/p62 with regard to the interferon signaling pathway. Thus, our results show that SQSTM1/p62 controls ISG levels in HCMV-infected cells and that differential regulation of the interferon pathway following infection with the different mutants explains the differences in progeny production.

5.4.3 Role of the phosphorylation at S272 of SQSTM1/p62 in the binding of cellular and HCMV proteins

The results did not reveal clear evidence for a role of the phosphorylation status of SQSTM1/p62 at S272 in determining the binding of the receptor to target proteins. Although the MS analyses showed that the non-phosphorylatable (-S272A) and also the phosphomimicking (-S272D) version of SQSTM1/p62 precipitated with a larger number of cellular proteins than SQSTM1/p62-S272wt (Figure 17A), this finding could not be confirmed for a number of cellular proteins by a Western blot (Figure 17B). Still, this does not exclude that the binding to selected other proteins was affected by the phosphorylation status at 272. Based on our findings, however, it is likely that the phosphorylation of SQSTM1/p62 at S272 has no impact on the affinity and specificity of the receptor to target proteins. This may be explained by the localization of this phosphosite because S272 is localized neither in the UBD nor in the LIR motif. Phosphosites in these two domains control the axis between cargo and the autophagic machinery. One example is the phosphorylation at S403 in the UBD, which promotes the interaction with ubiquitinated proteins and, subsequently, their clearance (Lim et al., 2015; Matsumoto et al., 2011).

Interestingly, there are two publications describing that the phosphorylation at T269 and S272 could impair the binding to autophagosomes either under stress conditions or upon proteasomal inhibition (Kehl et al., 2019; Zhang et al., 2022). Thus, not the cargo specificity but the interaction with proteins linked to autophagosomal membranes could be influenced by the phosphorylation at S272. The interaction between SQSTM1/p62 in dependence on its phosphorylation level with both LC3 and GABARAP proteins in HCMV-infected cells was not addressed in this work, thus leaving the question unanswered whether the phosphorylation at S272 affects the interplay of the receptor with autophagosomes.

Both the MS and the Western blot analyses demonstrated that SQSTM1/p62 specifically interacted with the cellular protein POM121 upon HCMV infection. Again, this interaction seems to be independent of the receptor's phosphorylation status at S272. POM121 is a transmembrane protein of the nuclear pore complex (NPC). The protein plays an important role in initiating NPC assembly by anchoring the complex to the membrane of the nuclear envelope (Casem, 2016; Doucet et al., 2010; Funakoshi et al., 2011). Moreover, the protein-protein network analyses revealed that several other proteins associated to the NPC and nucleocytoplasmic transport were co-precipitated by SQSTM1/p62-S272wt, -S272A, and -S272D (Figure 19).

These data are in agreement with the role of SQSTM1/p62 as a shuttle protein between the nucleus and the cytoplasm (Pankiv et al., 2010; Thakar et al., 2013). So far, the shuttle process of SQSTM1/p62 and the interaction with proteins of NPC are poorly understood. The data in this work showed that the variants of SQSTM1/p62 interacted with a largely overlapping set of NPC proteins upon HCMV infection as -S272wt or -S272D. These proteins, belonging to NPC, are either located at the outer nuclear membrane or in the lumen of the complex,

representing an interaction with the NPC in the cytoplasm (Beck and Hurt, 2017). According to the STRING database, a protein-protein interaction between SQSTM1/p62 and any of the identified members of the NCP family has not yet been described, suggesting that these interactions of SQSTM1/p62 could be specific in HCMV-infected HFF.

Interestingly, Pankiv et al. demonstrated that phosphorylation of SQSTM1/p62 at T269 and S272 can accelerate nuclear import activity (Pankiv et al., 2010). Thus, phosphorylation at S272 may also play a regulatory role in modulating nucleocytoplasmic shuttling of SQSTM1/p62 in HCMV-infected cells. Enhanced nuclear import of SQSTM1/p62 may result in an early interaction of the receptor with components of nascent HCMV capsids, leading to a transport of capsid protein to the autophagosomes for degradation. The results from this work support this and may be the basis for further research to elucidate the molecular mechanisms behind the shuttling of SQSTM1/p62 between the cytoplasm and the nucleus in HCMV-infected cells.

Two further specific biological processes have been identified in the STRING analysis, which could be influenced by SQSTM1/p62 independent of its phosphorylation status at S272, namely the Golgi vesicle transport and the postsynaptic neurotransmitter receptor internalization (Figure 18). Proteins related to the respective processes were found to co-immunoprecipitate with SQSTM1/p62. In order to determine the impact of SQSTM1/p62 on those two processes, the confirmation of the interaction with the respectively associated proteins is pending. Besides these specific processes, rather general processes such as macromolecule localization and partly metabolic process and gene expression were affected by SQSTM1/p62 (Figure 18).

The phosphorylation status at S272 had little impact on the binding of HCMV proteins to SQSTM1/p62 (Figure 20). This is evidenced by the fact that the non-phosphorylatable (272A) variant of SQSTM1/p62 precipitated with the same proteins as its the phosphomimicking variant of SQSTM1/p62 (-272D). Thus, the specificity of the receptor to viral proteins was not altered by the phosphorylation level at S272, as also seen for cellular target proteins. Interestingly, most of the precipitated proteins are structural capsid components. Even proteins of low abundance, such as pUL77 and pUL93, interacted with SQSTM1/p62. In conclusion, the data show that the interaction of SQSTM1/p62 with both cellular and viral proteins is independent of its phosphorylation level at its site S272.

In summary, a model of the major findings of SQSTM1/p62 and its role in HCMV infection is shown in Figure 32.

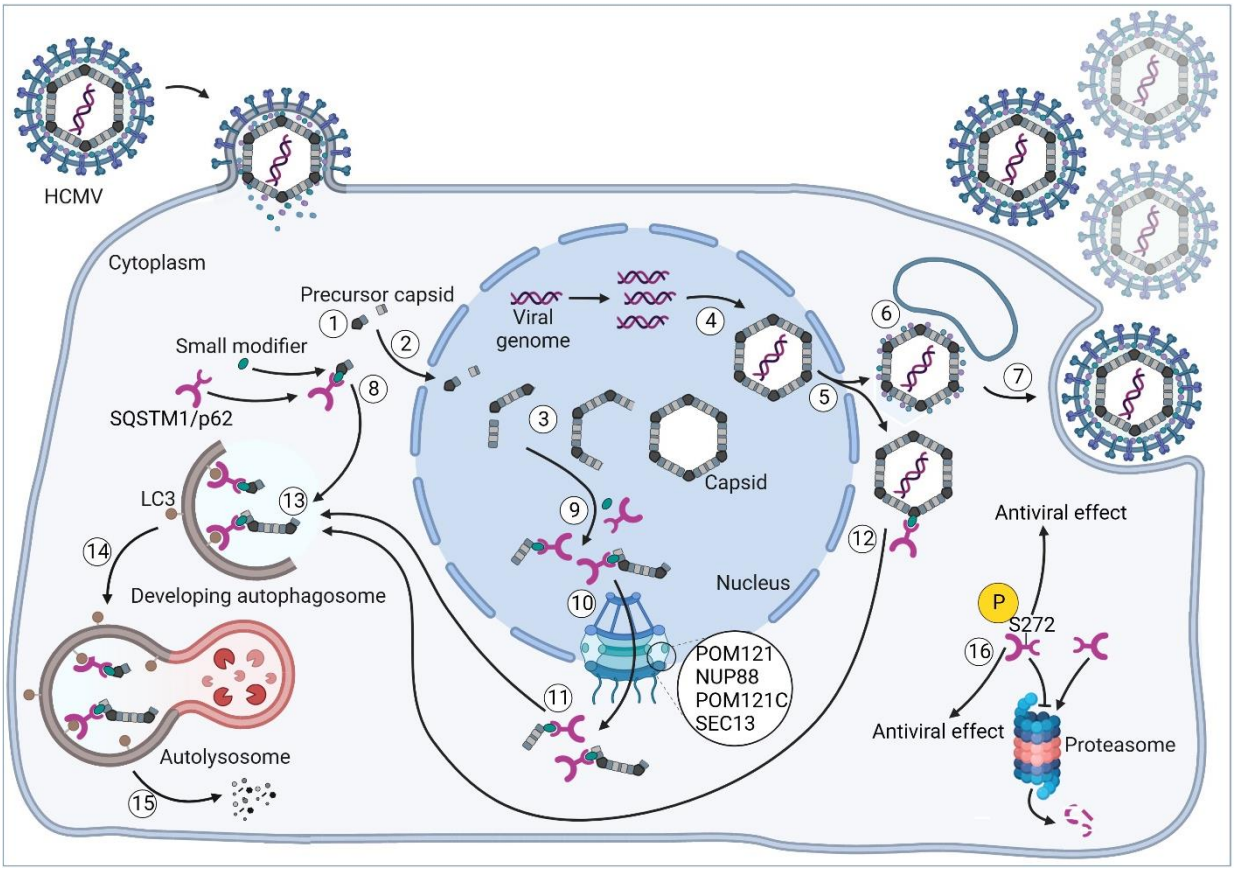

Figure 32. Schematic interaction between SQSTM1/p62 and HCMV capsid components and its impact on HCMV infection. (1) In HCMV-infected cells, precursor capsids assemble in the cytoplasm in the process of particle morphogenesis. (2) These viral structures are translocated in the nucleus. (3) Here, precursor capsid components coalesce to form an icosahedral capsid. (4) After this process, the viral genome is packaged into capsids, (5) followed by nuclear egress of the DNA-containing capsids into the cytoplasm. (6) Capsids are transported to cytoplasmic virion assembly compartments (cVACs), where they associate with tegument proteins and are enveloped by cellular membranes. (7) Finally, particles are transported to the cell membrane, where they are released into the extracellular space by membrane fusion. The results of this work indicate that the autophagy receptor SQSTM1/p62 affects the assembly of capsids and their precursor structures at different points during HCMV infection, resulting in reduced viral progeny release. (8) SQSTM1/p62 may already recognize precursor capsid components in the cytoplasm, which are probably attached to small modifiers such as ubiquitin for recognition. SQSTM1/p62 transports the capsid components to the developing autophagosome. (9) A second interaction between SQSTM1/p62 and capsid structures occurs in the nucleus. (10) As SQSTM1/p62 shuttles between the cytoplasm and the nucleus, the assumption is that the receptor interacts with pro-capsid structures to mediate their export into the cytoplasm through the nuclear pore complex (NPC) via the interaction with proteins of NPC such as POM121, NUP88, POM121C, and SEC13. (11) The exported pro-capsid structures are then transported to the developing autophagosome. (12) The mature capsids released from the nucleus into the cytoplasm could also be recognized by SQSTM1/p62 and be directed to autophagosomes. (13) SQSTM1/p62 binds LC3B, anchored on the autophagosomal membrane. (14) The autophagosome fuses with a lysosome to form the autolysosome. The viral proteins are subsequently degraded in the autolysosome. (15) The resulting material is released into the cytoplasm

to be recycled. (16) Upon HCMV infection, SQSTM1/p62 is phosphorylated at S272, preventing the receptor from proteasomal degradation and leading to its enrichment and mediating an antiviral effect. The mechanism behind this effect has yet to be determined. The model was created with BioRender.com.

5.5 Impact of pUL97 and CDK1 on SQSTM1/p62 S272 phosphorylation

The finding that SQSTM1/p62 was hyperphosphorylated upon HCMV infection suggested that the viral kinase pUL97 was involved. This kinase is known to control the course of HCMV infection by phosphorylating both cellular and viral proteins (Schütz et al., 2021; Steingruber and Marschall, 2020). To investigate the role of a kinase, a general tool is the usage of analog-sensitive variants. Such modified enzymes can be selectively inhibited by an ATP analog that is not hydrolysable (Lopez et al., 2014). In this work, an HCMV mutant expressing such an analog-sensitive version of pUL97 (pUL-97-as1) was generated, allowing the study of the phosphorylation level of SQSTM1/p62 by preventing the activation of pUL97-as1 (Krämer et al., 2022; Umaña et al., 2018). Interestingly, cells infected with the mutant strain under conditions when pUL97-as1 activity was blocked displayed reduced phosphorylation of SQSTM1/p62 at S272 (Figure 21). This was confirmed by co-transfection experiments independent of HCMV infection (Figure 22). The data showed that pUL97 is directly or indirectly involved in the phosphorylation of SQSTM1/p62 at S272. *In-vitro*-kinase analyses, however, provided no evidence for direct phosphorylation of SQSTM1/p62 at S272 by pUL97 (Figure 23). Thus, the results suggest that pUL97 has an indirect role in SQSTM1/p62-S272 phosphorylation.

The fact that the viral kinase was involved in this modification was striking, considering the fact that SQSTM1/p62-S272 phosphorylation impaired HCMV infection and enhanced ISG protein levels. At this point, it is unknown why HCMV should benefit from phosphorylating this autophagy receptor by pUL97 and accepting the disadvantage for viral infection. One hypothesis would be that pUL97 activates a cellular kinase used for viral purposes to promote efficient HCMV infection, but that this kinase simultaneously activates a defense strategy. CDK1 is activated upon HCMV infection and can phosphorylate SQSTM1/p62 at S272 in a non-infectious background (Linares et al., 2011; Sanchez et al., 2003). *CDK1* expression is increased upon pUL97 activity to facilitate viral replication (Gill et al., 2012). Thus, it could be hypothesized that pUL97-mediated regulation of CDK1 is required for HCMV replication but that this is associated with collateral phosphorylation of SQSTM1/p62, mediating an antiviral effect. However, no clear evidence for a role of CDK1 for SQSTM1/p62-S272 phosphorylation upon HCMV infection could be obtained (Figure 24). More detailed analyses beyond the scope of this work are required to address the role of cellular kinases in SQSTM1/p62-S272 phosphorylation in HCMV-infected cells.

5.6 Impact of selected TRIMs on HCMV infection, regulation of both autophagy and ISG protein levels

TRIMs are known to regulate various antiviral cellular functions, such as autophagy and the IFN-I signaling pathway. They can also directly impair viral replication, e.g., through proteasome-mediated degradation of viral proteins (Mandell et al., 2014a; Sparrer et al., 2017). Moreover, the TRIM family may represent a new class of autophagy receptors, because some of the members have been shown to recognize viral proteins and mediate autophagosomal degradation (Mandell et al., 2014b).

The fact that several TRIM proteins were detected in purified HCMV particles fostered the assumption that these proteins repressed HCMV infection by targeting viral structural proteins as autophagy receptors and autophagy regulators. Consequently, the potential of these TRIMs, namely TRIM25, TRIM26, and TRIM32 to act as autophagy receptors was examined. In addition, two other TRIM proteins, TRIM21 and TRIM28, were investigated for their function as autophagy receptors, as they are known regulators of autophagy. The interaction of these TRIMs with selected HCMV proteins were investigated in infected fibroblasts. TRIM25 co-precipitated with HCMV capsid proteins (Figure 25). In previous work from our laboratory, TRIM21 and TRIM28 were also found to interact with capsid proteins (Afifi, 2021, unpublished). The fact that these TRIMs precipitated with capsid proteins leads to the hypothesis that immature viral particles are targeted by these molecules to transport them for degradation. Thus, this work provides initial evidence that TRIM21, TRIM25, and TRIM28 have the potential to function as autophagy receptors in HCMV-infected cells.

TRIMs are also known to regulate cellular processes such as the IFN-I pathway or autophagy and thereby contribute to an antiviral environment within the cell. For example, TRIM32 poly-ubiquitinates STING which enhances STING-mediated induction of IFN-β in order to increase the antiviral response during DNA-virus infection (Zhang et al., 2012). TRIM25 mediates activation of retinoic acid-inducible gene I (RIG-I)-like receptors (RLRs) signaling pathways, whereas TRIM26 promotes IRF3 activation, which in both cases induces IFN-β production after RNA-virus infection (Gack et al., 2007; Ran et al., 2016). Besides the IFN-I pathway, TRIMs regulate autophagy by serving as scaffold proteins or via ubiquitin-mediated mechanisms (Di Rienzo et al., 2020; Mandell et al., 2014b). Consequently, the role of the TRIM proteins in HCMV replication was analyzed in TRIM- knockout cell lines by investigating viral progeny release from these cells (Figure 26C). Indeed, viral progeny release was enhanced in each TRIM-ko cell line, except for ko-TRIM28. HCMV progeny release was most prominently enhanced from infected ko-TRIM25 and ko-TRIM32 fibroblasts. To evaluate the mechanism behind this effect, the regulation of proteins involved in the IFN-I pathway and the autophagy pathway were addressed (Figure 27 and Figure 28).

Surprisingly, in infected TRIM knockout cells, protein levels of selected ISGs known for their antiviral function were not impaired as assumed but increased. Thus, there was no down-regulation of Mx1 and ISG15 proteins after HCMV infection in TRIM knockout cells, which could explain the increased progeny. It remains unanswered why the antiviral effect of Mx1 and ISG15 was insufficient to attenuate HCMV infection in these cells. Still, other ISGs could be negatively regulated and could be responsible for the elevated progeny release in the absence of these TRIM proteins upon HCMV infection. Based on these initial data, the IFN-I pathway is affected by TRIMs upon HCMV infection, but further analysis of ISG product levels is required to determine the role of this cellular mechanism. Autophagic activity was also not affected by the TRIMs in the early stages of HCMV infection. However, the analysis showed that TRIM21, TRIM28 and TRIM32 reduced autophagy activity at late time points. The effect of these TRIMs on the regulation of autophagy during HCMV infection needs to be validated in further experiments.

These findings thus rather suggest that viral morphogenesis was directly impaired by the TRIMs, for example by facilitating proteasomal degradation of viral structural proteins. In line with this, SQSTM1/p62 was reduced in ko-TRIM25 and ko-TRIM32 cells, indicating that the receptor levels are partly dependent on the presence of TRIM25 and TRIM32. Because HCMV progeny release is also enhanced in the absence of SQSTM1/p62, the impact of TRIM25 and TRIM32 on viral infection may be mediated by influencing SQSTM1/p62 levels. An interaction with SQSTM1/p62 is described for TRIM32, which regulates the activity of SQSTM1/p62 by mono-ubiquitylating the receptor (Overå et al., 2019).

Together, these data provide evidence for a crucial role of the tested TRIMs in the cellular defense against HCMV infection, which could also explain their incorporation into HCMV virions. The molecular mechanisms that mediate their role in the cellular defense during HCMV infection, however, need to be addressed in future analyses.

5.7 Impairment of HCMV infection by IRGQ

IRGQ, a member of the IRG family of proteins, was recently shown to be involved in autophagy by Herhaus and colleagues (Bekpen et al., 2005; Herhaus, unpublished). They found that IRGQ interacts with GABARAP-L2 and LC3B. Interestingly, IRGQ was also identified as a new effector of *Salmonella* clearance by controlling the induction and completion of xenophagy via the interplay with TBK1 and GABARAP-L2. These results suggested that IRGQ functions in the autophagy-mediated defense against pathogens. So far Herhaus and colleagues assume that IRGQ does not function as an autophagy receptor (Herhaus, unpublished).

Intrigued by this finding, the role of IRGQ on viral infections, focusing on HCMV was investigated. Viral genome replication was unaltered following IRGQ-knockdown (Figure 30A). Strikingly, viral progeny release was distinctly elevated in the absence of IRGQ (Figure 30B). These first analyses indicated that IRGQ interfered with HCMV infection by impeding HCMV progeny production.

To further investigate this, a focus was laid on the interaction of IRGQ with GABARAP-L2. Herhaus had found that IRGQ bound GABARAP-L2 upon *Salmonella* infection and this was regulated by TBK1 phosphorylation (Herhaus, unpublished). We thus wished to determine if GABARAP-L2 would enhance the antiviral effect of IRGQ (Figure 31). Surprisingly, and contrary to our expectation, the analysis revealed that in cells in which both proteins were knocked-down, a reduced level of HCMV progeny release was found compared to the absence of only IRGQ (Figure 31C). This indicated that the antiviral effect of IRGQ is conditionally related to the presence of GABARAP-L2. This was supported by the finding that the impact of GABARAP-L2 knockdown on HCMV infection was moderate compared to IRGQ-knockdown, indicating that IRGQ is the key effector that is regulated by GABARAP-L2.

The molecular basis for the effects of IRGQ on HCMV infection remains unknown at this point. The hypothesis is that the induction and completion of autophagy is dependent on the signaling axis of TBK1-GABARAP-L2-IRGQ in HCMV-infected cells, comparable to *Salmonella* infection. Thus, the absence of IRGQ would lead to the interruption of this signaling cascade and would thus impair autophagy and explaining the enhancement of HCMV infection in the absence of IRGQ. Others have shown that TBK1 is activated upon viral infection (Sparrer et al., 2017; tenOever et al., 2004). Thus, further analyses will have to focus on the role of TBK1 kinase activity in regulating the TBK1-GABARAP-L2-IRGQ axis and autophagy during HCMV infection.

With these preliminary data, the finding by Herhaus that IRGQ functions as an interactor in pathogen elimination was corroborated. The role of IRGQ during viral infections has to be studied in further detail.

5.8 Conclusion and perspectives

To better understand the interplay between HCMV and autophagy, the role of autophagy receptors during infection was investigated. In this work, it is shown that the autophagy receptor SQSTM1/p62 is executing different roles during HCMV infection, thereby probably balancing the regulation of both viral infection and antiviral defense mechanisms. On the one hand, SQSTM1/p62 negatively affects the release of viral progeny by directing nascent virions to autophagosomal degradation. On the other hand, the receptor limits an excessive interferon response, thereby preventing cell damage. In addition, the phosphorylation at S272 of SQSTM1/p62 also restricts HCMV infection. These data underline SQSTM1/p62's multifunctional roles besides its task as an autophagy receptor to transport virus components to autophagosomes. In summary, SQSTM1/p62 was identified as an essential player in HCMV infection with diverse functions. In addition, TRIMs and IRGQ have been identified as novel regulators of HCMV infection, but their roles remain to be determined.

Based on these studies, some questions arise: (1) What is the relevance of SQSTM1/p62 shuttling via NPC during HCMV infection? (2) What is the role of phosphorylation of SQSTM1/p62 at 272 in the interaction of SQSTM1/p62 with the IFN-I pathway? (3) What is the impact of SQSTM1/p62 on HCMV infection in other cell types? (4) Does the interaction of autophagy receptors with pUL84 play a role? (5) What are the molecular mechanisms of the analyzed TRIM proteins to impair HCMV infection? (6) What are the molecular mechanisms behind the antiviral effect of IRGQ on HCMV infection?

6 Appendix

A1. Cellular precipitates of SQSTM1/p62-S272wt, -S272D and -S272A at 3 d.p.i. upon HCMV infection. Data are illustrated in a heat map (Figure 17A).

Threshold:	-Log Student's T-test p-value	$-\log_{10}(0.05) = 1.3$
	Student's T-test Difference	$\log_2(2) = 1$

	Proteins significantly co-precipitated with SQSTM1/p62-S272wt were sorted from their highest to lowest Student's T-test difference value.
	Proteins that did not or did not significantly precipitate with SQSTM1/p62-S272wt were sorted against SQSTM1/p62-S272D from highest to lowest Student's T-test Difference values.

				SQSTM1/p62-S272wt vs IgG (control)		**SQSTM1/p62-S272D vs IgG (control)**		**SQSTM1/p62-S272A vs IgG (control)**	
Gene names	**Protein ID**	**Protein names**	**Razor + unique peptides**	**-Log Student's T-test p-value**	**Student's T-test Difference**	**-Log Student's T-test p-value**	**Student's T-test Difference**	**-Log Student's T-test p-value**	**Student's T-test Difference**
POM121C	A8CG34	Nuclear envelope pore membrane protein POM 121C	19	4.459	7.671	5.200	9.968	5.200	9.968
SEC16A	O15027	Protein transport protein Sec16A	41	3.775	7.373	4.181	8.589	4.181	8.589
POM121	Q96HA1	Nuclear envelope pore membrane protein POM 121	3	4.504	7.211	5.567	9.242	5.567	9.242
SEC23IP	Q9Y6Y8	SEC23-interacting protein	23	2.222	6.426	2.697	7.867	2.697	7.867

				SQSTM1/p62-S272wt vs IgG (control)		SQSTM1/p62-S272D vs IgG (control)		SQSTM1/p62-S272A vs IgG (control)	
Gene names	**Protein ID**	**Protein names**	**Razor + unique peptides**	**-Log Student's T-test p-value**	**Student's T-test Difference**	**-Log Student's T-test p-value**	**Student's T-test Difference**	**-Log Student's T-test p-value**	**Student's T-test Difference**
DHX9	Q08211	ATP-dependent RNA helicase A	51	1.741	5.599	2.153	7.173	2.153	7.173
GTSE1	Q9NYZ3	G2 and S phase-expressed protein 1	3	3.156	5.322	4.008	7.133	4.008	7.133
TAF15	Q92804	TATA-binding protein-associated factor 2N	3	2.700	5.164	2.715	4.694	2.715	4.694
ARL6IP1	Q15041	ADP-ribosylation factor-like protein 6-interacting protein 1	2	1.517	4.653	2.210	7.102	2.210	7.102
AP2M1	Q96CW1	AP-2 complex subunit mu	7	1.409	4.518	2.058	6.769	2.058	6.769
CTSL	P07711	Procathepsin L	1	1.663	4.493	2.023	5.646	2.023	5.646
MYCBP2	O75592	E3 ubiquitin-protein ligase MYCBP2	29	4.526	4.099	5.660	6.684	5.660	6.684
DNAJC8	O75937	DnaJ homolog subfamily C member 8	1	1.867	4.085	2.535	3.866	2.535	3.866
NEU1	Q99519	Sialidase-1	6	1.544	4.019	2.218	5.978	2.218	5.978
SCAMP2	O15127	Secretory carrier-associated membrane protein 2	1	1.506	4.004	2.252	6.231	2.252	6.231
DCP1A	Q9NPI6	mRNA-decapping enzyme 1A	4	1.805	3.919	2.701	5.991	2.701	5.991
AGFG1	P52594	Arf-GAP domain and FG repeat-containing protein 1	3	1.558	3.849	2.140	5.220	2.140	5.220
SEC13	P55735	Protein SEC13 homolog	6	2.557	3.699	3.327	5.481	3.327	5.481
OAT	P04181	Ornithine aminotransferase, mitochondrial	6	1.399	3.398	2.232	5.858	2.232	5.858
SUN2	Q9UH99	SUN domain-containing protein 2	2	2.795	3.150	3.486	3.164	3.486	3.164
NUP88	Q99567	Nuclear pore complex protein Nup88	3	1.990	3.026	3.105	4.111	3.105	4.111

				SQSTM1/p62-S272wt vs IgG (control)		SQSTM1/p62-S272D vs IgG (control)		SQSTM1/p62-S272A vs IgG (control)	
Gene names	**Protein ID**	**Protein names**	**Razor + unique peptides**	**-Log Student's T-test p-value**	**Student's T-test Difference**	**-Log Student's T-test p-value**	**Student's T-test Difference**	**-Log Student's T-test p-value**	**Student's T-test Difference**
PLD3	Q8IV08	5-3 exonuclease PLD3	3	1.483	3.019	1.477	3.005	3.055	4.790
SPRYD3	Q8NCJ5	SPRY domain-containing protein 3	1	2.561	3.005			3.773	4.500
RPS14	P62263	40S ribosomal protein S14	10	1.909	2.881	1.854	2.741	2.378	3.675
RAE1	P78406	mRNA export factor RAE1	3	1.524	2.768			2.049	4.326
KIF4A	O95239	Chromosome-associated kinesin KIF4A	3	2.000	2.520	1.435	1.830	3.638	3.821
OSGEP	Q9NPF4	Probable tRNA N6-adenosine threonylcarbamoyltransferase	3	1.681	2.485	1.950	3.119	2.651	4.360
UMPS	P11172	Uridine 5-monophosphate synthase	2	1.345	2.030	1.519	2.278	2.581	4.216
CYP51A1	Q16850	Lanosterol 14-alpha demethylase	5	1.396	1.509	2.886	2.872	3.120	3.529
CNIH4	Q9P003	Protein cornichon homolog 4	1	NaN	0	2.010	7.471	2.177	8.166
DAD1	P61803	Dolichyldiphosphooligosaccharide-protein glycosyltransferase subunit DAD1	3	1.285	3.834	1.802	5.923	3.181	7.054
P3H1	Q32P28	Prolyl 3-hydroxylase 1	13	1.257	3.984	1.757	5.687	2.107	6.830
SPCS3	P61009	Signal peptidase complex subunit 3	2	1.289	4.112	2.567	5.452	2.727	6.222
UQCRFS1P1	P47985 P0C7P4	Cytochrome b-c1 complex subunit Rieske, mitochondrial	3	1.298	3.625	1.842	4.849	2.255	6.003
RAB8A	P61006	Ras-related protein Rab-8A	4	1.216	2.799	2.120	4.751	2.354	5.299
STT3A	P46977	Dolichyl-diphosphooligosaccharide--protein glycosyltransferase subunit STT3A	11	0.912	2.623	1.723	4.628	2.374	6.251
MYADM	Q96S97	Myeloid-associated differentiation marker	3	NaN	0	2.955	4.549	3.160	5.131

				SQSTM1/p62-S272wt vs IgG (control)		SQSTM1/p62-S272D vs IgG (control)		SQSTM1/p62-S272A vs IgG (control)	
Gene names	**Protein ID**	**Protein names**	**Razor + unique peptides**	**-Log Student's T-test p-value**	**Student's T-test Difference**	**-Log Student's T-test p-value**	**Student's T-test Difference**	**-Log Student's T-test p-value**	**Student's T-test Difference**
RNPEP	Q9H4A4	Aminopeptidase B	7	1.179	2.980	1.644	4.518	2.125	5.804
COPZ1	P61923	Coatomer subunit zeta-1	4	NaN	0	1.302	4.428	2.244	6.736
LYZ	P61626	Lysozyme C		NaN	0	2.323	4.297		
ATP5MG	O75964	ATP synthase subunit g, mitochondrial		NaN	0	2.025	4.152	2.757	6.111
TFG	Q92734	Protein TFG	5	NaN	0	1.388	4.115	2.151	5.552
NDRG3	Q9UGV2	Protein NDRG3	3	NaN	0	1.733	4.062	2.618	5.735
MCM7	P33993	DNA replication licensing factor MCM7	14	1.182	2.959	1.659	3.921	2.212	5.296
ALG2	Q9H553	Alpha-1,3/1,6-mannosyltransferase ALG2	3		0	2.459	3.919	3.084	5.144
TM9SF3	Q9HD45	Transmembrane 9 superfamily member 3	3	1.098	2.365	1.563	3.915	2.173	5.141
INF2	Q27J81	Inverted formin-2	6	NaN	0	2.169	3.895	2.913	4.576
CARS1	P49589	Cysteine--tRNA ligase, cytoplasmic	6	1.237	3.205	1.514	3.870	2.197	5.674
RO60	P10155	RNA-binding protein RO60	7	1.219	2.766	1.647	3.860	2.042	4.904
USP7	Q93009	Ubiquitin carboxyl-terminal hydrolase 7	5	0.827	1.188	3.254	3.813	3.664	4.531
TOR1AIP2	Q8NFQ8	Torsin-1A-interacting protein 2	3	0.926	1.958	1.612	3.750	2.121	4.930
CUL2	Q13617	Cullin-2	11	1.037	2.435	1.423	3.662	2.056	5.076
GLB1	P16278	Beta-galactosidase	4	1.208	2.574	1.638	3.649	2.011	4.605
HAT1	O14929	Histone acetyltransferase type B catalytic subunit	1	NaN	0	2.371	3.634		
TRAPPC5	Q8IUR0	Trafficking protein particle complex subunit 5	1	NaN	0	1.717	3.622	2.420	4.145

				SQSTM1/p62-S272wt vs IgG (control)		SQSTM1/p62-S272D vs IgG (control)		SQSTM1/p62-S272A vs IgG (control)	
Gene names	**Protein ID**	**Protein names**	**Razor + unique peptides**	**-Log Student's T-test p-value**	**Student's T-test Difference**	**-Log Student's T-test p-value**	**Student's T-test Difference**	**-Log Student's T-test p-value**	**Student's T-test Difference**
PGRMC2	O15173	Membrane-associated progesterone receptor component 2	3	NaN	0	1.843	3.617	2.495	4.839
OCIAD2	Q56VL3	OCIA domain-containing protein 2	4	0.899	2.595	1.440	3.594	2.354	5.170
DIAPH1	O60610	Protein diaphanous homolog 1	8	1.008	1.754	2.086	3.564	2.756	4.774
IARS2	Q9NSE4	Isoleucine--tRNA ligase, mitochondrial	7	0.740	1.523	1.526	3.544	2.281	5.002
IPO9	Q96P70	Importin-9	5	NaN	0	2.115	3.540	2.919	4.341
STEAP3	Q658P3	Metalloreductase STEAP3	1	NaN	0	1.303	3.523	2.158	3.921
FAM162A	Q96A26	Protein FAM162A	1	NaN	0	2.490	3.489	3.210	4.752
AP2A2	O94973	AP-2 complex subunit alpha-2	4	0.866	2.084	1.775	3.487	2.300	4.773
DDX39A	O00148	ATP-dependent RNA helicase DDX39A	5	1.169	2.338	1.587	3.417	2.344	4.853
IMPA1	P29218	Inositol monophosphatase 1	2	NaN	0	1.428	3.362	2.577	4.154
MYO6	Q9UM54	Unconventional myosin-VI	9	1.064	1.996	1.754	3.349	2.461	4.607
SLC25A4	P12235	ADP/ATP translocase 1	3	1.125	2.260	1.571	3.299	2.250	4.689
EIF2AK2	P19525	Interferon-induced, double-stranded RNA-activated protein kinase	6	NaN	0	1.389	3.298	2.049	4.163
ECM1	Q16610	Extracellular matrix protein 1	3	1.247	2.403	1.629	3.272	2.148	4.320
PRKDC	P78527	DNA-dependent protein kinase catalytic subunit	68	1.062	2.148	1.423	3.262	2.227	4.890
ODR4	Q5SWX8	Protein odr-4 homolog	2	NaN	0	2.143	3.260	2.680	3.830

				SQSTM1/p62-S272wt vs IgG (control)		SQSTM1/p62-S272D vs IgG (control)		SQSTM1/p62-S272A vs IgG (control)	
Gene names	**Protein ID**	**Protein names**	**Razor + unique peptides**	**-Log Student's T-test p-value**	**Student's T-test Difference**	**-Log Student's T-test p-value**	**Student's T-test Difference**	**-Log Student's T-test p-value**	**Student's T-test Difference**
NAA15	Q9BXJ9	N-alpha-acetyltransferase 15, NatA auxiliary subunit	7	0.776	1.398	1.431	3.230	2.199	4.646
CTNNB1	P35222	Catenin beta-1	5	NaN	0	2.200	3.220	2.979	4.707
NUP205	Q92621	Nuclear pore complex protein Nup205	8	1.204	1.734	2.146	3.196	2.746	4.276
ABCD3	P28288	ATP-binding cassette sub-family D member 3	7	1.122	2.208	1.658	3.185	2.354	4.553
TNPO3	Q9Y5L0	Transportin-3	4	NaN	0	2.470	3.154	1.989	3.648
UNC45A	Q9H3U1	Protein unc-45 homolog A	8	1.111	1.871	1.617	3.129	2.500	4.732
KCMF1	Q9P0J7	E3 ubiquitin-protein ligase KCMF1	1	NaN	0	1.958	3.098	2.879	2.847
TTLL12	Q14166	Tubulin--tyrosine ligase-like protein 12	3	NaN	0	1.379	3.086	2.147	4.685
PIGT	Q969N2	GPI transamidase component PIG-T	2	NaN	0	2.386	3.010	3.087	3.511
ARMT1	Q9H993	Damage-control phosphatase ARMT1	2	NaN	0	1.678	2.934	3.580	5.297
METAP2	P50579	Methionine aminopeptidase 2	2	NaN	0	2.044	2.930	2.649	3.391
MTA2	O94776	Metastasis-associated protein MTA2	3	0.813	1.403	1.792	2.919	2.451	3.812
NUP93	Q8N1F7	Nuclear pore complex protein Nup93	11	0.928	1.544	1.617	2.905	2.024	4.044
NAT10	Q9H0A0	RNA cytidine acetyltransferase	2	0.532	0.553	1.899	2.895	2.099	3.193
DPP7	Q9UHL4	Dipeptidyl peptidase 2	2	0.743	1.308	1.781	2.889	2.156	3.708
PBK	Q96KB5	Lymphokine-activated killer T-cell-originated protein kinase	2	1.070	2.606	1.778	2.870	2.237	3.898

				SQSTM1/p62-S272wt vs IgG (control)		SQSTM1/p62-S272D vs IgG (control)		SQSTM1/p62-S272A vs IgG (control)	
Gene names	**Protein ID**	**Protein names**	**Razor + unique peptides**	**-Log Student's T-test p-value**	**Student's T-test Difference**	**-Log Student's T-test p-value**	**Student's T-test Difference**	**-Log Student's T-test p-value**	**Student's T-test Difference**
UFL1	O94874	E3 UFM1-protein ligase 1	4	NaN	0	1.510	2.846	2.701	3.906
PDS5B	Q9NTI5	Sister chromatid cohesion protein PDS5 homolog B	3	0.780	1.097	1.623	2.842	2.258	3.715
SNX27	Q96L92	Sorting nexin-27	2	NaN	0	1.952	2.838	2.541	4.459
GNE	Q9Y223	Bifunctional UDP-N-acetylglucosamine 2-epimerase/N-acetylmannosamine kinase	2	NaN	0	1.398	2.833	2.063	3.534
CDK1	P06493	Cyclin-dependent kinase 1	6	0.938	1.631	1.631	2.826	2.098	3.683
SCARB2	Q14108	Lysosome membrane protein 2	2	0.985	2.813	1.399	2.792	2.265	4.433
TNPO2	O14787	Transportin-2	2	1.122	1.475	2.018	2.765	2.280	3.610
AP2A1	O95782	AP-2 complex subunit alpha-1	12	0.439	0.564	1.488	2.689	2.244	4.220
PRPF6	O94906	Pre-mRNA-processing factor 6	3	1.162	2.111	1.841	2.684	2.841	4.365
GMDS	O60547	GDP-mannose 4,6 dehydratase	2	NaN	0	1.302	2.680	2.198	3.968
CSTF3	Q12996	Cleavage stimulation factor subunit 3	3	NaN	0	1.596	2.595	3.208	4.997
MRPS5	P82675	28S ribosomal protein S5, mitochondrial	3	0.654	1.191	1.357	2.563	2.097	4.170
ATP5F1A	P25705	ATP synthase subunit alpha, mitochondrial	33	1.102	1.901	1.351	2.459	2.109	3.925
IGF2R	P11717	Cation-independent mannose-6-phosphate receptor	9	0.800	0.969	1.808	2.421	2.640	3.484
PFKM	P08237	ATP-dependent 6-phosphofructokinase, muscle type	7	1.137	1.816	1.497	2.403	2.019	3.522
ATP2B1	P23634; P20020	Plasma membrane calcium-transporting ATPase 4	5	0.208	-0.388	1.369	2.356	2.169	3.908

				SQSTM1/p62-S272wt vs IgG (control)		SQSTM1/p62-S272D vs IgG (control)		SQSTM1/p62-S272A vs IgG (control)	
Gene names	**Protein ID**	**Protein names**	**Razor + unique peptides**	**-Log Student's T-test p-value**	**Student's T-test Difference**	**-Log Student's T-test p-value**	**Student's T-test Difference**	**-Log Student's T-test p-value**	**Student's T-test Difference**
PELP1	Q92888	Proline-, glutamic acid- and leucine-rich protein 1	2	0.426	0.320	1.501	2.302	2.164	2.919
DNAJC13	O75165	DnaJ homolog subfamily C member 13	6	0.624	0.508	2.567	2.302	2.980	3.154
UAP1L1	Q3KQV9	Nodal modulator 2	2	0.947	1.770	1.631	2.277	2.633	3.828
MYBBP1A	Q9BQG0	UDP-N-acetylhexosamine pyrophosphorylase-like protein 1	6	0.385	0.243	1.403	2.255	2.043	2.888
CHD3	Q14839; Q12873; Q8TDI0	Myb-binding protein 1A	4	NaN	0	2.371	2.176	4.330	4.311
FAM120A	Q9NZB2	Lysosomal alpha-mannosidase	3	0.942	1.540	1.496	2.173	2.200	3.323
CUL4B	Q13620	Cullin-4B	8	0.598	0.810	1.518	2.139	2.000	3.119
SEC24D	O94855	Protein transport protein Sec24D	3	NaN	0	2.761	2.071	2.280	3.769
CNOT1	A5YKK6	CCR4-NOT transcription complex subunit 1	2	0.585	0.536	1.368	1.879	2.107	2.599
BASP1	P80723	Brain acid soluble protein 1	7	0.116	-0.795	1.539	1.611	2.350	2.563

A2. Cellular proteins precipitated only by SQSTM1/p62-S272A at 3 d.p.i. upon HCMV infection.

Threshold:	-Log Student's T-test p-value	$-\log_{10}(0.05) = 1.3$
	Student's T-test Difference	$\log_2(2) = 1$

Cellular proteins that significantly co-precipitated only with SQSTM1/p62-S272A were sorted by their highest to lowest Student's T-test Difference value.

				SQSTM1/p62-S272wt vs IgG		**SQSTM1/p62-S272D vs IgG**		**SQSTM1/p62-S272A vs IgG**	
Gene names	**Protein ID**	**Protein names**	**Razor + unique peptides**	**-Log Student's T-test p-value**	**Student's T-test Difference**	**-Log Student's T-test p-value**	**Student's T-test Difference**	**-Log Student's T-test p-value**	**Student's T-test Difference**
DPM3	Q9P2X0	Dolichol-phosphate mannosyltransferase subunit 3	2	0	NaN	0	NaN	4.125	9.192
RBX1	P62877	E3 ubiquitin-protein ligase RBX1	2	0	NaN	0	NaN	4.947	7.592
MRPS14	O60783	28S ribosomal protein S14, mitochondrial	1	0	NaN	0	NaN	3.921	6.777
NDUFA4	O00483	Cytochrome c oxidase subunit NDUFA4	1	0	NaN	0	NaN	2.085	5.857
PEX11B	O96011	Peroxisomal membrane protein 11B	2	0	NaN	0	NaN	3.490	5.752
CYRIB	Q9NUQ9	CYFIP-related Rac1 interactor B	1	0	NaN	0	NaN	3.102	5.637

				SQSTM1/p62-S272wt vs IgG		SQSTM1/p62-S272D vs IgG		SQSTM1/p62-S272A vs IgG	
Gene names	**Protein ID**	**Protein names**	**Razor + unique peptides**	**-Log Student's T-test p-value**	**Student's T-test Difference**	**-Log Student's T-test p-value**	**Student's T-test Difference**	**-Log Student's T-test p-value**	**Student's T-test Difference**
FBXO45	P0C2W1	F-box/SPRY domain-containing protein 1	3	0	NaN	0	NaN	4.515	5.525
OSTC	Q9NRP0	Oligosaccharyltransferase complex subunit OSTC	1	0	NaN	0	NaN	3.744	5.502
TMED1	Q13445	Transmembrane emp24 domain-containing protein 1	1	0	NaN	0	NaN	3.296	5.447
ATP6V1G1	O75348	V-type proton ATPase subunit G 1	1	0	NaN	0	NaN	2.665	5.287
STRN3	Q13033	Striatin-3	2	0	NaN	0	NaN	2.168	4.785
FDFT1	P37268	Squalene synthase	1	0	NaN	0	NaN	3.367	4.758
DNAJB3	O75190	DnaJ homolog subfamily B member 6	2	0	NaN	0	NaN	4.775	4.694
BID	P55957	BH3-interacting domain death agonist	2	0	NaN	0	NaN	2.725	4.637
TP53I11	O14683	Tumor protein p53-inducible protein 11	1	0	NaN	0	NaN	3.065	4.193

				SQSTM1/p62-S272wt vs IgG		SQSTM1/p62-S272D vs IgG		SQSTM1/p62-S272A vs IgG	
Gene names	**Protein ID**	**Protein names**	**Razor + unique peptides**	**-Log Student's T-test p-value**	**Student's T-test Difference**	**-Log Student's T-test p-value**	**Student's T-test Difference**	**-Log Student's T-test p-value**	**Student's T-test Difference**
CLPTM1L	Q96KA5	Cleft lip and palate transmembrane protein 1-like protein	1	0	NaN	0	NaN	2.545	4.180
NT5DC1	Q5TFE4	5-nucleotidase domain-containing protein 1	1	0	NaN	0	NaN	2.651	4.055
ARMC1	Q9NVT9	Armadillo repeat-containing protein 1	2	0	NaN	0	NaN	2.010	3.975
FAM83G	A6ND36	Protein FAM83G	5	0	NaN	0	NaN	3.200	3.912
SLC25A10	Q9UBX3	Mitochondrial dicarboxylate carrier	2	0	NaN	0	NaN	2.070	3.863
RRP12	Q5JTH9	RRP12-like protein	3	0	NaN	0	NaN	2.492	3.736
DOHH	Q9BU89	Deoxyhypusine hydroxylase	1	0	NaN	0	NaN	2.495	3.732
CELF1	Q92879	CUGBP Elav-like family member 1	1	0	NaN	0	NaN	3.213	3.695
UBE2Q1	Q7Z7E8	Ubiquitin-conjugating enzyme E2 Q1	1	0	NaN	0	NaN	3.397	3.578
VPS16	Q9H269	Vacuolar protein sorting-associated protein 16 homolog	4	0	NaN	0	NaN	3.114	3.560

				SQSTM1/p62-S272wt vs IgG		SQSTM1/p62-S272D vs IgG		SQSTM1/p62-S272A vs IgG	
Gene names	**Protein ID**	**Protein names**	**Razor + unique peptides**	**-Log Student's T-test p-value**	**Student's T-test Difference**	**-Log Student's T-test p-value**	**Student's T-test Difference**	**-Log Student's T-test p-value**	**Student's T-test Difference**
DNAJC7	Q99615	DnaJ homolog subfamily C member 7	1	0	NaN	0	NaN	2.636	3.536
MRPL38	Q96DV4	39S ribosomal protein L38, mitochondrial	1	0	NaN	0	NaN	2.472	3.523
GLMN	Q92990	Glomulin	1	0	NaN	0	NaN	2.206	3.402
EXOC2	Q96KP1	Exocyst complex component 2	2	0	NaN	0	NaN	2.226	3.278
DCTN4	Q9UJW0	Dynactin subunit 4	1	0	NaN	0	NaN	2.946	3.224
SQOR	Q9Y6N5	Sulfide:quinone oxidoreductase, mitochondrial	1	0	NaN	0	NaN	3.551	3.077
UBA2	Q9UBT2	SUMO-activating enzyme subunit 2	2	0	NaN	0	NaN	2.782	3.023
PPFIBP1	Q86W92	Liprin-beta-1	1	0	NaN	0	NaN	2.226	2.988
MAP3K20	Q9NYL2	Mitogen-activated protein kinase kinase kinase 20	1	0	NaN	0	NaN	3.059	2.539

A3. Selected cellular precipitates of SQSTM1/p62-S272wt, -S272A and -S272D at 3 d.p.i. upon HCMV infection, which were analyzed by Western blot. These proteins possessed a high log2 fold change and a low p-value. Data are illustrated in a Western blot (Figure 17B).

Threshold:	-Log Student's T-test p-value	-log10(0.03) = 1.5
	Student's T-test Difference	$\log_2(4) = 2$

Selected cellular proteins that coprecipitated significantly with all SQSTM1/p62-S272 mutants or only some of them analyzed in Figure 17B.

					SQSTM1/p62-S272wt vs IgG		**SQSTM1/p62-S272A vs IgG**		**SQSTM1/p62-S272D vs IgG**	
Gene names	**Protein ID**	**Protein names**	**Razor + unique peptides**	**Mol. weight [kDa]**	**-Log Student's T-test p-value**	**Student's T-test Difference**	**-Log Student's T-test p-value**	**Student's T-test Difference**	**-Log Student's T-test p-value**	**Student's T-test Difference**
POM121	Q96HA1	Nuclear envelope pore membrane protein POM 121	3	127.72	4.504	7.211	5.567	9.242	4.826	6.594
TAF15	Q92804	TATA-binding protein-associated factor 2N	3	61.829	2.700	5.164	2.715	4.694	NaN	0
ARL6IP1	Q15041	ADP-ribosylation factor-like protein 6-interacting protein 1	2	23.362	1.517	4.653	2.210	7.102	NaN	0

					SQSTM1/p62-S272wt vs IgG		SQSTM1/p62-S272A vs IgG		SQSTM1/p62-S272D vs IgG	
Gene names	**Protein ID**	**Protein names**	**Razor + unique peptides**	**Mol. weight [kDa]**	**-Log Student's T-test p-value**	**Student's T-test Difference**	**-Log Student's T-test p-value**	**Student's T-test Difference**	**-Log Student's T-test p-value**	**Student's T-test Difference**
TRAM1	Q15629	Translocating chain-associated membrane protein 1	2	43.071	NaN	0.000	4.118	5.948	4.262	5.593
GGH	Q92820	Gamma-glutamyl hydrolase	1	35.964	2.632	4.452	2.753	5.384	3.385	5.490
ARF6	P62330	ADP-ribosylation factor 6	1	20.082	2.293	4.318	NaN	0	NaN	0

A4. Viral precipitates of SQSTM1/p62-S272wt, -S272D and -S272A at 3 d.p.i. upon HCMV infection. Data are illustrated in a heat map (Figure 20A).

Threshold:	-Log Student's T-test p-value	$-\log_{10}(0.05) = 1.3$
	Student's T-test Difference	$\log_2(2) = 1$

	Proteins significantly co-precipitated with SQSTM1/p62-S272wt were sorted from their highest to lowest Student's T-test difference value.
	Proteins that did not or did not significantly precipitate with SQSTM1/p62-S272wt were sorted against SQSTM1/p62-S272D from highest to lowest Student's T-test Difference values.

				SQSTM1/p62-S272wt vs IgG		**SQSTM1/p62-S272D vs IgG**		**SQSTM1/p62-S272A vs IgG**	
Gene names	**Majority protein IDs**	**Protein names**	**Razor + unique peptides**	**-Log Student's T-test p-value**	**Student's T-test Difference**	**-Log Student's T-test p-value**	**Student's T-test Difference**	**-Log Student's T-test p-value**	**Student's T-test Difference**
UL86/MCP	P16729	Major capsid protein	74	1.427	4.740	1.221	3.964	2.008	6.793
CVC2	P16726	Capsid vertex component 2	13	1.422	4.201	1.456	3.868	2.472	7.098
UL104	P16735	Portal protein	15	1.387	3.235	1.444	3.260	2.320	5.631
CVC1	P16799	Capsid vertex component 1	7	1.747	3.201	1.687	2.628	4.410	5.814
UL36	P16767	Uncharacterized protein UL36	2	2.005	2.727	NaN	0	2.624	4.506
UL80	P16753	Capsid scaffolding protein	21	1.491	2.230	1.085	1.384	2.847	4.093

				SQSTM1/p62-S272wt vs IgG		SQSTM1/p62-S272D vs IgG		SQSTM1/p62-S272A vs IgG	
Gene names	**Majority protein IDs**	**Protein names**	**Razor + unique peptides**	**-Log Student's T-test p-value**	**Student's T-test Difference**	**-Log Student's T-test p-value**	**Student's T-test Difference**	**-Log Student's T-test p-value**	**Student's T-test Difference**
UL32	P08318	Large structural phosphoprotein	39	1.808	2.125	1.443	1.492	3.712	4.444
RIR1	P16782	Ribonucleoside-diphosphate reductase large subunit-like protein	28	1.453	1.161	1.252	1.331	2.751	3.047
UL80	P16753-2	Isoform pAP of Capsid scaffolding protein	1	1.237	5.032	1.478	4.648	2.698	7.694
UL88	P16731	Protein UL88	10	1.217	2.934	1.724	4.330	2.492	6.300
UL102	P16827	DNA helicase/primase complex-associated protein	10	1.054	2.398	1.622	3.853	2.079	4.955
gL	P16832	Envelope glycoprotein L	4	1.063	2.424	1.752	3.758	2.577	5.168
gH	P12824	Envelope glycoprotein H	10	1.074	2.014	1.609	3.156	2.445	4.897
UL69	P16749	mRNA export factor ICP27 homolog	15	1.015	1.454	1.349	2.048	2.187	3.422

A5. Viral precipitates of only SQSTM1/p62-S272A at 3 d.p.i. upon HCMV infection.

Threshold:	-Log Student's T-test p-value	-log10(0.05) = 1.3
	Student's T-test Difference	$\log_2(2) = 1$

Cellular proteins that significantly co-precipitated only with SQSTM1/p62-S272A were sorted by their highest to lowest Student's T-test Difference value.

				SQSTM1/p62-S272wt vs IgG		**SQSTM1/p62-S272D vs IgG**		**SQSTM1/p62-S272A vs IgG**	
Gene names	**Protein ID**	**Protein names**	**Razor + unique peptides**	**-Log Student's T-test p-value**	**Student's T-test Difference**	**-Log Student's T-test p-value**	**Student's T-test Difference**	**-Log Student's T-test p-value**	**Student's T-test Difference**
UL41A	O39920	Protein UL41A	1	0	NaN	0	NaN	4.587	8.461
UL43	P16781	Tegument protein UL43	5	0.794	1.997	1.128	2.551	2.138	5.091
UL13	P16755	Uncharacterized protein UL13	2	1.047	2.033	1.029	2.004	2.668	4.016
UL33	P16849	G-protein coupled receptor homolog UL33	2	0.549	0.473	0.372	0.136	2.040	2.138

viruses

A6.

MDPI

Article

Recombinant Human Cytomegalovirus Expressing an Analog-Sensitive Kinase pUL97 as Novel Tool for Functional Analyses

Nadine Krämer [1], Martin Schütz [2], Uxía Gestal Mato [3], Lina Herhaus [3], Manfred Marschall [2] and Christine Zimmermann [1,4,*]

[1] University Medical Center, Institute for Virology, University of Mainz, 55131 Mainz, Germany
[2] Institute for Clinical and Molecular Virology, Friedrich-Alexander Universität Erlangen-Nürnberg (FAU), 91054 Erlangen, Germany
[3] School of Medicine, Institute of Biochemistry II, Goethe University, 60598 Frankfurt, Germany
[4] Research Center for Immunotherapy (FZI), University Medical Center, University of Mainz, 55131 Mainz, Germany
* Correspondence: chrzimme@uni-mainz.de; Tel.: +49-61-3117-9072

Abstract: The human cytomegalovirus (HCMV) is a member of the beta-herpesvirus family and inflicts life-long latent infections in its hosts. HCMV has been shown to manipulate and dysregulate many cellular processes. One major interactor with the cellular host is the viral kinase pUL97. The UL97 gene is essential for viral replication, and kinase-deficient mutants of pUL97 display a severe replication defect. Recently, another group established an analog-sensitive version of the pUL97 protein. This mutant kinase can be treated with a non-hydrolysable ATP analog, thereby inhibiting its kinase function. This process is reversible by removing the ATP analog by media change. We introduced this mutant version of the pUL97 protein into the laboratory strain Ad169 of HCMV, BADwt, creating a BAD-UL97-as1 viral mutant. This mutant virus replicated normally in infected cells in the absence of the ATP analog and maintained its ability to phosphorylate its cellular substrates. However, when treated with the ATP analog, BAD-UL97-as1 displayed a defect in the production of intra- and extracellular viral DNA and in the production of viral progeny. Furthermore, in the presence of 3MB-PP1, a well-established substrate of pUL97 was no longer hyperphosphorylated. This effect was detectable as early as 4 h post treatment, which allows for studies on pUL97 without the complication of low viral titers. Nevertheless, we observed off-target effects of 3MB-PP1 on several cellular processes, which should be considered with this approach.

Keywords: human cytomegalovirus (HCMV); BACmid-derived recombinant HCMV; viral kinase activity; protein kinase pUL97; analog-sensitive pUL97 variant; functional analyses; pUL97-specific inhibitors

check for updates

Citation: Krämer, N.; Schütz, M.; Mato, U.G.; Herhaus, L.; Marschall, M.; Zimmermann, C. Recombinant Human Cytomegalovirus Expressing an Analog-Sensitive Kinase pUL97 as Novel Tool for Functional Analyses. *Viruses* **2022**, *14*, 2285. https://doi.org/10.3390/v14102285

Academic Editor: Barry Slobedman

Received: 6 September 2022
Accepted: 12 October 2022
Published: 17 October 2022

Publisher's Note: MDPI stays neutral with regard to jurisdictional claims in published maps and institutional affiliations.

Copyright: © 2022 by the authors. Licensee MDPI, Basel, Switzerland. This article is an open access article distributed under the terms and conditions of the Creative Commons Attribution (CC BY) license (https://creativecommons.org/licenses/by/4.0/).

1. Introduction

The human cytomegalovirus (HCMV) is a member of the beta-herpesvirus family and shows a worldwide prevalence of 40–95% in the human population, depending on the socioeconomic, regional circumstances. Like all herpesviruses, HCMV inflicts life-long infections by establishing latency. HCMV infection is normally asymptomatic in healthy, immunocompetent individuals. However, in immunocompromised patients, such as bone-marrow recipients, HCMV reactivation can cause severe and even life-threatening complications, rendering this virus clinically highly relevant. Most importantly, HCMV represents the most frequent infection-based risk factor during pregnancy, so that congenital HCMV infection (cCMV) can cause serious and even life-threatening disease in the unborn and neonates [1].

HCMV manipulates several cellular processes in infected cells, whereby, however, many of those virus–host interactions are incompletely understood. One major viral factor

of host interaction is the protein kinase pUL97, an ortholog of human cyclin-dependent kinases (CDKs) [2]. pUL97 phosphorylates many cellular and viral substrates and thus dysregulates CDK–cyclin complexes, eventually leading to a cell-cycle arrest in G1/S-phase [3]. pUL97 also serves an important role in HCMV nuclear egress, a crucial step in the viral replication cycle, by phosphorylating lamins A/C in a site-specific manner [4,5], resulting in the local distortion of the nuclear lamina during nuclear egress, [6–8]. Hence, kinase-depleted mutants of pUL97 display a severe replication defect, making it difficult to produce viral stock titers sufficient for experimental procedures [9,10].

A particularly useful tool for the study of functional aspects of kinases is the creation of so-called analog-sensitive (as) kinase versions. Basically, these mutants carry a point mutation within the ATP binding pocket of the kinase, maintaining the ability to bind ATP and maintain its kinase activity. However, the addition of a non-hydrolysable ATP-analog to the media blocks the ATP binding pocket, thereby inhibiting the phosphorylation of kinase substrates [11–13]. Members of Robert Kalejta's research laboratory recently established an analog-sensitive version of the pUL97 protein, as transiently expressed using settings of plasmid transfection [14]. An important achievement of the study was the identification of a single amino acid replacement mutation within the ATP binding pocket of pUL97, which indeed, on the one hand, maintained the kinase activity of this mutant protein under normal conditions. On the other hand, however, the addition of bio-orthogonal ATP 3-methylbenzyl pyrazolopyrimidine (3MB-PP1) to the media caused a selective inhibition of pUL97 kinase activity, thereby preventing the phosphorylation of known pUL97 substrates. In the present work, we generated a recombinant HCMV expressing the analog-sensitive version of pUL97 and performed a phenotypical characterization. The use of this recombinant that expressed the pUL97 as a mutant proved to be a quick and easy way to inhibit the kinase function at any time of infection without the complication of low viral titers. In addition, the inhibition of the kinase function can be adjusted in a dose-dependent manner and is reversible when the cell media are replaced with fresh media without 3MB-PP1. Thus, we established a viral tool that enables us to study the various functions of pUL97 in the context of HCMV infection, including the topics of substrate recognition, specificity of protein binding and phosphorylation, and the in vitro efficacy of pUL97-selective inhibitory drugs.

2. Materials and Methods

2.1. BAC-Mutagenesis and Virus Reconstitution

To create the BAD-UL97-as1 BAC DNA, the nucleotides between 1177 and 1286 of UL97 of the parental strain Ad169/BADwt, kindly provided by Thomas Shenk [15], were replaced by a DNA fragment encoding the bacterial galactokinase galK as previously described [16]. Afterwards, the galK cassette was replaced by a DNA fragment, which encodes the sequence of UL97-as1 in which the histidin on position 411 of wild-type UL97 was replaced by a glycin by changing the coding triplet from cat to ggg. We chose the UL133-UL138-missing backbone as one part of the rationale for our studies. The deletion of the genomic region UL133-UL138 in the chosen virus context is linked to an increased dependence of the virus on pUL97 kinase activity [17–20]. For reasons of a complex regulatory interference between the viral proteins that normally are expressed by this genomic region (e.g., the early regulators of ORF-UL138 proteins and others) with the pUL97 functionality, such an HCMV strain, and mutants derived from it, are expected to be particularly sensitive to any regulatory or drug-mediated impairment of pUL97.

For virus reconstitution BAC-clones were used to transfect HFF with BAC DNA, as described in [21]. The genomes of Ad169/BADwt and its derivatives contain a self-excisable BAC vector, leading to automatic deletion of the BAC sequence upon transfection into HFF through the expression of the CRE-recombinase [15].

2.2. Cell Culture

Primary human foreskin fibroblasts (HFF) were cultured in T175 flasks, containing MEM with 10% FCS, at 37 °C, 80% humidity and 5% CO_2, as described previously [22]. Briefly, to harvest HFF, cells were washed with 1× DPBS (Sigma-Aldrich, Burlington, MA, USA, D8537) and incubated with 1× trypsin/EDTA (Gibco/Thermo Fisher Scientific, 1540054, Waltham, MA, USA) at 37 °C. After five minutes the digestion was stopped by the addition of MEM medium, cells were centrifuged at 432× *g* for five minutes and the supernatant was discarded. According to that, the cells were counted and seeded in the appropriate cell culture dishes with the corresponding cell amount.

The following strains were used in this study: BADwt/Ad169 [15] kindly provided by Thomas Shenk, BAD-UL97-as1 was created by the exchange of the nucleotide triplet cat, coding for the amino acid histidine to ggg, coding for a glycine at position 411 in the gene of UL97 in the BADwt parental strain via homologues recombination [16].

2.3. The 3MB-PP1 and Maribavir Treatment

3MB-PP1 (Calbiochem Merck, 529582-5MG) and maribavir (MBV; MedChem Express, HY-16305) were added to the cell culture in a concentration of 40 µM for 3MB-PP1 or 20 µM for MBV once up to 18 h before infection or at different time points during infection.

2.4. TaqMan/Kinetics

Virus titers were determined by quantitation of viral genomes in cell culture by quantitative PCR as described in [23]. The main aspects and the modifications are briefly described in the following sentences. The genome copies were estimated in infected cells as follows: 0.5 × 10^6 cells were seeded in 10 cm dishes. On the next day, cells were infected with Ad169/BAD-wt or BAD-UL97-as1, using different virus dilutions (10 µL, 50 µL, 100 µL und 500 µL). After 6 h post-infection, the cells were harvested, adjusted to 1 × 10^6/mL in PBS and analyzed by quantitative PCR, using an ABI 7500 Fast real-time PCR detection system. Analysis of intracellular viral DNA replication and extracellular viral DNA were performed by quantitative PCR analysis, as previously described [21]. For this, 0.5 × 10^6 cells were seeded in 10 cm dishes and infected with 4 genomes/cell on the next day. On different days post-infection, both supernatant and cells were harvested. The supernatant was transferred into a 50 mL reaction tube, centrifuged at 2800 rpm for 10 min and stored in 1 mL aliquots at −80 °C. At 6 h post-infection and different days post-infection, the cells were washed with 1× DPBS, harvested by 1× trypsin/EDTA, centrifuged, counted and adjusted to 1 × 10^6/mL with 1× DPBS and stored at −20 °C. The DNA was isolated both from 200 µL supernatant and 1 × 10^5 cells by using the High Pure viral nucleic acid kit (Roche Holding AG, 11858874001) according to the manufacturer's instructions. The quantification was performed by qPCR.

2.5. Western BLOT

A total of 0.5 × 10^6 HFF were seeded in 10 cm^2 dishes and were either treated with 3MB-PP1, MBV or DMSO as a negative control. On the next day, the cells were infected with the respective HCMV strains with different genomes per cell (4 genomes per cell). On different days post-infection, the cells were harvested, adjusted to 1 × 10^5 cells and lysed in 2× Laemmli sample buffer. Protein samples were separated on 10% SDS-PAGE (Life Technologies, NP0301BOX, Carlsbad, CA, USA) and transferred to PVDF membranes (Immobilon, ISEQ00010). The filters were probed with specific primary antibodies phospho-Rb (Ser807/811) (Cell Signaling, 8516S), Rb (Cell Signaling, 9309S), pp28 (kindly provided by William Britt), GAPDH (Sigma-Aldrich, G8795), pAb-UL97 (kindly provided by D.M. Coen, Harvard Medical School, Boston, MA, USA), mAb-Cyclin B1 (sc-245, Santa Cruz Biotechnology), Fluorescent-conjugated secondary antibodies (Invitrogen, A10043; Licor,926-32212) were used for detection by using the Odyssey Infrared Imager CLx (LI-COR Biotechnology, Lincoln, NE, USA).

2.6. Coimmunoprecipitation Experiments (CoIP)

For the investigation of interaction patterns, HCMV-infected HFFs (in T175 flasks) were harvested and lysed 4 days post-infection (d.p.i). If indicated, cells were incubated with 40 µM of 3MB 4 h before collecting the cellular material and again during cell lysis. The coimmunoprecipitation assay (CoIP) was performed as described previously [24]. Cyclin B1 was immunoprecipitated using a pAb-cyclin B1 antibody (AF6000, R&D Systems). Immunoprecipitated samples (IP) and lysate control were subjected to standard SDS-PAGE/Wb procedures [25,26].

2.7. TMT-Based Total Proteome Analysis

The experiments were performed similar as described in [27]: cells were lysed in (2% SDS, 50 mM Tris-HCl pH 8, 150 mM NaCl, 10 mM TCEP, and 40 mM chloracetamide), heated at 95 °C for 10 min, and sonicated with Sonics Vibra-Cell. Protein lysates were precipitated by methanol/chloroform using four volumes of ice-cold methanol, one volume of chloroform, and three volumes of water. The mixture was centrifuged at 20,000× *g* for 30 min, the upper aqueous phase was removed and three volumes of ice-cold methanol added. Proteins were pelleted by centrifugation and washed twice with one volume of ice-cold methanol and air-dried. The resulting protein pellet was resuspended in 8 M urea with 10 mM EPPS pH 8.2. Protein concentration was determined with Pierce™ BCA Protein Assay Kit. For digestion, 50 µg proteins were diluted to 2 M urea and incubated 1:100 with LysC and 1:100 with Trypsin overnight. The reaction was acidified using TFA (0.5%) and purified using Sep-Pakt C18 according to manufacturer's protocol. Peptide estimation was determined with Micro BCA™ Protein Assay Kit (Thermo Fischer Scientific, Waltham, MA, USA), 10 µg of peptides were TMT labeled and channels adjusted to equimolar ratios as jugged by single-injection measurements by liquid chromatography (LC)-mass spectrometry (MS). Peptides were cleaned up by C18 stage tip (washed with 3% ACN, 0.1% TFA) and fractionated according to manufacturer's instructions using the Pierce™ High pH Reversed-Phase Kit (Thermo Scientific/Thermo Fischer Scientific, Waltham, MA, USA). Samples were vacuum-dried for LC-MS measurements.

3. Results

3.1. An Analog-Sensitive Version of the Viral Kinase pUL97

In order to create a viral mutant in which the kinase function of pUL97 can be reduced or inhibited in a dose-dependent manner and at a desired time point during infection, we inserted the point mutation described in [14] into the UL97 gene of the Ad169 laboratory strain of HCMV (Figure 1). For this purpose, we made use of the BAC recombination method described by others [16]. The resulting BACmid was then transfected into HFF cells to produce the viral mutant.

Although analog-sensitive kinases can still bind the normal ATP molecule, a slight reduction in kinase activity of these kinases has been described in some cases [13]. To determine a possible replication defect of the UL97-as1 mutant, we performed replication kinetics of both the intracellular viral DNA, as well as the viral genomes that were released from infected human foreskin fibroblasts (HFF) (Figure 2A). Over a course of 8 days post-infection, we collected samples of UL97-as1-infected cells at 6 h, and 1, 3, 6 and 8 days post-infection (Figure 2A upper graph). Although the starting point of the UL97-as1 mutant appeared slightly delayed compared to the wild-type virus (wt), we detected no significant growth defect of the mutant. We also collected samples from the supernatants of infected cells at 1, 3, 6 and 8 days post-infection (Figure 2A lower graph) and measured the amount of viral DNA released from infected cells. We found no differences in the amount of viral DNA released from cells infected with the as1 mutant, compared to the wt virus.

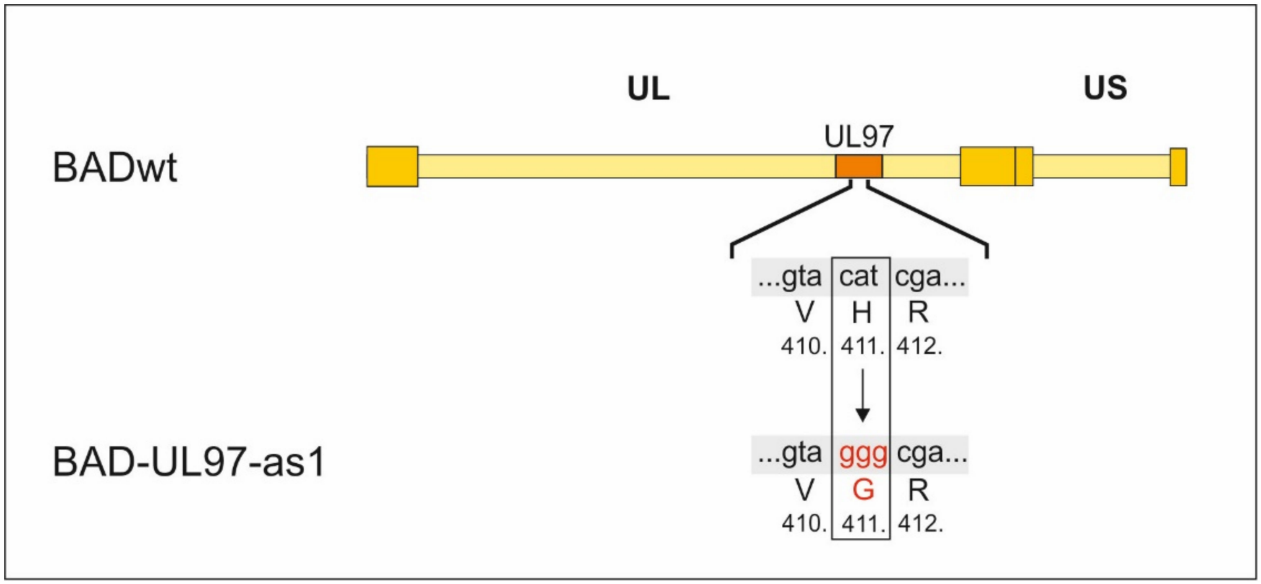

Figure 1. Construction of BAD-UL97-as1. The triplet cat coding for histidin on position 411 within the UL97 gene was replaced by ggg coding for glycin using the BAC recombination technique described in [16].

While the amount of viral DNA is an indicator for successful viral DNA replication, it is possible, that some of these genomes are not incorporated into functional viral progeny. We therefore infected HFF cell cultures with the supernatant of wild-type or mutant-infected cells, respectively. Staining for the HCMV immediate-early protein 1 (IE1) was performed two days after inoculation. There was no major difference in the amount of viral progeny released from cells infected with the BAD-UL97-as1 mutant, compared to cells infected with the parental strain (Figure 2B).

3.2. Inhibition of BAD-UL97-as1 Using an ATP Analog

In [14], the authors tested several ATP analogs on the pUL97-as1 kinase mutant protein and found 3MB-PP1 to inhibit the kinase function most effectively. We followed that lead and chose 3MB-PP1 as the ATP-analog for further experiments. To test, whether 3MB-PP1 would indeed have an effect on the BAD-UL97-as1 mutant virus, we treated cells with 40 µM of 3MB-PP1 or DMSO the day before infection. The next day, we infected cells with either BADwt or BAD-UL97-as1. We then collected samples from infected cells at different time points and measured the amount of viral DNA present in these cells (Figure 3 upper graph). As expected, intracellular viral genomes of BAD-UL97-as1 were reduced when treated with 3MB-PP1, but not when treated with DMSO, compared to the wild type. Similarly, the amount of viral DNA released from cells infected with BAD-UL97-as1 was lower when the cells were treated with 3MB-PP1, compared to wild-type-infected cells (Figure 3 lower graph). As the literature from recent years has demonstrated, that inhibition of the pUL97 kinase activity causes viral replication defects, these results suggested, that 3MB-PP1 indeed reduced the replication of the BAD-pUL97-as1 viral strain. Interestingly, the release of viral DNA from BADwt-infected cells seemed also delayed in the presence of 3MB-PP1, even though this effect was not significant. This was surprising, because the ATP-analog was not expected to affect molecules other than the mutant kinase. However, this finding hints at off-target effects of 3MB-PP1 either on cellular processes or on other viral proteins.

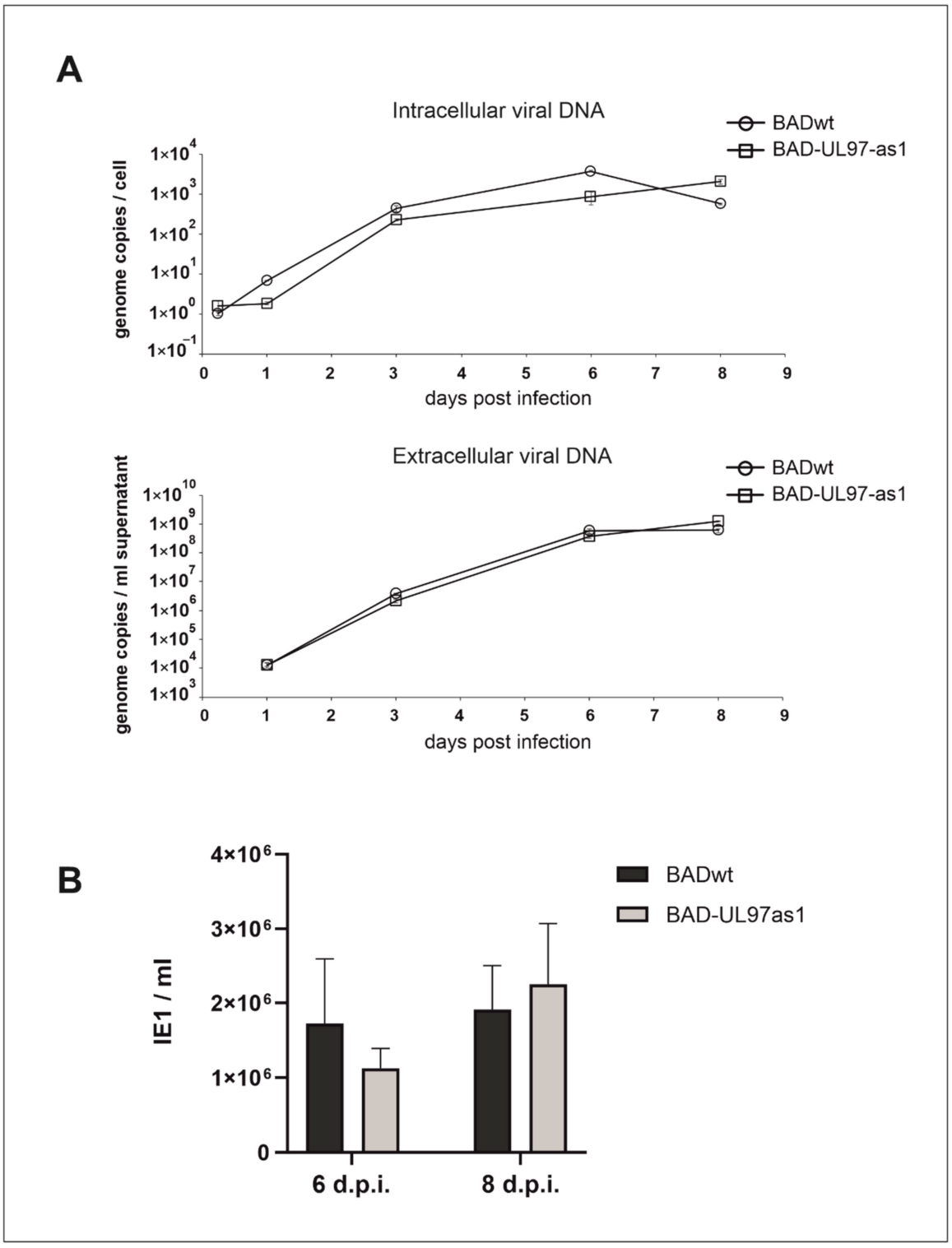

Figure 2. Replication kinetics of BADwt and BAD-UL97-as1. (**A**) Cells were infected with BADwt or BAD-UL97-as1 with 4 genomes/cell. Samples were taken and viral DNA was extracted from infected cells and the cell supernatant at the indicated time points. The intracellular and extracellular viral genome copies were quantified by quantitative PCR analysis. (**B**) HFF were infected with 4 genomes per cell with either BADwt or BAD-UL97-as1. After 6 and 8 days post infection, supernatants were collected and used to analyze the level of viral infectivity by serial dilution on indicator cell cultures, using staining for the immediate-early protein 1 (IE1) of HCMV at two days after inoculation. Bars represent the mean of eight technical replicates and the standard deviation is indicated by error bars.

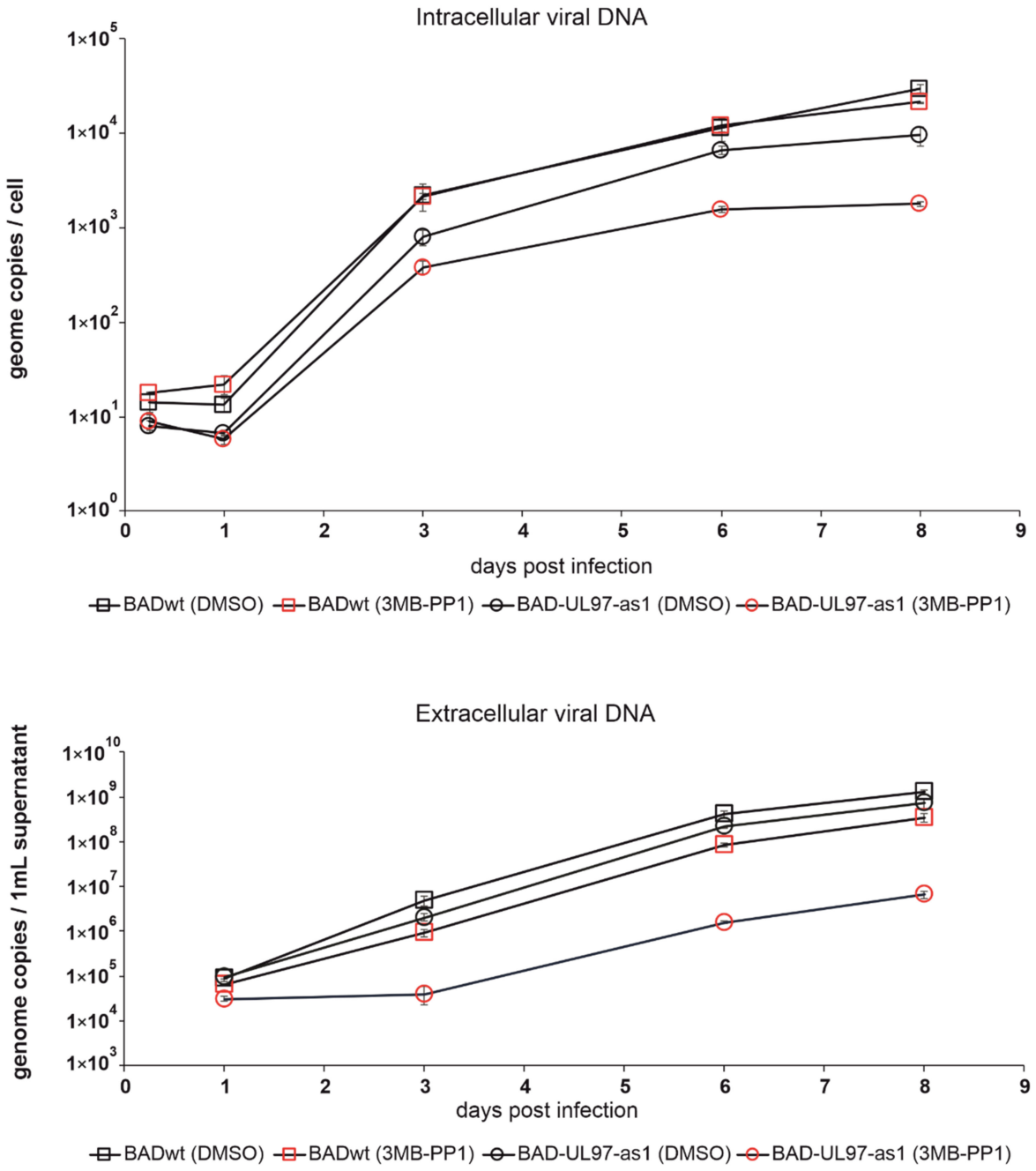

Figure 3. Replication kinetics of BADwt and BAD-UL97-as1 after treatment with 3MB-PP1. Cells were treated with either 40 µM of 3MB-PP1 or with DMSO one day before infection. The next day, cells were infected with BADwt or BAD-UL97-as1 with 4 genomes/cell. Samples were taken and viral DNA was extracted from infected cells and the cell supernatant at the indicated time points. The intracellular and extracellular viral genome copies were quantified by quantitative PCR analysis.

3.3. Phosphorylation Activity of BAD-UL97-as1

The cellular retinoblastoma protein (Rb) is a confirmed target of pUL97. pUL97 phosphorylates Rb on Serines 807 and 811 [2,28]. In the next step, we monitored the phosphorylation status of Rb in cells infected with either BADwt or the BAD-UL97-as1 mutant, using a specific antibody for these residues (Figure 4). Cells were treated with 40 µM 3MB-PP1 or with DMSO the day before infection and samples were collected at 5 days post-infection (d.p.i.). As a positive control, we also treated cells with 20 µM of a

known inhibitor of pUL97, maribavir (MBV), Livtencity™ [29] and analyzed the samples using SDS-PAGE and Western blot. Uninfected (mock) cells were also treated as control.

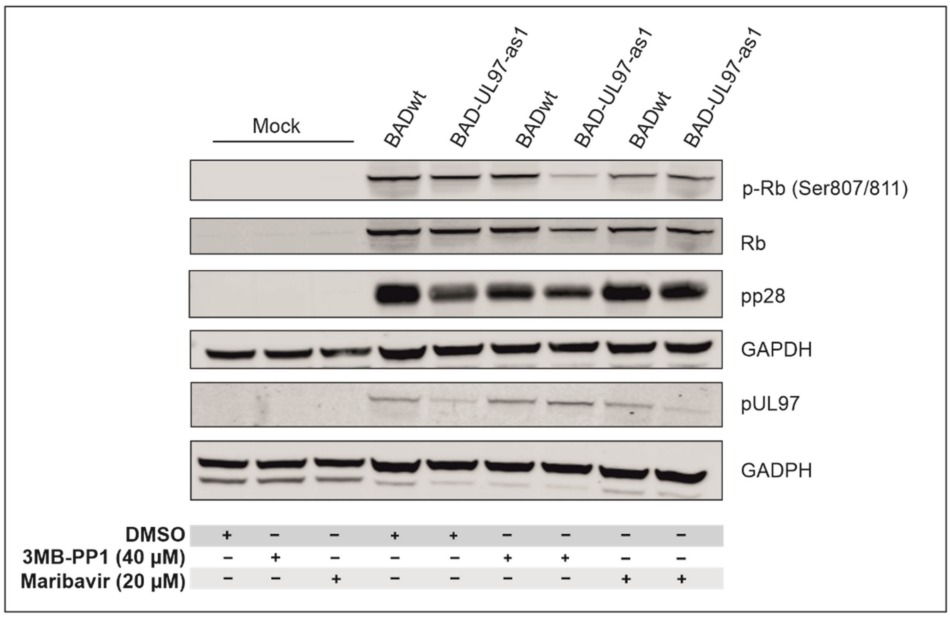

Figure 4. Phosphorylation of the retinoblastoma protein (Rb). Cells were pre-treated with DMSO, 3MB-PP1 or MBV one day before infection. The next day, cells were infected with BADwt or BAD-UL97-as1. Cells were harvested and lysed at 5 d.p.i. and analyzed in an SDS-PAGE and Western blot using a phospho-specific antibody for residues 807/811 of Rb. Antibodies against full protein Rb, the viral proteins pp28 and pUL97 were probed for reference.

As expected, the phosphorylation levels of Serines 807/811 of Rb increased when infected with either BADwt or BAD-UL97-as1 in the absence of 3MB-PP1 and MBV, compared to mock-infected cells. However, when BAD-UL97-as1-infected cells were treated with 3MB-PP1, the phosphorylation of Rb residues 807/811 hardly increased and instead, remained close to mock levels (Figure 4). The protein levels of pUL97 were comparable in both 3MB-PP1-treated samples, excluding the possibility that the reduction in substrate phosphorylation might result from lower pUL97-as1 protein levels. This indicates, that 3MB-PP1 indeed blocks the kinase activity of pUL97-as1 during infection. As expected, MBV reduced the levels of Rb phosphorylation in both BADwt and BAD-UL97-as1-infected cells.

3.4. Incubation Duration and Off-Target Effects of 3MB-PP1

While an analog-sensitive version of pUL97 is a promising tool to study the function of this kinase in an infection background, the replication defect and resulting low viral titers of BAD-UL97-as1 during long-term treatment with the analog might cause problems in various experimental procedures. To this end, we determined the minimal period of 3MB-PP1 treatment that ensures a substantial reduction in pUL97 kinase activity without reducing the viral replication and intracellular load. For this, we infected cells with either BADwt or BAD-UL97-as1 and treated with 3MB-PP1 for either 5, 2 or 1 days or for 4 h before harvesting the cells at 5 d.p.i. Cell lysates were then run in SDS-PAGE and Western blot and analyzed using the Ser807/811-specific antibody of Rb. To monitor the viral load, we also probed for a viral protein pp28, indicating the onset of viral replication in these cells.

We observed a reduction of the phosphorylation of Ser807/811 of Rb as soon as 4 h post-treatment with 3MB-PP1 (Figure 5). A treatment of 2 or even 5 days resulted in a reduction in the Rb full protein as well as in a reduction in the viral protein pp28 (Figure 5A). Furthermore, viral titers in the supernatant of BAD-UL97-as1-infected cells were reduced

when treated with 3MB-PP1 for one day or longer, while viral titers remained comparable to untreated samples when only treated for 4 h (Figure 5B).

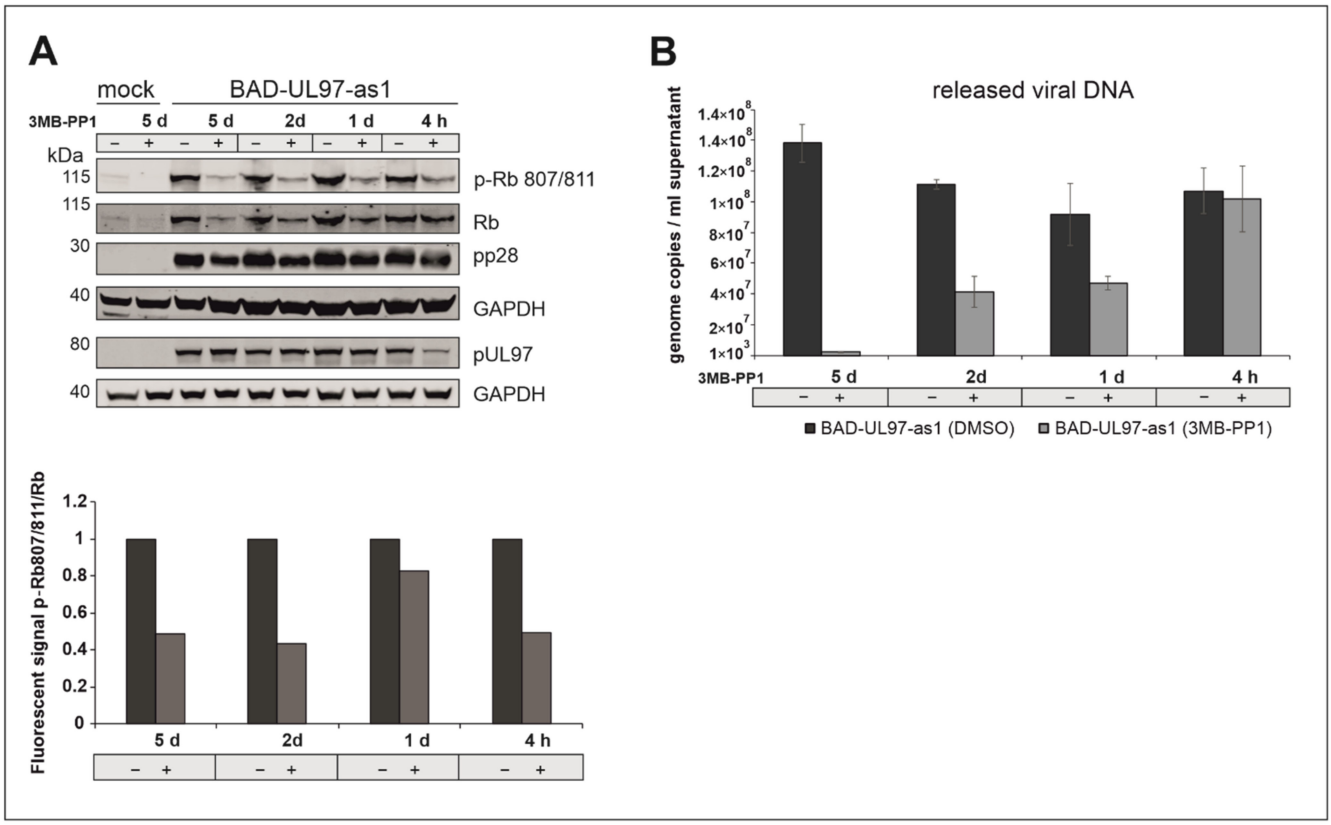

Figure 5. (**A**) BAD-UL97-as1 infected cells (10 genomes/cell) were harvested at 5 d.p.i. 40 µM of 3MB-PP1 was added at either 5 days, 2 days, 1 day or 4 h before harvest. The samples were analyzed by SDS-Page and Western blot analysis, using a specific antibody against the phosphosite 807/811 of Rb. The quantification was performed by measuring the protein intensity of pRb and Rb using Image Studio Lite Version 5.2.5. The ratios (pRb807/811/Rb) in dependence of 3MB-PP1 are shown. Thereby the corresponding DMSO sample was indicated as 1 (n = 2). (**B**) BAD-UL97-as1 (2 genomes/cell) infected HFFs were treated with 3MB-PP1 at different time points during infection. At 5 days, 2 days, 1 day or 4 h before harvest, the inhibitor was added. After 5 days post-infection, the supernatant was collected, DNA was isolated and the viral DNA of three technical replicates was quantified by TaqMan-PCR. The means ± standard deviations of each sample are shown.

ATP analogs supposedly inhibit analog-sensitive kinases specifically and are not expected to interfere with other cellular processes. However, during the course of these experiments, we regularly observed an effect of 3MB-PP1 on cells infected with the wild-type virus and even uninfected cells. To exclude any severe off-target effects, we submitted lysates of uninfected cells that we had treated for 5 days with 40 µM of 3MB-PP1 to mass spectrometry to analyze possible proteome changes triggered by the ATP analog (Figure 6, Supplementary Figure S1 and Table S1).

We observed an upregulation of cellular processes listed in Figure 6A. Many of these processes were involved in the ATP metabolism of the cell. In contrast, a number of cellular processes were downregulated, many of which intensely require ATP (Figure 6B). These findings may not be a counter-argument against the use of this tool but should be considered when analog-sensitive kinases are used.

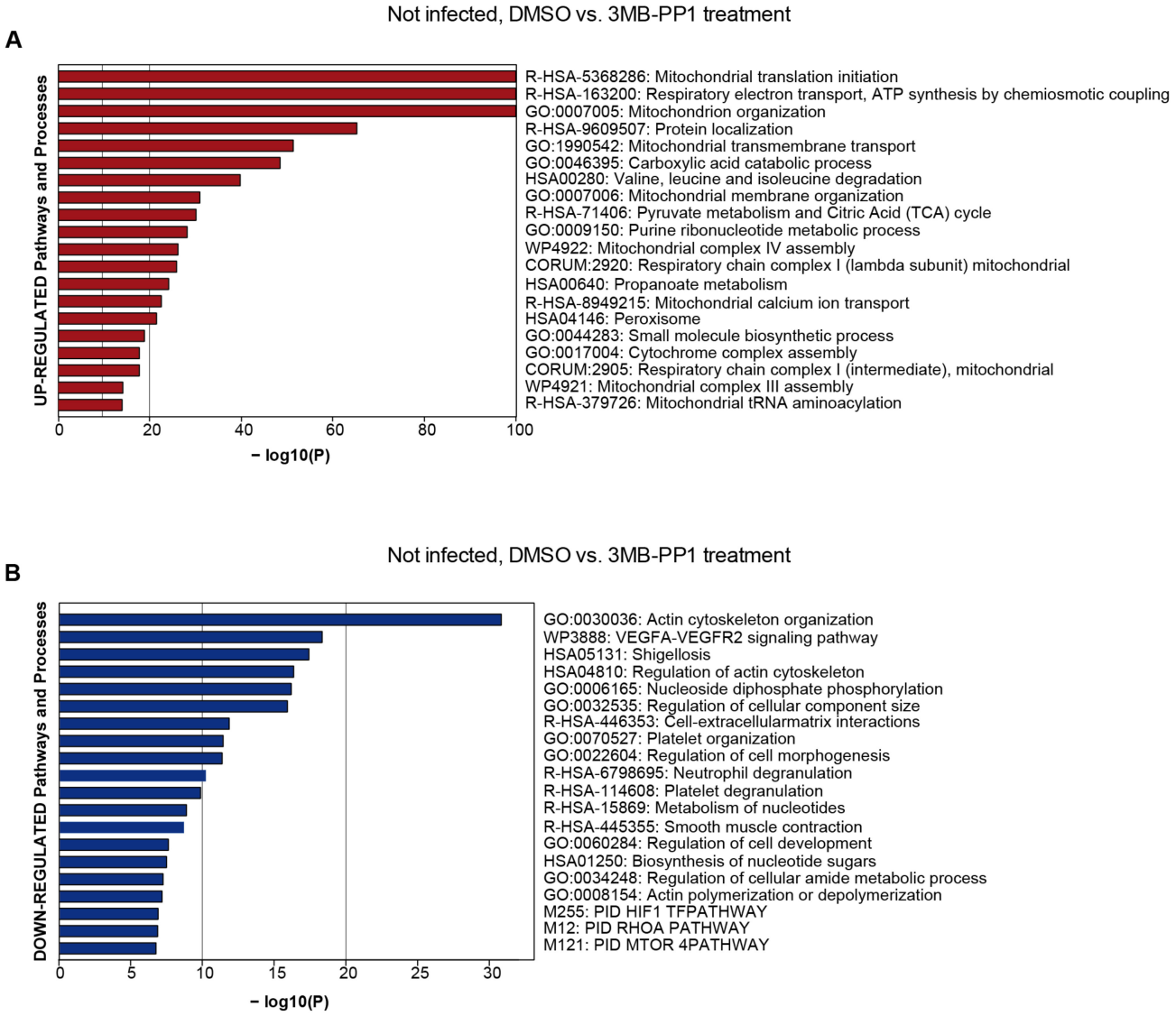

Figure 6. Dysregulated protein groups after 3MB-PP1 treatment in uninfected HFF. Pathway and process enrichment analysis of proteins up-regulated after 3MB-PP1 treatment (log2 ≥ 0.7 and *p*-value ≤ 0.05) (**A**). The top 20 clusters with their representative enriched terms are plotted according to their *p*-value in log base 10 (Log10 (P)). Enrichment analysis was performed with Metascape [30]. Pathway and process enrichment analysis of proteins down-regulated after 3MB-PP1 treatment (log2 ≤ -0.7 and *p*-value ≤ 0.05) (**B**). The top 20 clusters with their representative enriched terms are plotted according to their *p*-value in log base 10 (Log10 (P)). Enrichment analysis was performed with Metascape [30]. Pathway results are shown with the number of proteins found in the dataset and computed FDR for pathway enrichment (FDR < 0.001).

3.5. The Mutant pUL97-as1 Expressed by Recombinant HCMV Binds to Cyclins

In order to address the question of whether the BAD-UL97-as1 mutant retained its ability to interact with human cyclins [31,32], a CoIP experiment was performed using BAD-UL97-as1-infected cell material in comparison to the parental wild-type pUL97 (Figure 7). Cyclin B1 was used representatively for other cyclin types since the interaction of cyclin B1 with pUL97 is uniquely dependent on pUL97 kinase activity [26]. The CoIP data indicated the interaction of cyclin B1 with pUL97-wt as described before (Figure 7A, upper panel, lane 3) [24,33]. Importantly, also the pUL97-as1 mutant clearly showed this cyclin B1 interaction (lane 5). Notably, the treatment with 3MB-PP1 led to a complete loss of cyclin B1 interaction with pUL97-as1 (lane 6), but not with wt (lane 4). Although the expression level

of pUL97-as1 was found to be reduced under 3MB-PP1 treatment, we did not only note a reduced level of cyclin B1 CoIP, but found a complete loss of this signal (Figure 7, lane 6). This indicates that 3MB-PP1 treatment specifically inhibited the activity of the pUL97-as1 mutant, thus preventing cyclin B1 interaction. It should also be noted that the IP control of cyclin B1 indicated a relatively strong variation of bands. For this reason, independent replicates of this CoIP experiment were performed and clearly showed that cyclin B1 was more constant in individual other cases of this experimental setup (Figure 7B). However, we also noted a partial reduction in the pUL97-wt's interaction with cyclin B1 (lanes 3–4) by 3MB-PP1 possibly indicating some minor effect on pUL97-wt as well. This treatment with 3MB-PP1 did not show an impairment of the expression levels of cyclin B1 and pUL97-wt, but some effect on the pUL97-as1 mutant (Figure 7A,B, lower two panels, lysate controls). As far as the detectable level of immunoprecipitated cyclin B1 was concerned, reduced signals were noted under 3MB-PP1 treatment compared to DMSO control (as possibly referring to some technical limitation of the IP efficiency caused by 3MB-PP1; Figure 7A, panel cyclin IP control, lanes 4 and 6; this was not seen in the second replicate, Figure 7B). In essence, positive signals of cyclin B1 interaction were detected for pUL97-as1 including a specific sensitivity to 3MB-PP1. Combined, the inhibition of pUL97-as1 activity by 3MB-PP1 completely blocked the detectable levels of interaction with cyclin B1 (Figure 7A,B, lanes 6). Thus, the successful cyclin B1–pUL97-as1 CoIP pointed to the preservation of a wt-like cyclin interaction phenotype of this mutant.

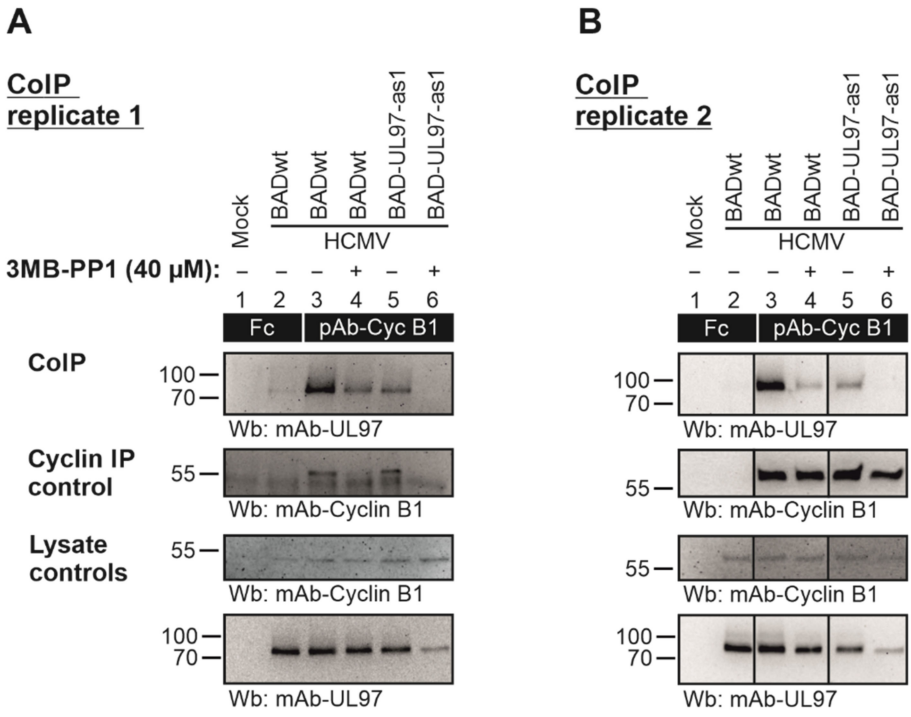

Figure 7. HFFs were cultivated in T175 flasks and used for infection with parental HCMV BADwt or recombinant BAD-UL97-as1 at a MOI of 0.5 for 4 d. An optional treatment with 40 µM of 3MB-PP1 (+, 3MB-PP1; −, DMSO solvent controls) was performed starting 4 h prior to sample collection and again during cell lysis. Total cell lysates were prepared and used for cyclin B1-specific CoIP with the indicated antibodies (see black boxes; Fc fragment was used as a negative control) under the continuous presence of 3MB. (**A**,**B**) show two independently produced biological replicates of this CoIP experiment, in order to illustrate the range of variability of individual signal strengths of detected protein bands. The CoIP samples were subjected to SDS-PAGE/Wb analysis (CoIP) and additional control stainings were performed to verify successful immunoprecipitation (cyclin IP control) and protein expression levels (lysate controls).

4. Discussion

Analog-sensitive kinases have been employed in various organisms for quite some time [11–13]. These kinases are useful tools to study any kinase and allow the inhibition of the kinase activity at any given time point in infection and in a dose-dependent manner. Additionally, this inhibition is reversible when the medium is washed off and replaced by fresh media not containing an ATP analog (Supplementary Figure S2). A possible reduction in kinase activity even without the inhibiting analog might occur in some cases but is usually not severe. In this work, we made use of a previously established analog-sensitive kinase protein of the viral kinase pUL97 of HCMV by introducing the respective mutation into the gene of UL97 in the Ad169 viral strain BADwt.

Over a time course of 8 days, the mutant virus BAD-UL97-as1 did not display a defect of viral replication, compared to the parental strain BADwt, although the replication of intracellular viral DNA appeared slightly reduced to a non-significant amount. This indicated that the BAD-UL97-as1 virus replicates normally in the absence of 3MB-PP1.

For experiments under impaired or blocked kinase activity, we used reasonably high doses of 3MB-PP1 (40 μM), hoping to sufficiently block the kinase activity of BAD-UL97-as1. While the literature suggests lower doses of 3MB-PP1 to be sufficient, we found the best reduction in the phosphorylation of the pUL97 substrate Rb using 40 μM of 3MB-PP1 (Supplementary Figure S3). Upon infection with BAD-UL97-as1, 3MB-PP1 reduced the amounts of intracellular as well as extracellular viral DNA over a time course of 8 days, while having only little effect on titers of the parental strain BADwt. This was not surprising, because a loss of the kinase activity of pUL97 has been described previously as non-beneficial for viral replication [31,34].

3MB-PP1 successfully prevented the phosphorylation of the pUL97-as1 substrate Rb, as was demonstrated on the Rb residues Ser807/811. This was not observed when BAD-UL97-as1-infected cells were treated with DMSO instead, demonstrating the functionality of the mutant kinase in the absence of the inhibitor. However, a long-term treatment with 3MB-PP1 led to a replication defect of BAD-UL97-as1, as was expected. This could be a problem for several experimental procedures, when high viral titers or titers comparable to those of parental strains are required. Our findings showed, that a short-term treatment of 3MB-PP1 also led to the desired effect of inhibiting pUL97-as1 substrate phosphorylation, while having no effect on the phosphorylation activity of the wild-type kinase. Together, these results indicate a specific inhibition of the mutant viral kinase by 3MB-PP1.

It should be mentioned that pUL97 was reported to be an active player in the HCMV-induced cellular cell cycle modulation and the induction of pseudomitosis. In this process, the main activity of pUL97, which contributes to this entire and complex phenomenon of pseudomitosis deregulation, is the massive, multisite-specific hyperphosphorylation of Rb by pUL97, leading to a G1-S phase transition of HCMV-infected cells. Our data showed that both wild-type and recombinant pUL97 were still able to perform Rb phosphorylation. However, according to the generally accepted understanding of this phenomenon, the cell cycle arrest is not a direct cause of the sole pUL97 activity, but more viral proteins appear to contribute and play additional regulatory roles [3,32,35]. Others, however, recently suggested that the reported phenotype of abnormal centrosome numbers seen in cells infected with the Ad169 strain of HCMV is rather caused by glycoprotein B (gB)-mediated cell fusion [36,37]. All together these complicated and carefully orchestrated regulatory mechanisms will require further investigation.

It should be pointed out, that 3MB-PP1 does not leave other cellular processes completely unaffected and seems to interfere with the binding of cyclins to the kinase, even in cells infected with the wild-type virus. Nevertheless, this interference does not seem to block the kinase activity or prevent target phosphorylation. In addition, a number of cellular proteins were dysregulated when cells were treated with 3MB-PP1, even in the absence of infection. Notably, ATP-producing processes were upregulated, hinting at a reaction of the cell to the presence of the non-hydrolysable ATP analog. Subsequently, processes demanding a high energy supply were decreased in the presence of 3MB-PP1.

While an analog-sensitive version of the viral kinase can be a very useful tool to study the role of the kinase during infection and its manipulation of cellular targets, these findings should be considered during experimental planning.

Supplementary Materials: The following supporting information can be downloaded at: https://www.mdpi.com/article/10.3390/v14102285/s1. Figure S1: Vulcano plot illustrating differentially abundant proteins of cells treated with 3MB-PP1 treatment. Figure S2: Reversible effect of 3MB-PP1 treatment. Figure S3: Dose-dependend effect of 3MB-PP1 on pUL97-as1.

Author Contributions: Conceptualization, C.Z., N.K. and M.M.; methodology, C.Z., N.K., M.M., L.H., U.G.M. and M.S.; validation, N.K., C.Z., M.S., M.M., U.G.M. and L.H.; formal analysis, N.K., C.Z. and M.M.; investigation, N.K., C.Z., M.S., U.G.M., L.H. and M.M.; resources, M.M., C.Z. and L.H.; writing—original draft preparation, C.Z. and N.K.; writing—review and editing, C.Z., N.K., M.M. and L.H.; supervision, C.Z., L.H. and M.M.; project administration, C.Z.; funding acquisition, C.Z., M.M. and L.H. All authors have read and agreed to the published version of the manuscript.

Funding: This research was funded by the Deutsche Forschungsgemeinschaft (DFG) grant ZI 1810/1-1 and the Interdisciplinary Center of Clinical Research of the Medical Center/Universitätsklinikum Erlangen (IZKF project A88-M.M./H.S.). Research in the Herhaus group is funded by the Dr. Rolf M. Schweite Stiftung (project 13/2017) and grants from the Goethe University Frankfurt (Nachwuchswissenschaftler grant (710000624) and GRADE A/B Focus (PID003790)). Additionally, this work was supported by the Clusterproject ENABLE funded by the Hessian Ministry for Science and the Arts, as well as the SFB 1177 'Molecular and Functional Characterization of Selective Autophagy'.

Institutional Review Board Statement: Not applicable.

Informed Consent Statement: Not applicable.

Data Availability Statement: The responsible authors declare that this article fully complies with the Data Availability Statements in the section "MDPI Research Data Policies" at https://www.mdpi.com/ethics (accessed on 5 September 2022). The mass spectrometry proteomic data have been deposited in the ProteomeXchange Consortium via the PRIDE partner repository with the following dataset identifier: PXD036455.

Acknowledgments: The authors appreciate the donation of monoclonal antibodies by William Britt and the donation of the BADwt BACmid by Thomas Shenk.

Conflicts of Interest: The authors declare no conflict of interest. The funders had no role in the design of the study; in the collection, analyses, or interpretation of data; in the writing of the manuscript; or in the decision to publish the results.

References

1. Griffiths, P.; Reeves, M. Pathogenesis of human cytomegalovirus in the immunocompromised host. *Nat. Rev. Microbiol.* **2021**, *19*, 759–773. [CrossRef] [PubMed]
2. Hume, A.J.; Finkel, J.S.; Kamil, J.P.; Coen, D.M.; Culbertson, M.R.; Kalejta, R.F. Phosphorylation of retinoblastoma protein by viral protein with cyclin-dependent kinase function. *Science* **2008**, *320*, 797–799. [CrossRef] [PubMed]
3. Hertel, L.; Chou, S.; Mocarski, E.S. Viral and cell cycle-regulated kinases in cytomegalovirus-induced pseudomitosis and replication. *PLoS Pathog.* **2007**, *3*, e6. [CrossRef] [PubMed]
4. Milbradt, J.; Hutterer, C.; Bahsi, H.; Wagner, S.; Sonntag, E.; Horn, A.H.; Kaufer, B.B.; Mori, Y.; Sticht, H.; Fossen, T.; et al. The Prolyl Isomerase Pin1 Promotes the Herpesvirus-Induced Phosphorylation-Dependent Disassembly of the Nuclear Lamina Required for Nucleocytoplasmic Egress. *PLoS Pathog.* **2016**, *12*, e1005825. [CrossRef]
5. Milbradt, J.; Webel, R.; Auerochs, S.; Sticht, H.; Marschall, M. Novel mode of phosphorylation-triggered reorganization of the nuclear lamina during nuclear egress of human cytomegalovirus. *J. Biol. Chem.* **2010**, *285*, 13979–13989. [CrossRef]
6. Hamirally, S.; Kamil, J.P.; Ndassa-Colday, Y.M.; Lin, A.J.; Jahng, W.J.; Baek, M.C.; Noton, S.; Silva, L.A.; Simpson-Holley, M.; Knipe, D.M.; et al. Viral mimicry of Cdc2/cyclin-dependent kinase 1 mediates disruption of nuclear lamina during human cytomegalovirus nuclear egress. *PLoS Pathog.* **2009**, *5*, e1000275. [CrossRef]
7. Marschall, M.; Marzi, A.; aus dem Siepen, P.; Jochmann, R.; Kalmer, M.; Auerochs, S.; Lischka, P.; Leis, M.; Stamminger, T. Cellular p32 recruits cytomegalovirus kinase pUL97 to redistribute the nuclear lamina. *J. Biol. Chem.* **2005**, *280*, 33357–33367. [CrossRef]
8. Sharma, M.; Bender, B.J.; Kamil, J.P.; Lye, M.F.; Pesola, J.M.; Reim, N.I.; Hogle, J.M.; Coen, D.M. Human cytomegalovirus UL97 phosphorylates the viral nuclear egress complex. *J. Virol.* **2015**, *89*, 523–534. [CrossRef]
9. Chou, S. Cytomegalovirus UL97 mutations in the era of ganciclovir and maribavir. *Rev. Med. Virol.* **2008**, *18*, 233–246. [CrossRef]

10. Prichard, M.N.; Britt, W.J.; Daily, S.L.; Hartline, C.B.; Kern, E.R. Human cytomegalovirus UL97 Kinase is required for the normal intranuclear distribution of pp65 and virion morphogenesis. *J. Virol.* **2005**, *79*, 15494–15502. [CrossRef]
11. Shokat, K.; Velleca, M. Novel chemical genetic approaches to the discovery of signal transduction inhibitors. *Drug Discov. Today* **2002**, *7*, 872–879. [CrossRef]
12. Witucki, L.A.; Huang, X.; Shah, K.; Liu, Y.; Kyin, S.; Eck, M.J.; Shokat, K.M. Mutant tyrosine kinases with unnatural nucleotide specificity retain the structure and phospho-acceptor specificity of the wild-type enzyme. *Chem. Biol.* **2002**, *9*, 25–33. [CrossRef]
13. Bishop, A.C.; Ubersax, J.A.; Petsch, D.T.; Matheos, D.P.; Gray, N.S.; Blethrow, J.; Shimizu, E.; Tsien, J.Z.; Schultz, P.G.; Rose, M.D.; et al. A chemical switch for inhibitor-sensitive alleles of any protein kinase. *Nature* **2000**, *407*, 395–401. [CrossRef]
14. Umana, A.C.; Iwahori, S.; Kalejta, R.F. Direct Substrate Identification with an Analog Sensitive (AS) Viral Cyclin-Dependent Kinase (v-Cdk). *ACS Chem. Biol.* **2018**, *13*, 189–199. [CrossRef]
15. Yu, D.; Smith, G.A.; Enquist, L.W.; Shenk, T. Construction of a self-excisable bacterial artificial chromosome containing the human cytomegalovirus genome and mutagenesis of the diploid TRL/IRL13 gene. *J. Virol.* **2002**, *76*, 2316–2328. [CrossRef]
16. Warming, S.; Costantino, N.; Court, D.L.; Jenkins, N.A.; Copeland, N.G. Simple and highly efficient BAC recombineering using galK selection. *Nucleic Acids Res.* **2005**, *33*, e36. [CrossRef]
17. Li, G.; Rak, M.; Nguyen, C.C.; Umashankar, M.; Goodrum, F.D.; Kamil, J.P. An epistatic relationship between the viral protein kinase UL97 and the UL133-UL138 latency locus during the human cytomegalovirus lytic cycle. *J. Virol.* **2014**, *88*, 6047–6060. [CrossRef]
18. Wang, D.; Li, G.; Schauflinger, M.; Nguyen, C.C.; Hall, E.D.; Yurochko, A.D.; von Einem, J.; Kamil, J.P. The ULb' region of the human cytomegalovirus genome confers an increased requirement for the viral protein kinase UL97. *J. Virol.* **2013**, *87*, 6359–6376. [CrossRef]
19. Mlera, L.; Moy, M.; Maness, K.; Tran, L.N.; Goodrum, F.D. The Role of the Human Cytomegalovirus UL133-UL138 Gene Locus in Latency and Reactivation. *Viruses* **2020**, *12*, 714. [CrossRef]
20. Kempova, V.; Lenhartova, S.; Benko, M.; Nemcovic, M.; Kudelova, M.; Nemcovicova, I. The power of human cytomegalovirus (HCMV) hijacked UL/b' functions lost in vitro. *Acta Virol.* **2020**, *64*, 117–130. [CrossRef]
21. Zimmermann, C.; Buscher, N.; Krauter, S.; Kramer, N.; Wolfrum, U.; Sehn, E.; Tenzer, S.; Plachter, B. The Abundant Tegument Protein pUL25 of Human Cytomegalovirus Prevents Proteasomal Degradation of pUL26 and Supports Its Suppression of ISGylation. *J. Virol.* **2018**, *92*, e01180-18. [CrossRef] [PubMed]
22. Besold, K.; Wills, M.; Plachter, B. Immune evasion proteins gpUS2 and gpUS11 of human cytomegalovirus incompletely protect infected cells from CD8 T cell recognition. *Virology* **2009**, *391*, 5–19. [CrossRef]
23. Krommelbein, N.; Wiebusch, L.; Schiedner, G.; Buscher, N.; Sauer, C.; Florin, L.; Sehn, E.; Wolfrum, U.; Plachter, B. Adenovirus E1A/E1B Transformed Amniotic Fluid Cells Support Human Cytomegalovirus Replication. *Viruses* **2016**, *8*, 37. [CrossRef]
24. Steingruber, M.; Kraut, A.; Socher, E.; Sticht, H.; Reichel, A.; Stamminger, T.; Amin, B.; Coute, Y.; Hutterer, C.; Marschall, M. Proteomic Interaction Patterns between Human Cyclins, the Cyclin-Dependent Kinase Ortholog pUL97 and Additional Cytomegalovirus Proteins. *Viruses* **2016**, *8*, 219. [CrossRef]
25. Hutterer, C.; Wandinger, S.K.; Wagner, S.; Muller, R.; Stamminger, T.; Zeittrager, I.; Godl, K.; Baumgartner, R.; Strobl, S.; Marschall, M. Profiling of the kinome of cytomegalovirus-infected cells reveals the functional importance of host kinases Aurora A, ABL and AMPK. *Antivir. Res.* **2013**, *99*, 139–148. [CrossRef]
26. Thomas, M.; Rechter, S.; Milbradt, J.; Auerochs, S.; Muller, R.; Stamminger, T.; Marschall, M. Cytomegaloviral protein kinase pUL97 interacts with the nuclear mRNA export factor pUL69 to modulate its intranuclear localization and activity. *J. Gen. Virol.* **2009**, *90 Pt 3*, 567–578. [CrossRef]
27. Hahn, M.; Covarrubias-Pinto, A.; Herhaus, L.; Satpathy, S.; Klann, K.; Boyle, K.B.; Munch, C.; Rajalingam, K.; Randow, F.; Choudhary, C.; et al. SIK2 orchestrates actin-dependent host response upon Salmonella infection. *Proc. Natl. Acad. Sci. USA* **2021**, *118*, e2024144118. [CrossRef]
28. Iwahori, S.; Hakki, M.; Chou, S.; Kalejta, R.F. Molecular Determinants for the Inactivation of the Retinoblastoma Tumor Suppressor by the Viral Cyclin-dependent Kinase UL97. *J. Biol. Chem.* **2015**, *290*, 19666–19680. [CrossRef]
29. Kang, C. Maribavir: First Approval. *Drugs* **2022**, *82*, 335–340. [CrossRef]
30. Zhou, Y.; Zhou, B.; Pache, L.; Chang, M.; Khodabakhshi, A.H.; Tanaseichuk, O.; Benner, C.; Chanda, S.K. Metascape provides a biologist-oriented resource for the analysis of systems-level datasets. *Nat. Commun.* **2019**, *10*, 1523. [CrossRef]
31. Schutz, M.; Steingruber, M.; Socher, E.; Muller, R.; Wagner, S.; Kogel, M.; Sticht, H.; Marschall, M. Functional Relevance of the Interaction between Human Cyclins and the Cytomegalovirus-Encoded CDK-Like Protein Kinase pUL97. *Viruses* **2021**, *13*, 1248. [CrossRef] [PubMed]
32. Steingruber, M.; Marschall, M. The Cytomegalovirus Protein Kinase pUL97: Host Interactions, Regulatory Mechanisms and Antiviral Drug Targeting. *Microorganisms* **2020**, *8*, 515. [CrossRef] [PubMed]
33. Steingruber, M.; Keller, L.; Socher, E.; Ferre, S.; Hesse, A.M.; Coute, Y.; Hahn, F.; Buscher, N.; Plachter, B.; Sticht, H.; et al. Cyclins B1, T1, and H differ in their molecular mode of interaction with cytomegalovirus protein kinase pUL97. *J. Biol. Chem.* **2019**, *294*, 6188–6203. [CrossRef] [PubMed]
34. Prichard, M.N.; Gao, N.; Jairath, S.; Mulamba, G.; Krosky, P.; Coen, D.M.; Parker, B.O.; Pari, G.S. A recombinant human cytomegalovirus with a large deletion in UL97 has a severe replication deficiency. *J. Virol.* **1999**, *73*, 5663–5670. [CrossRef]

Viruses **2022**, *14*, 2285

35. Marschall, M.; Feichtinger, S.; Milbradt, J. Regulatory roles of protein kinases in cytomegalovirus replication. *Adv. Virus Res.* **2011**, *80*, 69–101.
36. Tang, J.; Frascaroli, G.; Lebbink, R.J.; Ostermann, E.; Brune, W. Human cytomegalovirus glycoprotein B variants affect viral entry, cell fusion, and genome stability. *Proc. Natl. Acad. Sci. USA* **2019**, *116*, 18021–18030. [CrossRef]
37. Bogdanow, B.; Phan, Q.V.; Wiebusch, L. Emerging Mechanisms of G1/S Cell Cycle Control by Human and Mouse Cytomegaloviruses. *mBio* **2021**, *12*, e0293421. [CrossRef]

7 References

Afifi, A., 2021, unpublished. Viral interaction of the human cytomegalovirus with components of the autophagy machinery, Institute for Virology. University Medical Center of Johannes Gutenberg University Mainz

Ames, J., Yadavalli, T., Suryawanshi, R., Hopkins, J., Agelidis, A., Patil, C., Fredericks, B., Tseng, H., Valyi-Nagy, T., Shukla, D., 2021. OPTN is a host intrinsic restriction factor against neuroinvasive HSV-1 infection. Nature Communications 12, 5401.

Andreoni, M., Faircloth, M., Vugler, L., Britt, W.J., 1989. A rapid microneutralization assay for the measurement of neutralizing antibody reactive with human cytomegalovirus. J Virol Methods 23, 157-167.

Ashley, C.L., Abendroth, A., McSharry, B.P., Slobedman, B., 2019. Interferon-Independent Upregulation of Interferon-Stimulated Genes during Human Cytomegalovirus Infection is Dependent on IRF3 Expression. Viruses 11.

Babu, J.R., Geetha, T., Wooten, M.W., 2005. Sequestosome 1/p62 shuttles polyubiquitinated tau for proteasomal degradation. J Neurochem 94, 192-203.

Baek, M.C., Krosky, P.M., Pearson, A., Coen, D.M., 2004. Phosphorylation of the RNA polymerase II carboxyl-terminal domain in human cytomegalovirus-infected cells and in vitro by the viral UL97 protein kinase. Virology 324, 184-193.

Bansal, M., Moharir, S.C., Sailasree, S.P., Sirohi, K., Sudhakar, C., Sarathi, D.P., Lakshmi, B.J., Buono, M., Kumar, S., Swarup, G., 2018. Optineurin promotes autophagosome formation by recruiting the autophagy-related Atg12-5-16L1 complex to phagophores containing the Wipi2 protein. Journal of Biological Chemistry 293, 132-147.

Barde, I., Rauwel, B., Marin-Florez, R.M., Corsinotti, A., Laurenti, E., Verp, S., Offner, S., Marquis, J., Kapopoulou, A., Vanicek, J., Trono, D., 2013. A KRAB/KAP1-miRNA cascade regulates erythropoiesis through stage-specific control of mitophagy. Science 340, 350-353.

Beck, M., Hurt, E., 2017. The nuclear pore complex: understanding its function through structural insight. Nature Reviews Molecular Cell Biology 18, 73-89.

Becke, S., Fabre-Mersseman, V., Aue, S., Auerochs, S., Sedmak, T., Wolfrum, U., Strand, D., Marschall, M., Plachter, B., Reyda, S., 2010. Modification of the major tegument protein pp65 of human cytomegalovirus inhibits virus growth and leads to the enhancement of a protein complex with pUL69 and pUL97 in infected cells. J Gen Virol 91, 2531-2541.

Bekpen, C., Hunn, J.P., Rohde, C., Parvanova, I., Guethlein, L., Dunn, D.M., Glowalla, E., Leptin, M., Howard, J.C., 2005. The interferon-inducible p47 (IRG) GTPases in vertebrates: loss of the cell autonomous resistance mechanism in the human lineage. Genome Biol 6, R92.

Belzile, J.P., Sabalza, M., Craig, M., Clark, A.E., Morello, C.S., Spector, D.H., 2016. Trehalose, an mTOR-Independent Inducer of Autophagy, Inhibits Human Cytomegalovirus Infection in Multiple Cell Types. J Virol 90, 1259-1277.

Berkamp, S., Mostafavi, S., Sachse, C., 2021. Structure and function of p62/SQSTM1 in the emerging framework of phase separation. The FEBS Journal 288, 6927-6941.

Bigley, T.M., Reitsma, J.M., Terhune, S.S., 2015. Antagonistic Relationship between Human Cytomegalovirus pUL27 and pUL97 Activities during Infection. J Virol 89, 10230-10246.

Birgisdottir, Å.B., Lamark, T., Johansen, T., 2013. The LIR motif – crucial for selective autophagy. Journal of Cell Science 126, 3237-3247.

Bjørkøy , G., Lamark , T., Brech , A., Outzen , H., Perander , M., Øvervatn , A., Stenmark , H., Johansen , T., 2005. p62/SQSTM1 forms protein aggregates degraded by autophagy and has a protective effect on huntingtin-induced cell death. Journal of Cell Biology 171, 603-614.

Boppana, S.B., Pass, R.F., Britt, W.J., Stagno, S., Alford, C.A., 1992. Symptomatic congenital cytomegalovirus infection: neonatal morbidity and mortality. Pediatr Infect Dis J 11, 93-99.

Borden, K.L., 1998. RING fingers and B-boxes: zinc-binding protein-protein interaction domains. Biochem Cell Biol 76, 351-358.

Borst, E.M., Messerle, M., 2005. Analysis of human cytomegalovirus oriLyt sequence requirements in the context of the viral genome. J Virol 79, 3615-3626.

Buckingham, E.M., Carpenter, J.E., Jackson, W., Grose, C., 2014. Autophagy and the effects of its inhibition on varicella-zoster virus glycoprotein biosynthesis and infectivity. J Virol 88, 890-902.

Canfield, D., Gabby, L., Vaziri Fard, E., Gyamfi-Bannerman, C., 2023. Cytomegalovirus in Pregnancy. Obstetrics and Gynecology Clinics of North America 50, 263-277.

Casem, M.L., 2016. Chapter 4 - The Nucleus, in: Casem, M.L. (Ed.), Case Studies in Cell Biology. Academic Press, Boston, pp. 73-103.

Chaumorcel, M., Lussignol, M., Mouna, L., Cavignac, Y., Fahie, K., Cotte-Laffitte, J., Geballe, A., Brune, W., Beau, I., Codogno, P., Esclatine, A., 2012. The human cytomegalovirus protein TRS1 inhibits autophagy via its interaction with Beclin 1. J Virol 86, 2571-2584.

Chen, M., Meng, Q., Qin, Y., Liang, P., Tan, P., He, L., Zhou, Y., Chen, Y., Huang, J., Wang, R.F., Cui, J., 2016. TRIM14 Inhibits cGAS Degradation Mediated by Selective Autophagy Receptor p62 to Promote Innate Immune Responses. Mol Cell 64, 105-119.

Choi, Y., Bowman, J.W., Jung, J.U., 2018. Autophagy during viral infection — a double-edged sword. Nature Reviews Microbiology 16, 341-354.

Chou, S.W., Scott, K.M., 1988. Rapid quantitation of cytomegalovirus and assay of neutralizing antibody by using monoclonal antibody to the major immediate-early viral protein. J Clin Microbiol 26, 504-507.

Chu, C.T., Ji, J., Dagda, R.K., Jiang, J.F., Tyurina, Y.Y., Kapralov, A.A., Tyurin, V.A., Yanamala, N., Shrivastava, I.H., Mohammadyani, D., Wang, K.Z.Q., Zhu, J., Klein-Seetharaman, J., Balasubramanian, K., Amoscato, A.A., Borisenko, G., Huang, Z., Gusdon, A.M., Cheikhi, A., Steer, E.K., Wang, R., Baty, C., Watkins, S., Bahar, I., Bayir, H., Kagan, V.E., 2013. Cardiolipin externalization to the outer mitochondrial membrane acts as an elimination signal for mitophagy in neuronal cells. Nat Cell Biol 15, 1197-1205.

Chu, Y., Yang, X., 2011. SUMO E3 ligase activity of TRIM proteins. Oncogene 30, 1108-1116.

Chun, Y., Kim, J., 2018. Autophagy: An Essential Degradation Program for Cellular Homeostasis and Life. Cells 7.

Clark, A.E., Sabalza, M., Gordts, P., Spector, D.H., 2018. Human Cytomegalovirus Replication Is Inhibited by the Autophagy-Inducing Compounds Trehalose and SMER28 through Distinctively Different Mechanisms. J Virol 92.

Concordet, J.-P., Haeussler, M., 2018. CRISPOR: intuitive guide selection for CRISPR/Cas9 genome editing experiments and screens. Nucleic Acids Research 46, W242-W245.

Dai, X., Yu, X., Gong, H., Jiang, X., Abenes, G., Liu, H., Shivakoti, S., Britt, W.J., Zhu, H., Liu, F., Zhou, Z.H., 2013. The smallest capsid protein mediates binding of the essential tegument protein pp150 to stabilize DNA-containing capsids in human cytomegalovirus. PLoS Pathog 9, e1003525.

de Jong, M.D., Galasso, G.J., Gazzard, B., Griffiths, P.D., Jabs, D.A., Kern, E.R., Spector, S.A., 1998. Summary of the II International Symposium on Cytomegalovirus. Antiviral Res 39, 141-162.

Dell'Oste, V., Gatti, D., Gugliesi, F., De Andrea, M., Bawadekar, M., Lo Cigno, I., Biolatti, M., Vallino, M., Marschall, M., Gariglio, M., Landolfo, S., 2014. Innate nuclear sensor IFI16 translocates into the cytoplasm during the early stage of in vitro human cytomegalovirus infection and is entrapped in the egressing virions during the late stage. J Virol 88, 6970-6982.

Di Rienzo, M., Antonioli, M., Fusco, C., Liu, Y., Mari, M., Orhon, I., Refolo, G., Germani, F., Corazzari, M., Romagnoli, A., Ciccosanti, F., Mandriani, B., Pellico, M.T., De La Torre, R., Ding, H., Dentice, M., Neri, M., Ferlini, A., Reggiori, F., Kulesz-Martin, M., Piacentini, M., Merla, G., Fimia, G.M., 2019. Autophagy induction in atrophic muscle cells requires ULK1 activation by TRIM32 through unanchored K63-linked polyubiquitin chains. Sci Adv 5, eaau8857.

Di Rienzo, M., Romagnoli, A., Antonioli, M., Piacentini, M., Fimia, G.M., 2020. TRIM proteins in autophagy: selective sensors in cell damage and innate immune responses. Cell Death & Differentiation 27, 887-902.

Ding, W.X., Yin, X.M., 2012. Mitophagy: mechanisms, pathophysiological roles, and analysis. Biol Chem 393, 547-564.

Diosi, P., Babusceac, L., Nevinglovschi, O., Kun-Stoicu, G., 1967. Cytomegalovirus infection associated with pregnancy. Lancet 2, 1063-1066.

Dong, X., Levine, B., 2013. Autophagy and viruses: adversaries or allies? J Innate Immun 5, 480-493.

Doucet, C.M., Talamas, J.A., Hetzer, M.W., 2010. Cell Cycle-Dependent Differences in Nuclear Pore Complex Assembly in Metazoa. Cell 141, 1030-1041.

Drew, W.L., 1992. Cytomegalovirus infection in patients with AIDS. Clin Infect Dis 14, 608-615.

Eldin, P., Papon, L., Oteiza, A., Brocchi, E., Lawson, T.G., Mechti, N., 2009. TRIM22 E3 ubiquitin ligase activity is required to mediate antiviral activity against encephalomyocarditis virus. Journal of General Virology 90, 536-545.

Fan, L., Yin, S., Zhang, E., Hu, H., 2018. Role of p62 in the regulation of cell death induction. Apoptosis 23, 187-193.

Farré, J.-C., Burkenroad, A., Burnett, S.F., Subramani, S., 2013. Phosphorylation of mitophagy and pexophagy receptors coordinates their interaction with Atg8 and Atg11. EMBO reports 14, 441-449.

Fleckenstein, B., Müller, I., Collins, J., 1982. Cloning of the complete human cytomegalovirus genome in cosmids. Gene 18, 39-46.

Fowler, K.B., Boppana, S.B., 2018. Congenital cytomegalovirus infection. Semin Perinatol 42, 149-154.

Funakoshi, T., Clever, M., Watanabe, A., Imamoto, N., 2011. Localization of Pom121 to the inner nuclear membrane is required for an early step of interphase nuclear pore complex assembly. Molecular Biology of the Cell 22, 1058-1069.

Fusco, C., Mandriani, B., Di Rienzo, M., Micale, L., Malerba, N., Cocciadiferro, D., Sjøttem, E., Augello, B., Squeo, G.M., Pellico, M.T., Jain, A., Johansen, T., Fimia, G.M., Merla, G., 2018. TRIM50 regulates Beclin 1 proautophagic activity. Biochim Biophys Acta Mol Cell Res 1865, 908-919.

Gack, M.U., Albrecht, R.A., Urano, T., Inn, K.-S., Huang, I.C., Carnero, E., Farzan, M., Inoue, S., Jung, J.U., García-Sastre, A., 2009. Influenza A Virus NS1 Targets the Ubiquitin Ligase TRIM25 to Evade Recognition by the Host Viral RNA Sensor RIG-I. Cell Host & Microbe 5, 439-449.

Gack, M.U., Shin, Y.C., Joo, C.H., Urano, T., Liang, C., Sun, L., Takeuchi, O., Akira, S., Chen, Z., Inoue, S., Jung, J.U., 2007. TRIM25 RING-finger E3 ubiquitin ligase is essential for RIG-I-mediated antiviral activity. Nature 446, 916-920.

Galluzzi, L., Baehrecke, E.H., Ballabio, A., Boya, P., Bravo-San Pedro, J.M., Cecconi, F., Choi, A.M., Chu, C.T., Codogno, P., Colombo, M.I., Cuervo, A.M., Debnath, J., Deretic, V., Dikic, I., Eskelinen, E.L., Fimia, G.M., Fulda, S., Gewirtz, D.A., Green, D.R., Hansen, M., Harper, J.W., Jäättelä, M., Johansen, T., Juhasz, G., Kimmelman, A.C., Kraft, C., Ktistakis, N.T., Kumar, S., Levine, B., Lopez-Otin, C., Madeo, F., Martens, S., Martinez, J., Melendez, A., Mizushima, N., Münz, C., Murphy, L.O., Penninger, J.M., Piacentini, M., Reggiori, F., Rubinsztein, D.C., Ryan, K.M., Santambrogio, L., Scorrano, L., Simon, A.K., Simon, H.U., Simonsen, A., Tavernarakis, N., Tooze, S.A., Yoshimori, T., Yuan, J., Yue, Z., Zhong, Q., Kroemer, G., 2017. Molecular definitions of autophagy and related processes. Embo j 36, 1811-1836.

Gill, R.B., James, S.H., Prichard, M.N., 2012. Human cytomegalovirus UL97 kinase alters the accumulation of CDK1. J Gen Virol 93, 1743-1755.

Giraldo, M.I., Hage, A., van Tol, S., Rajsbaum, R., 2020. TRIM Proteins in Host Defense and Viral Pathogenesis. Current Clinical Microbiology Reports 7, 101-114.

Goderis, J., De Leenheer, E., Smets, K., Van Hoecke, H., Keymeulen, A., Dhooge, I., 2014. Hearing loss and congenital CMV infection: a systematic review. Pediatrics 134, 972-982.

Griffiths, P., Reeves, M., 2021. Pathogenesis of human cytomegalovirus in the immunocompromised host. Nature Reviews Microbiology 19, 759-773.

Griffiths, P.D., Clark, D.A., Emery, V.C., 2000. Betaherpesviruses in transplant recipients. J Antimicrob Chemother 45 Suppl T3, 29-34.

Gu, H., Jan Fada, B., 2020. Specificity in Ubiquitination Triggered by Virus Infection. Int J Mol Sci 21.

Gubas, A., Dikic, I., 2022. A guide to the regulation of selective autophagy receptors. The FEBS Journal 289, 75-89.

Gugliesi, F., Coscia, A., Griffante, G., Galitska, G., Pasquero, S., Albano, C., Biolatti, M., 2020. Where do we Stand after Decades of Studying Human Cytomegalovirus? Microorganisms 8.

Haeussler, M., Schönig, K., Eckert, H., Eschstruth, A., Mianné, J., Renaud, J.B., Schneider-Maunoury, S., Shkumatava, A., Teboul, L., Kent, J., Joly, J.S., Concordet, J.P., 2016. Evaluation of off-target and on-target scoring algorithms and integration into the guide RNA selection tool CRISPOR. Genome Biol 17, 148.

Hamirally, S., Kamil, J.P., Ndassa-Colday, Y.M., Lin, A.J., Jahng, W.J., Baek, M.C., Noton, S., Silva, L.A., Simpson-Holley, M., Knipe, D.M., Golan, D.E., Marto, J.A., Coen, D.M., 2009. Viral mimicry of Cdc2/cyclin-dependent kinase 1 mediates disruption of nuclear lamina during human cytomegalovirus nuclear egress. PLoS Pathog 5, e1000275.

Handsfield, H.H., Chandler, S.H., Caine, V.A., Meyers, J.D., Corey, L., Medeiros, E., McDougall, J.K., 1985. Cytomegalovirus infection in sex partners: evidence for sexual transmission. J Infect Dis 151, 344-348.

Hennig, P., Fenini, G., Di Filippo, M., Karakaya, T., Beer, H.D., 2021. The Pathways Underlying the Multiple Roles of p62 in Inflammation and Cancer. Biomedicines 9.

Herhaus, L., unpublished.

Herhaus, L., Bhaskara, R.M., Lystad, A.H., Gestal-Mato, U., Covarrubias-Pinto, A., Bonn, F., Simonsen, A., Hummer, G., Dikic, I., 2020. TBK1-mediated phosphorylation of LC3C and GABARAP-L2 controls autophagosome shedding by ATG4 protease. EMBO reports 21, e48317.

Horwitz, C.A., Henle, W., Henle, G., Snover, D., Rudnick, H., Balfour, H.H., Jr., Mazur, M.H., Watson, R., Schwartz, B., Muller, N., 1986. Clinical and laboratory evaluation of cytomegalovirus-induced mononucleosis in previously healthy individuals. Report of 82 cases. Medicine (Baltimore) 65, 124-134.

Hume, A.J., Finkel, J.S., Kamil, J.P., Coen, D.M., Culbertson, M.R., Kalejta, R.F., 2008. Phosphorylation of retinoblastoma protein by viral protein with cyclin-dependent kinase function. Science 320, 797-799.

Ikeda, K., Inoue, S., 2012. TRIM proteins as RING finger E3 ubiquitin ligases. Adv Exp Med Biol 770, 27-37.

Imbert, F., Leavitt, G., Langford, D., 2022. SUMOylation and Viral Infections of the Brain. Pathogens 11.

Isomura, H., Stinski, M.F., Kudoh, A., Nakayama, S., Murata, T., Sato, Y., Iwahori, S., Tsurumi, T., 2008. A cis element between the TATA Box and the transcription start site of the major immediate-early promoter of human cytomegalovirus determines efficiency of viral replication. J Virol 82, 849-858.

Iwahori, S., Kalejta, R.F., 2017. Phosphorylation of transcriptional regulators in the retinoblastoma protein pathway by UL97, the viral cyclin-dependent kinase encoded by human cytomegalovirus. Virology 512, 95-103.

Iwahori, S., Umaña, A.C., VanDeusen, H.R., Kalejta, R.F., 2017. Human cytomegalovirus-encoded viral cyclin-dependent kinase (v-CDK) UL97 phosphorylates and inactivates the retinoblastoma protein-related p107 and p130 proteins. J Biol Chem 292, 6583-6599.

Jackson, W.T., 2015. Viruses and the autophagy pathway. Virology 479-480, 450-456.

Johansen, T., Lamark, T., 2011. Selective autophagy mediated by autophagic adapter proteins. Autophagy 7, 279-296.

Jordan, T.X., Randall, G., 2012. Manipulation or capitulation: virus interactions with autophagy. Microbes Infect 14, 126-139.

Judith, D., Mostowy, S., Bourai, M., Gangneux, N., Lelek, M., Lucas-Hourani, M., Cayet, N., Jacob, Y., Prévost, M.C., Pierre, P., Tangy, F., Zimmer, C., Vidalain, P.O., Couderc, T., Lecuit, M., 2013. Species-specific impact of the autophagy machinery on Chikungunya virus infection. EMBO Rep 14, 534-544.

Kabeya, Y., Mizushima, N., Yamamoto, A., Oshitani-Okamoto, S., Ohsumi, Y., Yoshimori, T., 2004. LC3, GABARAP and GATE16 localize to autophagosomal membrane depending on form-II formation. Journal of Cell Science 117, 2805-2812.

Kachaner, D., Génin, P., Laplantine, E., Weil, R., 2012. Toward an integrative view of Optineurin functions. Cell Cycle 11, 2808-2818.

Kalejta, R.F., 2008a. Functions of human cytomegalovirus tegument proteins prior to immediate early gene expression. Curr Top Microbiol Immunol 325, 101-115.

Kalejta, R.F., 2008b. Tegument proteins of human cytomegalovirus. Microbiol Mol Biol Rev 72, 249-265, table of contents.

Kehl, S.R., Soos, B.A., Saha, B., Choi, S.W., Herren, A.W., Johansen, T., Mandell, M.A., 2019. TAK1 converts Sequestosome 1/p62 from an autophagy receptor to a signaling platform. EMBO Rep 20, e46238.

Kenneson, A., Cannon, M.J., 2007. Review and meta-analysis of the epidemiology of congenital cytomegalovirus (CMV) infection. Rev Med Virol 17, 253-276.

Khaminets, A., Behl, C., Dikic, I., 2016. Ubiquitin-Dependent And Independent Signals In Selective Autophagy. Trends in Cell Biology 26, 6-16.

Kim, P.K., Hailey, D.W., Mullen, R.T., Lippincott-Schwartz, J., 2008. Ubiquitin signals autophagic degradation of cytosolic proteins and peroxisomes. Proc Natl Acad Sci U S A 105, 20567-20574.

Kimura, T., Jain, A., Choi, S.W., Mandell, M.A., Johansen, T., Deretic, V., 2017a. TRIM-directed selective autophagy regulates immune activation. Autophagy 13, 989-990.

Kimura, T., Jain, A., Choi, S.W., Mandell, M.A., Schroder, K., Johansen, T., Deretic, V., 2015. TRIM-mediated precision autophagy targets cytoplasmic regulators of innate immunity. J Cell Biol 210, 973-989.

Kimura, T., Jia, J., Kumar, S., Choi, S.W., Gu, Y., Mudd, M., Dupont, N., Jiang, S., Peters, R., Farzam, F., Jain, A., Lidke, K.A., Adams, C.M., Johansen, T., Deretic, V., 2017b. Dedicated SNAREs and specialized TRIM cargo receptors mediate secretory autophagy. The EMBO Journal 36, 42-60.

Kirkin, V., Rogov, V.V., 2019. A Diversity of Selective Autophagy Receptors Determines the Specificity of the Autophagy Pathway. Molecular Cell 76, 268-285.

Koepke, L., Gack, M.U., Sparrer, K.M., 2021. The antiviral activities of TRIM proteins. Curr Opin Microbiol 59, 50-57.

König, P., Svrlanska, A., Read, C., Feichtinger, S., Stamminger, T., 2021. The Autophagy-Initiating Protein Kinase ULK1 Phosphorylates Human Cytomegalovirus Tegument Protein pp28 and Regulates Efficient Virus Release. J Virol 95.

Korac, J., Schaeffer, V., Kovacevic, I., Clement, A.M., Jungblut, B., Behl, C., Terzic, J., Dikic, I., 2013. Ubiquitin-independent function of optineurin in autophagic clearance of protein aggregates. J Cell Sci 126, 580-592.

Krämer, N., Schütz, M., Mato, U.G., Herhaus, L., Marschall, M., Zimmermann, C., 2022. Recombinant Human Cytomegalovirus Expressing an Analog-Sensitive Kinase pUL97 as Novel Tool for Functional Analyses. Viruses 14.

Kuang, Y., Ma, K., Zhou, C., Ding, P., Zhu, Y., Chen, Q., Xia, B., 2016. Structural basis for the phosphorylation of FUNDC1 LIR as a molecular switch of mitophagy. Autophagy 12, 2363-2373.

Kuma, A., Mizushima, N., 2010. Physiological role of autophagy as an intracellular recycling system: with an emphasis on nutrient metabolism. Semin Cell Dev Biol 21, 683-690.

Kumar, A.V., Mills, J., Lapierre, L.R., 2022. Selective Autophagy Receptor p62/SQSTM1, a Pivotal Player in Stress and Aging. Frontiers in Cell and Developmental Biology 10.

Kuny, C.V., Chinchilla, K., Culbertson, M.R., Kalejta, R.F., 2010. Cyclin-dependent kinase-like function is shared by the beta- and gamma- subset of the conserved herpesvirus protein kinases. PLoS Pathog 6, e1001092.

Lamark, T., Johansen, T., 2012. Aggrephagy: selective disposal of protein aggregates by macroautophagy. Int J Cell Biol 2012, 736905.

Lamark, T., Svenning, S., Johansen, T., 2017. Regulation of selective autophagy: the p62/SQSTM1 paradigm. Essays in Biochemistry 61, 609-624.

Lamberson, H.V., Dock, N.L., 1992. Prevention of transfusion-transmitted cytomegalovirus infection. Transfusion 32, 196-198.

Lan, K., Luo, M.H., 2017. Herpesviruses: epidemiology, pathogenesis, and interventions. Virol Sin 32, 347-348.

Lang, D., Stamminger, T., 1993. The 86-kilodalton IE-2 protein of human cytomegalovirus is a sequence-specific DNA-binding protein that interacts directly with the negative autoregulatory response element located near the cap site of the IE-1/2 enhancer-promoter. J Virol 67, 323-331.

Le-Trilling, V.T.K., Becker, T., Nachshon, A., Stern-Ginossar, N., Schöler, L., Voigt, S., Hengel, H., Trilling, M., 2020. The Human Cytomegalovirus pUL145 Isoforms Act as Viral DDB1-Cullin-Associated Factors to Instruct Host Protein Degradation to Impede Innate Immunity. Cell Reports 30, 2248-2260.e2245.

Levine, B., Mizushima, N., Virgin, H.W., 2011. Autophagy in immunity and inflammation. Nature 469, 323-335.

Lim, J., Lachenmayer, M.L., Wu, S., Liu, W., Kundu, M., Wang, R., Komatsu, M., Oh, Y.J., Zhao, Y., Yue, Z., 2015. Proteotoxic stress induces phosphorylation of p62/SQSTM1 by ULK1 to regulate selective autophagic clearance of protein aggregates. PLoS Genet 11, e1004987.

Lin, X., Li, Shuang , Zhao, Yue, Ma, Xiaofeng, Zhang, Kai, He, Xinglan and Wang, o 2013. Interaction Domains of p62: A Bridge Between p62 and Selective Autophagy. DNA and Cell Biology 32, 220-227.

Linares, J.F., Amanchy, R., Greis, K., Diaz-Meco, M.T., Moscat, J., 2011. Phosphorylation of p62 by cdk1 controls the timely transit of cells through mitosis and tumor cell proliferation. Mol Cell Biol 31, 105-117.

Linares, J.F., Duran, A., Reina-Campos, M., Aza-Blanc, P., Campos, A., Moscat, J., Diaz-Meco, M.T., 2015. Amino Acid Activation of mTORC1 by a PB1-Domain-Driven Kinase Complex Cascade. Cell Rep 12, 1339-1352.

Liu, L., 2014. Fields Virology, 6th Edition. Clinical Infectious Diseases 59, 613-613.

Liu, W.J., Ye, L., Huang, W.F., Guo, L.J., Xu, Z.G., Wu, H.L., Yang, C., Liu, H.F., 2016. p62 links the autophagy pathway and the ubiqutin–proteasome system upon ubiquitinated protein degradation. Cellular & Molecular Biology Letters 21, 29.

Liu, Z., Chen, P., Gao, H., Gu, Y., Yang, J., Peng, H., Xu, X., Wang, H., Yang, M., Liu, X., Fan, L., Chen, S., Zhou, J., Sun, Y., Ruan, K., Cheng, S., Komatsu, M., White, E., Li, L., Ji,

H., Finley, D., Hu, R., 2014. Ubiquitylation of autophagy receptor Optineurin by HACE1 activates selective autophagy for tumor suppression. Cancer Cell 26, 106-120.

Lobb, I.T., Morin, P., Martin, K., Thoms, H.C., Wills, J.C., Lleshi, X., Olsen, K.C.F., Duncan, R.R., Stark, L.A., 2021. A Role for the Autophagic Receptor, SQSTM1/p62, in Trafficking NF-κB/RelA to Nucleolar Aggresomes. Mol Cancer Res 19, 274-287.

Lomonte, P., 2017. Herpesvirus Latency: On the Importance of Positioning Oneself. Adv Anat Embryol Cell Biol 223, 95-117.

Lopez, M.S., Kliegman, J.I., Shokat, K.M., 2014. Chapter Eight - The Logic and Design of Analog-Sensitive Kinases and Their Small Molecule Inhibitors, in: Shokat, K.M. (Ed.), Methods in Enzymology. Academic Press, pp. 189-213.

Malumbres, M., 2014. Cyclin-dependent kinases. Genome Biology 15, 122.

Mandell, M.A., Jain, A., Arko-Mensah, J., Chauhan, S., Kimura, T., Dinkins, C., Silvestri, G., Münch, J., Kirchhoff, F., Simonsen, A., Wei, Y., Levine, B., Johansen, T., Deretic, V., 2014a. TRIM proteins regulate autophagy and can target autophagic substrates by direct recognition. Dev Cell 30, 394-409.

Mandell, M.A., Kimura, T., Jain, A., Johansen, T., Deretic, V., 2014b. TRIM proteins regulate autophagy: TRIM5 is a selective autophagy receptor mediating HIV-1 restriction. Autophagy 10, 2387-2388.

Marschall, M., Freitag, M., Suchy, P., Romaker, D., Kupfer, R., Hanke, M., Stamminger, T., 2003. The protein kinase pUL97 of human cytomegalovirus interacts with and phosphorylates the DNA polymerase processivity factor pUL44. Virology 311, 60-71.

Matsumoto, G., Wada, K., Okuno, M., Kurosawa, M., Nukina, N., 2011. Serine 403 phosphorylation of p62/SQSTM1 regulates selective autophagic clearance of ubiquitinated proteins. Mol Cell 44, 279-289.

Meyer, R.D., Srinivasan, S., Singh, A.J., Mahoney, J.E., Gharahassanlou, K.R., Rahimi, N., 2011. PEST motif serine and tyrosine phosphorylation controls vascular endothelial growth factor receptor 2 stability and downregulation. Mol Cell Biol 31, 2010-2025.

Milbradt, J., Webel, R., Auerochs, S., Sticht, H., Marschall, M., 2010. Novel mode of phosphorylation-triggered reorganization of the nuclear lamina during nuclear egress of human cytomegalovirus. J Biol Chem 285, 13979-13989.

Mohamud, Y., Qu, J., Xue, Y.C., Liu, H., Deng, H., Luo, H., 2019. CALCOCO2/NDP52 and SQSTM1/p62 differentially regulate coxsackievirus B3 propagation. Cell Death Differ 26, 1062-1076.

Moscat, J., Karin, M., Diaz-Meco, M.T., 2016. p62 in Cancer: Signaling Adaptor Beyond Autophagy. Cell 167, 606-609.

Mouna, L., Hernandez, E., Bonte, D., Brost, R., Amazit, L., Delgui, L.R., Brune, W., Geballe, A.P., Beau, I., Esclatine, A., 2016. Analysis of the role of autophagy inhibition by two complementary human cytomegalovirus BECN1/Beclin 1-binding proteins. Autophagy 12, 327-342.

Münz, C., 2017. The Autophagic Machinery in Viral Exocytosis. Front Microbiol 8, 269.

Murphy, E., Shenk, T.E., 2008. Human Cytomegalovirus Genome, in: Shenk, T.E., Stinski, M.F. (Eds.), Human Cytomegalovirus. Springer Berlin Heidelberg, Berlin, Heidelberg, pp. 1-19.

Nance, W.E., Lim, B.G., Dodson, K.M., 2006. Importance of congenital cytomegalovirus infections as a cause for pre-lingual hearing loss. J Clin Virol 35, 221-225.

Niida, M., Tanaka, M., Kamitani, T., 2010. Downregulation of active IKK beta by Ro52-mediated autophagy. Mol Immunol 47, 2378-2387.

Ning, S., Wang, L., 2019. The Multifunctional Protein p62 and Its Mechanistic Roles in Cancers. Curr Cancer Drug Targets 19, 468-478.

Nowag, H., Guhl, B., Thriene, K., Romao, S., Ziegler, U., Dengjel, J., Münz, C., 2014. Macroautophagy Proteins Assist Epstein Barr Virus Production and Get Incorporated Into the Virus Particles. EBioMedicine 1, 116-125.

Orvedahl, A., Alexander, D., Tallóczy, Z., Sun, Q., Wei, Y., Zhang, W., Burns, D., Leib, D.A., Levine, B., 2007. HSV-1 ICP34.5 Confers Neurovirulence by Targeting the Beclin 1 Autophagy Protein. Cell Host & Microbe 1, 23-35.

Orvedahl, A., MacPherson, S., Sumpter, R., Jr., Tallóczy, Z., Zou, Z., Levine, B., 2010. Autophagy Protects against Sindbis Virus Infection of the Central Nervous System. Cell Host & Microbe 7, 115-127.

Overå, K.S., Garcia-Garcia, J., Bhujabal, Z., Jain, A., Øvervatn, A., Larsen, K.B., Deretic, V., Johansen, T., Lamark, T., Sjøttem, E., 2019. TRIM32, but not its muscular dystrophy-associated mutant, positively regulates and is targeted to autophagic degradation by p62/SQSTM1. Journal of Cell Science 132.

Ozato, K., Shin, D.-M., Chang, T.-H., Morse, H.C., 2008. TRIM family proteins and their emerging roles in innate immunity. Nature Reviews Immunology 8, 849-860.

Paludan, C., Schmid, D., Landthaler, M., Vockerodt, M., Kube, D., Tuschl, T., Münz, C., 2005. Endogenous MHC Class II Processing of a Viral Nuclear Antigen After Autophagy. Science 307, 593-596.

Pankiv, S., Clausen, T.H., Lamark, T., Brech, A., Bruun, J.-A., Outzen, H., Øvervatn, A., Bjørkøy, G., Johansen, T., 2007. p62/SQSTM1 Binds Directly to Atg8/LC3 to Facilitate Degradation of Ubiquitinated Protein Aggregates by Autophagy *<sup>
</sup>. Journal of Biological Chemistry 282, 24131-24145.

Pankiv, S., Lamark, T., Bruun, J.-A., Øvervatn, A., Bjørkøy, G., Johansen, T., 2010. Nucleocytoplasmic Shuttling of p62/SQSTM1 and Its Role in Recruitment of Nuclear Polyubiquitinated Proteins to Promyelocytic Leukemia Bodies *. Journal of Biological Chemistry 285, 5941-5953.

Pari, G.S., 2008. Nuts and bolts of human cytomegalovirus lytic DNA replication. Curr Top Microbiol Immunol 325, 153-166.

Parzych, K.R., Klionsky, D.J., 2014. An overview of autophagy: morphology, mechanism, and regulation. Antioxid Redox Signal 20, 460-473.

Pattingre, S., Tassa, A., Qu, X., Garuti, R., Liang, X.H., Mizushima, N., Packer, M., Schneider, M.D., Levine, B., 2005. Bcl-2 Antiapoptotic Proteins Inhibit Beclin 1-Dependent Autophagy. Cell 122, 927-939.

Paul, P., Münz, C., 2016. Autophagy and Mammalian Viruses: Roles in Immune Response, Viral Replication, and Beyond. Adv Virus Res 95, 149-195.

Phillips, S.L., Cygnar, D., Thomas, A., Bresnahan, W.A., 2012. Interaction between the human cytomegalovirus tegument proteins UL94 and UL99 is essential for virus replication. J Virol 86, 9995-10005.

Pilli, M., Arko-Mensah, J., Ponpuak, M., Roberts, E., Master, S., Mandell, M.A., Dupont, N., Ornatowski, W., Jiang, S., Bradfute, S.B., Bruun, J.-A., Hansen, Tom E., Johansen, T.,

Deretic, V., 2012. TBK-1 Promotes Autophagy-Mediated Antimicrobial Defense by Controlling Autophagosome Maturation. Immunity 37, 223-234.

Pineda, C.T., Ramanathan, S., Fon Tacer, K., Weon, J.L., Potts, M.B., Ou, Y.H., White, M.A., Potts, P.R., 2015. Degradation of AMPK by a cancer-specific ubiquitin ligase. Cell 160, 715-728.

Prabakaran, T., Bodda, C., Krapp, C., Zhang, B.C., Christensen, M.H., Sun, C., Reinert, L., Cai, Y., Jensen, S.B., Skouboe, M.K., Nyengaard, J.R., Thompson, C.B., Lebbink, R.J., Sen, G.C., van Loo, G., Nielsen, R., Komatsu, M., Nejsum, L.N., Jakobsen, M.R., Gyrd-Hansen, M., Paludan, S.R., 2018. Attenuation of cGAS-STING signaling is mediated by a p62/SQSTM1-dependent autophagy pathway activated by TBK1. Embo j 37.

Prichard, M.N., Britt, W.J., Daily, S.L., Hartline, C.B., Kern, E.R., 2005. Human cytomegalovirus UL97 Kinase is required for the normal intranuclear distribution of pp65 and virion morphogenesis. J Virol 79, 15494-15502.

Prichard, M.N., Gao, N., Jairath, S., Mulamba, G., Krosky, P., Coen, D.M., Parker, B.O., Pari, G.S., 1999. A recombinant human cytomegalovirus with a large deletion in UL97 has a severe replication deficiency. J Virol 73, 5663-5670.

Rabinowitz, J.D., White, E., 2010. Autophagy and metabolism. Science 330, 1344-1348.

Rafailidis, P.I., Mourtzoukou, E.G., Varbobitis, I.C., Falagas, M.E., 2008. Severe cytomegalovirus infection in apparently immunocompetent patients: a systematic review. Virol J 5, 47.

Ran, Y., Zhang, J., Liu, L.L., Pan, Z.Y., Nie, Y., Zhang, H.Y., Wang, Y.Y., 2016. Autoubiquitination of TRIM26 links TBK1 to NEMO in RLR-mediated innate antiviral immune response. J Mol Cell Biol 8, 31-43.

Razonable, R.R., Inoue, N., Pinninti, S.G., Boppana, S.B., Lazzarotto, T., Gabrielli, L., Simonazzi, G., Pellett, P.E., Schmid, D.S., 2020. Clinical Diagnostic Testing for Human Cytomegalovirus Infections. J Infect Dis 221, S74-s85.

Rechsteiner, M., 1990. PEST sequences are signals for rapid intracellular proteolysis. Semin Cell Biol 1, 433-440.

Rechsteiner, M., Rogers, S.W., 1996. PEST sequences and regulation by proteolysis. Trends in Biochemical Sciences 21, 267-271.

Reddy, B.A., Etkin, L.D., Freemont, P.S., 1992. A novel zinc finger coiled-coil domain in a family of nuclear proteins. Trends Biochem Sci 17, 344-345.

Reymond, A., Meroni, G., Fantozzi, A., Merla, G., Cairo, S., Luzi, L., Riganelli, D., Zanaria, E., Messali, S., Cainarca, S., Guffanti, A., Minucci, S., Pelicci, P.G., Ballabio, A., 2001. The tripartite motif family identifies cell compartments. Embo j 20, 2140-2151.

Rezaie, T., Child, A., Hitchings, R., Brice, G., Miller, L., Coca-Prados, M., Héon, E., Krupin, T., Ritch, R., Kreutzer, D., Crick, R.P., Sarfarazi, M., 2002. Adult-onset primary open-angle glaucoma caused by mutations in optineurin. Science 295, 1077-1079.

Richetta, C., Faure, M., 2013. Autophagy in antiviral innate immunity. Cellular Microbiology 15, 368-376.

Richter, B., Sliter, D.A., Herhaus, L., Stolz, A., Wang, C., Beli, P., Zaffagnini, G., Wild, P., Martens, S., Wagner, S.A., Youle, R.J., Dikic, I., 2016. Phosphorylation of OPTN by TBK1 enhances its binding to Ub chains and promotes selective autophagy of damaged mitochondria. Proc Natl Acad Sci U S A 113, 4039-4044.

Rogers, S., Wells, R., Rechsteiner, M., 1986. Amino acid sequences common to rapidly degraded proteins: the PEST hypothesis. Science 234, 364-368.

Rogov, V., Dötsch, V., Johansen, T., Kirkin, V., 2014. Interactions between Autophagy Receptors and Ubiquitin-like Proteins Form the Molecular Basis for Selective Autophagy. Molecular Cell 53, 167-178.

Rogov, V.V., Suzuki, H., Marinković, M., Lang, V., Kato, R., Kawasaki, M., Buljubašić, M., Šprung, M., Rogova, N., Wakatsuki, S., Hamacher-Brady, A., Dötsch, V., Dikic, I., Brady, N.R., Novak, I., 2017. Phosphorylation of the mitochondrial autophagy receptor Nix enhances its interaction with LC3 proteins. Scientific Reports 7, 1131.

Sagnier, S., Daussy, C.F., Borel, S., Robert-Hebmann, V., Faure, M., Blanchet, F.P., Beaumelle, B., Biard-Piechaczyk, M., Espert, L., 2015. Autophagy restricts HIV-1 infection by selectively degrading Tat in CD4+ T lymphocytes. J Virol 89, 615-625.

Sampaio, K.L., Weyell, A., Subramanian, N., Wu, Z., Sinzger, C., 2017. A TB40/E-derived human cytomegalovirus genome with an intact US-gene region and a self-excisable BAC cassette for immunological research. Biotechniques 63, 205-214.

Sanchez, V., McElroy, A.K., Spector, D.H., 2003. Mechanisms governing maintenance of Cdk1/cyclin B1 kinase activity in cells infected with human cytomegalovirus. J Virol 77, 13214-13224.

Sanz, L., Sanchez, P., Lallena, M.-J., Diaz-Meco, M.T., Moscat, J., 1999. The interaction of p62 with RIP links the atypical PKCs to NF-κB activation. The EMBO Journal 18, 3044-3053.

Schaaf, M.B.E., Keulers, T.G., Vooijs, M.A., Rouschop, K.M.A., 2016. LC3/GABARAP family proteins: autophagy-(un)related functions. The FASEB Journal 30, 3961-3978.

Schauflinger, M., Villinger, C., Mertens, T., Walther, P., von Einem, J., 2013. Analysis of human cytomegalovirus secondary envelopment by advanced electron microscopy. Cell Microbiol 15, 305-314.

Schlegel, A., Giddings, T.H., Jr., Ladinsky, M.S., Kirkegaard, K., 1996. Cellular origin and ultrastructure of membranes induced during poliovirus infection. J Virol 70, 6576-6588.

Schneider, W.M., Chevillotte, M.D., Rice, C.M., 2014. Interferon-Stimulated Genes: A Complex Web of Host Defenses. Annual Review of Immunology 32, 513-545.

Schoggins, J.W., 2019. Interferon-Stimulated Genes: What Do They All Do? Annu Rev Virol 6, 567-584.

Schoggins, J.W., Rice, C.M., 2011. Interferon-stimulated genes and their antiviral effector functions. Curr Opin Virol 1, 519-525.

Schottstedt, V., Blümel, J., Burger, R., Drosten, C., Gröner, A., Gürtler, L., Heiden, M., Hildebrandt, M., Jansen, B., Montag-Lessing, T., Offergeld, R., Pauli, G., Seitz, R., Schlenkrich, U., Strobel, J., Willkommen, H., von König, C.H., 2010. Human Cytomegalovirus (HCMV) - Revised. Transfus Med Hemother 37, 365-375.

Schütz, M., Steingruber, M., Socher, E., Müller, R., Wagner, S., Kögel, M., Sticht, H., Marschall, M., 2021. Functional Relevance of the Interaction between Human Cyclins and the Cytomegalovirus-Encoded CDK-Like Protein Kinase pUL97. Viruses 13.

Seibenhener, M.L., Babu, J.R., Geetha, T., Wong, H.C., Krishna, N.R., Wooten, M.W., 2004. Sequestosome 1/p62 is a polyubiquitin chain binding protein involved in ubiquitin proteasome degradation. Mol Cell Biol 24, 8055-8068.

Shi, J., Fung, G., Piesik, P., Zhang, J., Luo, H., 2014. Dominant-negative function of the C-terminal fragments of NBR1 and SQSTM1 generated during enteroviral infection. Cell Death & Differentiation 21, 1432-1441.

Smith, R.M., Kosuri, S., Kerry, J.A., 2014. Role of human cytomegalovirus tegument proteins in virion assembly. Viruses 6, 582-605.

Sparrer, K.M.J., Gableske, S., Zurenski, M.A., Parker, Z.M., Full, F., Baumgart, G.J., Kato, J., Pacheco-Rodriguez, G., Liang, C., Pornillos, O., Moss, J., Vaughan, M., Gack, M.U., 2017. TRIM23 mediates virus-induced autophagy via activation of TBK1. Nature Microbiology 2, 1543-1557.

Stagno, S., Pass, R.F., Dworsky, M.E., Britt, W.J., Alford, C.A., 1984. Congenital and perinatal cytomegalovirus infections: clinical characteristics and pathogenic factors. Birth Defects Orig Artic Ser 20, 65-85.

Steingruber, M., Marschall, M., 2020. The Cytomegalovirus Protein Kinase pUL97:Host Interactions, Regulatory Mechanisms and Antiviral Drug Targeting. Microorganisms 8.

Steininger, C., 2007. Clinical relevance of cytomegalovirus infection in patients with disorders of the immune system. Clin Microbiol Infect 13, 953-963.

Stolz, A., Ernst, A., Dikic, I., 2014. Cargo recognition and trafficking in selective autophagy. Nat Cell Biol 16, 495-501.

Sun, D., Wu, R., Zheng, J., Li, P., Yu, L., 2018. Polyubiquitin chain-induced p62 phase separation drives autophagic cargo segregation. Cell Res 28, 405-415.

Taisne, C., Lussignol, M., Hernandez, E., Moris, A., Mouna, L., Esclatine, A., 2019. Human cytomegalovirus hijacks the autophagic machinery and LC3 homologs in order to optimize cytoplasmic envelopment of mature infectious particles. Scientific Reports 9, 4560.

Tanida, I., Minematsu-Ikeguchi, N., Ueno, T., Kominami, E., 2005. Lysosomal turnover, but not a cellular level, of endogenous LC3 is a marker for autophagy. Autophagy 1, 84-91.

Tanida, I., Ueno, T., Kominami, E., 2008. LC3 and Autophagy, in: Deretic, V. (Ed.), Autophagosome and Phagosome. Humana Press, Totowa, NJ, pp. 77-88.

tenOever, B.R., Sharma, S., Zou, W., Sun, Q., Grandvaux, N., Julkunen, I., Hemmi, H., Yamamoto, M., Akira, S., Yeh, W.C., Lin, R., Hiscott, J., 2004. Activation of TBK1 and IKKvarepsilon kinases by vesicular stomatitis virus infection and the role of viral ribonucleoprotein in the development of interferon antiviral immunity. J Virol 78, 10636-10649.

Thakar, K., Karaca, S., Port, S.A., Urlaub, H., Kehlenbach, R.H., 2013. Identification of CRM1-dependent Nuclear Export Cargos Using Quantitative Mass Spectrometry. Mol Cell Proteomics 12, 664-678.

Thinwa, J.W., Zou, Z., Parks, E., Sebti, S., Hui, K., Wei, Y., Singh, V., Urquhart, G., Jewell, J.L., Pfeiffer, J.K., Levine, B., Reese, T.A., Shiloh, M.U., 2022. CDKL5 regulates p62-mediated selective autophagy and host antiviral defense. bioRxiv, 2022.2009.2020.508746.

Umaña, A.C., Iwahori, S., Kalejta, R.F., 2018. Direct Substrate Identification with an Analog Sensitive (AS) Viral Cyclin-Dependent Kinase (v-Cdk). ACS Chem Biol 13, 189-199.

Van Damme, E., Van Loock, M., 2014. Functional annotation of human cytomegalovirus gene products: an update. Frontiers in Microbiology 5.

van den Berg, A.P., van Son, W.J., Jiwa, N.M., van der Bij, W., Schirm, J., van der Giessen, M., The, T.H., 1990. Recent advances in the diagnosis of active cytomegalovirus infection after organ transplantation. Transplant Proc 22, 226-228.

van Gent, M., Sparrer, K.M.J., Gack, M.U., 2018. TRIM Proteins and Their Roles in Antiviral Host Defenses. Annu Rev Virol 5, 385-405.

van Zeijl, M., Fairhurst, J., Baum, E.Z., Sun, L., Jones, T.R., 1997. The human cytomegalovirus UL97 protein is phosphorylated and a component of virions. Virology 231, 72-80.

Vargas, J.N.S., Hamasaki, M., Kawabata, T., Youle, R.J., Yoshimori, T., 2023. The mechanisms and roles of selective autophagy in mammals. Nature Reviews Molecular Cell Biology 24, 167-185.

Verpooten, D., Ma, Y., Hou, S., Yan, Z., He, B., 2009. Control of TANK-binding kinase 1-mediated signaling by the gamma(1)34.5 protein of herpes simplex virus 1. J Biol Chem 284, 1097-1105.

Verweij, M.C., Horst, D., Griffin, B.D., Luteijn, R.D., Davison, A.J., Ressing, M.E., Wiertz, E.J., 2015. Viral inhibition of the transporter associated with antigen processing (TAP): a striking example of functional convergent evolution. PLoS Pathog 11, e1004743.

Viret, C., Duclaux-Loras, R., Nancey, S., Rozières, A., Faure, M., 2021. Selective Autophagy Receptors in Antiviral Defense. Trends in Microbiology 29, 798-810.

Wang, C.C., Peng, H., Wang, Z., Yang, J., Hu, R.G., Li, C.Y., Geng, W.J., 2022. TRIM72-mediated degradation of the short form of p62/SQSTM1 rheostatically controls selective autophagy in human cells. Mil Med Res 9, 35.

Wang, W., Xia, Z., Farré, J.C., Subramani, S., 2018. TRIM37 deficiency induces autophagy through deregulating the MTORC1-TFEB axis. Autophagy 14, 1574-1585.

Warming, S., Costantino, N., Court, D.L., Jenkins, N.A., Copeland, N.G., 2005. Simple and highly efficient BAC recombineering using galK selection. Nucleic Acids Res 33, e36.

Weidberg, H., Shvets, E., Shpilka, T., Shimron, F., Shinder, V., Elazar, Z., 2010. LC3 and GATE-16/GABARAP subfamilies are both essential yet act differently in autophagosome biogenesis. Embo j 29, 1792-1802.

Wild, P., Farhan, H., McEwan, D.G., Wagner, S., Rogov, V.V., Brady, N.R., Richter, B., Korac, J., Waidmann, O., Choudhary, C., Dötsch, V., Bumann, D., Dikic, I., 2011. Phosphorylation of the Autophagy Receptor Optineurin Restricts Salmonella Growth. Science 333, 228-233.

Wolf, D.G., Courcelle, C.T., Prichard, M.N., Mocarski, E.S., 2001. Distinct and separate roles for herpesvirus-conserved UL97 kinase in cytomegalovirus DNA synthesis and encapsidation. Proc Natl Acad Sci U S A 98, 1895-1900.

Wu, Q., Xiang, M., Wang, K., Chen, Z., Long, L., Tao, Y., Liang, Y., Yan, Y., Xiao, Z., Qiu, S., Yi, B., 2020a. Overexpression of p62 Induces Autophagy and Promotes Proliferation, Migration and Invasion of Nasopharyngeal Carcinoma Cells through Promoting ERK Signaling Pathway. Curr Cancer Drug Targets 20, 624-637.

Wu, S.F., Xia, L., Shi, X.D., Dai, Y.J., Zhang, W.N., Zhao, J.M., Zhang, W., Weng, X.Q., Lu, J., Le, H.Y., Tao, S.C., Zhu, J., Chen, Z., Wang, Y.Y., Chen, S., 2020b. RIG-I regulates myeloid differentiation by promoting TRIM25-mediated ISGylation. Proc Natl Acad Sci U S A 117, 14395-14404.

Wurzer, B., Zaffagnini, G., Fracchiolla, D., Turco, E., Abert, C., Romanov, J., Martens, S., 2015. Oligomerization of p62 allows for selection of ubiquitinated cargo and isolation membrane during selective autophagy. Elife 4, e08941.

Xu, Y., Cei, S.A., Huete, A.R., Pari, G.S., 2004a. Human cytomegalovirus UL84 insertion mutant defective for viral DNA synthesis and growth. J Virol 78, 10360-10369.

Xu, Y., Cei, S.A., Rodriguez Huete, A., Colletti, K.S., Pari, G.S., 2004b. Human cytomegalovirus DNA replication requires transcriptional activation via an IE2- and UL84-responsive bidirectional promoter element within oriLyt. J Virol 78, 11664-11677.

Yang, Q., Liu, T.T., Lin, H., Zhang, M., Wei, J., Luo, W.W., Hu, Y.H., Zhong, B., Hu, M.M., Shu, H.B., 2017. TRIM32-TAX1BP1-dependent selective autophagic degradation of TRIF negatively regulates TLR3/4-mediated innate immune responses. PLoS Pathog 13, e1006600.

Yang, Y., Fiskus, W., Yong, B., Atadja, P., Takahashi, Y., Pandita, T.K., Wang, H.G., Bhalla, K.N., 2013. Acetylated hsp70 and KAP1-mediated Vps34 SUMOylation is required for autophagosome creation in autophagy. Proc Natl Acad Sci U S A 110, 6841-6846.

Ying, H., Yue, B.Y., 2012. Cellular and molecular biology of optineurin. Int Rev Cell Mol Biol 294, 223-258.

Ying, H., Yue, B.Y., 2016. Optineurin: The autophagy connection. Exp Eye Res 144, 73-80.

Ylä-Anttila, P., 2021. Autophagy receptors as viral targets. Cell Mol Biol Lett 26, 29.

Yu, D., Smith, G.A., Enquist, L.W., Shenk, T., 2002. Construction of a self-excisable bacterial artificial chromosome containing the human cytomegalovirus genome and mutagenesis of the diploid TRL/IRL13 gene. J Virol 76, 2316-2328.

Zhang, C., Huang, C., Xia, H., Xu, H., Tang, Q., Bi, F., 2022. Autophagic sequestration of SQSTM1 disrupts the aggresome formation of ubiquitinated proteins during proteasome inhibition. Cell Death Dis 13, 615.

Zhang, J., Hu, M.M., Wang, Y.Y., Shu, H.B., 2012. TRIM32 protein modulates type I interferon induction and cellular antiviral response by targeting MITA/STING protein for K63-linked ubiquitination. J Biol Chem 287, 28646-28655.

Zimmermann, C., unpublished.

Zimmermann, C., Krämer, N., Krauter, S., Strand, D., Sehn, E., Wolfrum, U., Freiwald, A., Butter, F., Plachter, B., 2021. Autophagy interferes with human cytomegalovirus genome replication, morphogenesis, and progeny release. Autophagy 17, 779-795.

Acknowledgments/Danksagung

Curriculum Vitae